ParaNoise

Traffic noise simulation using parametric design and optimizing building configurations to reduce traffic noise

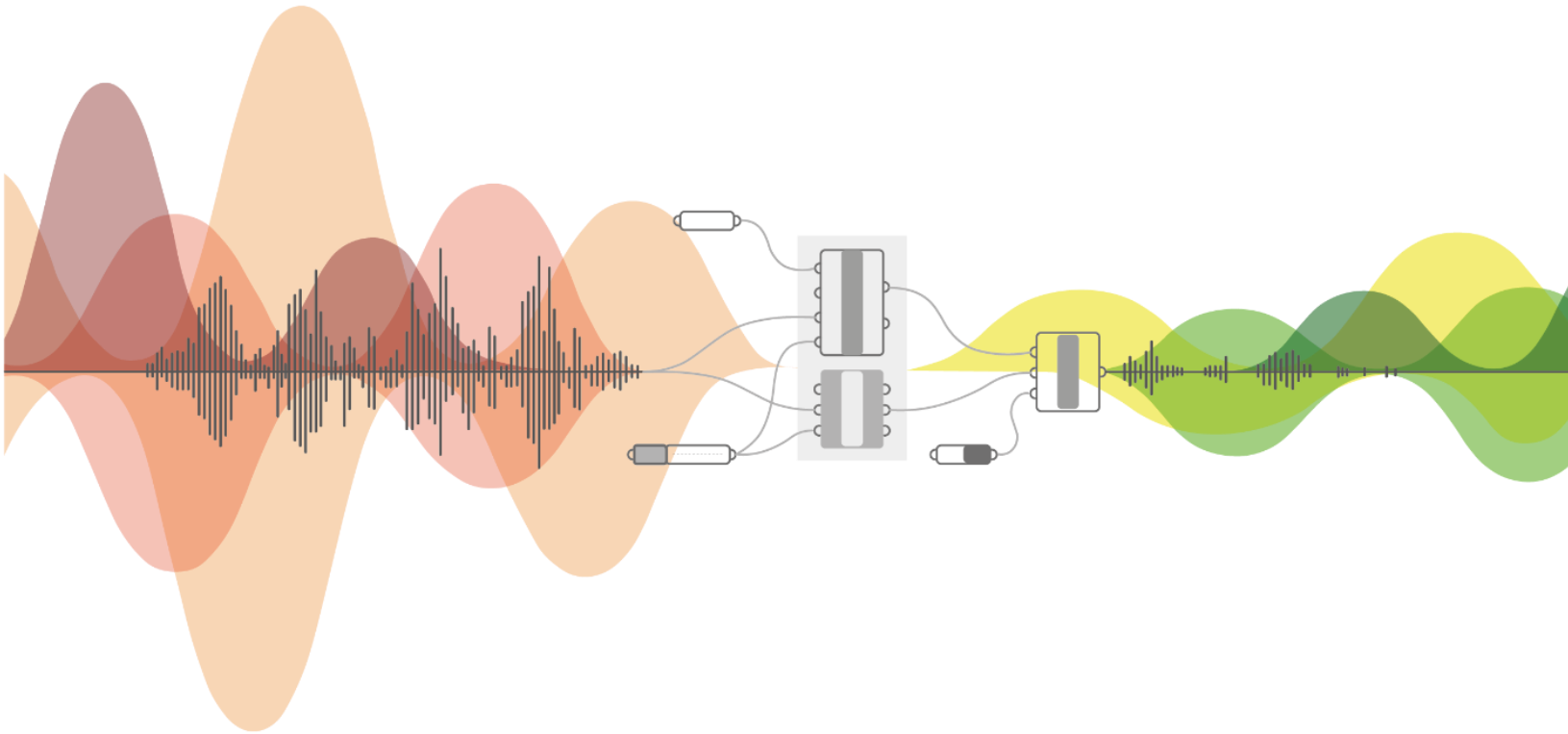

Graduation report
Parikshit Nikumbh
5077907

Traffic noise simulation using parametric design and optimizing building configurations to reduce traffic noise

June 4th, 2022

Graduation Report by,

Parikshit D. Nikumbh
5077907
TU Delft
Faculty of Civil Engineering & Geosciences

Master Track	Building Engineering
Specialization	Building Technology and Physics

Graduation committee:

Dr.ir. H.R. (Roel) Schipper (Chair)	Applied Mechanics | CiTG
Dr.ir. M.J. (Martin) Tenpierik	Building Physics | AE+T
Dr.ir. M.C. (Martijn) Lugten	Building Physics | AE+T
Dr. M. (Michela) Turrin	Design Informatics | AE+T
ir. J.D. (Douwe) de Jong	Building Physics | RHDHV

TU Delft

Royal HaskoningDHV
Enhancing Society Together

Preface

A quiet environment is a pretty rare commodity these days and we are all paying a price for it in terms of our health. Reducing environmental noise and realization of silent spaces has become a key objective for governments and designers like architects and urban planners have a big role to play.

For the past eight months, I've been focusing on how we can predict traffic noise early in the design process, allowing the designer to improve the quality of the urban environment. This master thesis presents the findings of this expedition which I believe will contribute to improving the quality of life in future cities.

During my bachelor's in Civil Engineering, I realized that the indoor environment determines how we experience the building, rather than the skeleton of the structure. With that intention, I enrolled myself in the TU Delft to help me understand more about the subject I truly adore. There have been exciting challenges I faced during my time at TU but working on this thesis was one of the most exciting. It pushed me to my limits and made me a better student. I think working on a master's thesis is like running a marathon where consistency is more important than speed. This whole marathon would not have been possible without the push from many people, and I would like to take this opportunity to show my gratitude to them.

First of all, I want to express my gratitude to Roel Schipper for being my mentor not just during this thesis but also over the past two years, and for assisting me in overcoming academic challenges. Martin Tenpierik and Michela deserve a huge thank you for teaching me acoustics and computational design during my first year, which inspired this thesis project. Additionally, their timely feedback was essential throughout the research. I'd also want to thank Martijn, who was extremely helpful in finding a case study and writing this thesis, as well as supporting me throughout the process by providing useful pointers for improvement.

I am grateful to Douwe de Jong, Vivian Timmermans, and all of my RHDHV colleagues for their technical assistance and positive feedback during the process. Special thanks to Marc Tavenier for helping me in the development of the workflow. Last but not least, I'd like to express my gratitude to my family for believing in me and my friends for providing emotional support along the journey.

Abstract

Environmental noise has become a large health concern in Europe with at least one in five people exposed to levels considered harmful to health. Additionally, prolonged exposure to excessive levels of noise has a negative economic impact.

The rapid development of urban areas makes the effect of noise pollution even worse. However, architects and urban designers who define the shape of a neighbourhood rarely give attention to this aspect. Decisions regarding the sound environment are often taken in the latter stages of design when the least design exploration is possible. Moreover, environmental acoustic involves complex urban physics which makes it more difficult for designers.

Therefore, in this master thesis, a parametric simulation workflow is developed which can predict the traffic noise in the early phases of design. The approach would be easy to use for architects and urban designers to overcome some of the main drawbacks of traditional practices.

The project followed five-step processes of research, development, validation, testing and optimization. To better understand urban noise, atmospheric acoustics, and how buildings affect sound propagation, a literature review was conducted. The parametric workflow was then created using Grasshopper, the visual scripting plugin for Rhino3D, in conjunction with other plugins such as Pachyderm and Ladybug.

After development stage, the parametric workflow is validated against on-site measurements and Geomilieu (environmental noise calculation software). Further, the simulation results from the design stage demonstrate that the tool can include urban microscale features like building shape, façade extrusions and materiality which can have an impact on reducing the traffic noise levels. It is found that the building shape of the lower levels may amplify or quieten the sound on upper levels. Façade extrusions have the least impact but variations in their positions and sizes may influence the results. It was further predicted that the green façade has a great potential to reduce reflected noise and lower the values inside the courtyard.

In addition, the findings of the optimization study show that the workflow may be used with other performance criteria and help to explore design solutions. Overall, the workflow can help identify the relationships between design aspects and acoustic performance in the early stages of design by taking into account simplifications and restrictions such as edge diffraction.

List of frequently used abbreviations

α	Absorption coefficient
dB	Decibels
dB(A)	A-weighed decibels
Hz	Hertz
λ	Wavelength of sound (in meters)
SPL	Sound Pressure level, mostly in dB of dB(A)
RT	Reverberation time (in seconds)
L_p	Sound pressure level (dB)
L_{den}	Sound pressure level (dB(A)) day-evening-night, European noise metric
Pachy_RH	Pachyderm plugin inside Rhino
Pachy_GH	Pachyderm plugin inside Grasshopper
RT-1	Residential tower-1
RT-2	Residential tower-2

Table of Contents

1

Introduction

Part 1 Introduction

1.1 Problem Context

1.1.1 Impact of environmental noise

Noise is a major environmental issue in urban areas and features among the top environmental risks to physical and mental health and wellbeing[1]. Health impacts of environmental noise are growing concerns among the general public and policymakers in Europe [2].

European Union publications suggest that about 40% of the population in 33 EU countries is exposed to road traffic noise at levels exceeding 55dB(A) and 20% are exposed to levels exceeding 65 dB(A) during the daytime [3], [4].

WHO defines environmental noise as "Noise emitted from all the sources except for noise at the industrial workplace" [5]. However, EU directive 2002/49/EC defines environmental noise as "unwanted or harmful outdoor sound created by human activities, including noise from the road, rail, airports and industrial sites"[1].

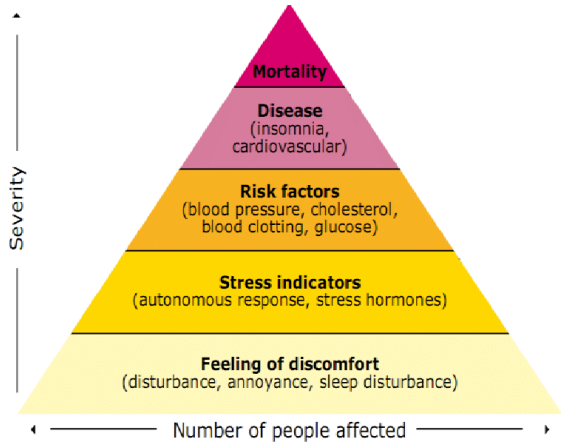

Figure 1 WHO pyramid of health effects of noise (Source: Babisch, 2002, based on WHO, 1972.)

Prolonged exposure to high noise levels is associated with adverse health effects and can cause many short-and long-term health problems[3]. Often these adverse effects are consequences of exceeding traffic noise and include annoyance, sleep disturbance, cardiovascular diseases, cognitive impairment and mental stress [4], [6].

Furthermore, noise pollution has adverse impacts on the economy as well. The economic costs related to noise involve a reduction in housing prices, increased medical costs, loss of productivity, medical expenses and decreases revenues from tourism [7]. In its Green Paper on Future Noise Policy 1996, the European commission estimated the damage due to environmental noise ranges from 13 million to 30 billion euros[8]. Subsequently, the 2011 report on the implementation of END estimates around 40-million-euro social cost of road noise related to disease and premature deaths [9].

Therefore, the effects of noise on society as well as on individuals should be taken seriously. Architecand urban designers can play an important role to reduce noise levels and creating healthy living in an urban environment through design intervention.

1.1.2 Expansion of cities

The population of Europe has grown consistently over the last 50 years, but projections estimate that the size of the European population will remain stable for the next two decades [10]. However, World Urbanization Prospect[11] and JRC report on European Territorial Trends shows that the population will be continuing to rise in urban areas [12]. This will lead to an increase in the demand for housing as well as more transport and infrastructure. Urban morphological zone (UMZ) data show that the expansion of cities also known as urban sprawl is generally along the major highways connecting to suburbs [13]. This colossal densification trend is classified as a major global health issue in the 21st century[14] and will further worsen the problem of traffic noise pollution.

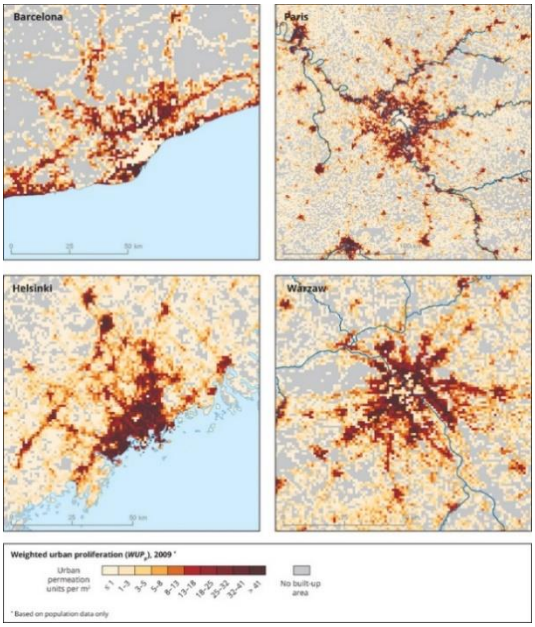

Figure 2 Urban-sprawl-in-Barcelona-Paris-Helsinki-Warzaw (Source: Urban morphological zones, EEA (europa.eu))

1.1.3 Urban sound planning

Optimizing the urban areas on a microscale level could reduce noise pollution and improve the acoustic environment. Urban microscale involves parameters like width and height of street, degree of façade irregularities and openings in façade (cross street openings). However, the role of acoustics in the planning for urban areas has not been considered in most of the projects [15], [16]. Optimizing the design for urban acoustics is a complex affair[16] and comprehensive knowledge of urban acoustics is important to understand the noise control measures, prediction methods and sound design [15]. This process becomes more complicated for most urban designers and architects. Oftentimes, an acoustic specialist gets consulted after the design is finalized. Although some localized solutions are being considered, acoustics is rarely given special consideration in the early phases of design. SONORUS an EU initiative for urban sound planning demonstrates the importance of involving urban sound planning in the design process from the beginning [17]. Thus, the involvement of urban acoustics in the earlier planning process can provide an integrated solution.

1.1.4 Acoustic simulation and Performance-based design

Computational acoustics is majorly divided into geometrical methods and wave-based methods, both having their advantages and disadvantages. In geometrical methods, also known as engineering methods, the sound wave is approximated as rays and is mostly used for sound mapping[16]. The advantage of the geometrical approach is that these methods are relatively cheaper and consume less time in calculations. However, the geometric approach is only suitable for higher frequencies and meteorological effects are generally approximated. On the other hand, the wave-based approach gives many accurate results at lower frequencies, and meteorological effects can be included in the simulation. Despite these advantages, wave-based methods are computationally expensive and need a longer computation time.

Over the last three decades, 3D computer modelling tools have revolutionized architectural practices. Well established acoustic simulation tools like Odeon, CATT-Acoustics, EASE, and Olive tree Lab are in continuous development and are widely used by acousticians for acoustical analysis [18]. These 3D modelling software and computational tools have allowed the analysis of complex geometries and acoustics in architecture design[19]. Many of these acoustic simulation software, however, run in an external modelling environment, which requires the preparation of a compatible 3D model. The transition between 3D modelling software and acoustic simulation software consumes a great amount of time. Another constraint is that the computational power required by these software is substantial, which limits their application in iterative design processes.

Programs like Rhino3D and Grasshopper introduced new territories in architecture design in which geometries can be easily controlled to meet functional objectives [19]. This performance-based (parametric) approach has gained popularity in recent years among the design community as well as students in the design field [20]. The design process involves gathering the performance aspects in the early stages of design, assigning the variables and iteratively optimizing the outcomes [19], [20].

Urban sound propagation is influenced by numerous factors, including sound reflection from surfaces, diffraction due to building edges, refraction by temperature gradient and wind, and air absorption [16]. Thus, the implementation of a parametric approach in the urban acoustic field can greatly support designers in combining acoustic performance objectives with architectural goals [20] and subsequently performing optimization. On the other hand, the number of parameters also makes the simulation much more complicated and thus simplifications are often implemented in geometrical acoustics.

The use of parametric tools, like Grasshopper and Rhino3D to design and optimize spaces intended for artistic performances, such as operas [21] and theatres [19] or open office plans [22] are well established. Pachyderm acoustics for Grasshopper is a widely known plugin and has been used in recent years for the design of spaces with specific indoor acoustic requirements. A recent study [23] investigated the impact of façade materials to maximize environmental noise mitigation using Rhino3D, Grasshopper and Pachyderm simulation plugins. But there is very limited application of Grasshopper and performance-based design applied for urban acoustics simulations.

1.1.5 Problem statement

Considering all the above aspects, the problem posed is the absence of the parametric design approach to evaluate environmental noise in an urban context. The approach would be useful for architects and urban designers to overcome some of the main drawbacks of traditional practices. The design tool can aid in identifying the dependencies between the design features and acoustic performance to further optimize the project in the early design stages.

1.2 Research Definition

1.2.1 Research objective

Based on the research gaps described in the problem context, the goal of this master thesis would be:

> To develop and test parametric simulation workflow that can be used to simulate traffic noise in the early phases of the design process, allowing evaluation and optimization of building configurations in an urban microscale.

1.2.2 Research questions

The research gap and objectives lead to the following main research question:

> How can a parametric-driven workflow help to predict traffic noise levels in an urban environment and help to analyse the building configurations in the early phases of the design process?

The main question will be divided into two major disciplines, one related to simulation and the other related to design. Thus, the main questions lead to the following sub-questions:

1) Sub questions related to simulation:
   a) What are the various meteorological effects which influence the propagation of noise in an urban context and to what extent do these aspects need to be considered in the early-stage acoustic design?
   b) To what extent are the results of a (simplified) parametric urban acoustic simulation workflow comparable to the reference measurements and acoustic software (Geomileu)?

2) Sub-questions related to the design:
   a) How do sound waves emitted by the traffic interact with the geometrical features of the building?
   b) How can different geometrical features and facade materials of the building contribute to enhancing the urban sound environment?
   c) How can parametric optimization be implemented in urban acoustical design?

1.2.3 Research outline

The research outline is summarized in Figure 3. In part 1 of the research, the problem context is described, leading to research objectives and research questions. In part 2, the theoretical framework is introduced that serves as the backbone of the design part. Part

3 introduces the calculation principle behind the parametric workflow and part 4 explains the development of the workflow. The workflow is then followed by the validation of results in part 5. The accumulated knowledge from literature and simulation is used to test different design variations in Part 6. Then part 7 illustrate a few limitations of the design workflow, simplifications to overcome those limitations and recommendation to improve the workflow. Finally, part 8 consists of conclusions, practical relevance and the future scope of the research.

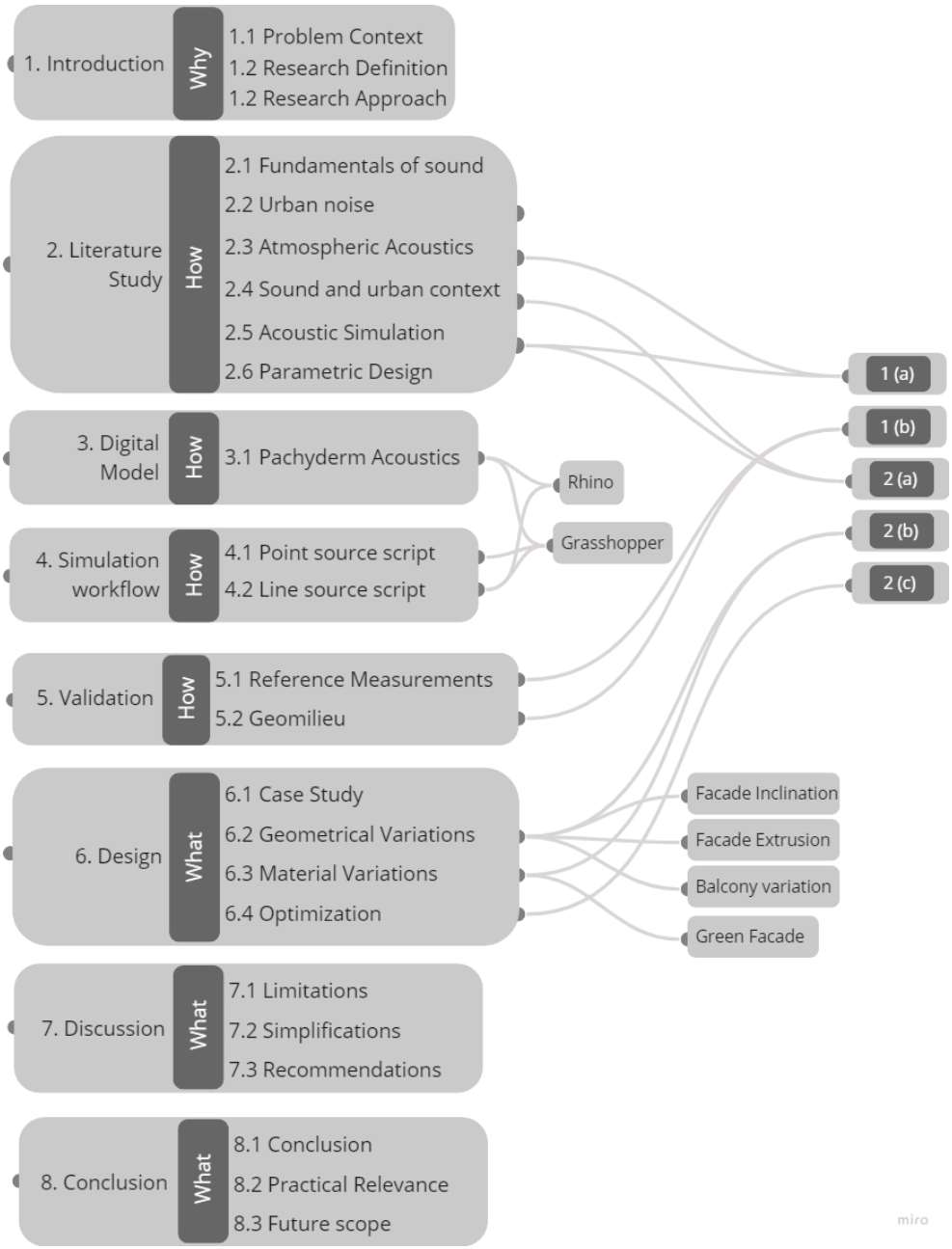

Figure 3 Research outline with research question relationship (own illustration)

1.3 Research Approach

To answer all the research questions, different approaches or methods will be used. This is a further explanation of the chapters mentioned in Figure 3.

1.3.1 Research Definition

This part has already been explained in the previous section.

1.3.2 Literature study

After defining the scope of the research, the literature review is carried out to gather sufficient knowledge about relevant topics in the research. Figure 4 explains the different topics involved in the literature study. Sound fundamentals like sound characteristics and sound perception are covered in chapter 2.1. Furthermore, chapter 2.2 goes through traffic noise, its health effects, and current regulations on noise pollution.

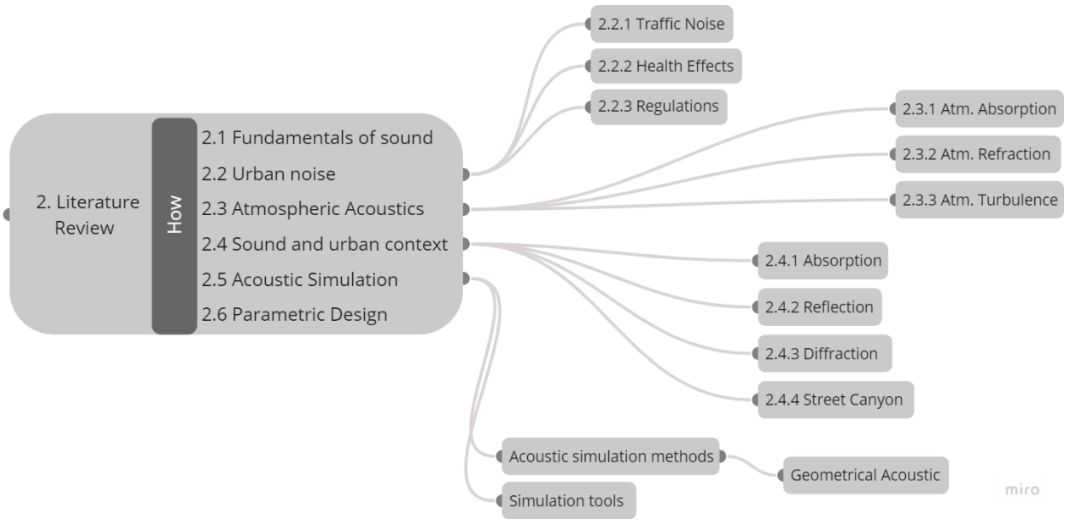

Figure 4 Overview of literature study (own illustration)

The literature study in chapter 2.3 demonstrates how sound propagates in an urban environment. The chapter introduces the meteorological effects like scattering from wind turbulence, refraction by wind and air absorption which are important in urban acoustic simulations. Further, how urban context influences sound propagation is explained in chapter 2.4. This chapter contains existing and theoretical ways to reduce the impact of noise in the urban environment like reflection, absorption, transmission and diffraction. These reviewed references are used in the design phase. And finally, chapter 6 will contain a brief summary of computational methods and software used in urban acoustics. During the literature review, search engines such as Google and Scopus were mostly

used. Terms like urban acoustics, atmospheric acoustics, computational method, parametric design etc. are used as filters to better navigate through the available literature.

1.3.3 Workflow development

To perform a parametric simulation, a Grasshopper definition is made. Grasshopper is a parametric form generating tool, integrated into Rhinoceros 3D and developed in such a way that it can be connected to multiple third-party plugins. In the Grasshopper, workflow is defined using visual components which contain predefined code. The Grasshopper definition is made using Pachyderm acoustics, a third-party simulation plugin that can perform raytracing and image source acoustic simulation. Pachyderm acoustic simulation uses the Finite Volume Method, including eigenfrequencies, 3d scattering coefficient prediction, ray-tracing and Transfer Matrix techniques for calculation of acoustic absorption [24].

During the set-up of the parametric script, ISO 9613-1/2 will be followed as a reference method. This international standard was developed by the technical body ISO/TC 43 to make it possible to predict noise levels in the community from known sound sources [25]. The method consists of two parts under the general title "Acoustics- Attenuation of sound during propagation outdoors":

Part 1: Calculation of the absorption of sound by the atmosphere

Part 2: General method of calculation

1.3.4 Validation

The results from the parametric definition are then validated against reference case study measurements. For this, an existing study conducted in Nantes, France is used as a reference since the purpose of the study was to measure sound decay in urban street. Then the results from the parametric simulation are compared and validated against Geomilieu [26].

1.3.5 Design

To test the parametric simulation and design alternatives a case study project is chosen. For this project, it is important that the proposed geometrical and material variation can potentially contribute to a less noisy environment. Therefore, Entrée Zoetermeer is selected as the case study which is an innovative urban development that is going to be constructed in the new city district of Zoetermeer (Figure 5). The mixed neighbourhood will contain 4500 new homes, offices and commercial spaces and will be developed on

either side of Afrikaweg. Being near to A12 national highway and Afrikaweg, the buildings are exposed to high noise levels which makes it a useful case study

Figure 5 Schematic plan of De Entree Zoetermeer, retrieved from [27]

The final product of this research is to test different design alternatives which reduce noise in an urban environment. Figure 5 shows the concept of street environment that is used for the analysis and validation. Readers should note that this is a typical urban street scenario made for the introduction part, thus serving as a reference. For the base case, buildings and streets from the Entrée Zoetermeer case study are considered as the model is verified in an earlier stage. To evaluate the effects of urban context on noise reduction, several design variants are tested. The design variants are divided into two groups:

1. Acoustical consequences of geometrical variations
2. Acoustical consequences of material variations

1.3.5.1 Geometrical variations:

First, the acoustical consequences of geometrical variations are performed without considering material variation. The geometrical variations are divided into an urban micro-scale which are also the parameters designers consider in the early stages of design. For example, the distance of the building from the street, façade inclination, openings in the façade (cross-streets) and effects of semi-outdoor spaces (façade extrusions).

The inclination of the façade plays important role in sound reflection [28]–[30], therefore three cases; perfectly vertical, 80° downward inclination and 100° upward inclination are included in the study and can be seen in Figure 7. The effect of distance between source and receiver in an open field is rather simple to understand since the closer the road

more will be the noise level. Therefore, variation with respect to street distances is not tested.

Many multi-functional projects like Entrée includes courtyard, green spaces or open fields in urban planning. END in its report [31] highlights the importance of protecting these quiet areas or quiet façades. Therefore, it becomes necessary to check the noise levels of these protected areas which mostly depend on building heights, roof shapes and cross street openings [15]. Thus, the effect of width and location of cross-street (openings in façade/ entrance) on the inner courtyard and quiet façade are tested, see Figure 8. Finally, the effect of façade extrusions like triangular prominences (Figure 9) is evaluated.

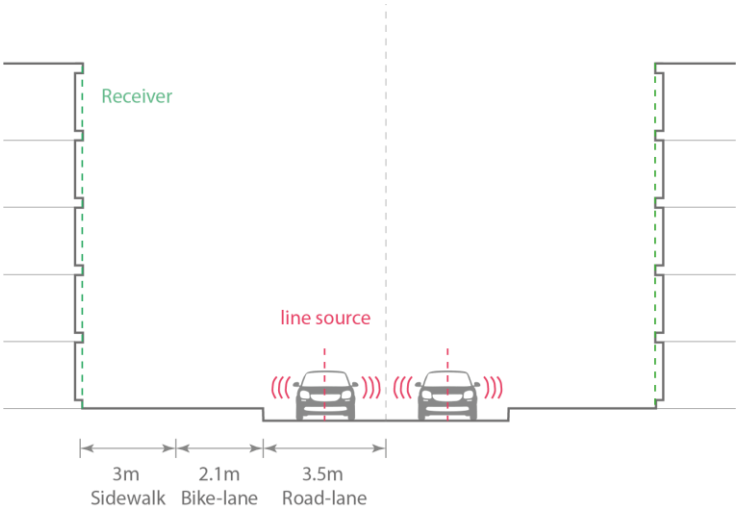

Figure 6 Base case for testing the design variations (own illustration)

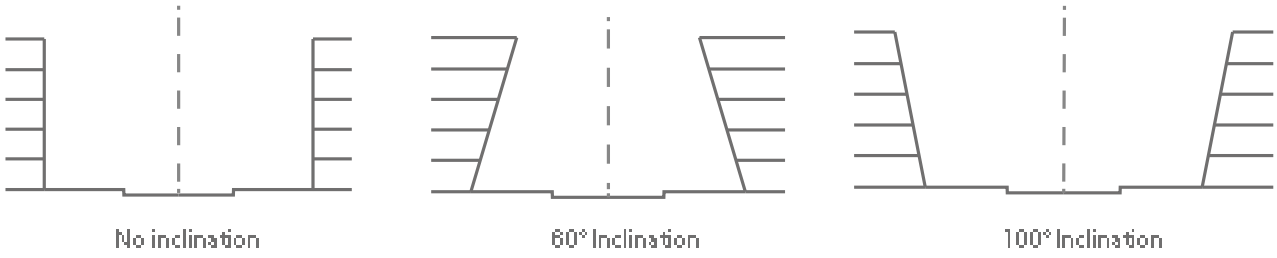

Figure 7 Variations in facade inclinations (own illustration)

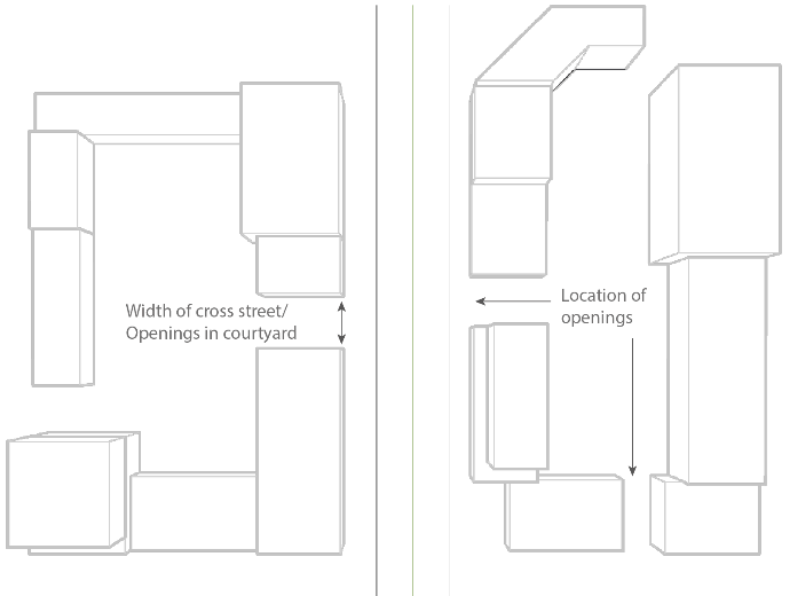

Figure 8 Variations in the cross-street opening (own illustration)

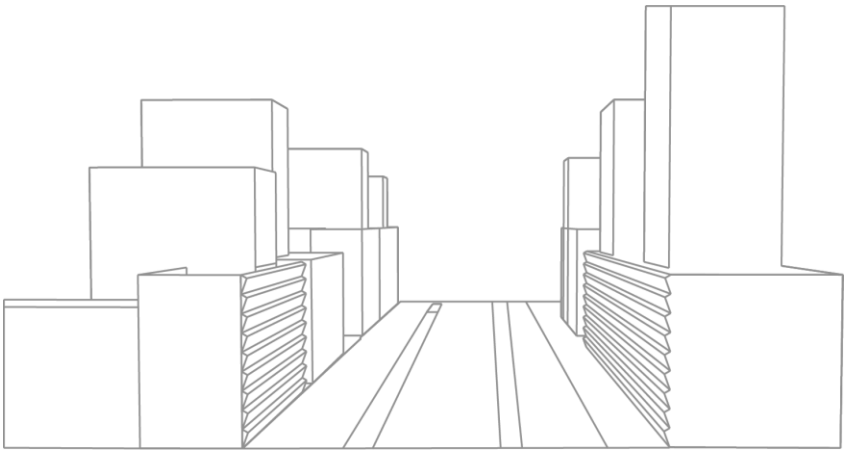

Figure 9 Façade with extrusions (own illustration)

1.3.5.2 Material Variation

Material variation is tested considering a few variants from the geometrical options. The green façade offers excellent sound absorption as well as sound scattering. Therefore, the effectiveness of the green wall is tested by creating a façade pattern (see Figure 10). Moreover, the effective reduction offered by the green wall on sound pressure levels inside the courtyard is tested. The application of absorption material on balcony ceilings to reduce noise levels is well tested by Hothersall et al. [32]. Considering that, balcony ceiling with absorption material is also investigated.

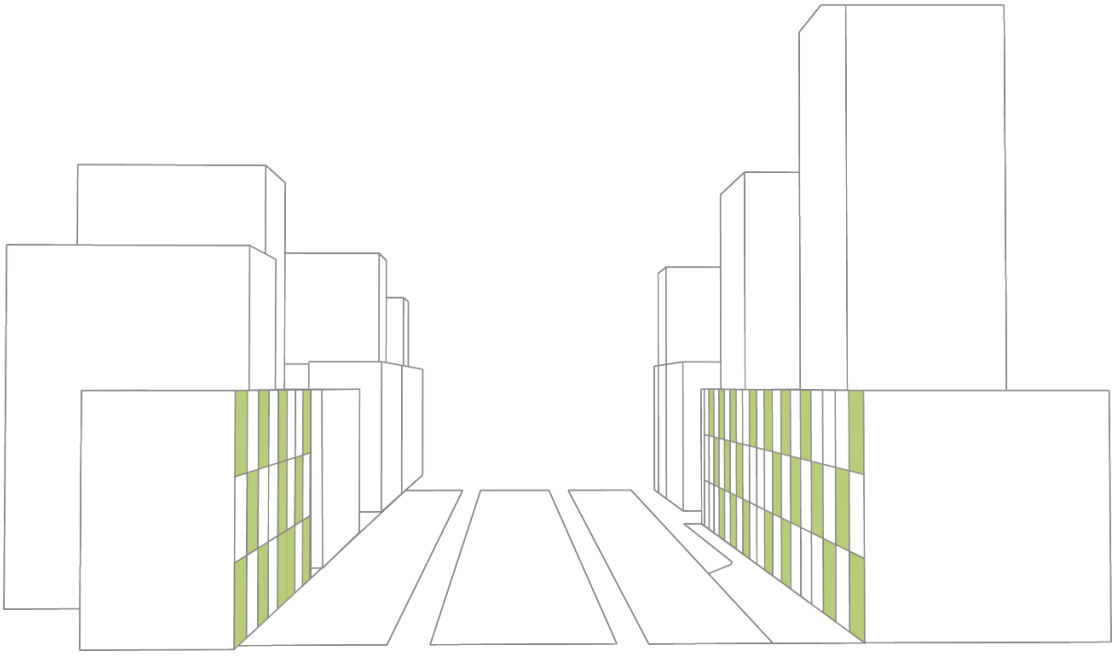

Figure 10 Material variation: Green Facade (own illustration)

1.3.6 Optimization

The final step in the research was to look into the optimization process using an acoustic parametric workflow. There are several third-party optimization plugins available that are supported by the Grasshopper environment like Galapagos, Octopus, Wallacei, Goat, modeFRONTIER etc. These plugins are based on AI evolutionary algorithms and can perform single or multi-objective optimization. The general steps of optimization are explained below to give an overview of the process:

- Identification of design variables and constraints

  In this step, the design variables and constraints are selected. The design variables are already explained in the previous chapter. Optimizing every design parameter is exhaustive and time-consuming work. Given the time frame of the study, only a single geometrical variation i.e. balcony variation is tested.

- Selection of simulation tool

  For optimization, the Wallacei plugin is used. It's an evolutionary solver which can accommodate multi-fitness criteria inside Grasshopper and can automate 3D building simulations and investigate complex geometry.

- Selection of objective function

  Reduction of sound pressure level was the main objective of the optimization. However, the goal was to create the baseline model script which can integrate

multiple design options so that the designer can choose its objective for the optimization. Therefore, the maximization of solar radiation in the winter months was selected as the 2nd objective.

- Simulating until optimization convergence is achieved
- Interpretation and visual representation of data

2

Literature

Part 2 Literature

2.1 Fundamentals of sound

In an elastic medium, a vibration produces pressure differences creating a wave motion due to compression and rarefaction of molecules [33]. This vibration propagates through a medium in the form of energy known as sound. The medium can be gas, liquid or solid, but given the context of the thesis, the sound is transmitted through air. On the other hand, noise is a sound above a certain threshold, and it is dependent on the subjective judgment of the listener.

Sound waves have certain characteristics like velocity, wavelength, amplitude, and frequency. The velocity depends on the physical properties of the fluid and generally for air at 20°C velocity of sound is 342.35 m/s [33]. Frequency is the number of complete cycles of motion (number of waves) in a one-time interval, generally one second [33]. The wavelength is the distance of the wave in a one-time period T and is often an important characteristic since it is the scale by which we judge the physical size of an object [33]. The relation between these characteristics is given by the equation (1) [33] in which, c is the speed of sound [m/s], f is the frequency [Hz], and λ is the wavelength [m]

$$c = f.\lambda \tag{1}$$

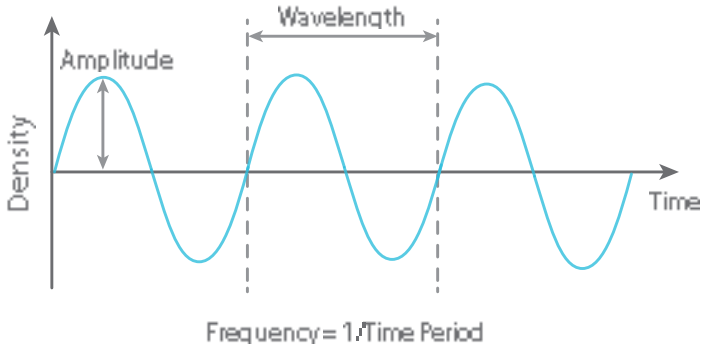

Figure 11 The wavelength, frequency, and amplitude of sound (own illustration)

Although the sound has different frequency ranges, this formula serves as the basics to understanding the relation between sound and an object. For example, at 1000Hz, in the middle of speech frequencies, the wavelength is about 0,34 meters. So, the sound will scatter off the surface of the object that is larger than 0,34 meters. On the other hand,

the sound will simply flow around the object, if the object is much smaller than the wavelength (0,34 in this case).

2.1.1 Sound Calculation

Sound is often measured in terms of effective pressure levels in the air and expressed on a logarithmic scale in decibels (dB) given by equation (2)[34],

$$L_p = 10\, log \frac{p^2}{p_0^2} \tag{2}$$

Where, L_p is the sound pressure level [dB], p is the effective sound pressure [Pa], p_0 is the pressure of the hearing threshold which is 2.10^-5 [Pa].

After hitting the surface, a sound wave is reflected unless the surface absorbs the entire sound energy. In this case, sound from the source to the receiver has two components, direct and reflected sound (echo) can be seen in Figure 12.

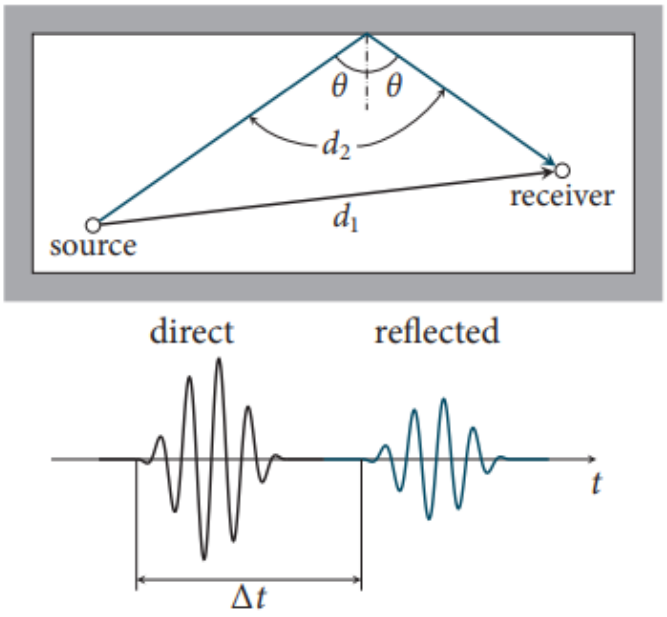

Figure 12 Direct and reflected sound in the closed field, retrieved from[35]

Because the reflected path d2 is larger than the direct sound path d1, a time delay of Δt occurs at the receiver [35]. This delay in combination with absorption from the surface leads to a smaller intensity of reflected sound. However, there are multiple reflections in a close field, which leads to a relatively constant sound pressure level and is identified as

a diffuse sound field [35]. Therefore, to calculate sound pressure level, direct sound and diffuse field are added and given by the Sabine-Franklin-Jaeger theory[36]

$$L_p = L_W + 10\log\left(\left(\frac{Q}{4\pi r^2}\right) + \left(\frac{4(1-\alpha)}{A}\right)\right) \quad (3)$$

In which, L_p is sound pressure level at receiver in [dB], L_W represents the sound power level of the source [dB], r is the distance to the source [m], A is the total absorption in a room [m^2 Sabine], α is the average absorption coefficient, Q is the directionality of the source.

According to Sabine-Franklin-Jaeger's theory, sound pressure level reaches a constant level far from the source, however, in reality, the sound keeps decreasing away from the source. Therefore, M. Barron added a correction to equation (3), which considers the reduction of a reverberant field with the distance [36], thus the equation becomes,

$$L_p = L_W + 10\log\left(\left(\frac{Q}{4\pi r^2}\right) + \left(\frac{4(1-\alpha)^{\frac{r}{mfp}}}{A}\right)\right) \quad (4)$$

Where V is a volume of space [m3], S is the total surface area [m2] and $mfp = \frac{4V}{S}$

The sound pressure levels in the free field depend on the characteristics of the source. In general, the distinction is made between a point source and a line source. In the case of a point source like a speaker, sound energy expands spherically while from a line source (traffic noise) the sound propagates cylindrically [34]. When the distance between sound and source increases, the sound energy produced by the source spread over a larger area, thus sound pressure level is lower at the receiver [37]. The sound pressure level as a function of distance is given by equation (5) for the point source and equation (6) for the line source. To put into perspective, sound pressure level is inversely proportional to the squared distance for the point source (decreases 6 dB for doubled the distance). And for line source, it is inversely proportional to the distance between source and receiver (decreases 3 dB for doubled the distance) [37].

$$L_p = L_{p0} - |20\log(r)| \quad (5)$$

$$L_p = L_{p0} - |10\log(r)| \quad (6)$$

Where, L_p is sound pressure level at the receiver [dB], L_{p0} is sound pressure level at 1m distance from the source [dB], and r is the distance between source and receiver [m].

Due to the logarithmic scale, multiple sound pressure levels cannot be added directly and therefore, the following equation is used to add multiple sound pressure levels [34],

$$L_{p;tot} = 10log\left(10^{\frac{Lp1}{10}} + 10^{\frac{Lp2}{10}} + 10^{\frac{Lp3}{10}} + \cdots\right) \quad (7)$$

Here, $L_{p;tot}$ represents the resulting sound pressure level [dB], L_{p1} is the sound pressure level of source 1 [dB] and L_{p2} is sound pressure level of source 2 [dB] etc. Therefore, when two equal (independent) sound pressures are added the resultant increase in sound pressure level is 3 dB.

2.1.2 Sound perception

The human ear can perceive sound in scales from 0 to 140 dB and can only hear frequencies between 20- 20000Hz. Each frequency has its own sensitivity [34]. For example, a sound of 105 dB with a frequency of 20 Hz is perceived as similar to the sound with 50 dB with 1000 Hz frequency (see Figure 13). Therefore, while evaluating the sound spectrum, the sensitivity of the ear to each octave band is considered and represented in a single (A-weighted) measurement expressed in dB(A)[35]. Table 1, represent A-weighting attenuation and amplification values in dB for the octave band.

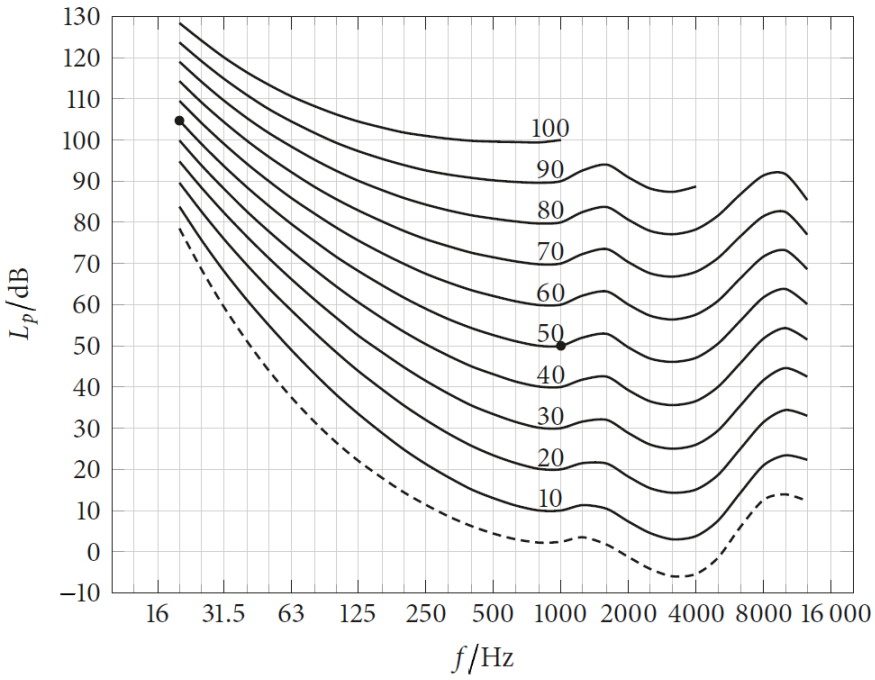

Figure 13 ISO equal-loudness contours for different frequency values, retrieved from[38]

Frequency [hz]	62.5	125	250	500	1000	2000	4000	8000
A-weighting [dB]	-26.2	-16.1	-8.6	-3.2	0	1.2	1	-1.1

Table 1 A-weighting correction for octave frequency band

However, in the case of sound pressure levels which vary over a time period for example motorway, a simple A-weighted measurement is not sufficient. Therefore, the equivalent sound pressure level (Leq) is given (equation (8)) to represent the sound that varies over a time period [34].

$$L_{eq} = 10 \log\left(\frac{1}{T}.\int \frac{p_t^2}{p_0^2}.dt\right) \quad (8)$$

Here, L_{eq} is the equivalent sound pressure level in dB or dB (A), *T* is exposure time [s], Pt represents the effective sound pressure during the exposure time [Pa] and P0 stands for the reference sound pressure in [Pa]. In addition to the frequencies and period, the time of exposure is also important but will be explained in detail in the following sections.

2.2 Urban Noise

Although urban noise includes sources like railways, airports, industrial sites, and sound created by human activities, the most influential source is road traffic. Therefore, this chapter will explain the characteristics of road traffic noise along with its effect on health and regulations taken by different governing bodies.

2.2.1 Traffic noise

Road traffic noise is defined as collective sound energy emitted from motor vehicles (cars, busses, lorries, motorcycles etc.) [39] This collective sound energy is produced by the vehicle's own characteristics, tire-road contact, and airflow around the vehicle. The aerodynamic noise (airflow around the vehicle) is generally not taken into account because it is only dominating for a vehicle travelling at a speed above 100 km/h [40].

The vehicle characteristics that influence the noise are engine, powertrain, air intake, and exhaust system [40]. Due to improvements in the automobile sector, engine and exhaust noise have significantly reduced. Also, considering the future scenario of electric vehicles, the noise pollution will be less when compared to vehicles with a combustion engine. However, if we consider the speed of vehicles above 50 km/h, both the improvements in the combustion engine and electric vehicle are not much of relevant as the noise is mainly dominated by contact between tire and road [41]. Figure 14 shows the development of car noise over a time span of 33 years in which the road wheel noise remains at a constant level.

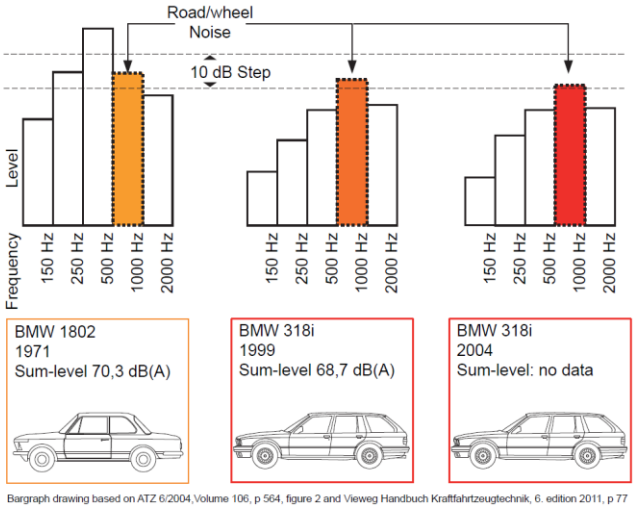

Figure 14- Development of road wheel noise between a 1971 model, a 1999 model and 2004 model, retrieved from [42]

In addition to the characteristics of a vehicle, traffic noise is also affected by traffic parameters like speed, density, traffic fluidity (traffic lights, one-way street) and type of vehicle. A traffic density of 2000 vehicles per hour produces twice the noise as 200 vehicles per hour [41] and with 50 vehicles/hour, a rise of 3-5 dB is noted when the speed is doubled [43]. Also, accelerating vehicles at signals can generate a noise that can be 15-20 dB(A) higher than the normal speed vehicles [43].

Mainly, traffic noise is represented in $L_{A,\,eq}$ (equivalent A-weighted sound pressure level (SPL)). However, spectral differences in road traffic noise are also important because the effect of noise reducers like noise barriers, road surfaces and absorption coefficient of façades are usually given in terms of an emitted spectrum. Current noise emission models like FHWA [44], the CoRTN model [45], the RLS90 model [46], CNOSSOS-EU [47] etc. calculates the equivalent sound pressure level based on vehicle type, driving speed, traffic volume and other flow parameters [48]. Figure 15 shows the A-weighted sound pressure levels for different types of vehicles for varying speeds.

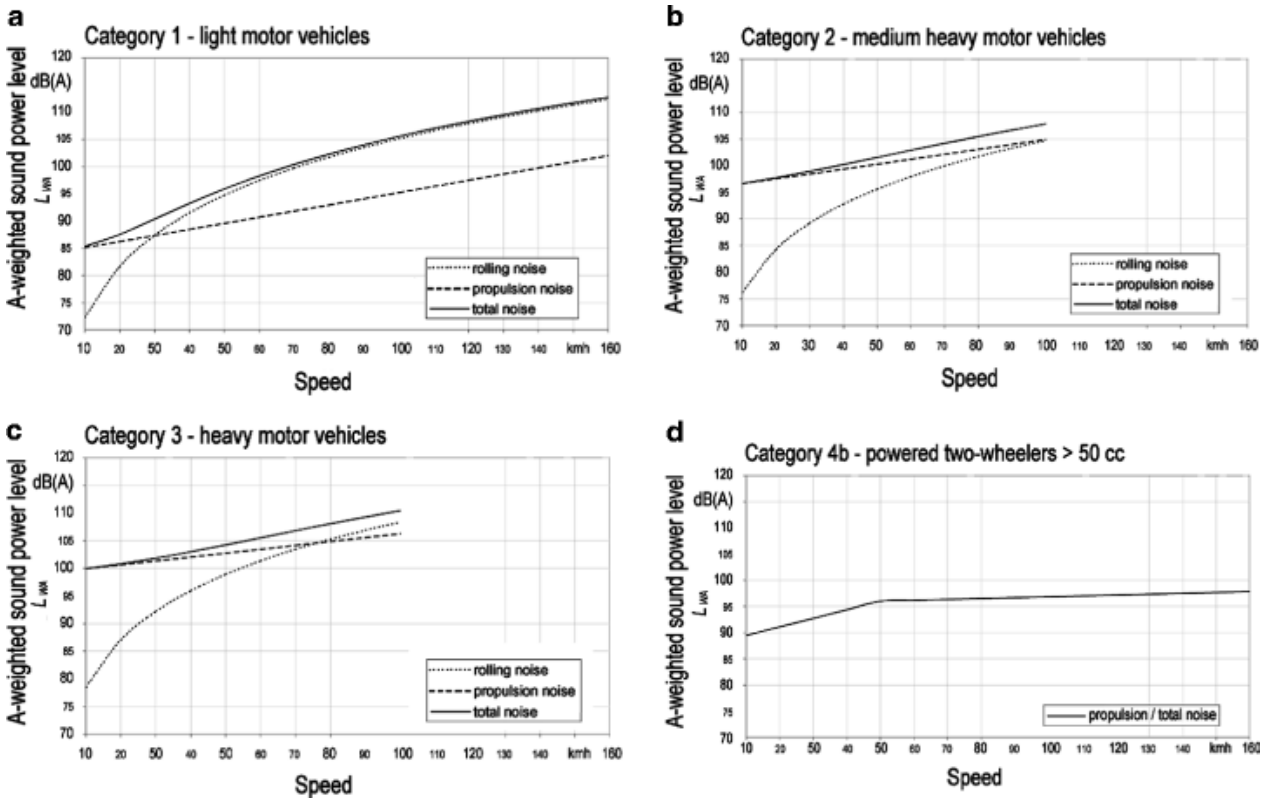

Figure 15 A-weighted sound pressure levels for a different type of vehicle and speed [49]

2.2.2 Health Effects

As mentioned earlier, environmental noise is one of the growing concerns due to its adverse effect on health. Environmental noise in Europe 2020 [50], estimated that around 84.3 million people will be exposed to road traffic noise above 55 dB (L_{den}) at the end of 2030. The adverse health effects of noise are mostly categorized in terms of annoyance, sleep disturbance, cardiovascular diseases, cognitive impairment and mental stress [4], [6].

The most common problem created by noise is annoyance. At a noise level of 55 dB(A), the previously set guideline by WHO, approximately 20% of those exposed are annoyed by traffic noise and some even experience annoyance at a level of 40 dB(A) and above[6]. Sleep disturbance is rated as the second most common problem and is mainly caused by traffic noise. The primary physiological effects induced by sleep disturbance can include immediate effects (e.g. arousal response, awakenings, body movements, blood pressure) after-effects (e.g. sleepiness, daytime performance) and long term effects (chronic sleep disturbance) [5].

In 2011, WHO published a report[1] where they introduced a single scale measure of disability-adjusted life years (DALY's), as the healthy years lost due to environmental

noise. The report estimated that in western Europe countries is equivalent to 61000 years for ischemic heart disease, 45000 years of cognitive impairment in children and 22000 years for tinnitus [1]. Therefore, WHO provide specific guidelines for environmental noise which are presented in the next section.

2.2.3 Regulations

The main objective of the regulations and guidelines is to protect human health from environmental noise. Although, the WHO provides guidelines against environmental noise, every country has its own regulations developed from studies on noise to healthy relationships and various policymaking. While defining the values, different aspects like type of noise source, the time of the day, type of development (new or existing), area type and sensitivity of the receiver are considered [50]. Given the context of the research, the only regulations for traffic noise are presented.

Many national legislations are based on (L_{day}) and (L_{night}) limit values, where L_{day} and L_{night} are A- weighted average during the day and night hours respectively [50]. On the other side, Environmental Noise Directive 2002/49/EC defines the limiting values based on the weighted average during the day-evening-night (L_{den}) design to assess annoyance and night-time (L_{night}) to indicate sleep disturbance [51]. These values are calculated by equation (9), in which an evening weighing of 5 dB and a night weighing of 10 dB are applied since people are more sensitive to the noise in those periods [51].

$$L_{den} = 10\,log\frac{1}{24}\left(12 * 10^{\frac{L_{day}}{10}} + 4 * 10^{\frac{L_{evening}+5}{10}} + 8 * 10^{\frac{L_{day}+10}{10}}\right) \quad (9)$$

In which,

L_{day} is the equivalent A-weighted average sound level determined over all day periods of a year (07:00 to 19:00)

$L_{evening}$ is the equivalent A-weighted average sound level determined overall evening periods of a year (19:00 to 23:00)

L_{night} is the equivalent A-weighted average sound level determined overall night periods of a year (23:00 to 07:00)

For average noise exposure, the WHO guidelines for Europe [52] strongly recommend noise levels produced by road traffic should be below 53 dB (L_{den}) and for nighttime exposure, the recommended values are below 45 dB (L_{night}), as road traffic noise above these levels is associated with adverse health effects [52].

In the Netherlands, the Noise Abatement Act states that the preferred value of sound for new homes should be less than 48 dB [53]. Under certain conditions (depending on the sensitivity of the area) the competent authority can set higher values. For inner-city areas, the maximum permitted noise level is set to 63 dB [53]. An overview of guidelines can be seen in Table 2.

Guideline	Standard value [dB]	Limit value [dB]
WHO (European region)	53	65
Noise abatement act (Netherlands)	48	63

Table 2 Noise exposure limits in Europe and Netherlands.

This means construction of new homes is not allowed if noise levels are above 63 dB and if the sound level is above 48 dB extra measures have to be taken to protect the noise going inside. According to article 110g of the Noise abatement act [53] for inner-city roads, a deduction of 5dB can be applied.

Mapping the noise levels offer little guidance regarding the health of the general public. Therefore, the GES method is developed by the GGD (municipal corporations in the Netherlands) to show which residents are exposed to which concentrations or noise levels [54]. Table 3 gives an overview of noise levels, GES scores and associated environmental health quality. Here, a new parameter L_{etm} is introduced which represents the highest sound level calculated over the day.

GES-Score	Environmental health quality	Noise level	
		L_{den} (dB(A))	L_{etm} L_{den} (dB(A))
0	Very good	<43	<45
1	Good	43-47	45-49
2	Reasonable/fair	48-52	50-54
3	Fairly moderate		
4	Moderate	53-57	55-59
5	Very moderate	58-62	60-64
6	Insufficient	63-67	65-69
7	More than insufficient	68-72	70-74
8	Very insufficient	>73	>75

Table 3 GES classification for traffic noise [54]

2.3 Atmospheric Effects

As discussed in earlier chapters, sound propagation depends on the medium, therefore, fluctuations in the medium can influence the path and the sound energy [55], [56]. The atmosphere is a complex medium for sound propagation because it is comprised of different layers with varying temperatures and wind speeds [55], [56]. Sound propagation is not only affected by the mean wind and atmosphere but also fluctuations of wind and temperature referred to as atmospheric turbulence [55]. Majorly three phenomena affect sound propagation in the atmosphere: atmospheric absorption, refraction by mean wind or temperature profiles, and scattering from atmospheric turbulence.

Sound absorptions occur due to fluctuations in temperature and humidity. These changes affect the viscosity of air and change the structure of gas molecules in the air [57]. Generally, the atmospheric absorption is given in terms of sound absorption factors (dB/m) which is a function of frequency, temperature and humidity (please see Appendix-A for the table). Atmospheric absorption plays a very important role when the distance between source and receiver is more and more often, and acoustic simulation software accounts for this effect.

Two media with different properties separates the sound wave at the interface of both media [57]. This separation results in the change of direction in a sound wave, known as atmospheric refraction [58]. When the distance between source and receiver is less than 100m in an open area, atmospheric refraction can be ignored [59]. However, for distances more than 100m, atmospheric refraction has a large effect on sound pressure levels, especially close to the ground [58]. The direction at which the ray will be diffracted is based on the temperature profile as well as the direction of the wind, which is itself a complex phenomenon. Therefore, most often, atmospheric refraction is excluded or approximated in acoustic simulations.

In the atmospheric absorption and refraction, the assumption is made that the vertical profiles of the temperature and the wind are constant over a period of time. However, on a time scale of seconds or minutes, wind and temperature profiles are hardly constant and show significant fluctuations [60]. These fluctuations are called atmospheric turbulence. Eddies generated due to the wind and temperature fluctuations carry the sound wave over a larger distance, thus resulting in higher sound pressure levels in the shadow region [60]. Atmospheric turbulence plays a very important role when the distance is greater and the source is located well above the ground, for example in the case of aircraft noise. Therefore, in traffic noise simulation they are of lesser significance [61]. All of these atmospheric factors, as well as their impact on sound transmission, are discussed in greater depth in Appendix A: Atmospheric effects on sound propagation.

2.4 Sound and Urban Context

When a sound wave propagates in an urban environment, it encounters different surfaces which influence its intensity and direction. As shown in Figure 16 the initial sound energy is absorbed, part of the energy is reflected, and the remaining sound energy is transmitted through the surface [62]. The degree to which this phenomenon happens depends on the acoustical properties of the surface and the angle of the incident [33]. The parameters commonly used to describe absorption, reflection, and transmission are often expressed in terms of respective coefficient ranges between 0 to 1. According to the law of conservation of energy, the sum of these three coefficients should be unity: $\alpha'+r+t=1$, where α', r and t represent absorption, reflection and transmission coefficients respectively.

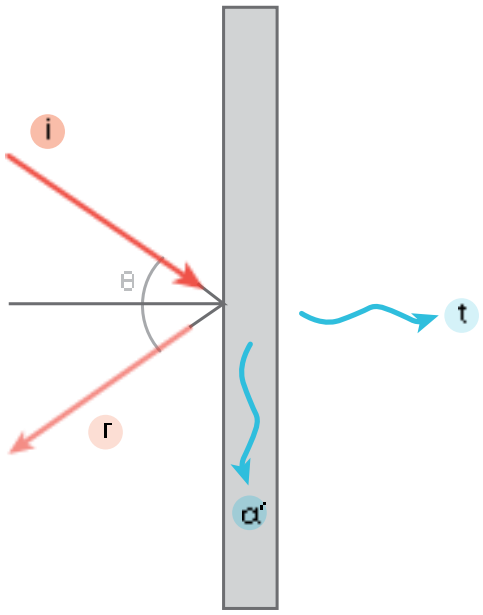

Figure 16 Three components of sound after interacting with a surface

2.4.1 Sound Absorption

Sound-absorbing materials are often used to decrease the sound pressure level in an urban environment. These materials convert the sound energy into thermal energy through the friction in the pores [56]. The successful implementation of these materials is determined by the material structures and the environment in which they are used [63].

The level of absorption can be expressed by the absorption coefficient, the impedance, or the flow resistivity [56]. Absorption coefficients represent the amount of energy that is either absorbed by the material or transmitted through the material, i.e. the energy

that doesn't return to the space as reflected energy. If the $\alpha > 0.5$, the material is considered a sound-absorbing material and if $\alpha < 0.2$, the material is often a reflecting material. Although the acoustic absorption coefficient is a common way to quantify absorption, it is dependent on the angle of incident and thus only suitable when the angle of incident is of lesser importance[64]. Therefore, when higher accuracy is required, flow resistivity is used which also determines the efficiency of the sound-absorbing material[4].

Flow resistivity is defined as the level of resistance air encounters when it moves through the material [56]. When airflow resistivity is high, fewer sound waves can enter the material. However, reducing the airflow resistivity leads to less transformation efficiency from sound energy to heat [63]. The porosity of the material also plays an important role in the amount of absorption. Increasing the porosity causes higher absorption coefficients as it results in more reflection of sound waves which leads to more friction and energy loss [4].

Moreover, sound absorption by the material is also influenced by the incident wave frequency. Lower frequencies have a higher wavelength, so less sound energy is absorbed when they interact with pore walls. On the other hand, higher frequencies with lower wavelengths collide more often with the pore and result in higher energy loss [63]. Therefore, different solutions are adopted based on the function of the space.

2.4.1.1 Types of sound absorbers:

Sound absorbers are broadly classified according to their working mechanism: friction and resonance. Porous and fibrous materials use the friction principle where compression and rarefaction of air molecules are restrained to convert sound energy into heat. Although their absorption coefficient increases with increasing frequency, they cover broadband frequency and therefore most commonly used in acoustics solutions [63]. The effectiveness of the porous absorber is influenced by the thickness, fibre orientation, and density [63]. Figure 17 and Figure 18 shows different porous absorbers along with their effectiveness in a frequency band.

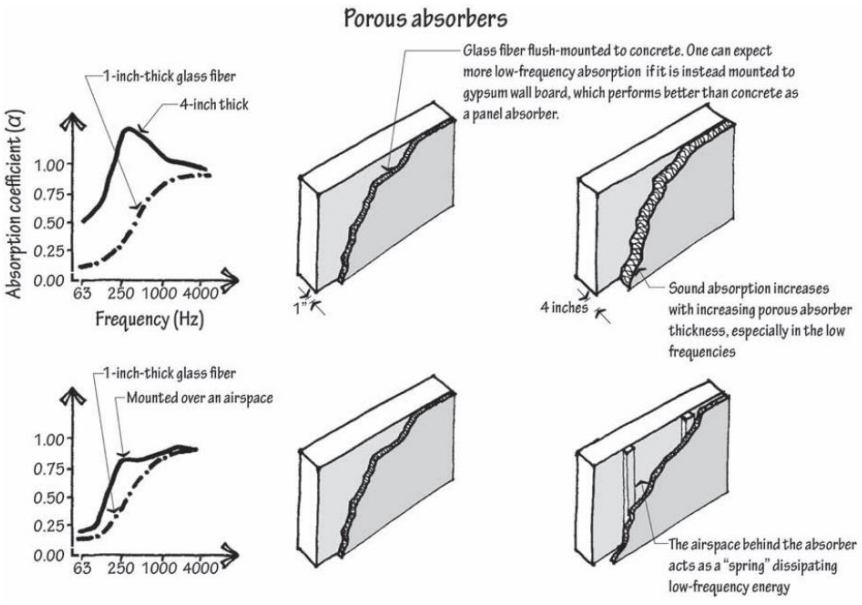

Figure 17 Porous Absorbers applied on wall with their effective frequency spectrum, retrieved from [63]

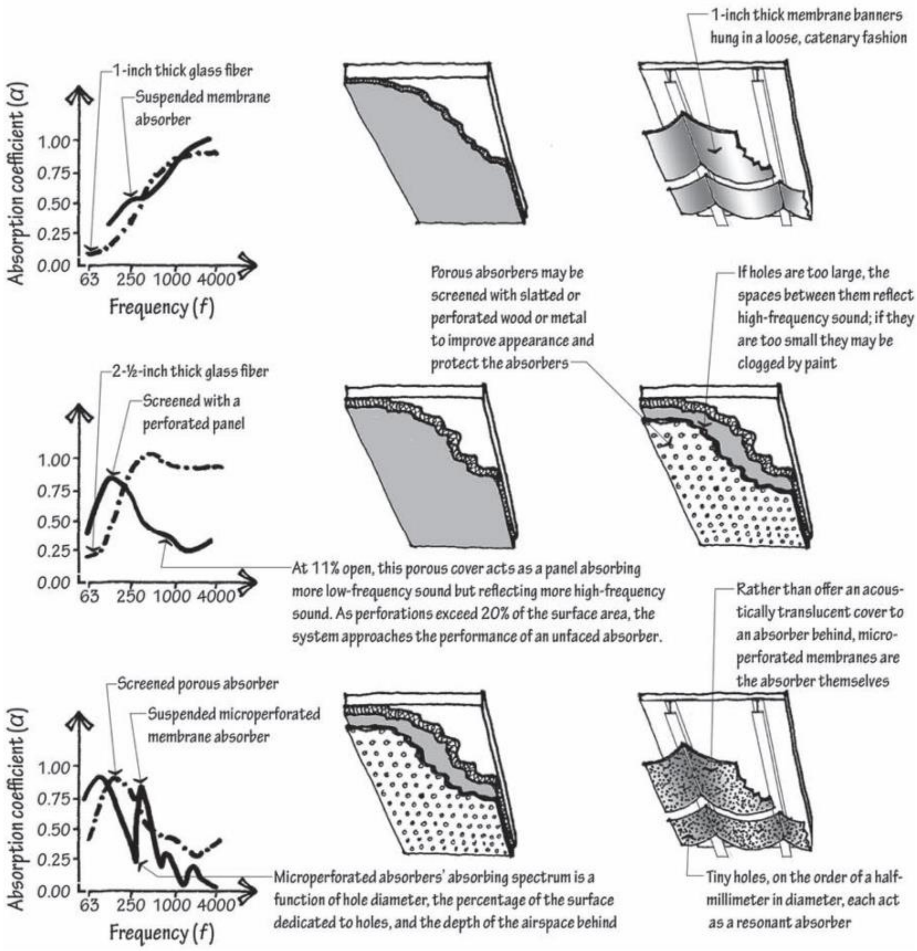

Figure 18 Porous Absorbers applied on the ceiling with their effective frequency spectrum, retrieved from [63]

Panel and resonant absorber work on the principle of resonance where the natural frequency of the material is tuned up according to incident sound frequency. These types of absorbers are more effective in narrow bands, as can be seen in Figure 19 and therefore used primarily in specialized applications [62]. By altering the absorber's mass, stiffness and geometry, panel and resonant absorbers can be tuned to increase their effectiveness in a particular frequency band. Due to the effectiveness of panel absorbers in the lower frequency range, they are used in combination with porous absorbers in a room like recording studios [62].

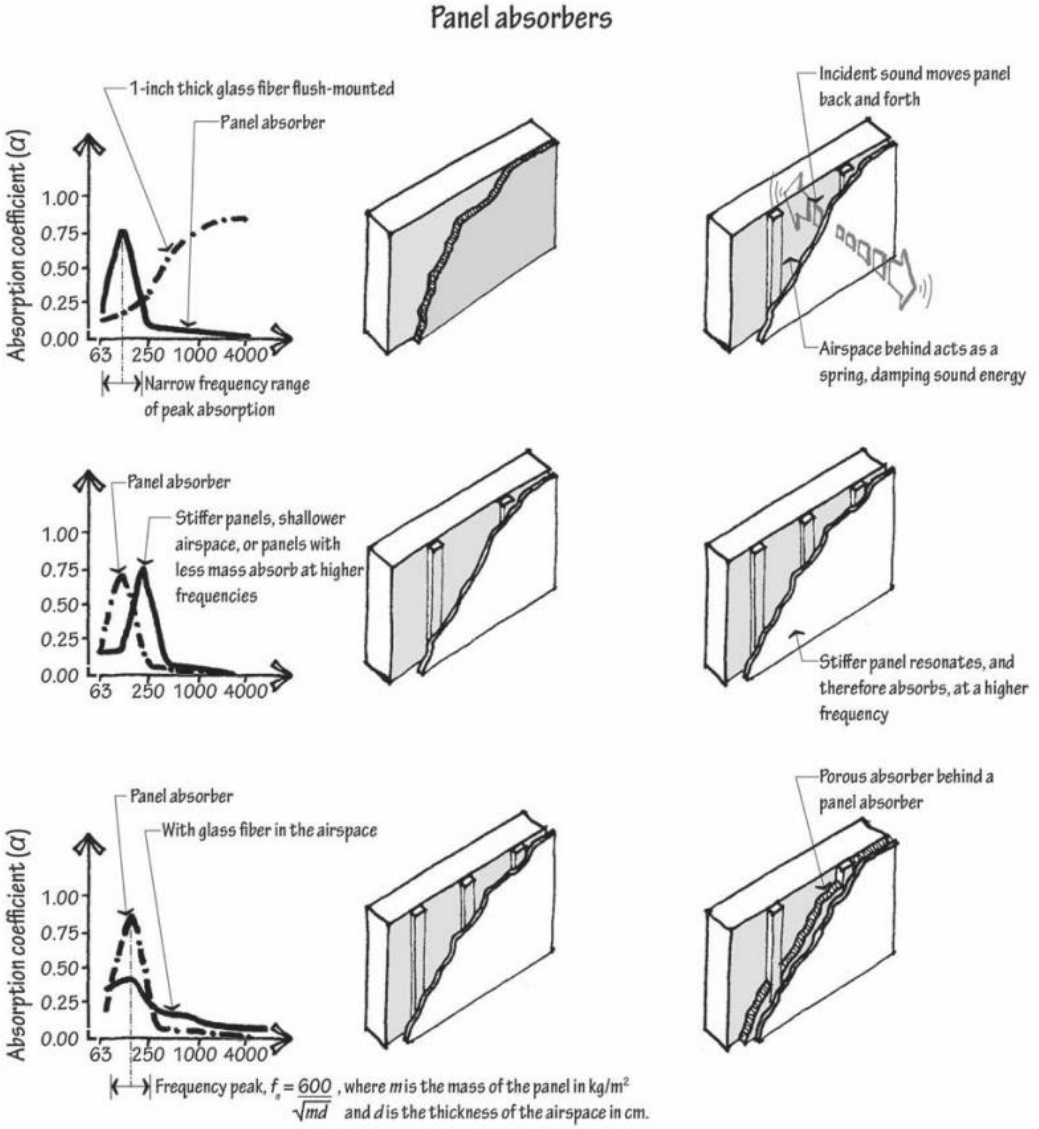

Figure 19 Panel Absorbers applied with their effective frequency spectrum, retrieved from [63]

2.4.2 Sound Reflection

As previously mentioned, when a sound wave hits a surface, part of the sound energy is reflected unless the surface absorbs sound energy entirely. In this case, the angle of reflection is taken as the angle of incident. If there is no barrier between source and receiver, the reflected wave always reaches the receiver after the direct wave [56]. However, sound sources often consist of multiple impulses. When the phase of a direct sound wave and the indirect (reflected) sound wave are the same, they will amplify each other. This condition, where the resultant sound wave has a higher amplitude than the original wave, is called constructive interference. On contrary, when direct and reflected waves move in opposite phases, they can cancel the sound level that reaches the receiver. This reduction in the sound wave is known as a destructive interface. Both the phenomena are explained in Figure 20 and Figure 21 respectively.

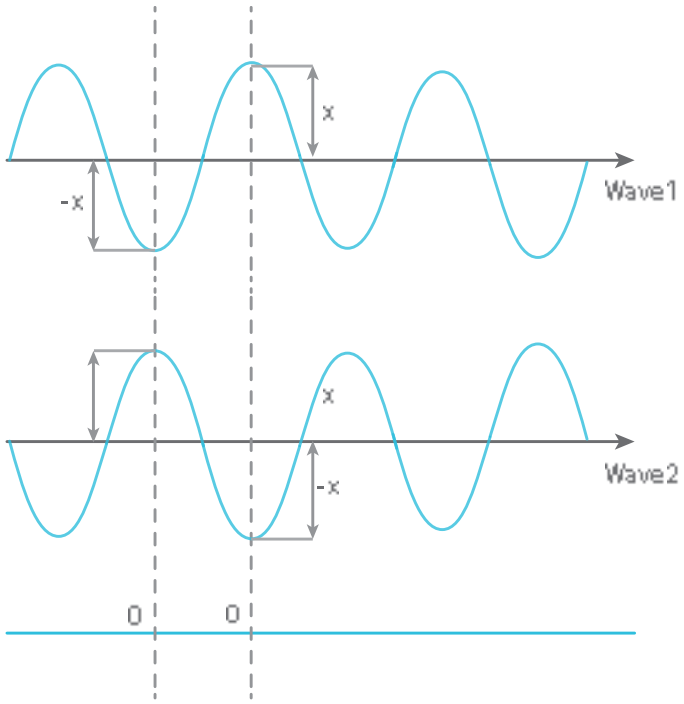

Figure 20 Example of destructive interference (own illustration)

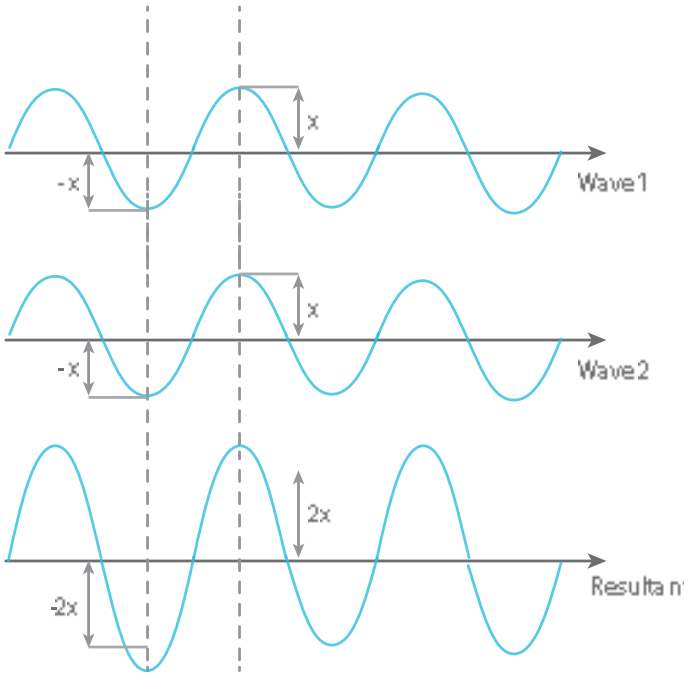

Figure 21 Example of constructive interference (own illustration)

In an urban environment, constructive and destructive interference frequently occur when both source and receiver are closer to the ground which is referred as the ground effect [61]. This effect is a function of the frequency and length of sound paths. For example in Figure 22, R1 is the direct sound path and R2 is a ground-reflected path, then the first minimum (destructive interference) occurs when $k(R2 - R1) = \pi$, or $f = c/2(R2 - R1)$, where, $k = w/c$ and $k = 2\pi f$ (c being the speed of sound and f being the frequency) [61].

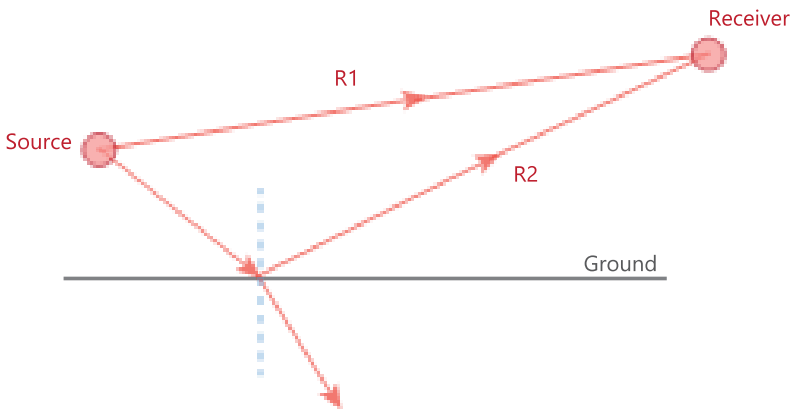

Figure 22 Sound propagation from a point source to receiver above the ground surface, (own illustration based on [61])

2.4.3 Sound Scattering

Sound scattering takes place when the surface is not smooth or contains some elements which have a size equal to the incident sound wavelength. Scattering reduces the sound intensity while it increases the area influenced by the sound. For wavelength much larger than the dimensions, i.e. for lower frequencies, the sound is reflected as if the surface would be flat [16]. While in the case of irregulars with a dimension greater than the wavelength, the reflection is specular, see Figure 23.

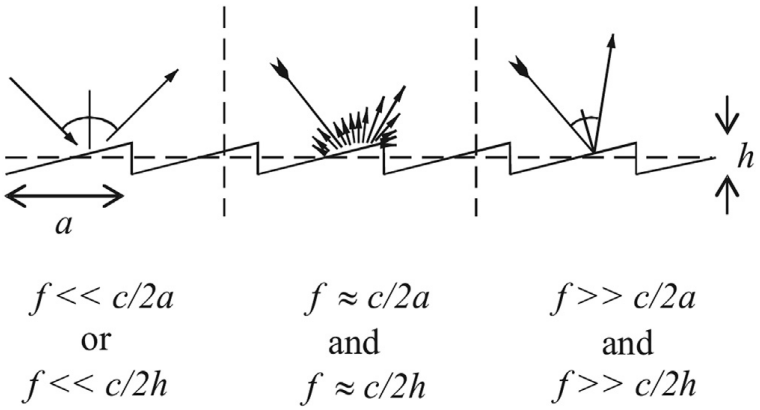

Figure 23 Influence of irregulars with distance 'a' and roughness depth 'h' on the direction of reflected sound waves[65]

Therefore, in general, the total reflected sound energy is divided into two parts; one containing specular reflection and the other with diffuse part, see Figure 24.

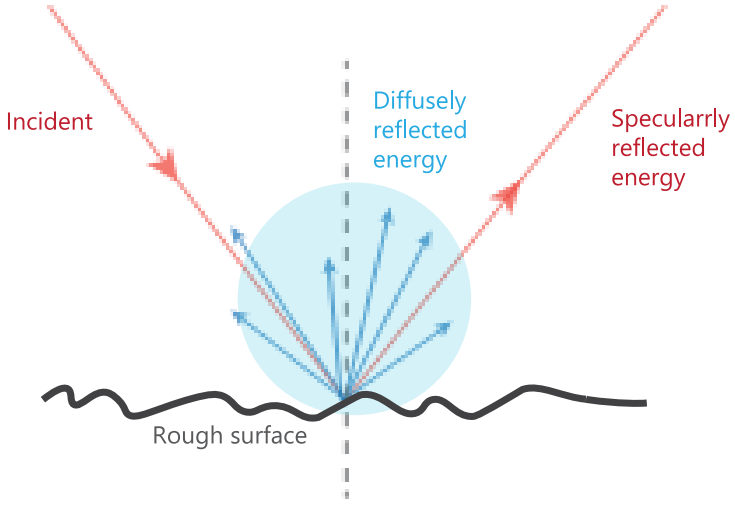

Figure 24 Specular reflection vs diffuse reflection

The diffuse reflection is independent of the angle of incident and given by Lambert's cosine law,

$$I(r) = I_0 \mathrm{d}S \frac{\cos\vartheta \cos\vartheta_0}{\pi r^2} \quad (10)$$

Where, $I(r)$ is the intensity of sound which is scattered in the direction given by angle ϑ, measured at a distance r from $\mathrm{d}S$, and ϑ_0 represent the angle made by incident ray with wall normal.

2.4.4 Sound Diffraction

The phenomenon in which sound waves bend around the edge of an object is known as diffraction of sound [8]. Realistically, this means sound still reaches behind the object, thus reducing the effect of the noise barrier. The ratio between frequency and the size of the object has a large influence on the amount of diffraction [8]. The diffraction is more pronounced with a low frequency that has a larger wavelength, while higher frequency sound does not diffract due to their short wavelength [67]. Moreover, greater diffraction angles also lead to more energy loss.

To calculate edge diffraction, several models have been developed. Sound diffraction can be considered similar to the diffraction of light and was first explained by Fresnel [68]. He used a wave propagation model put forth by Huygens in 1690 which imagines that each point on a wavefront serves as a new source of a wave with the same frequency and speed as the original wave [68]. Ultimately, the Huygens-Fresnel principle turns out to be an inspiration and led to the establishment of the geometrical theory of diffraction (GTD) [68] and its extension, the Uniform Theory of Diffraction (UTD)[69]

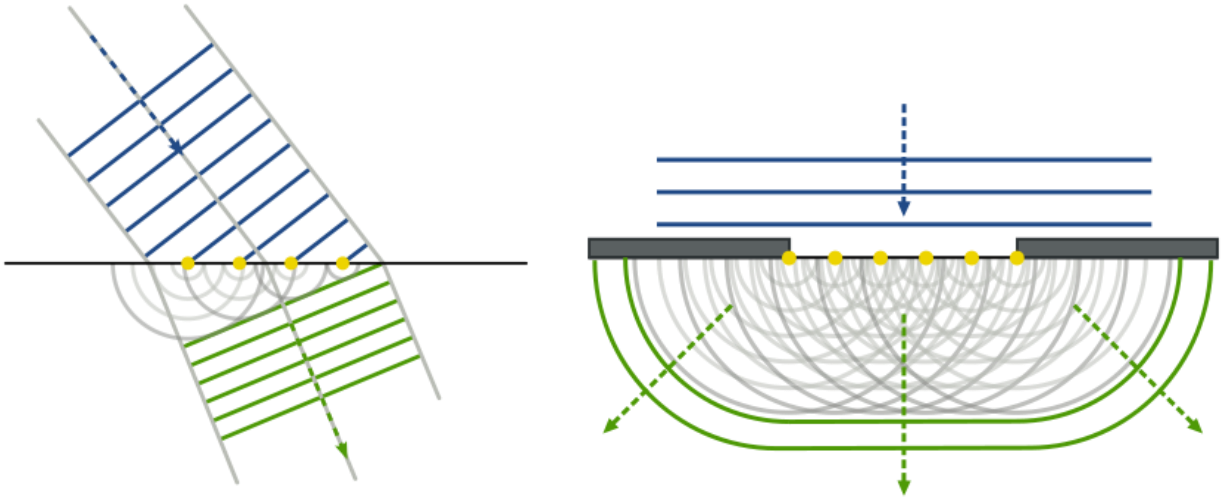

Figure 25 Illustration of the Huygens-Fresnel principle showing the gradual propagation of a plane wave through the excitation of secondary waves[70]

UTD applies to infinite-length wedges with rigid or pressure release surfaces [71], it is reasonably fast to compute for each diffraction path and it can approximate the amplitude response with reduced computation [72]. However, it has a limitation to computing lower frequencies when the source or receiver is close to the surface [72] and may only work well for a large model in outdoor scenes.

Another such model used in geometrical acoustics is given by Biot-Tolstoy-Medwin (BTM) [73]. BTM is theoretically superior which models diffraction around a finite edge in terms of many virtual points sources located along the edge. As a result, not only the shortest path over the edge is considered, but also paths that require a longer detour [69]. However, due to the numerical complication, BTM is more computationally intensive [72], [73].

Among all, the method given by Maekawa [74] is probably the simplest method for computing diffraction. It is an empirically based detour method that has gained a lot of attention, notably for noise emission predictions. Maekawa's approach calculates a transmission loss which is based on the wavelength and the height of an object [69]. This excess attenuation is given as ΔL, see equation 21. Other important details of the wedge, like the inner edge angle, wedge length and crossing angle of the shortest path, are overlooked [69].

$$\Delta L = L_0 - L_b = \Delta L_U - 10\log\left(1 + \frac{N_U}{N_1} + \frac{N_U}{N_2}\right) \tag{11}$$

Here, L_0 represent the sound pressure level without barrier while L_b gives pressure level with a barrier. The non-dimensional Fresnel number is given by N_U for the upper edge and N_1 and N_2 for two side edges. The excess attenuation resulting from only the upper edge is given by equation 22 and the Fresnel number is given by equation 23:

$$\Delta L_U = 10\log\left(3 + 20N_U\right) \tag{12}$$

$$N_i = \frac{2(s_2 - s_1)}{\lambda} \tag{13}$$

In which, s_1 and s_2 are the length of direct sound path and length of diffracted sound path respectively.

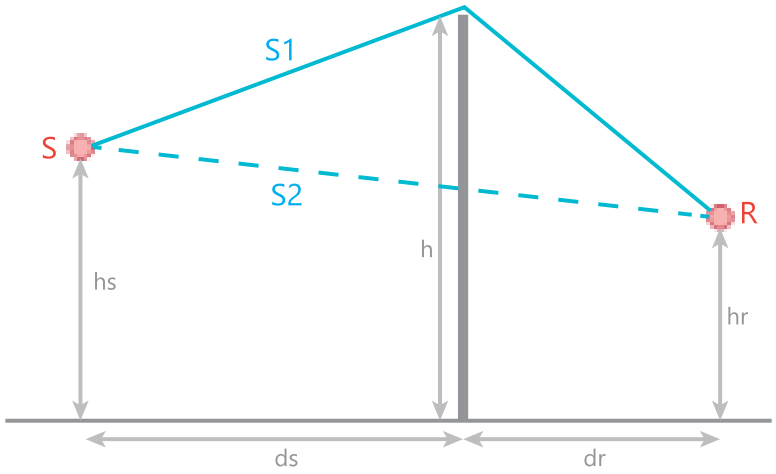

Figure 26 Source and receiver position with respect to the barrier (Maekawa's principle)

Not only limited point source, but Maekawa's theory is also further extended to calculate the excess authentication for a line source. This is given by different Fresnel numbers (see Table 4)[75]

Fresnel-Number	Reduction at line source	Reduction at point source
$N_f \leq -0.3$	0	
$-0.3 \leq N_f < 0$	$52 * (N_f + 0.3)^2$	$56 * (N_f + 0.3)^2$
$0 \leq N_f < 1$	$4.68 + 5.4\sqrt{N_f}$	$5.04 + 8\sqrt{N_f}$
$N_f \geq 1$	$10.08 + 8\log(N_f)$	$13.04 + 10\log(N_f)$

Table 4 sound reduction of an infinite long barrier given by Maekawa in dB(A) [75]

2.4.5 Street Canyon

When city streets are flanked on both sides by buildings, as in the case of many European cities, a canyon-like environment is created, which is commonly described as "Urban Street Canyon" [70]. In figure 27, an aerial photograph of the Riverenbuurt neighbourhood from South Amsterdam, shows a typical configuration, with straight streets and 3-4 floor buildings surrounding the streets. These canyons can alter local environmental conditions like temperature, wind, and air quality [70] but also affect the propagation of noise.

Figure 27 Aerial view of Reivernbuurt neighbourhood, South Amsterdam, source: Google earth

In an ideal cityscape, sound sources such as vehicles, public transportation, social events, pedestrians etc. are reflected by the building fronts, generating the "street canyon" effect. This phenomenon is influenced by the geometry as well as the materiality of the street. For example, an increased building height/street width ratio magnifies this effect, forcing soundwaves to be reflected multiple times before escaping the urban canyon, resulting in a rise in sound pressure level within the street [76].

The sound absorption and scattered reflection from the building surfaces also have a great impact [77]. Ground surfaces, such as road pavements and footpaths, are typically made of hard materials and thus contribute little to sound absorption or diffusion [78]. Lastly, the sky acts as a perfect absorbent surface, allowing soundwaves to escape the canyon when directed toward it [77], [78].

As mentioned earlier, when a soundwave hits a surface, a portion of the energy is absorbed, reflected, or scattered, thus the sound field in a street canyon is somewhere between the diffusing and geometrically reflecting [79]. Kang compared these street canyons with diffusely and geometrically reflecting boundaries using radiosity and image source methods respectively [79]. He investigated the effect of sound attenuation along the length and cross-section of the street, as well as the effect of building height and width. He concluded that it is better to design the street boundaries as diffusely reflective rather than geometrically reflective [79].

To account for both specular and diffuse reflection, Hiroshi Onaga combined the two approaches utilized by Kang [78]. The study focuses on the materials used on facades, examining different combinations of scattering coefficients (0-1) and absorption

coefficients (0-0.5). The findings reveal that scattering significantly decreases SPL at long distances from the source and a slight rise at close distances [78].

Moreover, Arnaud used a sound particle tracking code to mimic real-world street canyons, taking into account the scattering provided by buildings as well as street fixtures [80]. His findings are similar to Hiroshi's but go one step further by evaluating the street's H/W ratio in connection with the acoustical properties of the street (diffusion and absorption coefficients of façade and ground) [80].

2.4.5.1 Acoustic solutions for street canyon

In most cases, environmental noise issues are considered after the design process and preventive measures in terms of absorbing pavements or noise barriers are taken. On the other hand, the acoustician normally advises the client to improve the façade and window sound insulation as a solution to reduce the noise. However, the effectiveness of these solutions would be jeopardized by just opening the window [81]. Therefore, in the past few decades, many scholars have studied the architectural design approaches and façade alterations that could reduce noise in an urban context, which are reported below:

The general shape of the building:

Building façades are one of the largest elements in an urban environment, which increases the reverberation time and sound pressure level in the street [28][82]. Using the reflection principle, they can help to reduce the multiple reflections between buildings, reducing the sound pressure level [83]. Echevarria Sanchez et al. performed a study where she evaluated the impact of façade profiles with flat, stepped, convex, concave and inclined configurations. She found out that a flat upwardly inclined or concave façade is the most effective as it decreases the SPL by reflecting the sound upwards towards the sky [81]. The effectiveness is more noticeable when combined with material configurations [81].

Façade irregularities and diffusion:

Research like [78] [84] looks into the impact of façade extrusions on sound diffusion in the street. Judicael et al. [85] discovered that by considering diffusion with a relative surface area larger than 20%, significant sound attenuation can be obtained along the street. Further, Echevarria Sanchez et al. [81] considered triangular prominences with varied vertical and horizontal distances from the façade plane. She found that the noise decreases with increasing triangle size, furthermore, vertex position (down or up) also influences the sound pressure levels on the façade [81].

Improving absorption of façade:

Absorption is one of the best ways to reduce the overall noise level in a reverberant field like a street canyon and greatly studied in [78], [84], [85]. Hothersall et al. investigated

eight different applications of sound-absorbing material for a sound field near balconies along a tall building. It is found that treatment of the ceiling or the rear wall of the balcony is the most efficient location to apply sound-absorbing material, reducing 5 to 8 dB of traffic noise [32]. Considering the importance of quiet areas, Hornikx and Forssen [76] investigated different noise abatement schemes for shielded street canyons. The research concluded that the façade absorption is most effective when placed in the upper part of the canyon and can reduce noise up to 4 dB inside the courtyard [76].

Moreover, applying vegetation can be a very effective solution, since it provides both: effective absorption as well as the scattering of the sound. The impact of different vertical greenery systems is analysed in Ref [86]. The study reveals that the green systems can reduce up to 5-10 dB of sound in low to middle frequencies and 2-4 dB in higher frequencies. Van Renterghem et al. [87] analysed potential green wall systems, green roofs and vegetation on low screen barriers against traffic noise. His results are similar to [76] that greening of the upper storeys in the street and full façade inside the courtyard is the most efficient solution to protect the courtyards [87]. Moreover, these green measures are most useful when applied in combination rather than separately [87].

Width and position of façade opening (cross street opening):

Façade openings, especially which serve as the entrance to the quiet areas like a courtyard or urban parks influence the sound pressure levels inside quiet areas. Ref [88], [89] demonstrate the favourable impact of quiet urban areas as a mitigating approach. However, noise penetrates through the façade openings and reduces the effectiveness of these areas. Therefore, the location and width of such cross-street openings are investigated by Heutschi [90]. He found that the noise level increases with increasing the opening size and by reducing the distance between receiver and opening [90].

Balcony Geometry:

Semi-outdoor spaces like balconies or loggias are one of the important features of building design and they protect against direct exposure to traffic noise. Moreover, they act as diffusing elements in a street, and their presence and shape have been the topic of research in the past few decades. Although the balconies protect from direct noise, Tang [91] in his scale model study showed that their ceiling might lead to the amplification of noise. References [81][92][93] studied the effect of balcony depth and parapet form, presenting intriguing findings that architects and designers could consider.

Ultimately, El Dien et al. investigated the different combinations of balcony depth and ceiling angle on the sound field for a high-rise building façade [94]. He found that the maximum reduction occurs for balconies on higher floors with more than 2m depth [94], see Figure 28-Figure 30.

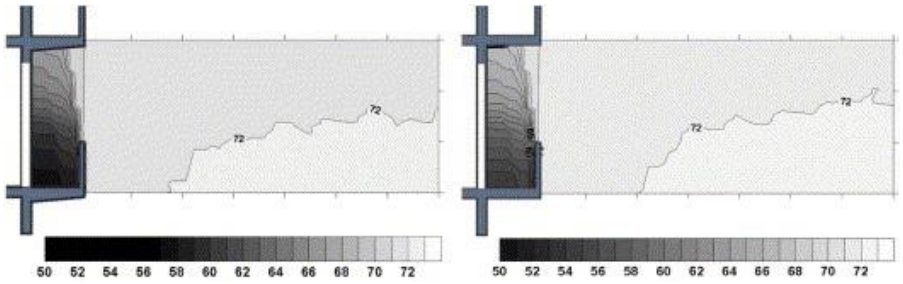

Figure 28 Balcony c/s for inclined ceiling 5° (left) and standard ceiling (right) with 1m depth at 16th floor[94]

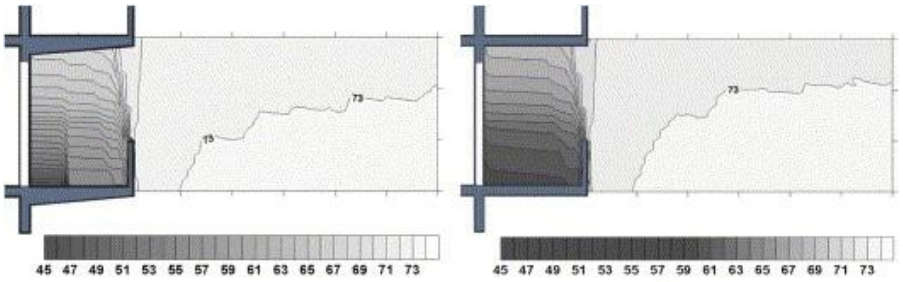

Figure 29 Balcony c/s for inclined ceiling 5° (left) and standard ceiling (right) with 2m depth on 13th floor[94]

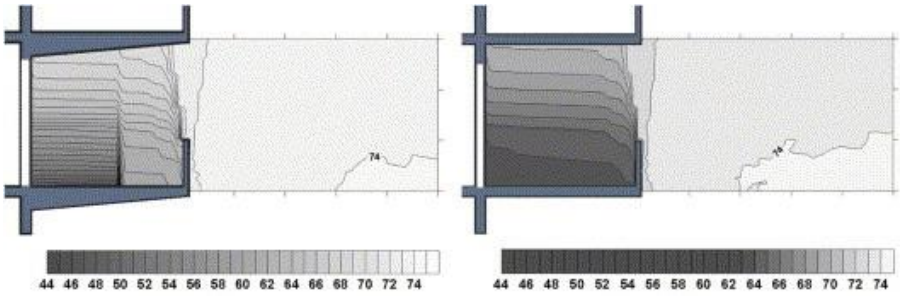

Figure 30 Balcony c/s for inclined ceiling 5° (left) and standard ceiling (right) with 3m depth at 11th floor[94]

2.5 Acoustic Simulation

2.5.1 Sound propagation methods:

In-room acoustics as well as in urban acoustics, various methods have been developed to simulate sound/noise. Acoustic simulations are broadly classified into two categories: wave-based approach and geometric acoustics (GA). An overview of these methods is given in Figure 31.

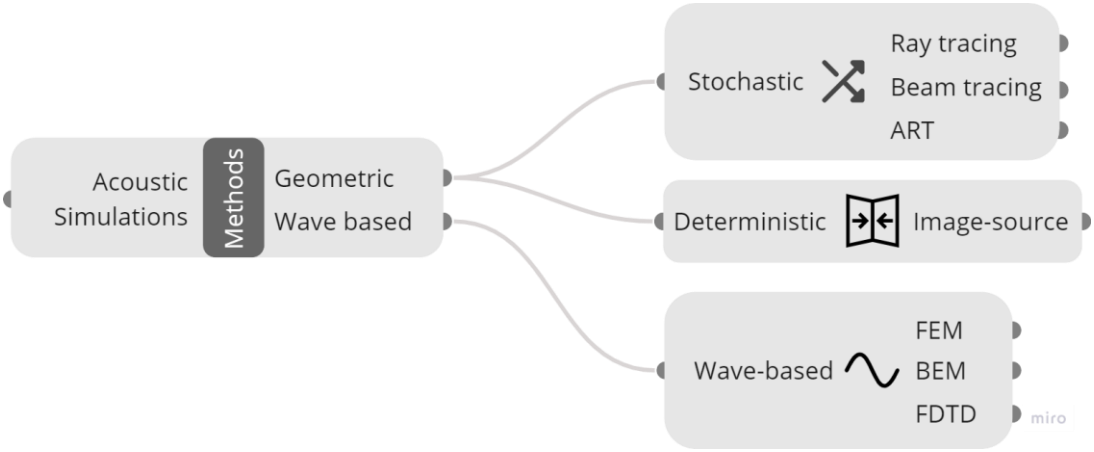

Figure 31 An overview of different acoustic simulation methods

Wave based methods replicate the actual behaviour of the sound wave in the design space, by solving the governing physical equations. These wave equations are derived from linearised Euler's equation and can include meteorological effects [16]. The wave approach is the most accurate way to predict sound since it can include source properties, geometrical data of urban topology, material properties and meteorological conditions [16]. On the contrary inclusion of all these parameters make this method time consuming and computationally- expensive, which increases with the highest frequency to be solved [16]. Due to advancements in computational power, the wave-based approach has been used by the scientific community to solve sound propagation in urban streets, cross-streets, squares, and courtyards [16]. Considering the complexity of the wave-based approach, references [95], [96] look into a simplified approach to model multiple reflections and sound propagation between adjacent streets.

Although wave-based methods are accurate, commercial acoustic simulation programs are usually based on a simplified method called Geometrical acoustics (GA). This approach is also known as Engineering methods, in which sound waves are approximated as sound rays or particles. These rays or particles behave similarly to the light ray with a well-defined direction of propagation, except for the propagation velocity [97]. This means, that in a free field the total energy carried by the ray remains constant unless and

until the medium itself does not cause any energy loss [97]. However, the general rule of spreading loss is still applicable to energy loss.

Even though all the tools based on geometrical acoustics can incorporate reflection and scattering, the transition of sound to another medium, as well as the refraction that goes with it, is generally not included [97][98]. This suggests that the effect of atmospheric conditions like turbulence and curvature of rays in a nonuniform medium is neglected. On the other side, the finite velocity of propagation is considered in many cases, since it affects important calculation parameters like reverberation time, echoes etc[97]. Likewise, many models can also incorporate atmospheric absorption, since it is calculated based on the distance travelled by the ray.

Furthermore, many geometrical simulation tools do not consider edge diffraction due to computational complexity [16], [97]. Therefore, GA methods are only applicable when object dimensions are larger than the wavelength of the sound [16][97][98], so approximately above 250 Hz in urban settings. Similarly, interference i.e. amplification and reduction of sound energy due to phase relationships are also excluded.

It goes without saying that geometrical acoustic methods can only reflect a portion of the acoustical events that occur in an urban environment. Despite that, GA models have been extensively used for noise mapping purposes [16]. Generally, noise maps are made at the macroscale (in km), however, they can be produced on microscale where accuracy of about 3dB is acceptable [16]. The following section explains the geometrical approach in detail.

2.5.2 Geometrical Acoustics

Geometrical room acoustics simulation produces time-energy and/or impulse response that can be used to compute various parameters like reverberation time, T60, clarity etc. Typical impulse response and time-energy response are illustrated in Figure 32.

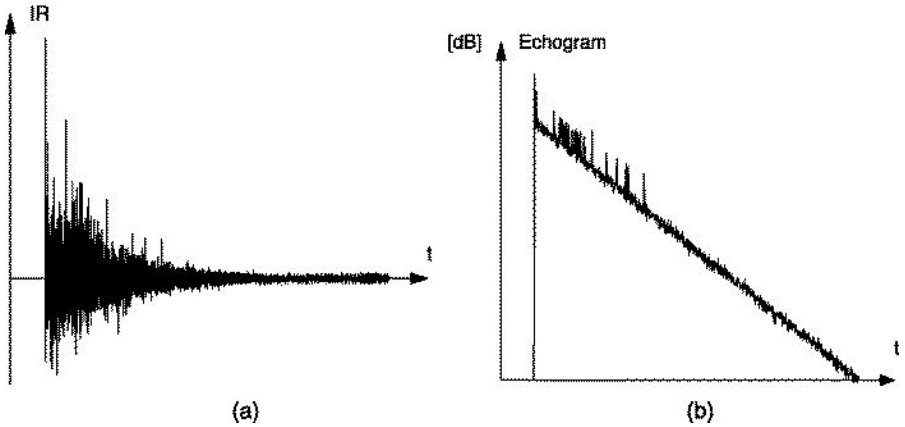

Figure 32 a) Impulse response and b) Time-energy response representing the propagation of sound energy [99]

Often, the time energy response is calculated first and then an impulse response is computed from the prior [99]. These types of responses consist of three parts: direct sound represented by the initial spike in Figure 32, then the later spikes show early reflection and finally the late reverberation.

To calculate the energy or/and impulse responses, various methods have been developed which are classified into two categories, stochastic approach and deterministic approach. The tools which use the stochastic approach simulate sound based on the statistical approximation, while the exact reflection path between source and receiver is calculated under the deterministic approach. The following sections give an overview of the image-source method (deterministic) and ray tracing (stochastic) approach.

2.5.2.1 Image source method:

The image source method was first developed in the field of electronics and later introduced in acoustics by Carslaw in 1899 [100]. However, the early stages have limitations over the infinite wedge and therefore, were first applied in room acoustics by Cremer in 1948 [101]. It represents the operating principle of all current deterministic approaches and provides an exact solution to the wave equation for a room with rigid walls [99].

The simulation is performed by creating virtual image sources, and by reflecting against all the surfaces in the model. To be valid, the line from the reflected source to each receiver must intersect the surface that served as the mirror. The first order path is completed by adding a second line segment from the intersection point to the original source (see Figure 33).

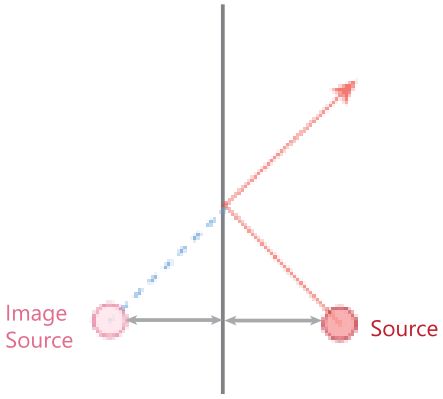

Figure 33 Concept of image source (own illustration)

Then the first order IS's are again reflected against all the surfaces and the process continues resulting in a set of image sources. For example, in Figure 34, S12 is an image source for a reflection that hit surface 1 and then surface 2. In the same way, we can find an image source S21. So, every image source is associated with an original source, a series of surfaces and a reflection order. This process ends when a predetermined

condition is reached, such as response length or reflection order [99]. At each reflection point, the specular reflection is reduced according to the absorption and scattering coefficient of the surface.

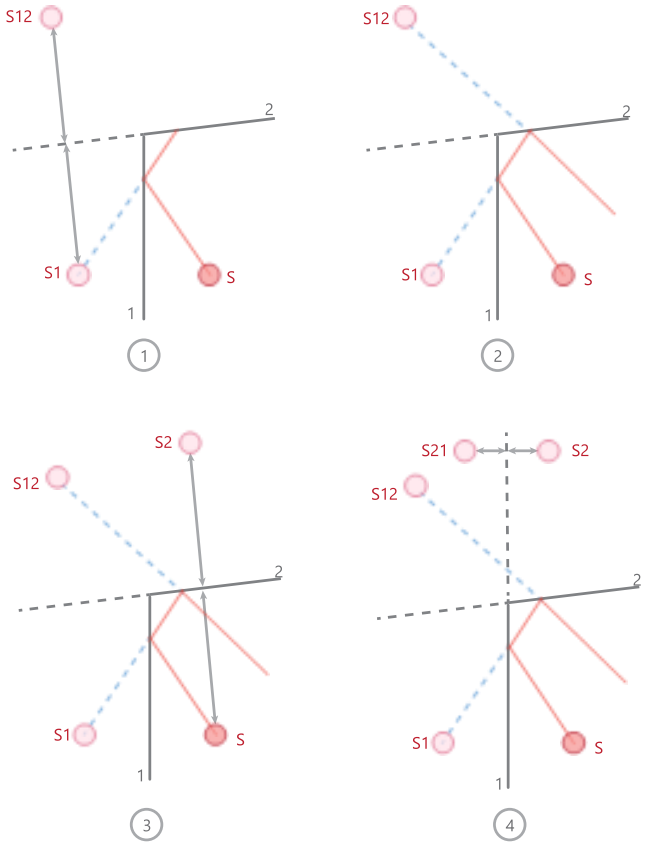

Figure 34 first and second-order image source principle for two surfaces

All the computational results of the image source can be seen as a hierarchical image source tree and the impulse response can be calculated as a sum of all the contributions of image sources in this tree [99].

The image source approach has the benefit of precisely locating all specular reflections and arrival times. However, as the number of IS increase exponentially, the higher-order image sources increase the computational power as well as the calculation time. For this reason, most of the calculation tools limit the reflection order up to two [99].

2.5.2.2 Ray tracing

Instead of calculating specular reflection paths deterministically, ray tracing is a stochastic approach that uses Monte Carlo's principle of reflection path[99]. The method was first introduced in 1958 by Allred and Newhouse[102] and first implemented by Krokstad et al. in 3D space to calculate the impulse response [103]. Soon after, when computer computers became powerful, this approach gain popularity to analyse more detailed geometries [99].

The operating principle of this method is to cast rays from a sound source, reflect them, and record the path history, (see Figure 35) [99]. The rays can be emitted from the source in one of two ways: according to a pre-defined distribution or randomly using the Monte Carlo principle [103]. If rays are cast based on the first technique, then the ray distribution can be weighted according to directivity [99]. The reflection path history of each ray alongside their intersection with a small volume at the receiver is recorded. Then the information like energy, arrival time and direction carried by the ray is represented in a time histogram and further converted into an impulse response.

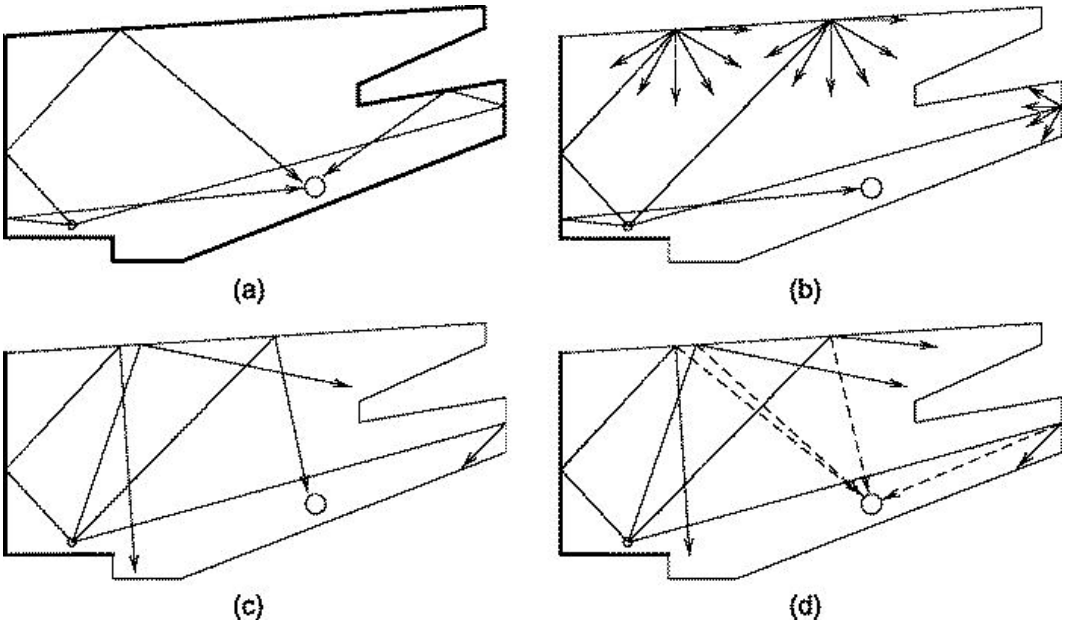

Figure 35 (a) specular reflection of ray (b) diffuse reflection of ray (c) non-specular reflection of rays (d) shadow ray to count non-specular ray to speed-up convergence process [99]

By defining a specific number of rays, the total emitted energy is distributed as a fraction carried by each ray [104]. When a ray hits the surface, part of this energy is absorbed according to the material properties of the reflector surface, while the remaining part is reflected in a specular or diffuse way. This can be done in frequency bands, with each band having its own set of energy information, and the material absorption being defined in the same band [99].

By defining a specific number of rays, the total emitted energy is distributed as a fraction carried by each ray [104]. When a ray hits the surface, part of this energy is absorbed according to the material properties of the reflector surface, while the remaining part is reflected in a specular or diffuse way. This can be done in frequency bands, with each band having its own set of energy information, and the material absorption being defined in the same band[99].

Relating to reflection, specular reflections are calculated based on geometrical law, while diffuse reflections are randomised and are defined by scattering coefficient. Therefore, to get high accuracy from the analysis, the surfaces of the model should be defined with proper absorption and scattering coefficients. Moreover, the stability of the results is also depending on the number of rays being cast. But the volume of the space and material properties defines the number of rays required for each scenario [99]. Therefore, each situation demands a different count and it is not possible to know the exact number before performing the simulation. Therefore, Kulowski [105] recommends the calculation of standard deviation between the runs to determine the suitable ray count. Subsequently, one can also use the relationship between the number of rays to the volume of space and absorption as suggested in [104].

2.5.3 Acoustic simulation tools:

A handful of software are available in the market for acoustic simulation, Table 5 gives an overview of these tools along with their calculation method and availability. Most of them use a complex combination of methods to simulate and analyse sound. Often the simulation is based on reflection order, for instance, lower-order reflection is simulated using the image source method and raytracing is preferred for higher-order reflection [106]. Both the simulation methods are based on geometrical acoustic as they are faster and cheaper. As a result, wave phenomena occurring at lower frequencies are ignored, resulting in a significant amount of inaccuracy. Considering the amount of computational overhead of wave-based methods, in most cases, the simplification made by geometrical methods is acceptable [16]. However, wave-based simulations are very important when analysing lower frequency sound fields. Therefore, recently many researchers are trying to develop a fusion of these simulation techniques which can utilize wave-approach in lower frequencies and raytracing in higher frequencies [107].

Name	Method	Availability
Odeon [108]	Geometric	Commercial
CATT-Acoustics[109]	Geometric	Commercial
Olive tree lab [110]	Geometric+wave	Commercial
EASE[111]	Geometric	Commercial
RAVEN	Geometric	None
RoomWeaver [112]	Wave-based	None
EAR [113]	Geometric	Free
Pachyderm Acoustics [114]	Geometric	Free
i-Simpa [115]	Geometric	Free
OpenPSTD [116]	Wave-based	Free

Table 5 Some of the common software used for acoustic simulation

Most of the software noted in Table 5 are commercial, and therefore used by professionals who can afford the cost. Only three tools are based on the wave-based approach, one of them is not available and one requires python or MATLAB scripting to run. OpenPSTD [117], is the only tool that is free and uses a wave-based approach. However, it requires a third-party design interface and documentation about modelling is very limited. All the listed software's are developed for the expert users (acousticians), as they all required technical knowledge to run [112][118]. Therefore, limits the possibility of use by acoustically unschooled architects and designers [118].

Furthermore, acoustic software requires a great deal of information on geometry and material, and it frequently necessitates format conversion[118]. Also, the simulation needs to be performed at every design modification, which makes it a time-consuming loop. The results contain a large amount of data with different acoustical parameters, which also makes it overwhelming for the architect to process and make design decisions[118].

The two major limitations of acoustic simulation tools are unclear guidelines and different software interfaces with different file formats [104]. The first one leads to misunderstanding about the data needed to execute the analysis and the second results in a poor level of data exchange between software [97], [104].

Most of the above-listed software are standalone, except EAR, OpenPSTD and Pachyderm, which make use of Blender and Rhino+Grasshpper respectively. Therefore, users often switch between modelling tools and acoustic simulation software, resulting in more time as well as cost. Given the iterative nature of the optimization process in design, the development of an acoustic simulation tool combined in a modelling environment appears to be a significant advantage [20].

2.6 Parametric Design and Optimization

2.6.1 Parametric design

Any form or geometry generated in a 2D or 3D modelling tool is based on the parameters. For example, a line drawn in Auto-CAD is based on two parameters (length and direction) or a box generated in a 3D tool has three parameters etc. Even though these examples use parameters to construct shape and form, they are not considered parametric design. Instead, it is a design approach that creates a functional/geometric relationship between objects (forms or groups of forms) so that certain characteristics of the forms can be changed while the original predetermined relationship remains [119]. One of the main advantages of parametric design is that it allows the designer to change features while keeping the basic logic [120]. This gives the designer a dynamic tool to analyse design possibilities.

The first application of parametric workflow dates back to the 19th century. The hanging chain model, used by Antoni Gaudi in the design of the Church of Colonia Guell, became the first analogue parametric model [121]. Since then, many applications of parametric design and constraints have been created, especially using scale models. The use of computer-aided design (CAD) software in the late nineteenth century greatly increased architects' capabilities. The 2D and 3D hand sketches became the 3D computer models. This gradually increased the complexity of design and thus lead to the new style in architecture defined as Parametricism [122].

2.6.1.1 Parametric tools

All kinds of digital applications are made in order to execute a specific task in a parametric fashion. This includes both engineering as well as non-engineering tools. Parametric tools are available as pre-built plugins or visual algorithm editors, but they can also be self-written code or scripts [121]. In 2003, Robert Aish first implemented this concept and created Generative Components while working for Bentley Systems [121]. Later in 2007, with the CAD software Rhinoceros3D, David Rutten created a counterpart, which is now known as Grasshopper. Similarly, in 2013 Autodesk introduced Dynamo to Revit.

Recently, Rhinoceros and Grasshopper have gained popularity because of their powerful modelling capabilities, flexible expandability and relatively low requirements on computer hardware [123]. The early developed tools for Rhino and Grasshopper were limited to architectural purposes. However, recently, the use of parametric models in conjunction with third-party applications/plugins to assess non-geometrical variables such as structural performance, building physics etc. has become the norm. For example, Karamba3D is a finite element package to evaluate the structural behaviour of trusses, frames, shells etc.[124]. Ladybug and Honeybee tools are developed for building physics analysis [125]. Similarly, for acoustics, Pachyderm plugin was developed for sound prediction and auralization[114]. Parallel to the development of these tools, online communities have emerged, sharing information and examples.

2.6.2 Performance-Based Optimization

Designing and analysing with parametric design results in a plethora of different design solutions that must be examined before deciding on the 'best' solution. These multiple scenarios in the (initial) design phase might be overwhelming for the designer to process [121]. Therefore, the term Performance-Based Design is introduced in which performance criteria guide the design process through the optimal solution with the support of digital analysis tools [123]. This method enhances both the design workflow and the final product by reducing cost and time while also increasing design potential and quality [126]. The ability to forecast performance from the start of the design process offers significant benefits, as design decisions made early in the process have the largest impact on the final design [127].

Just as there are many possible solutions to a design problem, there are also various methods available to help find the best results. Determining which technique to apply is a part of the challenge and also depends on the complexity of the problem [128]. One such method is evolutionary or genetic algorithms. This method uses the Darwinian theory of evolution to reach the optimal solution without working out all the solutions. This means options are generated according to set parameters, high scoring options are called parents. Then the new alternatives are generated through mutations from the parents to find the solutions (children's), which might outperform their parents. This process repeats several times (Figure 36) until the solution fulfils set requirements [121].

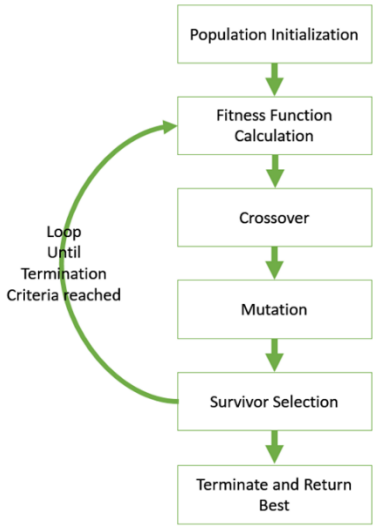

Figure 36 Evolutionary Optimization process diagram[129]

The first step might be to identify whether the optimization is applicable in the first place. Because many times the design space is very limited, thus finding out the optimal solution by the means of the trials is simpler than doing the optimization. To help with that Grobman analysed different optimization approaches, outlining their evolution over time, and categorizes them based on the design challenge they are attempting to solve, and the method used [128]. The same author in his research [130] concludes that the lack of coding skills among architects is one of the reasons why generative methods are still underutilised in practice. Simulation tools, on the other hand, are rapidly improving, becoming more accurate and user-friendly, allowing architects to conduct simple simulations and correctly interpret their results on their own. Moreover, Grasshopper plugins like Galapagos, Octopus, and Wallacei[131] are making the process easy by providing the predefined codes embedded into Grasshopper components.

2.7 Summary

The key findings from the literature study are as follows.

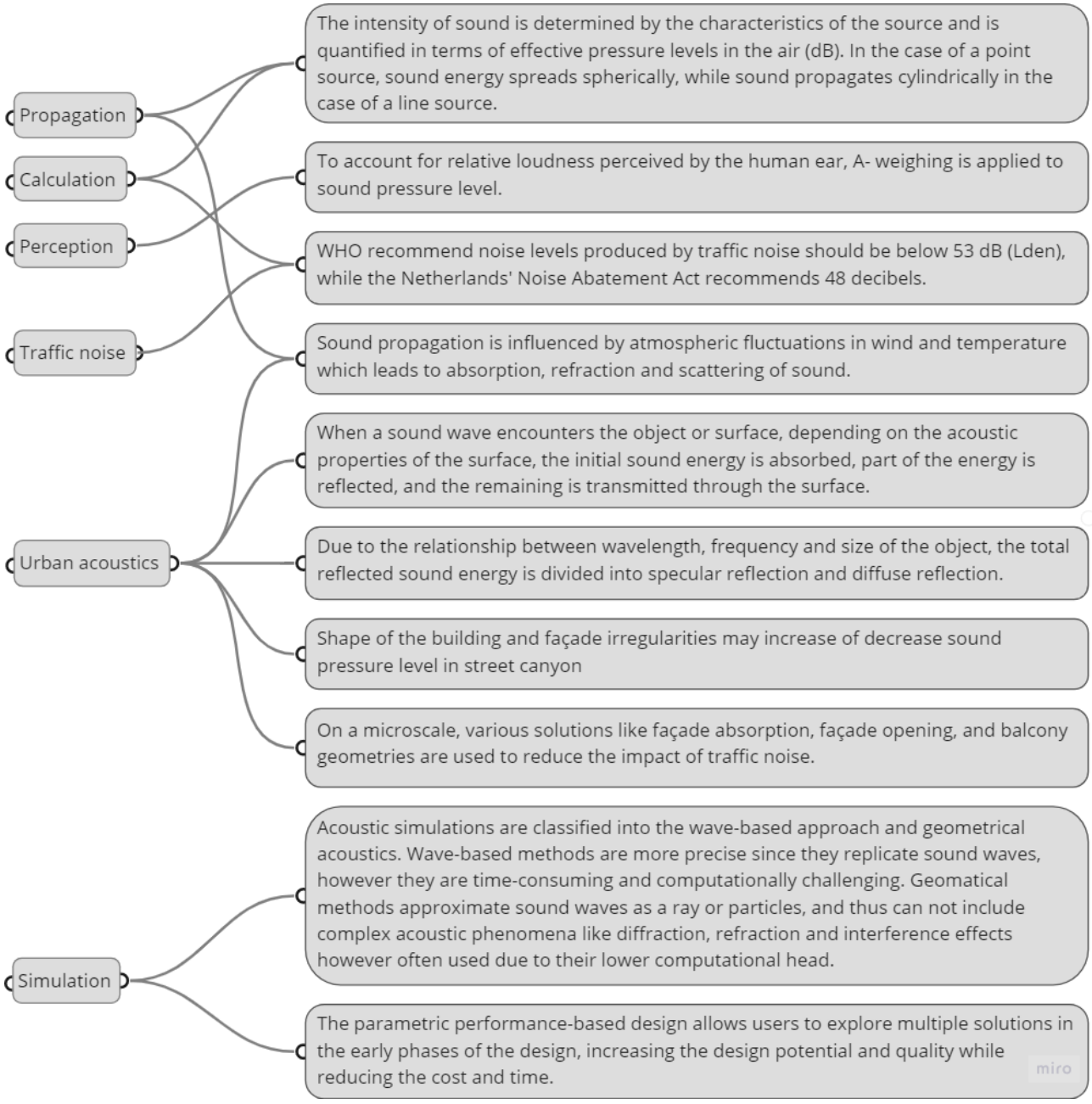

3

The Digital Model

Part 3 The Digital Model

This chapter explains the development process behind the parametric acoustic simulation workflow, which is also the main objective of this research. A brief overview of the Pachyderm acoustics plugin is given followed by calculation methods based on which the tool is developed. Finally, the development of the Grasshopper definition is outlined.

3.1 Software Requirements

In order to develop the proposed workflow, a series of tools need to be installed. In particular, the study will require a 3D modelling environment, a parametric modelling environment, acoustic simulation software and finally an optimizer. Rhinoceros 7 [132], Grasshopper[133] and Pachyderm acoustic [114] are considered the most suitable applications. Grasshopper is a parametric form generator that is integrated into Rhinoceros 3D and designed to work with a variety of third-party plugins. Logic is defined in the Grasshopper utilizing visual components that contain predefined code. The Grasshopper definition is made using native Grasshopper components, Ladybug components [125] and Pachyderm acoustics. All listed software and plugin can run on a machine having 64-bit Windows 8.1, or 10, and can also be used on Intel Mac or Apple Silicon Mac. More information about the software and its installation process can be found in [132] [133] [114] [125].

3.2 Pachyderm Acoustics

Pachyderm is an acoustical simulation plugin developed by Arthur van der Harten for Rhino and Grasshopper. The software plugin has been open-sourced since March 2015 and is in continuous development in terms of its features. The current version of Pachyderm is based on geometrical acoustics. The impulse response is calculated based on either the raytracing solution or image source modelling or a combination of both. The image source solution is a deterministic method in which the amount of wavefront is represented by a ray. While in a ray-tracing solution, the amount of the wavefront is represented by a ray which is proportional to the number of rays being cast. The assumption is made that these rays are evenly spaced on the surface of the spherical wavefront. However, with a large sample size, the amount of error reduces. Each method has its own advantages and disadvantages, which are already been discussed in the literature.

The Pachyderm Rhino plugin (*Pachy_RH*) is more developed in terms of its features as compared to Pachyderm Grasshopper (*Pachy_GH*) plugin. *Pachy_RH* offers a separate interface within the Rhino interface (see figure 37), where acoustical set-up is carried out.

Frequency-dependent absorption coefficient and scattering coefficient are applied to

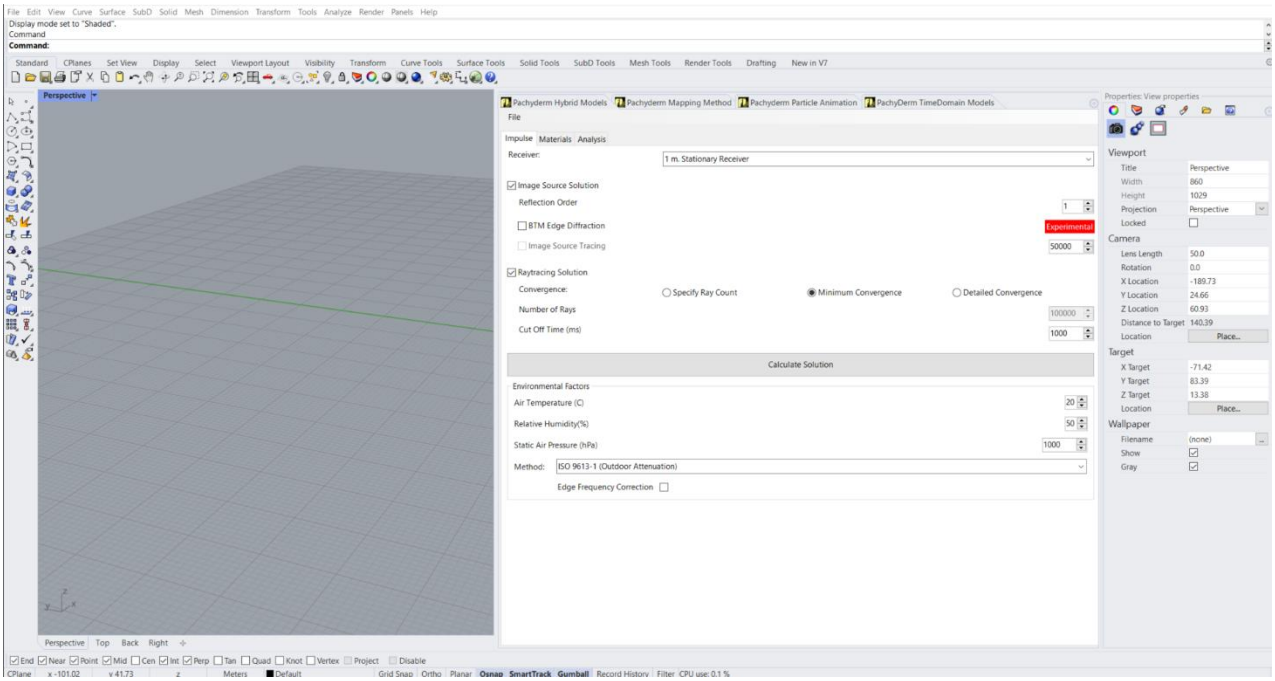

Figure 37 Integrated interface of Pachyderm inside Rhino

geometry via the model layer. The geometries which are not defined by layer are not included in the calculation, therefore, it is important to assign exact geometry to the associated layer. After running the simulation, the results can be expressed by several acoustic parameters. The only disadvantage of the *Pachy_RH* plugin is that parametric simulation is not possible and thus limits the option of optimization.

On the other side, parametrization of the geometry is possible by using the *Pachy_GH* plugin. However, it runs in tandem with the Rhino plugin, meaning that the absorption and scattering coefficients are retrieved from the Rhino model layers.

Even though the interface of the two environments is different, both work on the same principle of geometrical acoustics, i.e. image source and ray-tracing solution. Image source modelling works perfect with simple geometry like rectangular room, finding all the specular reflections and arrival time. However, not suitable for geometries involving complex shapes. The image sources inside Pachyderm are calculated similarly to the principle explained in section 2.5.2.1 and therefore only the calculation principle of raytracing is explained along with the source, receiver and impulse response calculations.

3.2.1 Ray-tracing in Pachyderm

In order to cover the disadvantages of the image-based solution, Pachyderm uses the Monte-Carlo ray-tracing method. The rays after hitting the object are either scattered, transmitted, reflected specularly or all three. The energy embodied by the ray is explained in the following expressions, where I_0 is the intensity of the ray after reflection [134].

$$I_0 = I_{\text{specular}} + I_{\text{scattered}} + I_{\text{transmitted}} \tag{14}$$

$$I_{\text{specular}} = I_{\text{incident}} * (1-\alpha) * (1-\tau) * (1-s)$$

$$I_{\text{scattered}} = I_{\text{incident}} * (1-\alpha) * (1-\tau) * s$$

$$I_{\text{transmitted}} = I_{\text{incident}} * (1-\alpha) * \tau$$

Where, I_{incident} is the intensity of a ray incident on the surface, α is the absorption coefficient (% of the energy absorbed by the reflected surface), s represents the scattering coefficient (% of energy scattered or reflected non-secularly) and τ is the transmission coefficient (% of energy transmitted through the surface).

The raytracing simulation in a Pachyderm occurs in three phases. During the first phase, after hitting the surface, each ray is split into its specular reflected energy, scattered energy and transmitted energy. The intensity of the ray is reduced by the absorption coefficient of the surface, and the remaining energy is scattered between both specular [$I_{\text{incident}}\ (1-s)$], and diffuse ($I_{\text{incident}} * s$) rays, in which s is defined as the scattering coefficient. If the transmission coefficient is also defined, then energy will be further divided between the rays and the third ray will hold the transmission portion. This first phase of ray tracing is only applicable when the casted ray is within 40 dB of its initial strength [134].

In the second phase, a random number check decides the state of the reflected ray. The scattering coefficient is given a region around it according to the following equation [134],

$$\begin{aligned} s_{max} &= s_{\text{center}} + |s_{\text{center}} - 0.5|/4 \\ s_{min} &= s_{\text{center}} - |s_{\text{center}} - 0.5|/4 \end{aligned} \tag{15}$$

In which, s_{center} is a scattering coefficient. If the random number is below the defined scattering region, then all the reflected energy is given to a single scattered ray and the direction is random. The ray is split into scattered and specular rays just like phase 1 if it is within the scattering region. And if the random number is above the scattering region, all the reflected energy is given to a single specular ray, whose direction is defined by Snell's law. The second phase lasts till the ray is 100 dB below its initial power, after that it shifts to the third phase [134].

The third phase is similar to the second phase, except the random number is compared with the scattering coefficient. So, if the random number is less than the scattering coefficient, all energy is given to a single scattered ray and if it is above the scattering coefficient the energy is assigned to a single specular ray. Figure 38 shows the specular and diffuse rays for multiple reflections and the complexity of this algorithm [134].

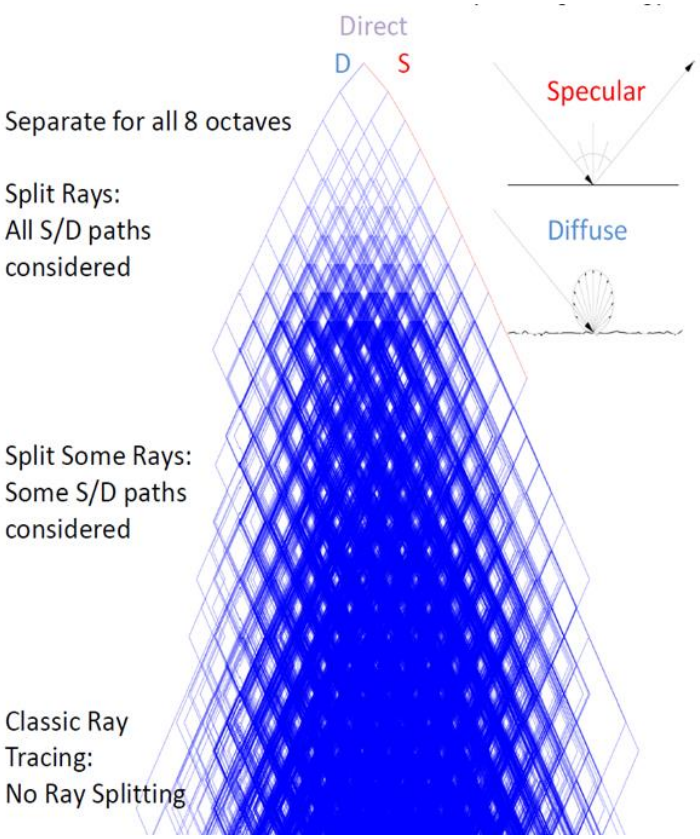

Figure 38 (Three-phase) Specular and diffuse reflection in Pachyderm [134]

3.2.2 Point Source

To ensure that the rays are distributed evenly and in all directions from a point, the surface of a sphere is divided into triangles with equal areas (see Figure 39). A barycentric coordinate system is used to divide the triangle into points, more information about the barycentric system can be found in [135]. Then the rays are cast from these points until every triangle has been used to generate the ray direction. This method not only allows quick generation of rays but also ensures even distribution [134].

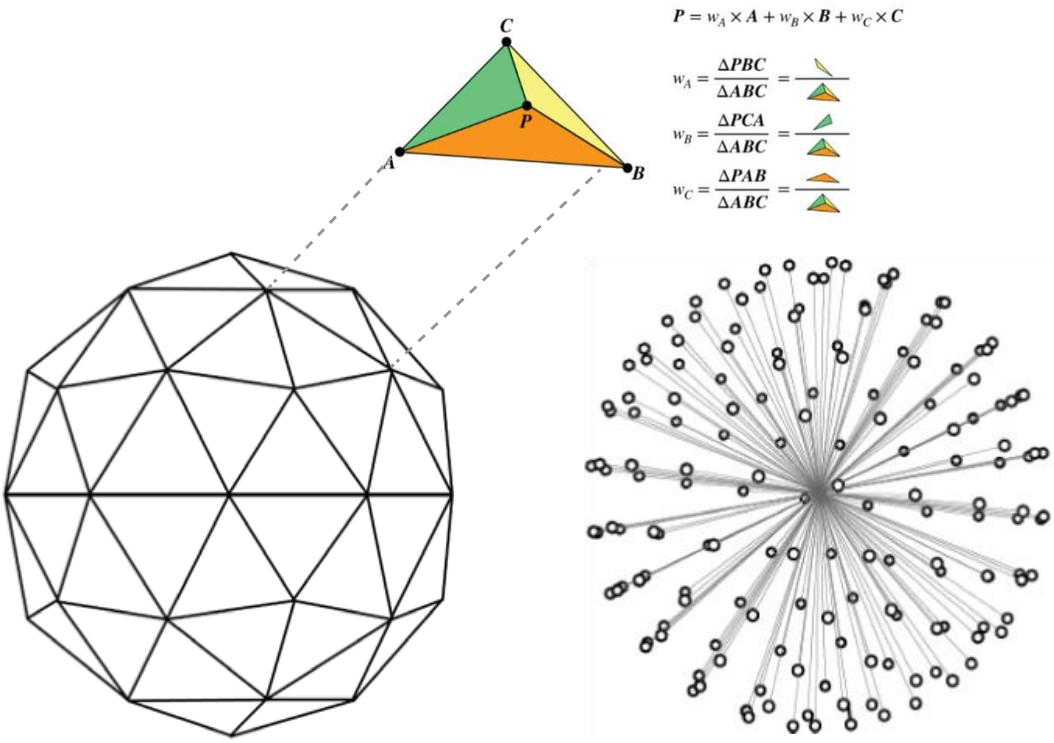

Figure 39 Left: Geodesic sphere with barycentric co-ordinates, right: rays cast from point 'p' (own illustration based on [136])

3.2.3 Point Receiver

The receiver in Pachyderm is also represented as a sphere. The rays that pass within a meter of a receiver point are recorded including the time of arrival and the sound power contained in the ray. The power embodied in the ray at the intersection point with the sphere is attenuated according to air absorption. Then weighing is applied according to the distance between the intersection point and centre of the receiver given by the following equation[134],

$$I = I_r * 10^{-\alpha * d/10} * l/2\pi \quad (16)$$

Where, I_r is the intensity carried by the ray, α is the air attenuation coefficient as per ISO 9613-1, the total distance the ray has travelled before the reaching the receiver sphere is represented by d and l is the distance between the two intersection points of the ray with the sphere (chord of the sphere), So, the longer the l (chord distance), the closer the ray to the centre, and the greater the impulse response will be [134].

3.2.4 Impulse response calculation

Pachyderm acoustics algorithm traces the energy from multiple sound sources (i.e. direct sound and reflected sound). When the ray carrying energy arrives at the receiver, it is

added to the set of echograms, depending on the time of its arrival and also the direction of arrival. An echogram is a time-based function of the sound intensity at a receiver. There are seven directional components represented by the echogram- one omnidirectional, and six directional (two for each axis). These seven echograms are represented for all frequencies in the octave band (63-8000hz), thus 56 echograms in total. Then the added energy is converted into decibels using the standard logarithmic formula [134],

$$I\ (dB) = 10 \log \left[\frac{I}{I_0}\right] \quad (17)$$

Where I is the intensity of sound ray [watts/m2] and I_0 is the intensity threshold of the least audible sound a human can hear = $1x10^{-12}$W/m2.

Over time the energy at the receiver reduces, this results in the decay of sound represented as the reverberation. Pachyderm uses the "Integrated impulse response" method to calculate the reverberation time (see EN ISO 3382-1 [137] for detailed calculation).

4

Acoustic Simulation Workflow

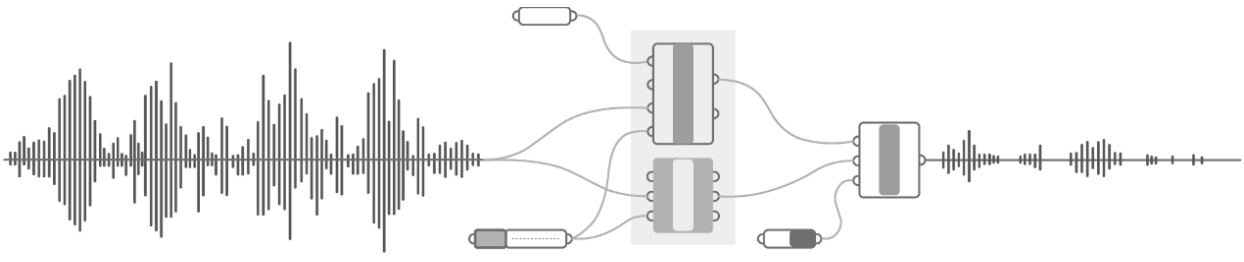

Part 4 Acoustic simulation workflow

The workflow used to set the acoustic simulations in Pachyderm is divided into two stages- first explaining the point source to point receiver definition and second describing the mapping definition. Point to not that the basic definition explained in the first part is valid for both the workflows. Other setting parameters like sound power level, number of rays, number of receivers and material properties are different for validation and design stage, thus addressed in respective chapters.

4.1 Point source to point receiver workflow

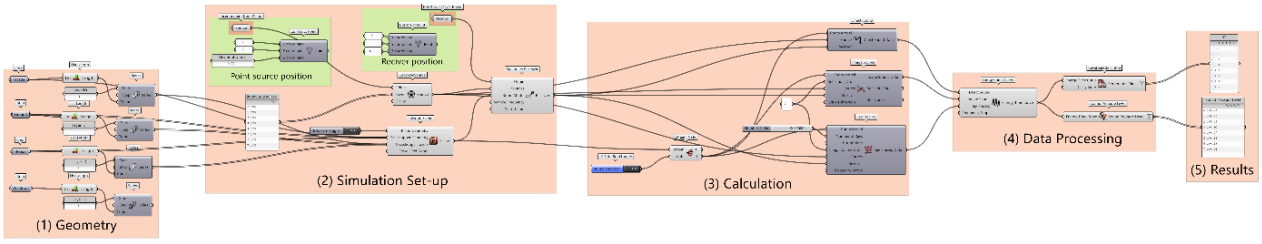

Figure 40 Point source to point receiver grasshopper definition

Figure 40 shows the complete Grasshopper definition for a point source to point receiver. The definition is fairly simple in logic and can be seen as a five-step process. While explaining it is assumed that the readers have a basic understanding of the Grasshopper environment. Text highlighted in *orange* represents the Grasshopper component while *blue* showcases input or output for the Grasshopper component.

4.1.1 Step 1: Geometry

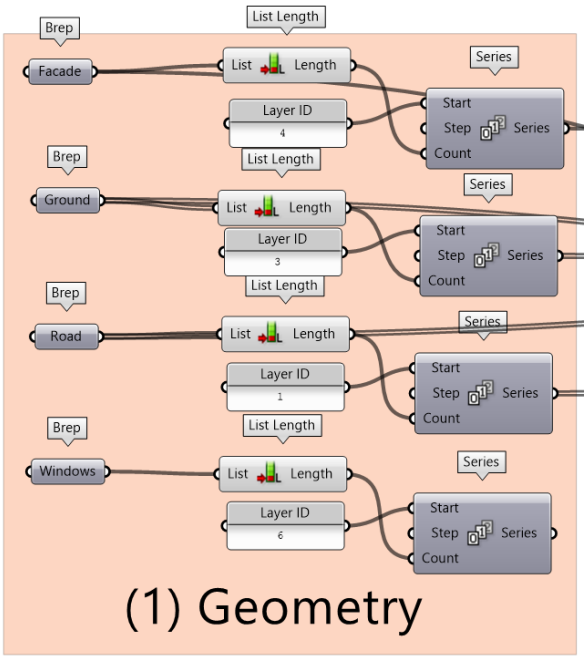

Figure 41 Step 1: Preparation of geometry

In the first step, the geometries from the Rhino are imported to the Grasshopper environment using a *brep*. Since material properties like absorption and scattering coefficient are assigned in the Rhino environment, *layer ID* is assigned manually by using the *panel* component. Therefore, it is important that separate brep should be used for separate geometry/surface. The number of items available in each brep is determined using *list length* and further attached to the *series* component. This workflow is important as it makes sure that all geometries are assigned to their respective material properties.

4.1.2 Step 2: Simulation set-up

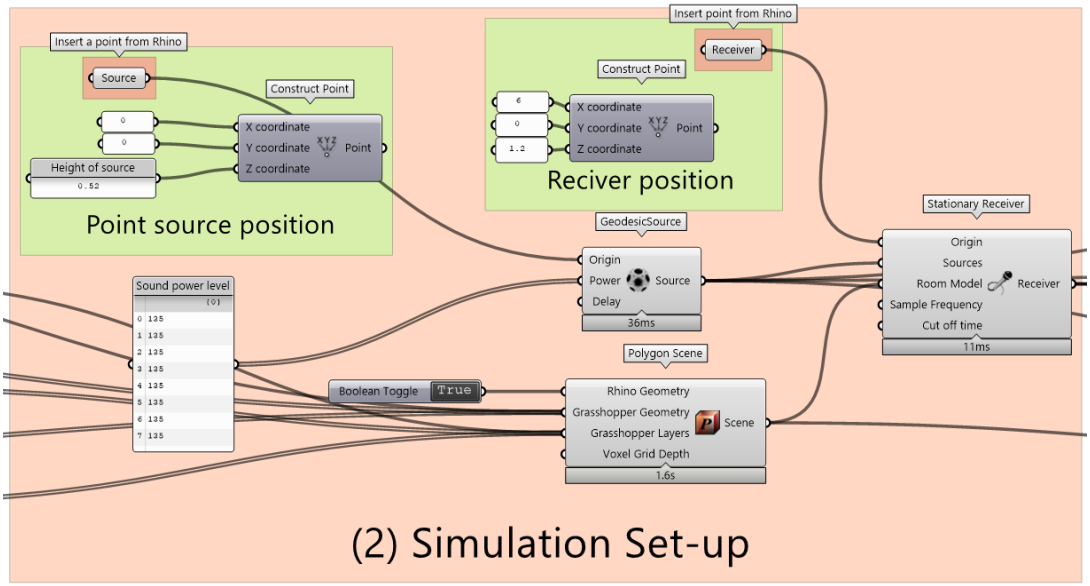

Figure 42 Step 2: Acoustic simulation set-up

In the second step, a virtual simulation context is created using the *polygon scene* component from Pachyderm. Here, the output from geometry *brep* and corresponding layers from *series* components are attached to *Grasshopper Geometry* and *Grasshopper Layer* respectively. A point source is created by using the *GeodesicSource* component. For that, the origin can be created by inserting the point from the Rho or assigning the coordinates in the *constructed point*. The sound power level for the source is assigned to each octave band using *panel* component in such a way that 0 corresponds to 62.5 Hz and 7 corresponds to 8000 Hz frequency. To create a receiver, the *origin* is defined by inserting a point or coordinates, the *source* takes the input from the *source* component and output from the *polygon scene* is inserted into the *Room model*.

4.1.3 Step 3: Calculation

A combination of *direct source*, *image source*, and *ray tracing* components is used in the calculating setup (see Figure 43). The calculation principle behind all these components is already explained in the earlier section. Because there is no parameter in Pachyderm components that can start the simulation process, when all the required strings are attached, it immediately starts the computation process. Therefore, to control the simulation manually, the *stream gate* component is introduced. It's linked to a *polygon scene* and a *false start switch*. All the three calculation components require *Room Mode, Source and Receiver* inputs in common. Reflection orders need to be set for the *image source* and *ray tracing* component which is given by simply setting the number in the

panel component. Additionally, a *slider* is introduced to control the number of rays used in the simulation.

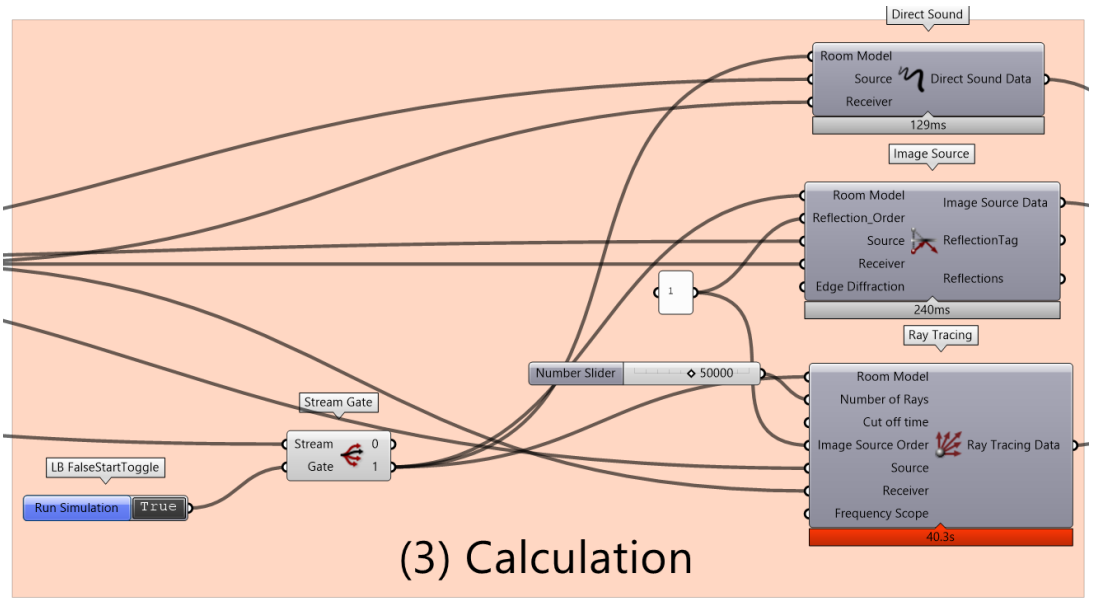

Figure 43 Step 3: calculation setup

4.1.4 Step 4: Data Processing

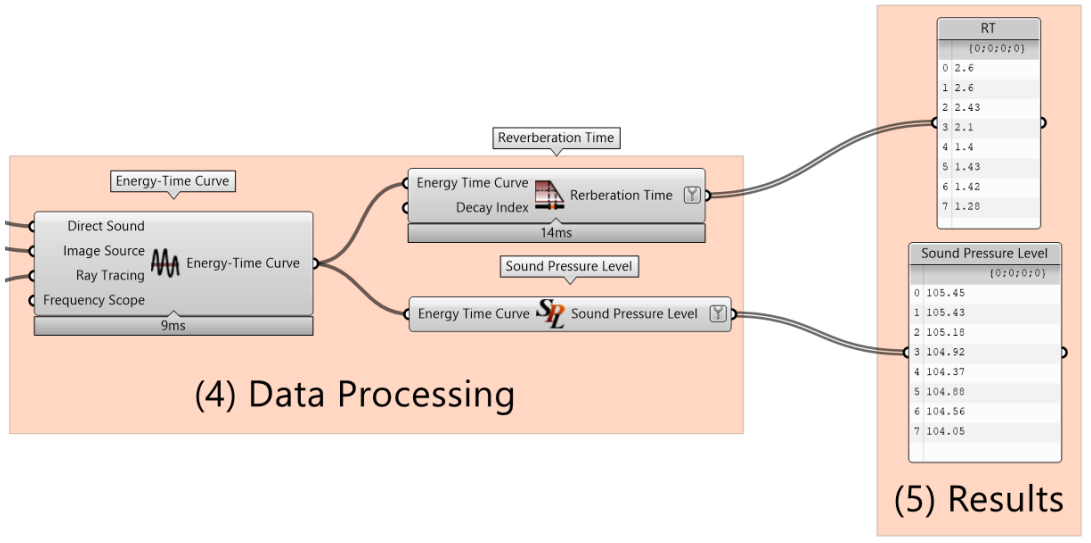

Figure 44 Step 4: Data processing and step 5: Results

Here the impulse response calculated from the previous step is converted into the *energy-time curve*. Therefore, the output from *direct sound, image source* and *ray-tracing* are plugged-in to the *Energy-Time Curve* component. Various calculation parameters like clarity, speech transmission index, RT etc, are available in Pachyderm, however, the research only involves the calculation of sound pressure level and reverberation time.

Therefore, the output from the *energy-time curve* is translated to *reverberation time* and *sound pressure level* components.

4.1.4.1 Step 5: Results

Finally, the results are simply represented by connecting the output from *RT* and *SPL* components to the *panel* component. This data then can be copied to excel for the statistical analysis.

4.2 Line Source to SPL Mapping Script

The point-source-to-point-receiver script is further modified to have the SPL values projected onto the façade or a surface. The logic and approach behind the script remain the same, however, slight changes are made to the previous workflow along with the addition of new workflows. The script grouped in blue in figure 45 represents the additional workflows. Steps 1 (geometry), step 4 (calculation) and step 5 (results) are the same as the previous definition, and thus not explained again.

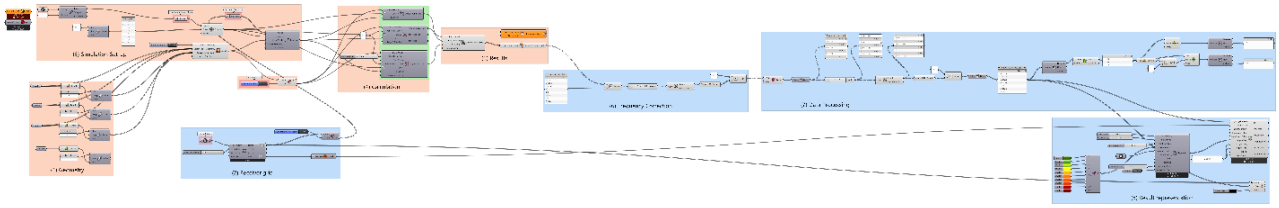

Figure 45 Sound pressure level mapping Grasshopper definition

4.2.1 Step 2: Receiver Grid

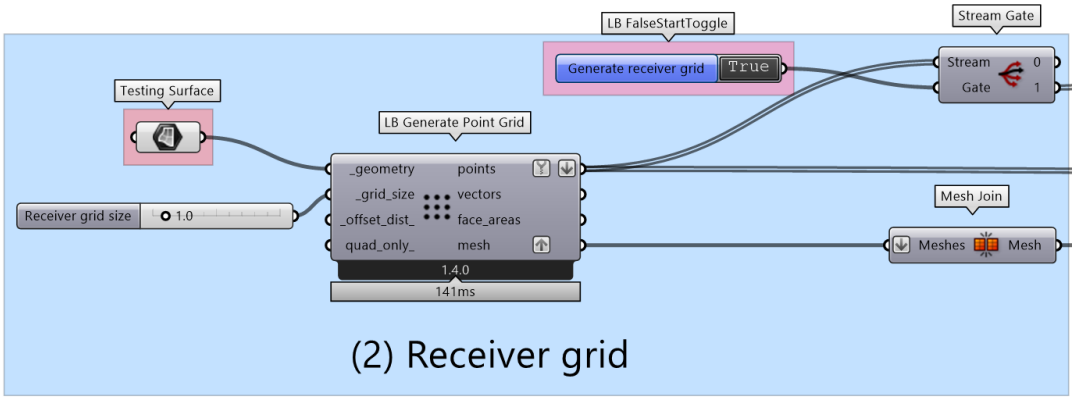

Figure 46 Step 2: Formation of receiver grid for analysis

A Receiver grid for the analysis surface is generated by using the *Ladybug generate point grid* component. The *surface* component is used to extract the surface from the rhino

model, which is subsequently coupled to the *geometry* input. Further, to control the *grid size* a *slider* is introduced. Each receiver is represented by the generated points from the grid component, which are then connected to the *receiver* component in the simulation step.

4.2.2 Step 3: Simulation set-up

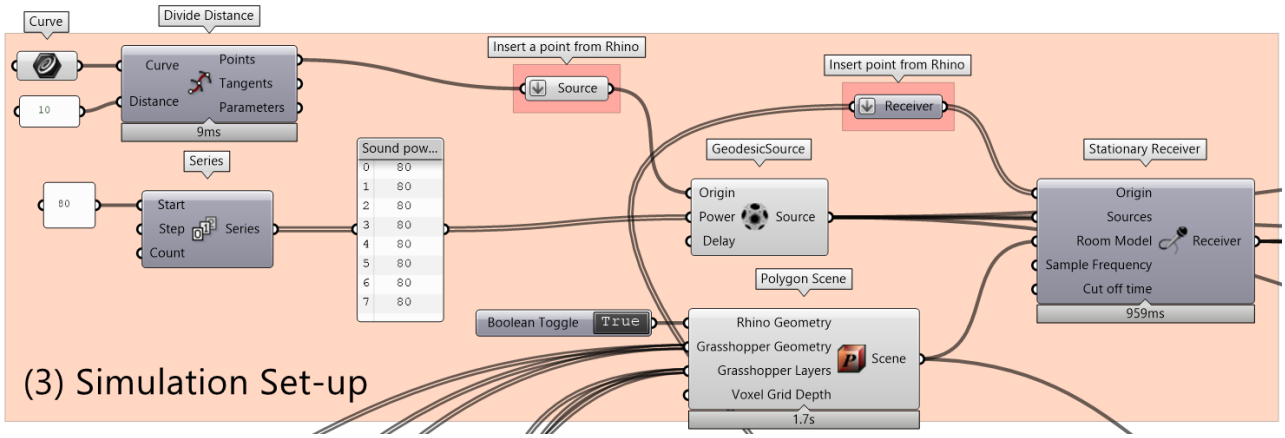

Figure 47 Step 3: Simulation setup

Pachyderm does not have a line source component. Therefore, the line is divided into points to represent the line source. The line can be created in Grasshopper using the *line* component, nevertheless, to increase the simplicity of the script, the line is modelled in Rhino and extracted by using the *curve* component. Then the spacing of the points along the line is created by using the *divide distance* component and distance input is given by the *panel*. The rest of the process in this step is the same as the point source script.

4.2.3 Step 6: Frequency correction

After the calculation of the sound pressure level for each receiver along the grid, a frequency correction workflow is presented. This workflow is important as it includes the human perception of sound and converts values into weighted sound pressure levels (dB(A)). Here, the correction is applied using the *panel* component with values from Table 1, and then, using the *addition* component, the results and corrections are combined. Since sound pressure level values are generated for each frequency band, a logarithmic addition has to be taken as per equation 7. This is accomplished by the use of the *expression*, the *mass addition*, the *logarithm*, and the *multiplication* component.

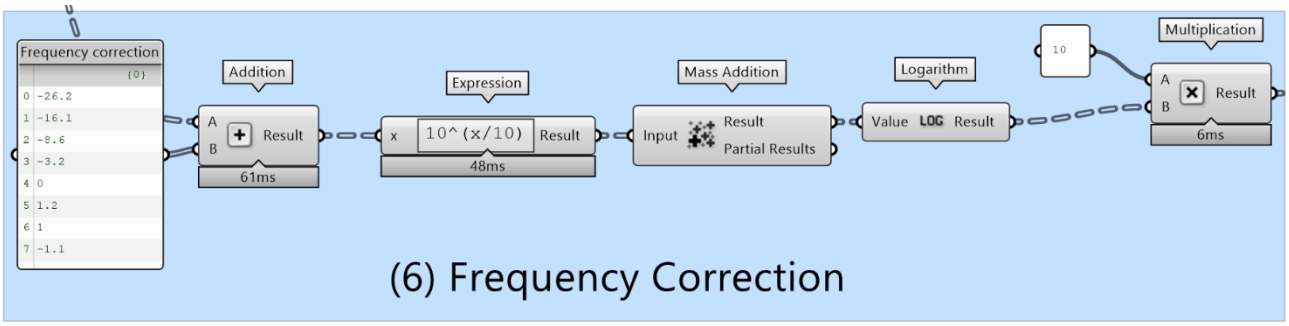

Figure 48 Step 6 frequency correction

4.2.3.1 Step 7: Data processing

Since the line is divided into several point sources, the receiver points record the SPL from each of these point sources. As a result, the data is processed afterwards to reflect the resultant single value at the receiver points. The simulated SPL are first rearranged using the *shit path* and *flip matrix* components. Then, similar to the previous step, a combination of *expression, mass addition*, *logarithm* and *multiplication* component is applied to logarithmically add the sound pressure levels. Further, the values are linked with a *round* component which round-off the values to the nearest digit. Moreover, maximum and minimum values are also calculated by sorting out the data using the sort *list, list length* and *list item* component.

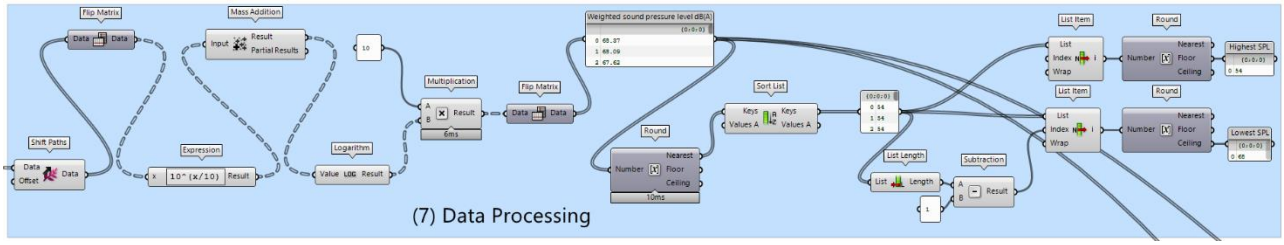

Figure 49 Step7: Post-processing the simulated results

4.2.4 Step 8: Representation of the results

Finally, the simulated values are represented in a colour grid. The parametric script allows us to set custom colours using the *swatch* component. A ten-colour scale is applied to cover a wide range. This colour grade is then merged and attached to the *Ladybug_Legendpar* component. This component also allows the user to set the lower and higher boundary which can be set by using a *slider* component or directly importing *minimum* and *maximum* values from the data processing step. Then this input from the *legendpar* component is linked to the *Ladybug recolour mesh* component. Here, the simulated results are combined with mesh from the receiver grid. And finally, the *text tag*

component is used to represent the sound pressure levels on the surface in the Rhino viewport.

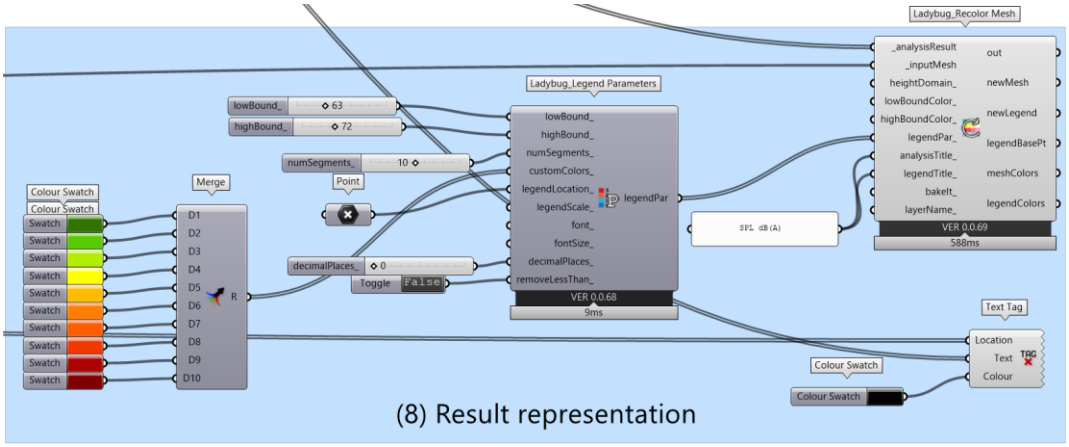

Figure 50 Step 8: Representation of the results

5

Validation

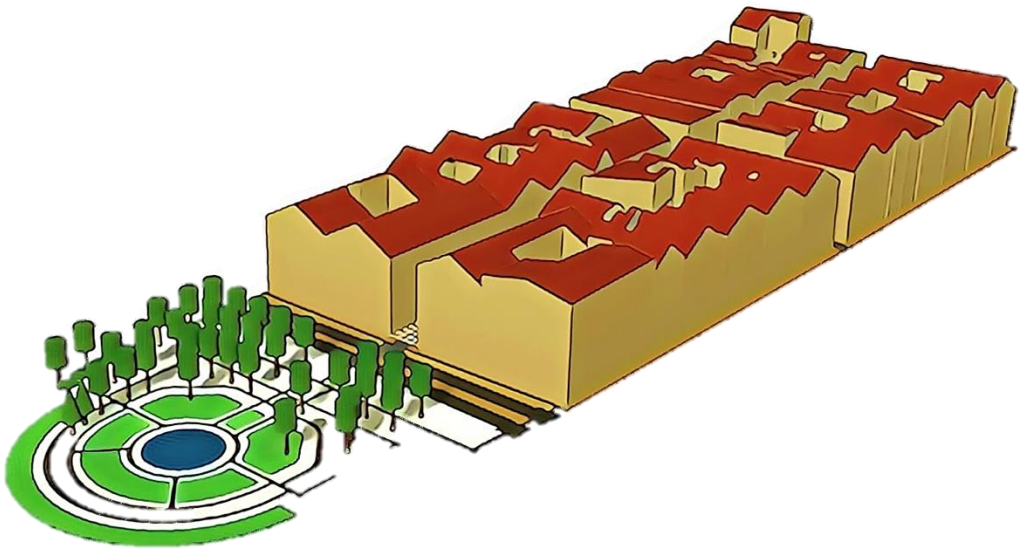

Part 5 Validation

In practice, all the computer simulation models are validated with the ultimate goal of producing accurate and creditable models. Model validation is defined as "substantiation that a computerized model within its domain of applicability possesses a satisfactory range of accuracy consistent with the intended application of the model" [138]. This step is important so that the users and the decision-makers using the information obtained from the results of these models have "trust" in the results[139].

In the acoustic simulation, different validation techniques are used by the scientific community depending on the scope of research and purpose of development. However, three approaches are common and widely used. The first one is a comparison of the computer simulation results against on-site measurements which is also considered the most reliable procedure. In this method, on-site measurements are taken, and the gathered data set is compared with simulated data. The second is a validation of the simulated results against the results of other (valid) models (software). And the third is a comparison with scale model measurement in which, a scale model is made the same as a computer model, then the measurements are taken and finally, the measured data is compared with the simulated data.

In this thesis, the first two approaches are considered for the validation process. Actual onsite measurements are not taken by the author instead, an experimented study of sound propagation in a street conducted by J. Picaut et al. [140] is used for the validation. The result of the experimental study and its comparison against the developed parametric workflow are explained in the next section. For the second approach, Geomilieu (geo-environment) software is chosen to verify the results of the Grasshopper simulation.

5.1.1 Case Study Measurements for Model Validation [140]

The original measurements were carried out in the city of Nantes, France, along the west side of Kervegan street Figure 51. The 210m long street has a constant height of 18m and a width of 7.9 meters. The First 50m of the Kervegan street is considered for the original measurements. The west end is opened to a large "Petite Hollande square". The east end is crossed by a perpendicular street of 6.58m width which is 55m beyond the experimental zone, thus not influencing the measurements.

The purpose of the study was to predict the behaviour of sound decay and sound attenuation in the street which is fairly aligned with the development of this thesis.

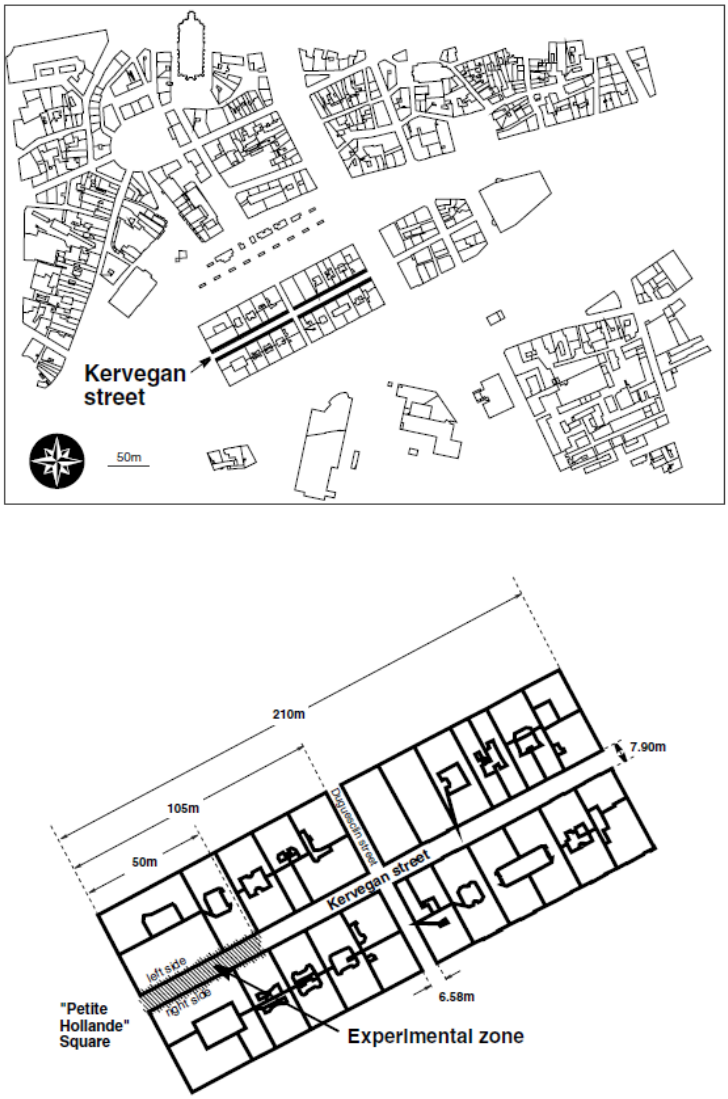

Figure 51 Top: Location of Kervegan street in Nantes, France, Bottom: Experimental zone (retrieved from [140])

The façade of the buildings is almost uniform along the entire street and is defined by a periodic array of windows. The old façade is mainly constructed with stone while the windows consist of glass and woodwork. The pavement can be considered perfectly reflective as it is made up of cobblestone.

5.1.1.1 Case-study measurement set-up:

Four different measurements setup were explored by the authors of the case study, each belongs to a specific position of the sound source. The setup is explained in Figure 52.

The sound sources S3-S4 were arranged at the beginning of the street while S1-S2 were set up in the middle of the street with heights of 0.52m and 1.65m respectively. Nine sets of microphones were used to measure the impulse response which includes AVM MI17 ICP microphones, Bruel and Kjær microphones (type 4135 and 4165), and GRAS microphones (type 40AF). This array of microphones M2-M10 (see Figure 53) was moved from 6 to 50 m in a step of 2m.

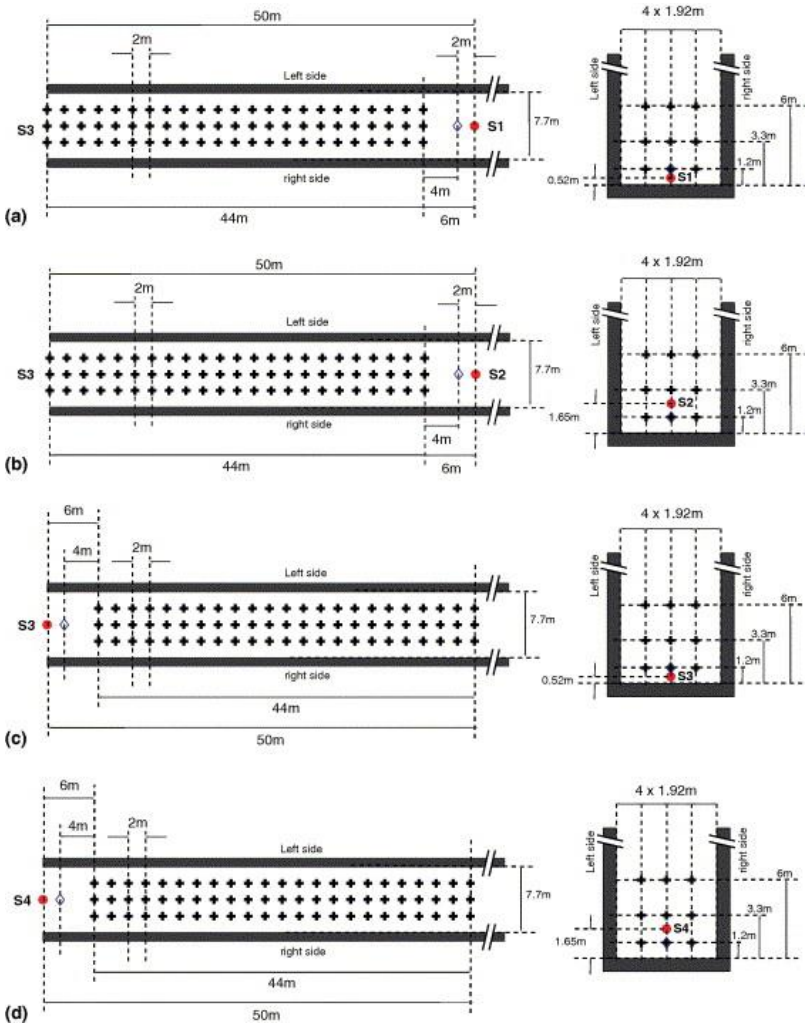

Figure 52 Case study measurement set-up for four source positions S1-S4 represented by (a)-(d) respectively (retrieved from [140])

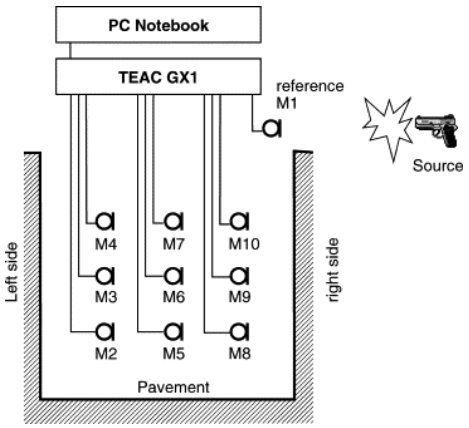

Figure 53 Nine receivers M2-M10 arranged in a grid along the cross-section of street (retrieved from [140])

5.1.2 Rhino set-up

The same street and neighbourhood are modelled in the Rhino file (Figure 54). To get the exact dimensions of the buildings an OSM file (street map information from OpenStreetMap) is used. Then the google earth coordinate system is utilized to retrieve exact heights and accordingly buildings are slightly adjusted to replicate the experimental situation.

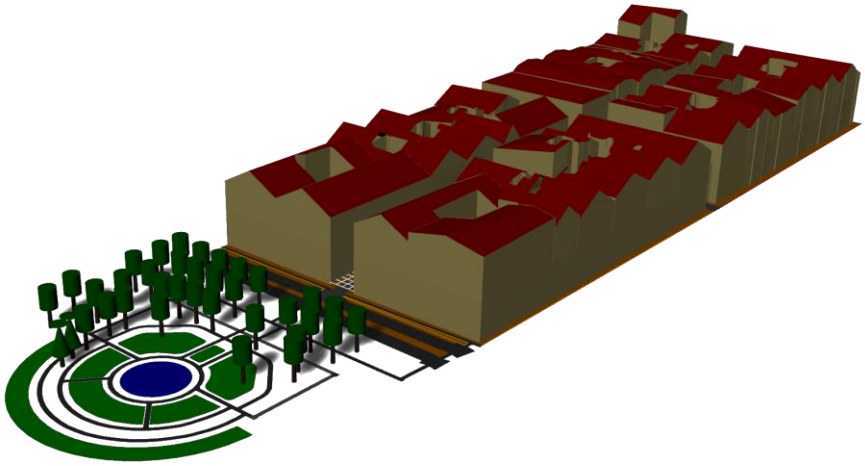

Figure 54 Rhino Model of Kervegan Street

For the first set of comparisons, only flat surfaces were modelled. Considering different street materiality, the absorption and scattering coefficients were applied to the surfaces. The following table shows different materials with their absorption and scattering coefficients implemented in the study.

	Cobblestone pavement		Hard Ground		Facade		Roof Tiles		Trees		Window	
Freq	AB	SC	AB	SC	AB	SC	AB	SC	AB	SC	AB	SC
62.5	0.01	0.01	0.01	0.3	0.04	0.01	0.02	0.4	0.40	0.5	0.10	0.01
125	0.02	0.01	0.02	0.3	0.04	0.01	0.02	0.4	0.40	0.5	0.06	0.01
250	0.02	0.01	0.03	0.3	0.05	0.01	0.03	0.4	0.40	0.5	0.04	0.01
500	0.04	0.02	0.03	0.3	0.06	0.02	0.04	0.4	0.45	0.5	0.03	0.01
1000	0.10	0.22	0.03	0.3	0.08	0.15	0.05	0.4	0.50	0.5	0.02	0.02
2000	0.08	0.41	0.04	0.3	0.04	0.23	0.04	0.4	0.30	0.5	0.02	0.22
4000	0.05	0.41	0.05	0.3	0.06	0.22	0.02	0.4	0.35	0.5	0.02	0.41
8000	0.05	0.41	0.05	0.3	0.06	0.22	0.02	0.4	0.35	0.5	0.02	0.41

Table 6 Absorption and scattering coefficients applied to Rhino geometry. (AB: Absorption coefficient, SC: Scattering coefficient)[64][141][142]

In the Rhino model, a similar grid of receivers is made, representing the array of onsite measurements (Figure 55). Once the geometrical model was set, acoustical simulation is first carried out using the *Pachy_RH* plugin. An omnidirectional sound source is used to represent the pistol gunshot of original measurements. The sound power level of the original source (gunshot) was unknown; therefore, the power level of the omnidirectional source is adjusted till the SPL at 6m receivers is the same as the case study measurements. After a few iterations, the sound pressure level of the source at 1m (SPL@ 1m) is found to be 124 dB and it is set constant over the octave band throughout the simulations.

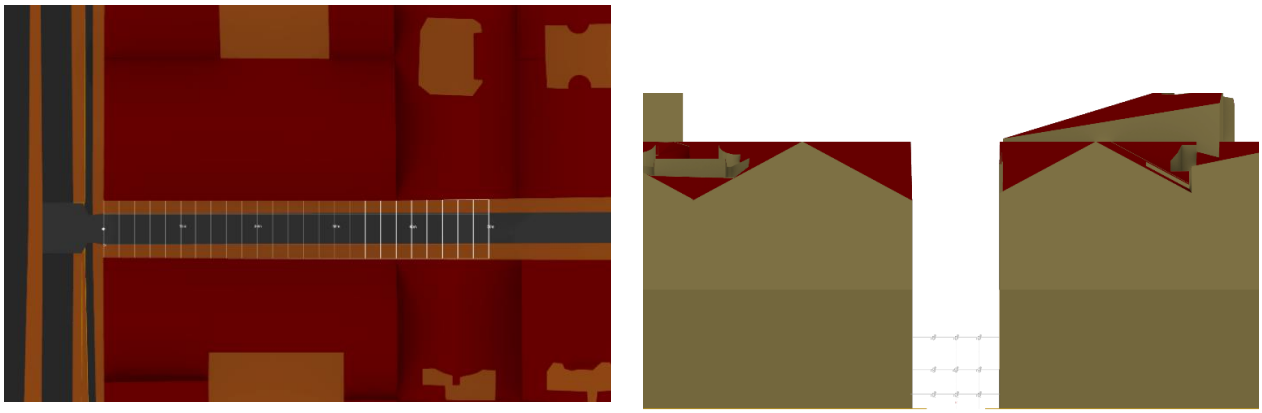

Figure 55 Left: Plan view of receiver grid, right: Section view of the receiver array

Although the *Pachy_RH* is more advanced, parametric simulation is not possible under the Rhino environment. Therefore, further, the Grasshopper script is developed using *Pachy_GH* and the results were compared with the Rhino plugin.

Table 7 represents the SPL comparison between *Pachy_RH* and *Pachy_GH*. As both plugins use the same calculation algorithm, the values are nearly identical with a maximum difference of 0.4 dB occurring at the M9 receiver. This difference is a result of

randomly distributed rays between the trials however, the variation is smaller than just a noticeable difference of SPL (1 dB). Therefore, from this point onward, the next discussion will only be concerning results simulated using the *Pachy_GH* plugin.

Receiver Position	M2	M3	M4	M5	M6	M7	M8	M9	M10
SPL (dB)-Rhino simulation	113.9	113.4	112.1	114.4	114.3	113.1	113.9	113.2	112.1
SPL (dB)-Grasshopper simulation	113.9	113.6	112.1	114.4	114.4	113.1	113.9	113.6	112.1

Table 7 SPL for Pachy_RH and Pachy_GH (Source: S3, receiver: 6m at 1000Hz frequency)

5.1.3 Results

5.1.3.1 Pre-setting

As described in chapter 2.5, simulation time and the accuracy of the results are dependent on the number of rays. If the number of calculations increases, which is in this case, then it might be time-consuming to adjust the ray count parameter every time. The formula for ray count, which is based on the volume of the space, is given by Pachyderm's creators for room acoustics modelling. The rule of thumb says the ray count should be 50 times the volume of space. However, in an urban environment, volume can be very large and may result in a delay in the simulation. Therefore, pre-calculations are performed to check the variability of results with respect to ray count, number of trails and the simulation time.

Figure 56 shows the deviation in the sound pressure level with respect to ray count. Five variants; 3k, 10k, 50k, 100k and 150K rays are tested for S3 configuration and receivers at 6m.

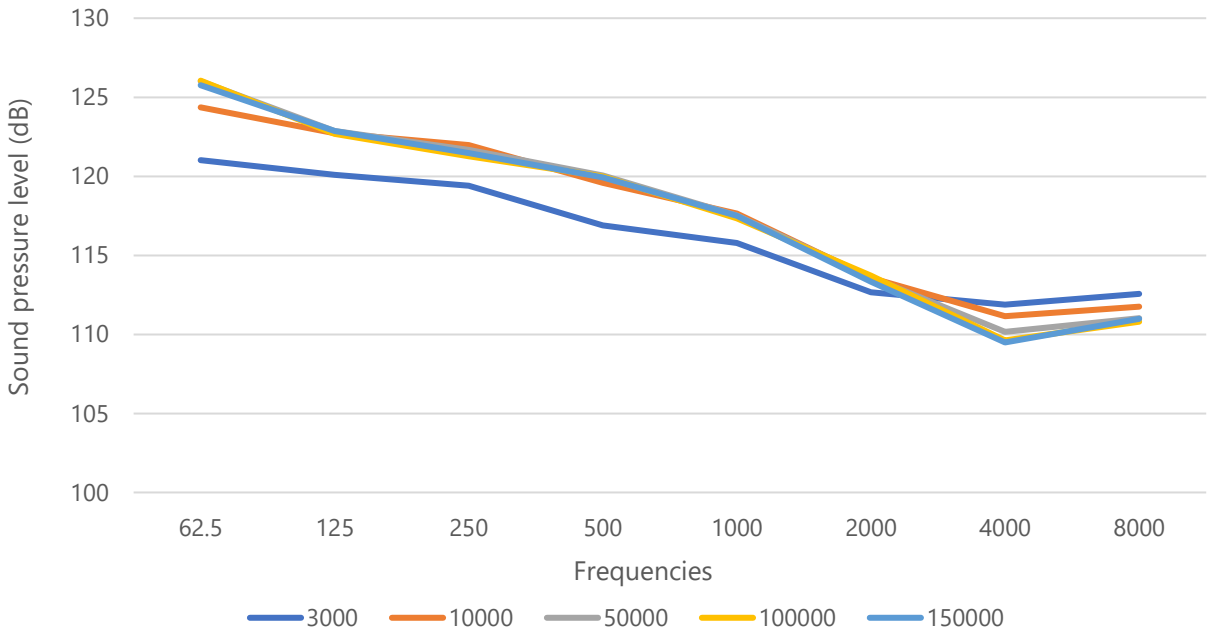

Figure 56 Sound pressure levels with respect to ray count (configuration: S3 at 6m)

Less number of rays leads to a smaller number of reflections and the probability that the reflected ray intersects the sphere of the receiver becomes less. Therefore, the sound pressure level with 3000 rays clearly deviates from the rest of the data set. As the initial ray count increases, more rays intersect the receiver sphere and after a certain point the weighing explained in equation 26 is no longer applicable. Therefore, for the ray count above ten thousand, the results are identical over all frequencies. "Ray count= volume x 50" is still applicable in this case and serves as the starting point for the calculation.

Further, the simulation time is also recorded for the considered ray counts. From Figure 57, we can see that the simulation time for 3000 and 10000 rays is just 3 seconds which is comparatively less than the simulation time required for 150000 rays. Nevertheless, 40-60 seconds for each simulation is acceptable given the accuracy of the results.

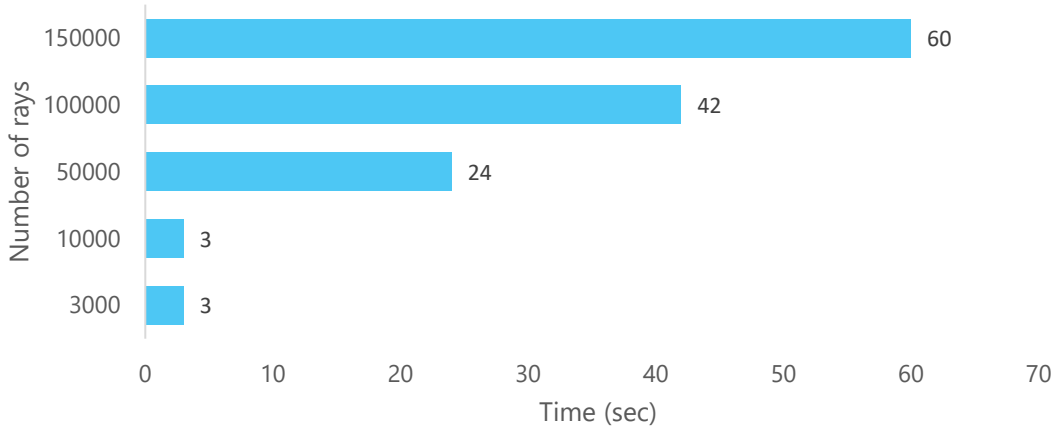

Figure 57 Variations in simulation time with respect to ray count

In the original case study setup, 5 measurements (i.e. 5 pistol shots) were carried out for each sound source position and each microphone array to minimize the error. Therefore, five trials were performed using 10000 rays for the S3 source and 10m receiver position using the Grasshopper workflow. The standard deviation in sound pressure level is calculated and can be seen in Figure 58. Although the lower and higher frequencies deviate more than the mid-range frequencies, the highest deviation in SPL is less than 0.2 dB. Thus, the error is well within the limit and a single simulation is also sufficient to produce acceptable results.

Therefore, in conclusion, 10000 rays and a single trail are selected as a pre-setting for further calculations and can be used in the early-stage design simulation.

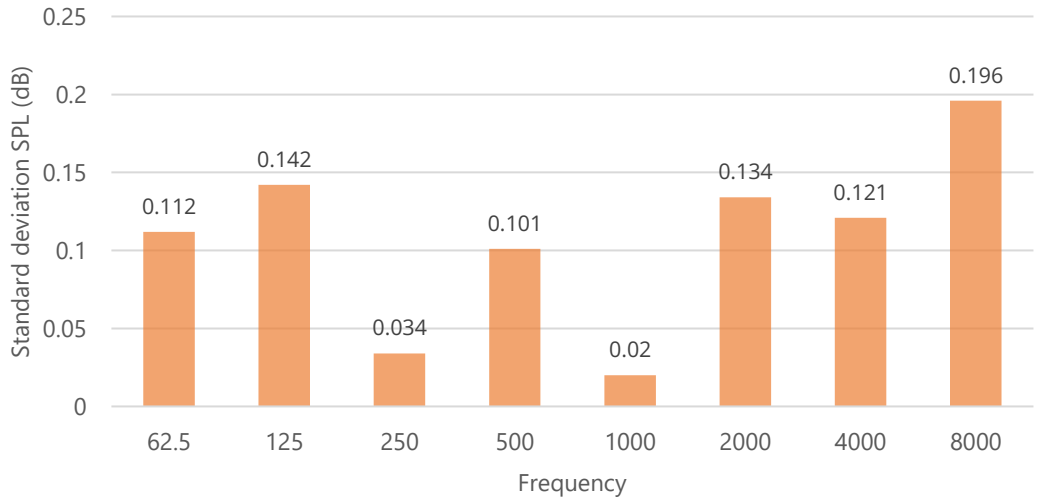

Figure 58 Trails response: standard deviation for five trails (configuration S3, receiver at 10m, at 1000Hz frequency)

5.1.3.2 Sound distribution in a street cross-section:

As an example, figure 59 and figure 60 represents the evolution of sound pressure levels in street cross-sections at 6m and 50m respectively. Differences on the same cross-section are of the order of 1.5-2.5 dB at 6m and 0.5-1.0 dB at 50m. This result shows that the sound distribution is rather uniform in the same cross-section. The higher differences at 6m indicate that the sound level close to the sound source is more influenced by the first reflection than the receivers far from the source. This variation may occur due to reflections and scattering by particular façade irregularities. On contrary, this effect has very little influence on the reverberant field far away from the source, which depends on the multiple-diffuse reflection by the building façade.

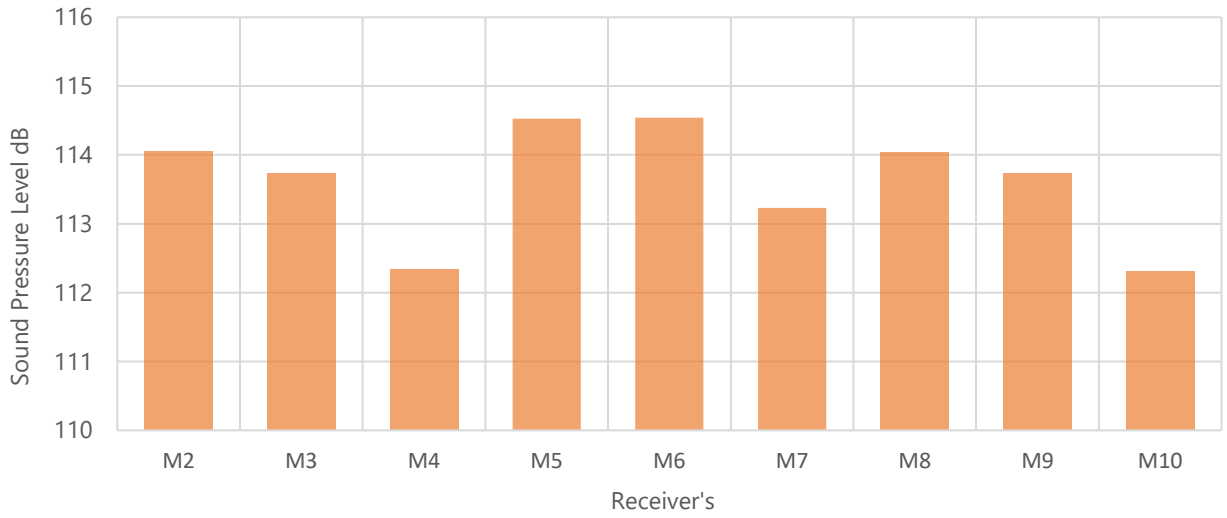

Figure 59 SPL at 6m for M2-M10 receivers (Configuration: S3, at 1000Hz frequency)

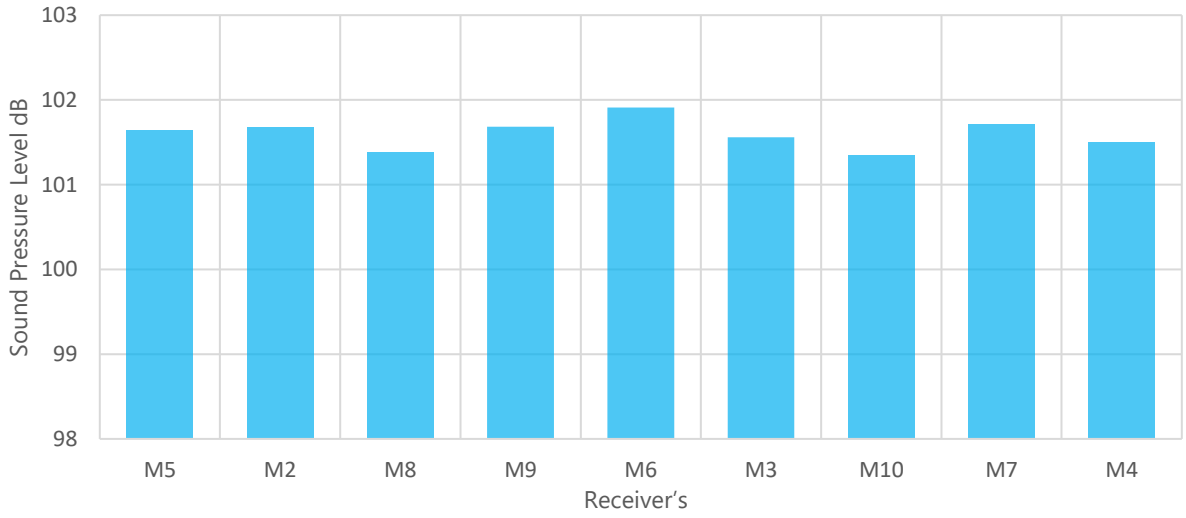

Figure 60 SPL at 50m for M2-M10 receivers (Configuration: S3, at 1000Hz frequency)

Further, these results are compared with on-site measurements. From figure 61 one can say that both the results follow similar trends. SPL for the receivers very near to the source (M2, M5 and M8) are almost equal as they are influenced by the direct sound path. However, in reality, multiple sound reflections occur in a street canyon. This effect of multiple reflections is generally not considered in a ray-tracing simulation like Pachyderm, and the reflection order is limited to a maximum of two. Therefore, the greater difference in SPL (3-4 dB) can be seen for the receivers M4, M7 and M10 which are far from the source.

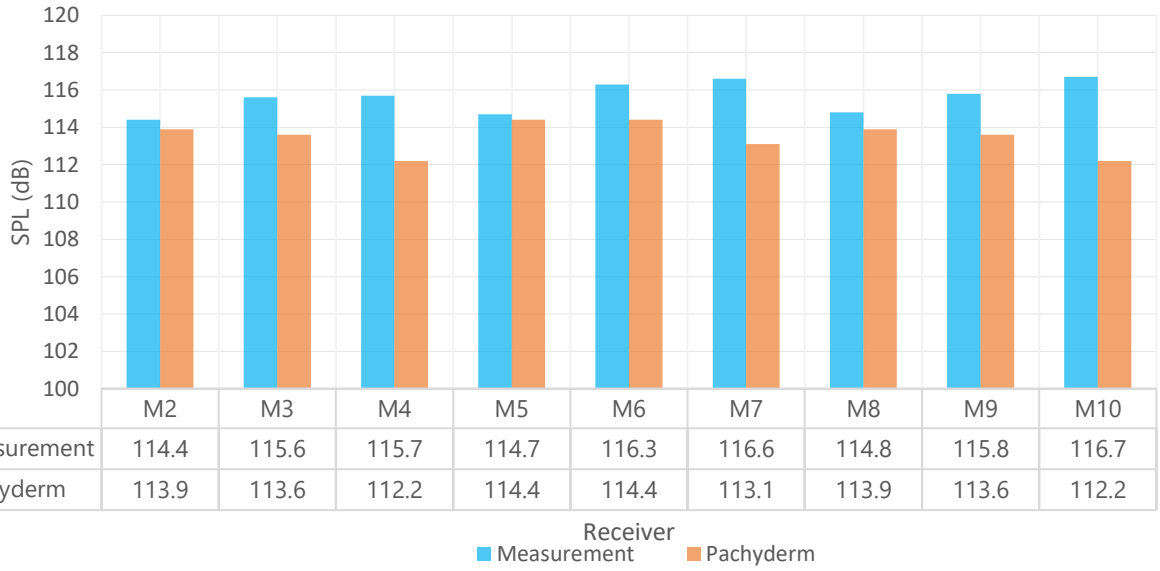

	M2	M3	M4	M5	M6	M7	M8	M9	M10
Measurement	114.4	115.6	115.7	114.7	116.3	116.6	114.8	115.8	116.7
Pachyderm	113.9	113.6	112.2	114.4	114.4	113.1	113.9	113.6	112.2

Figure 61 SPL comparison between measurements and Pachyderm at 6m for receivers M2-M10 street (S3 configuration at 1000 Hz)

Similarly, the results are obtained for reverberation time and compared with on-site measurements. Figure 62 demonstrate, the reverberation time in the street cross-section at 6m for the S3 configuration over all (octave) frequency bands.

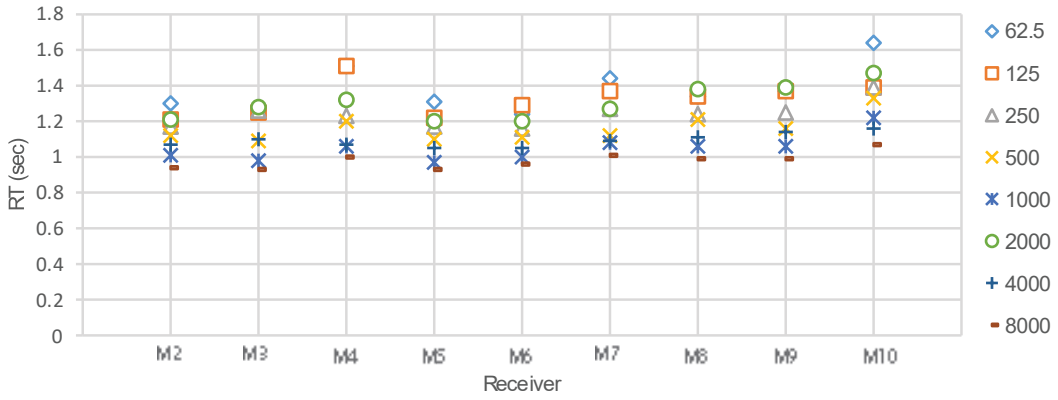

Figure 62 Reverberation time for M2-M10 receivers at 6m for octave frequency band (S3 configuration)

These results illustrate that the reverberation time is higher for low frequencies while the high frequencies are more quickly attenuated. This is because diffuse reflections from the building façade mostly consist of low frequencies and high frequencies are scattered out of the street (towards the sky). The result is in agreement with the common idea that the higher frequencies are reflected in more directions than the lower frequencies [140], also air absorption is more prominent in higher frequencies.

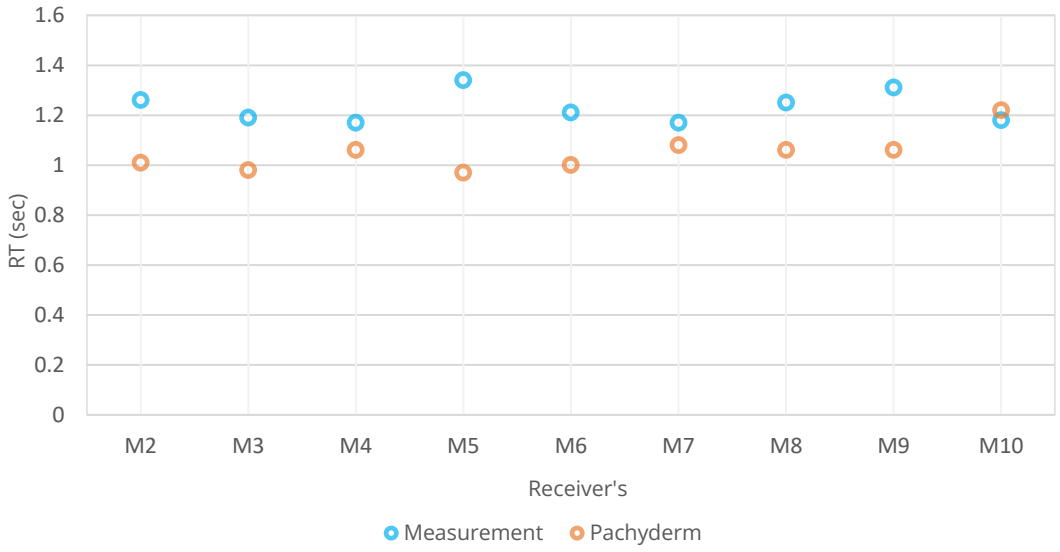

Figure 63 RT comparison between measurements and Pachyderm at 6m for receivers M2-M10 (S3 configuration at 1000 Hz)

When these results are compared with the on-site measurements, a similar conclusion can be made for RT that of sound pressure level. Figure 63 represents the RT comparison between measurements and Pachyderm at 6m. The higher RT values for measurements are the result of a longer reverberant field due to multiple reflections in real situations.

5.1.3.3 Sound distribution along the street:

Figure 64 presents the evolution of reverberation time as a function of the source to receiver distance over the octave frequency band. The graph clearly indicates that the RT increases with increasing distance between source and receiver. This increase is more noticeable up to 30m, after which the RT becomes more constant this might be due to the reduced effect of 1st order reflections and direct sound.

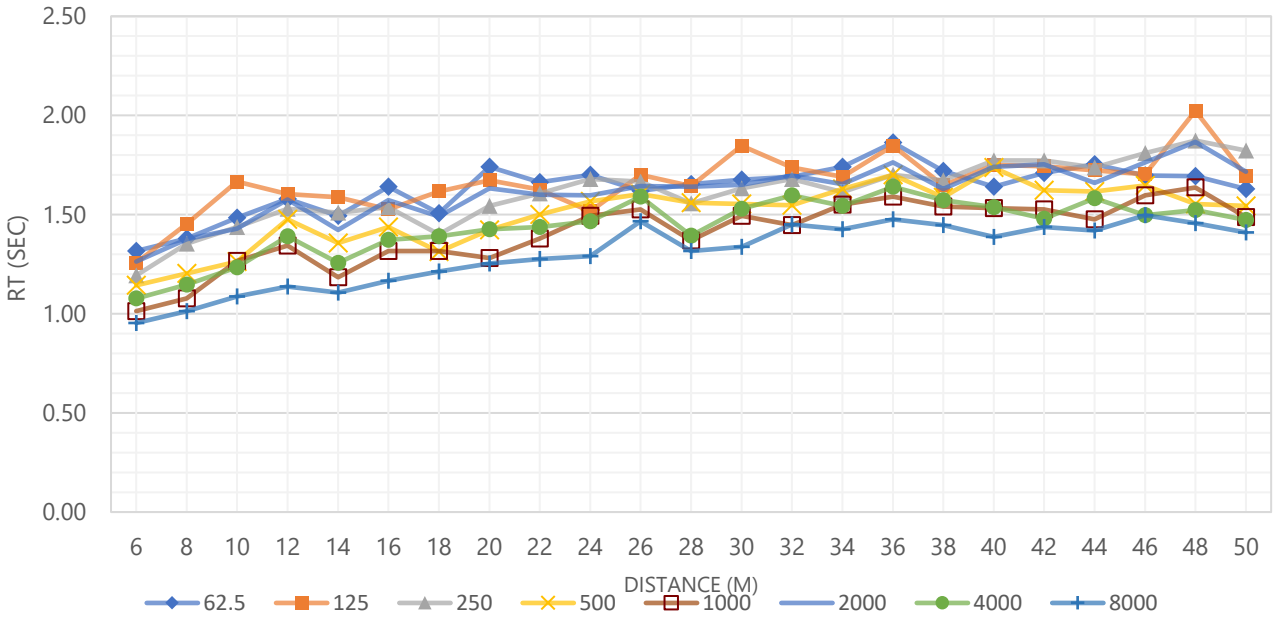

Figure 64 Evolution of average reverberation time along the street for each octave band (S3 configuration)

In figure 65, the average RT results at 1000Hz frequency are compared with on-site measurement. Although, both the calculations are based on decay between -5dB to -35dB and Schroeder's integration method, a Pachyderm is developed for room acoustic simulation. RT is highly dependent on the properties of the room (close space) and therefore, higher variations in RT can be seen for Pachyderm values when applied to the external situation.

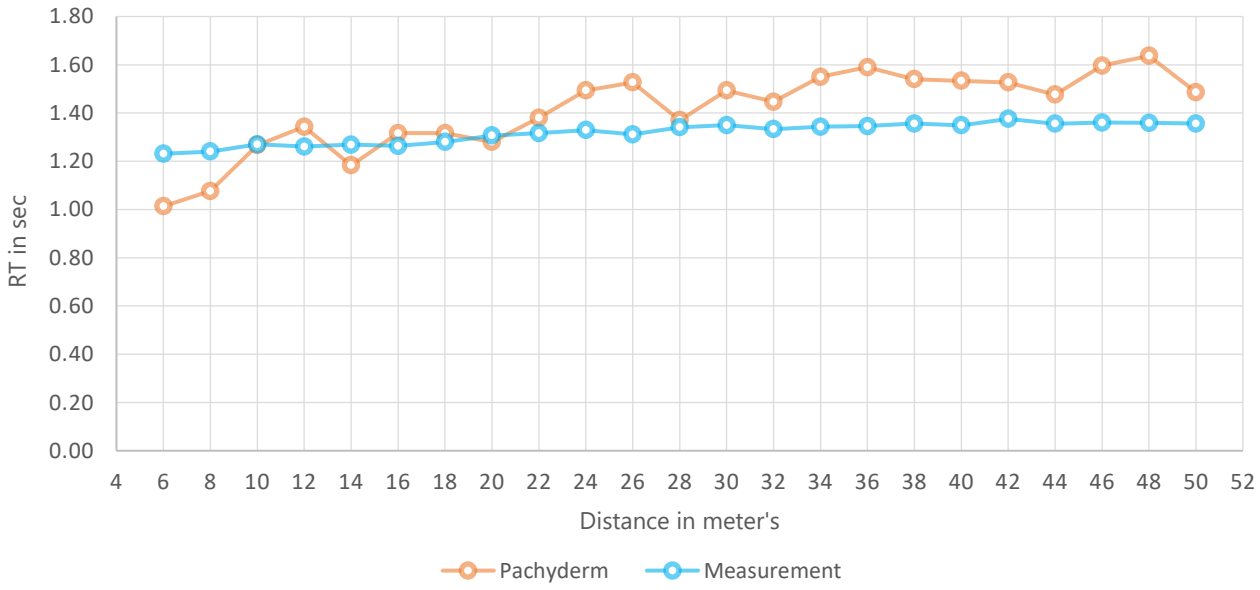

Figure 65 Evolution of average reverberation time for Pachyderm vs measurement along the (S3 configuration)

Since the sound source in Pachyderm is perfectly impulsive (i.e. same sound power level is applied for all frequencies) the sound energy is almost equal for the octave band. Therefore, SPL comparison is performed for 1000 Hz frequency between Pachyderm and on-site measurements (figure 66). The pressure level in Pachyderm follows the expected logarithmic decay as the software simulation is not influenced by the local geometrical features and is performed under constant atmospheric conditions. The logarithmic trend line for calculation follows the trend line for measurement, which indicates that the decay of sound along the street is comparable to the on-site measurements.

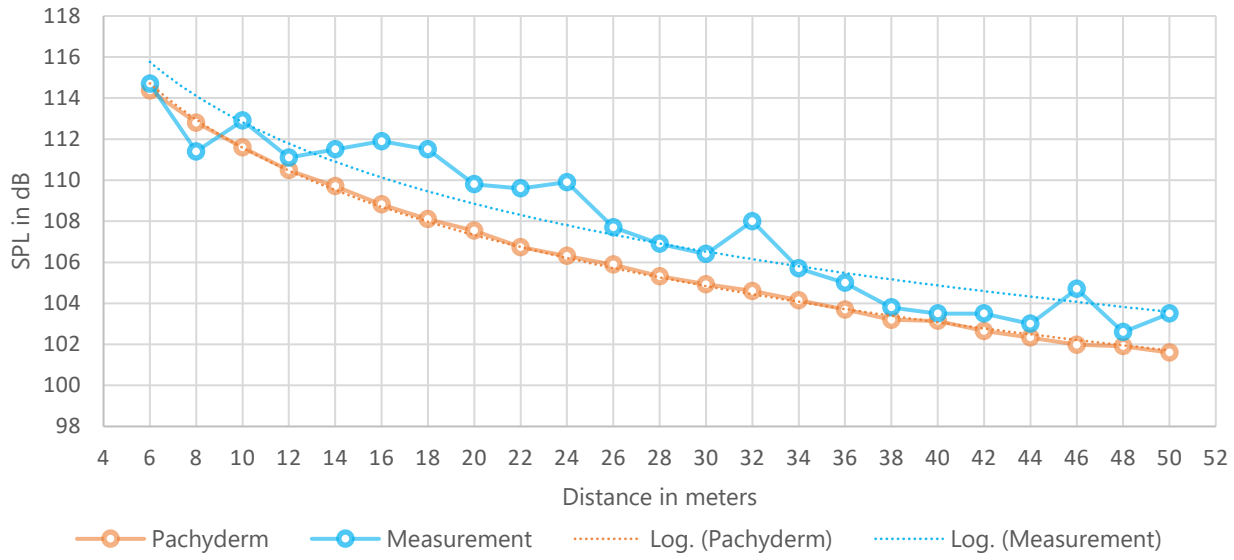

Figure 66 Evolution of sound pressure level along the street for Pachyderm and measurement (S3 configuration at 1000Hz)

Nevertheless, certain peaks can be seen in measurements for example at 24m, 32m and at 46m. The occurrence of these peaks might be the result of a constructive interface that occurs when reflected sound waves coincide with the direct sound wave and amplify. Therefore, manual calculations are performed to verify this phenomenon (please see Appendix B.2 Interference effect). According to calculations it is concluded that the occurrence of these peaks is a result of certain building irregularities present along the street or error in measurements rather than the constructive or destructive interface.

Moreover, the results from Pachyderm are compared with the Sabine-Franklin-Jaeger theory with a correction from Michael Barron (equation 4). Since the equation is used for room-acoustic calculation, few assumptions are made. For example, the entry, exit and roof of the street are assumed to be perfectly absorbent (α=1) and background noise of 40 dB. The comparison (Figure 67) demonstrates that the results conform to each other for only up to 10m, after that the calculated values follow a linear profile while sound pressure levels decrease logarithmically in Pachyderm. At the end of the street (50 m), a difference of 2 dB is noted. So, a larger decay in simulation is a result of more scattering objects in the model with their scattering coefficients than assumed by Barron's formula.

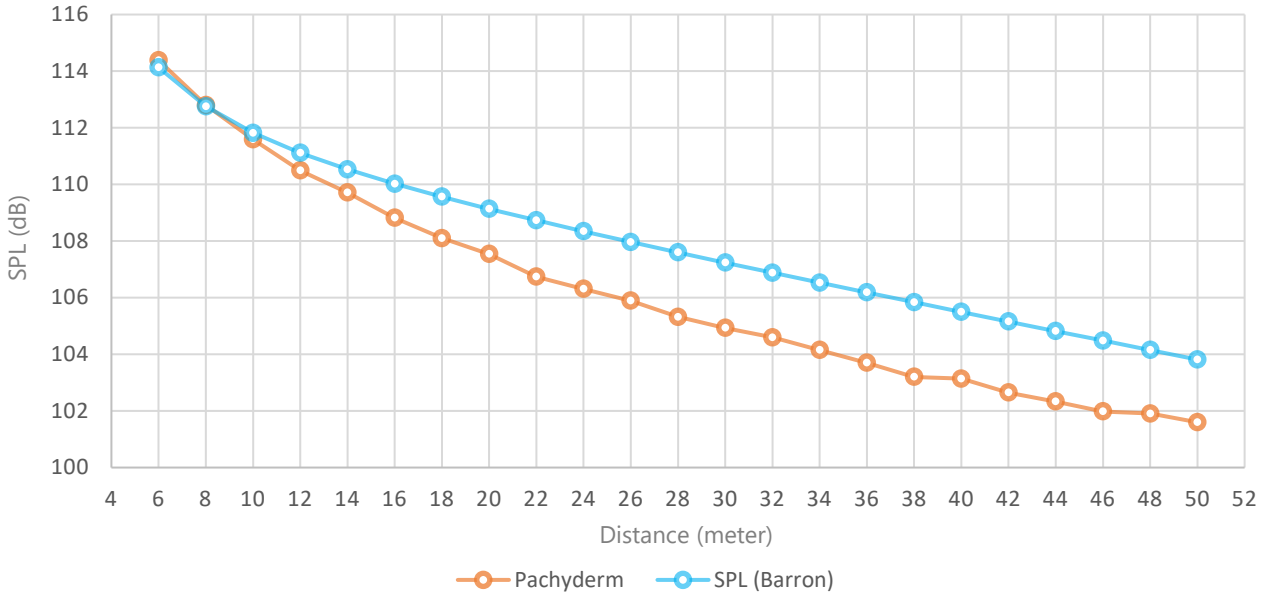

Figure 67 Evolution of sound pressure level along the street for pachyderm and calculation (Sabine-Franklin-Jaeger-Michael theory)

5.1.3.4 Effect of the source position along the street:

As an example, Figure 68 shows that the sound pressure levels in S1 configurations (source in the street) are larger than for S3 configuration (source at the end of the street). Although, not significant, the maximum difference reached up to 0.55 dB with an average of 0.34 dB along the entire street. This specific behaviour can be explained by Figure 69. When the source is at the start of the street (S3), most of the sound energy is lost through the open end. On contrary, when the source is located inside the street (S1), the part of sound energy radiated backwards can be reflected towards the receiver, depending on the building irregularities present in the street. This occurrence is known as back diffusion. However, Figure 68 also shows that the sound decay is not affected by the back diffusion. This is because the extra energy due to back diffusion appears in the late decay, therefore much smaller than the direct field.

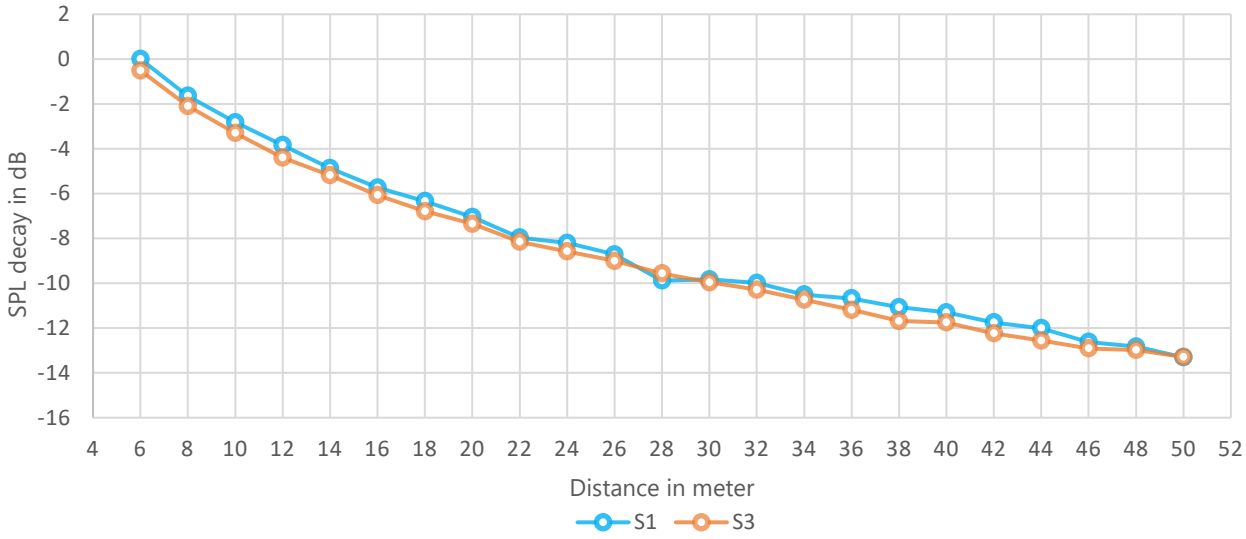

Figure 68 Evolution of the sound levels along the street for S1 and S3 (at 1000 Hz and M5 receiver)

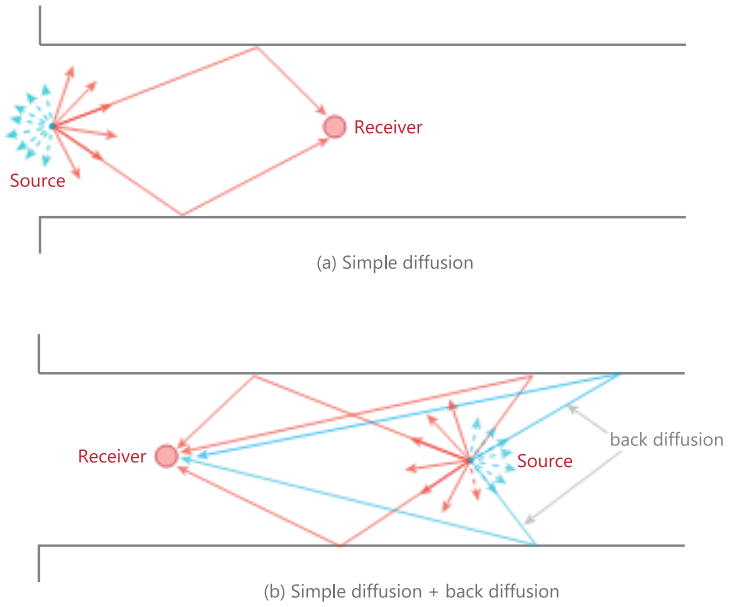

Figure 69 Schematic representation of back diffusion. a) Condition with source at start of the street b) Condition with source at middle of the street

5.1.3.5 Effect of façade irregularities and scattering coefficients

All the results explained in the previous sections are performed for the geometries considering flat surfaces. A totally smooth surface does not exist on a real city street. Irregularities can be seen on a variety of scales, ranging from millimetre-scale roughness on the façade to meter-scale window bays. Although scattering coefficients were given while modelling, it is still a simplification of actual façade surfaces. For instance, Figure 70 shows the building façades along the Kervegan street that consist of a great amount of

articulation. Therefore, to check the effect of these façade irregularities on sound pressure levels, a new 3D model is made considering widows and with a setbacks distance of 0.5 m.

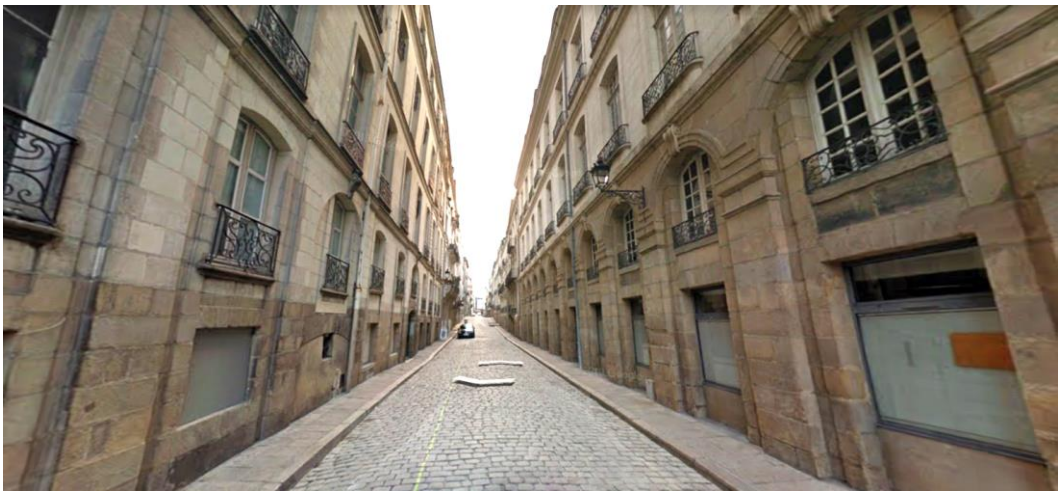

Figure 70 Kervegan street with facade articulations (Reference: Google Earth)

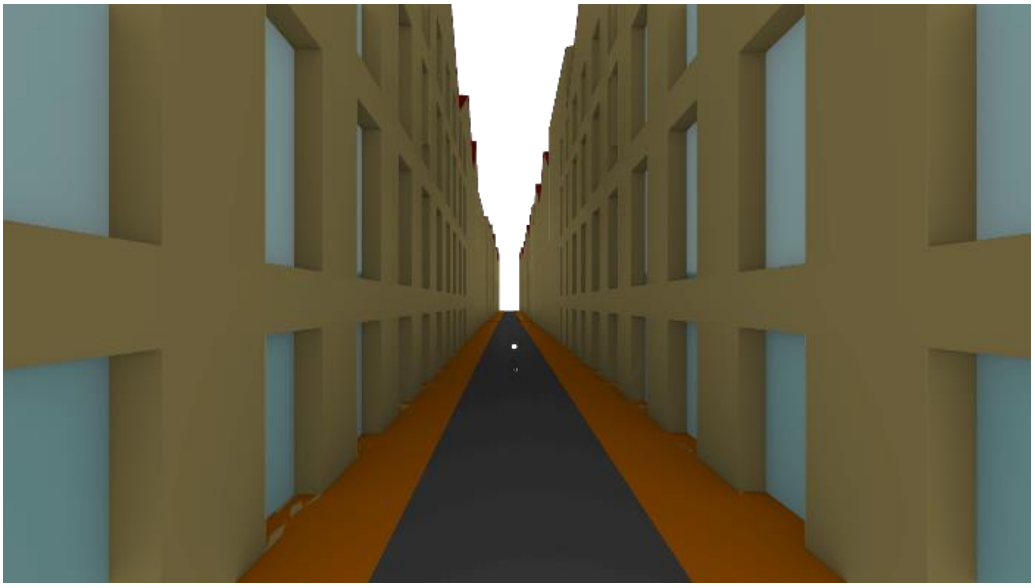

Figure 71 Rhino model with extruded façade

The SPL difference between the flat surface and extruded surface can be seen in Figure 72. For initial 10 meters, pressure levels remain equal, but as the distance from the source and receiver increases the difference also increases. For example, Figure 73 shows the same comparison at 50 m receiver over the octave frequency band. On average 2 dB deviation is noted for lower frequencies (62.5-500 Hz) and 1 dB difference for higher frequencies (1000-8000 Hz). Flat surfaces with scattering coefficient do not include the scattering of rays occurring due to large extrusions like window offset (i.e. more than 30

cm). Therefore, the large, extruded surface leads to more sound attenuation than the flat surface with scattering coefficients.

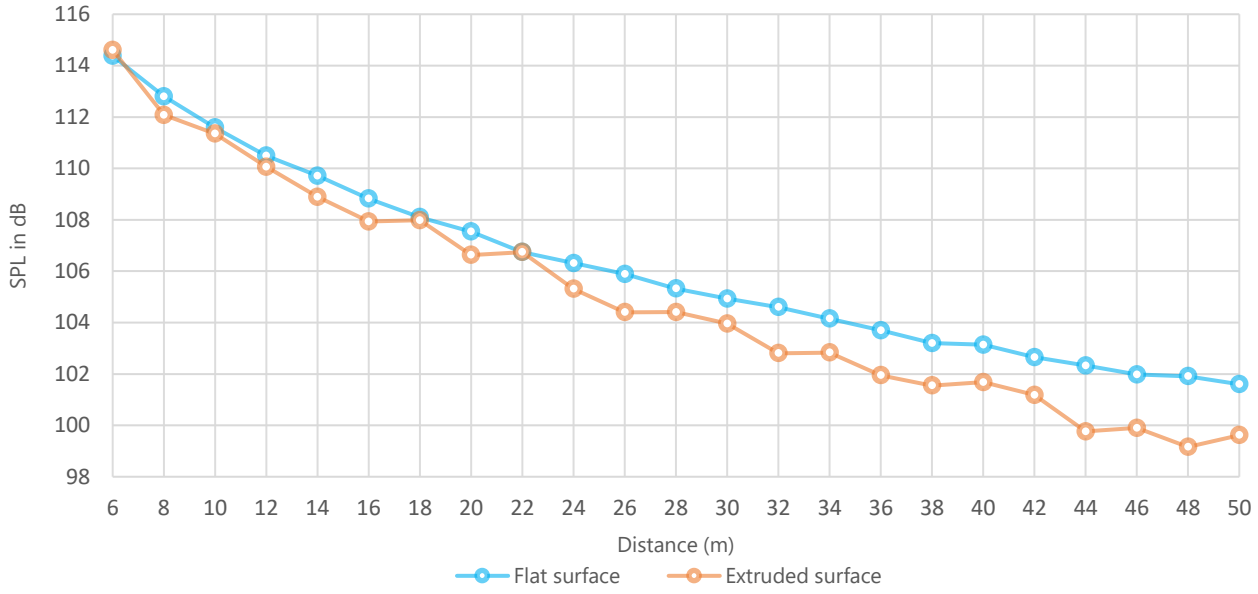

Figure 72 Evolution of sound pressure level for the flat surface and extruded surface (configuration: S3 and M5 receiver at 1000 Hz)

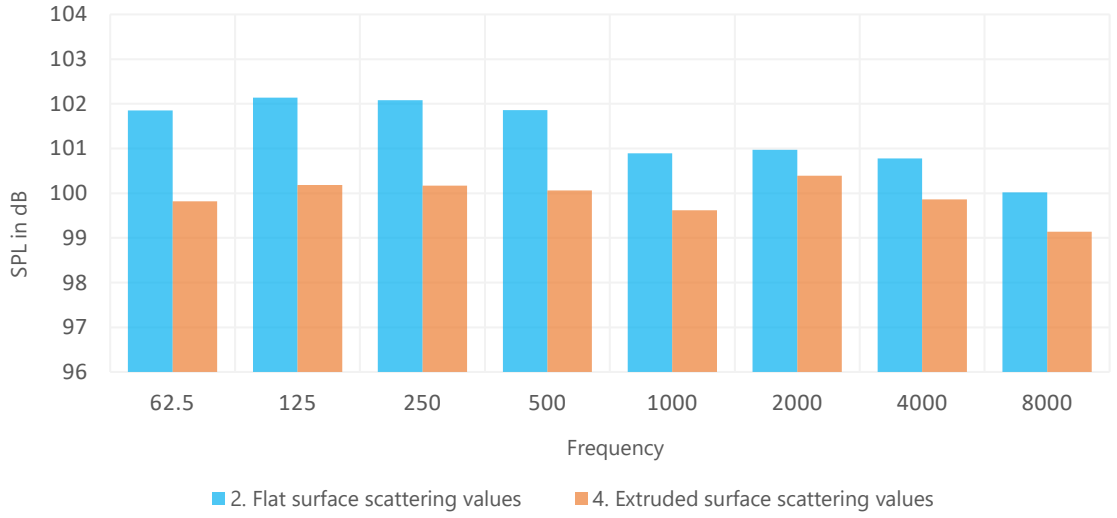

Figure 73 SPL comparison between the flat surface and extruded surface at 50m for octave frequency band (S3 configuration)

5.1.4 Sound pressure level on façade:

After validating the results with case study measurements, sound pressure levels on the façade are calculated using the *Pachy_RH* and *Pachy_GH* plugin. The same case study model (Kervegan street) is used for calculation and comparison purposes. Section 3.2.4.1, represents the results obtained from the *Pachy_RH* plugin and its comparison with

pachy_grasshopper. In section 3.2.5, the results from the Grasshopper simulation are compared against Geomilieu.

5.1.4.1 Mapping Results: Pachy_RH (Pachy_RH)

As discussed earlier, *Pachy_RH* is well advanced in its features and the recent version (Pachyderm acoustics 2.0RC26)[114] can perform traffic and aircraft noise simulation. It has a dedicated line source component where one can assign sound power level over octave frequency band or use the FHWA- Federal Highway Administration (U.S. Department of transportation) model, which uses several inputs described in Table 8.

Parameter	Input
1. Speed of traffic	Kph
2. Pavement type	Dense graded asphalt
	PCC concrete
	Open-graded asphalt
3. Automobiles	NOS/Per hour
4. Medium trucks	NOS/Per hour
5. Heavy trucks	NOS/Per hour
6. Buses	NOS/Per hour
7. Motorcycles	NOS/Per hour
8. Full throttle	Yes/No

Table 8 Input parameters used in FHWA traffic model inside Pachyderm

However, for the analysis, a constant sound power level of 80 dB is used for all frequencies and calculations are based on ISO9613: Part 2 [25] outdoor sound propagation model. To reduce simulation time and consistency of the results only the first 50m of the façade is considered, other simulation parameters are presented in table 9.

Parameter	Value
Sound power level	80 dB
Number of rays	100000
Distance between source to receiver surface	3.7m
Air temperature	20°C
Relative Humidity	50%
Static Air Pressure	10^5 Pa

Table 9 Simulation parameters used for Pachy_RH simulation

Figure 74 represents the results obtained from the *Pachy_RH* simulation. As can be noticed, the sound pressure levels are gradually reducing with increasing height. Moreover, lower values can be observed near the left end, since more sound power is lost towards the open park area. Although the values in the scale can be changed, the

colour scale is not well distributed over the values. For example, values between 54-60 dB are represented by the same green colour (Figure 74). So, if the result range is longer, then it is difficult to comprehend the results.

Although the sound pressure levels are uniformly reducing, the results are 5-6 dB less than expected by the numerical equation. For example, considering the distance between point source and receiver as 3.7m, the SPL should be around 68 dB according to equation (6), however, the observed values are between 62-63 dB. This is because the SPL for different frequencies are not added logarithmically and also geometrical damping is considered in the calculation. Pachyderm uses ISO9613-2 [25] outdoor sound propagation method to predict SPL. Therefore, hand calculations are made to check the validity of the results using the ISO9613-2 model which can be found in Appendix B. The values simulated using *Pachy_RH* follow the hand calculation.

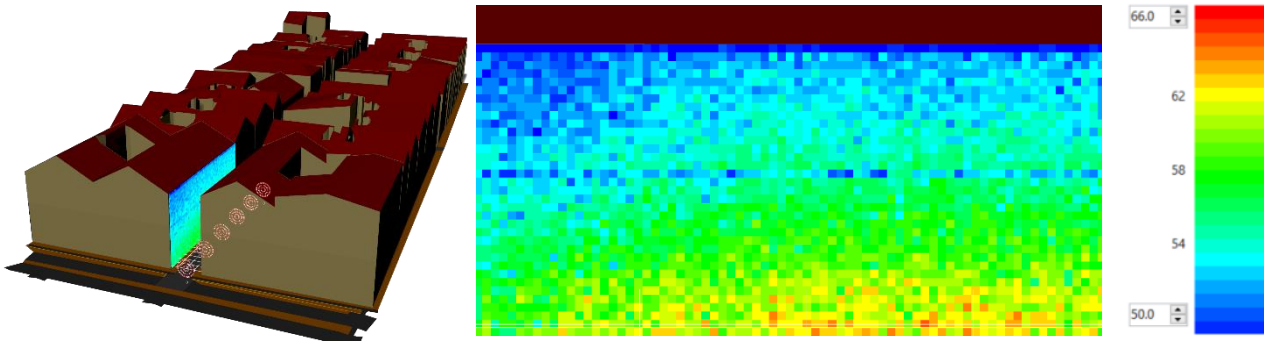

Figure 74 Left: Pachy_RH results in context, right: Pachy_RH results front view

5.1.4.2 Mapping Results: Pachyderm_Grasshopper (Pachy_GH)

To get results from the Grasshopper simulation, the Grasshopper script is further developed. *Pachy_GH* is limited in terms of its features and has no option to model a line source. Therefore, the line is divided into multiple points sources in Grasshopper. The other simulation parameters are kept similar to the Rhino simulation (Table 10).

Figure 75, shows the result from the Grasshopper simulation. The values are in agreement with Rhino simulation i.e. gradually decreasing with the height from 64 dB to 55 dB. However, as explained earlier these values are the flat average over the frequency band, thus 5-6 dB less than expected. Also, Regulations and guidelines are often given in terms of A-weighted values which include sensitivity of the human ear. Therefore, a post-processing frequency correction, as well as logarithmic addition for the frequency band is applied in the Grasshopper workflow. After applying the correction, the values are increased by 6 to 7 dB (Figure 76).

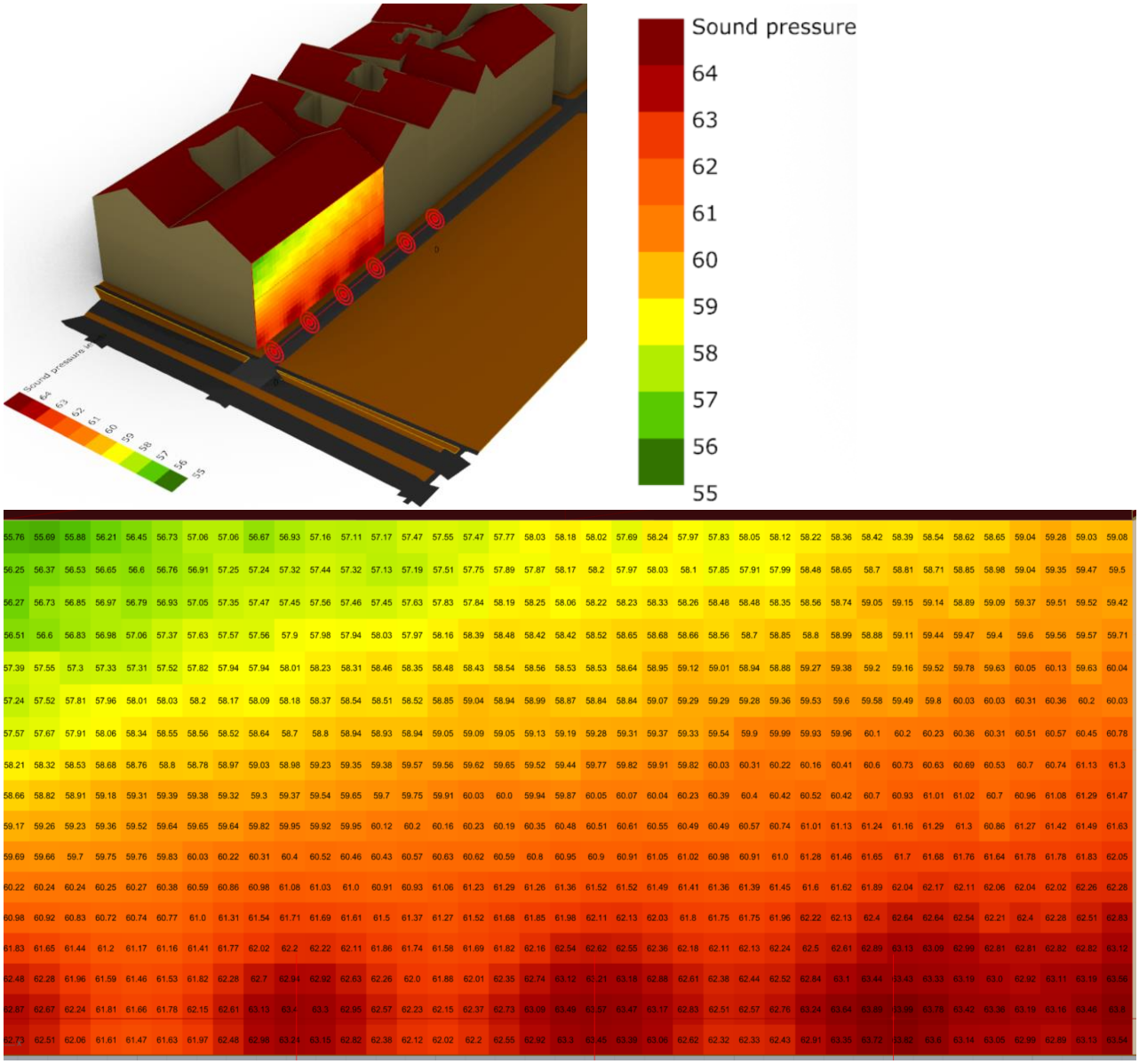

Figure 75 Mapping results for Pachyderm Grasshopper without frequency correction

Although the values are reducing uniformly, peaks with a rise of 1 dB can be observed where the point sources along the line are located. This effect is solved by establishing the relationship between the spacing of point source and distance between source and receiver, given by,

$$X = 2 \times Y \tag{18}$$

here, X is the distance between point sources along the line and Y is the shortest distance between the line source and receiver grid. Figure 77 shows that when the distance between the source to the receiver increases from 3.7m to 5m (half of the spacing between point sources) the effect of point sources disappeared. However, the

relationship is not applicable when the distance between source to the receiver is large. Therefore, it is recommended to perform a few trails to decide the exact distance between point sources along the line.

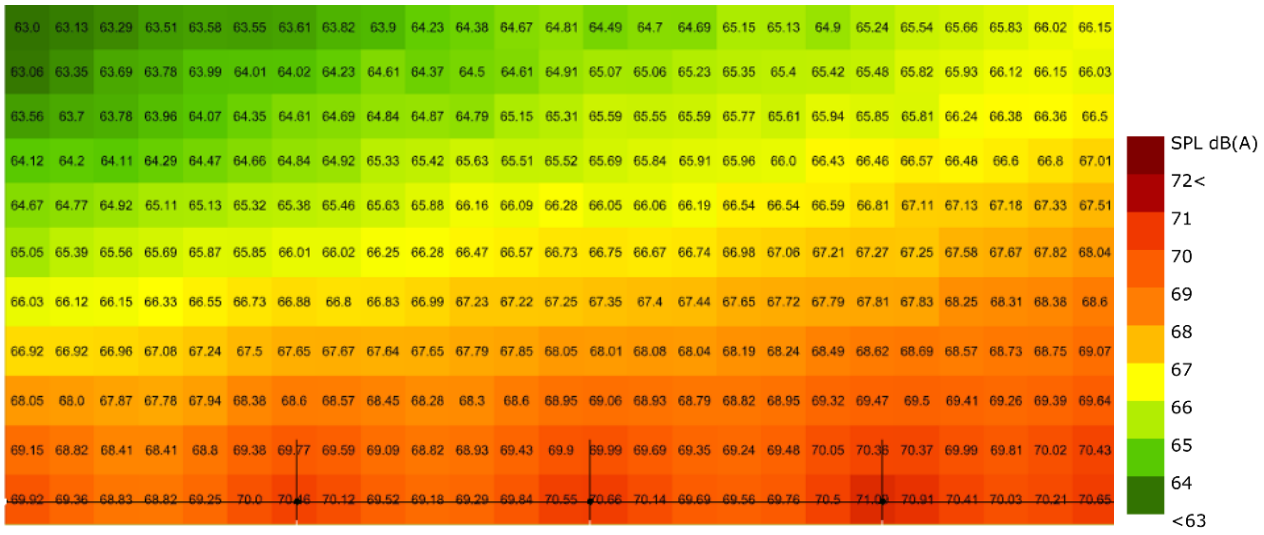

Figure 76 A-weighted SPL on the facade (X=3.5m and Y=10m)

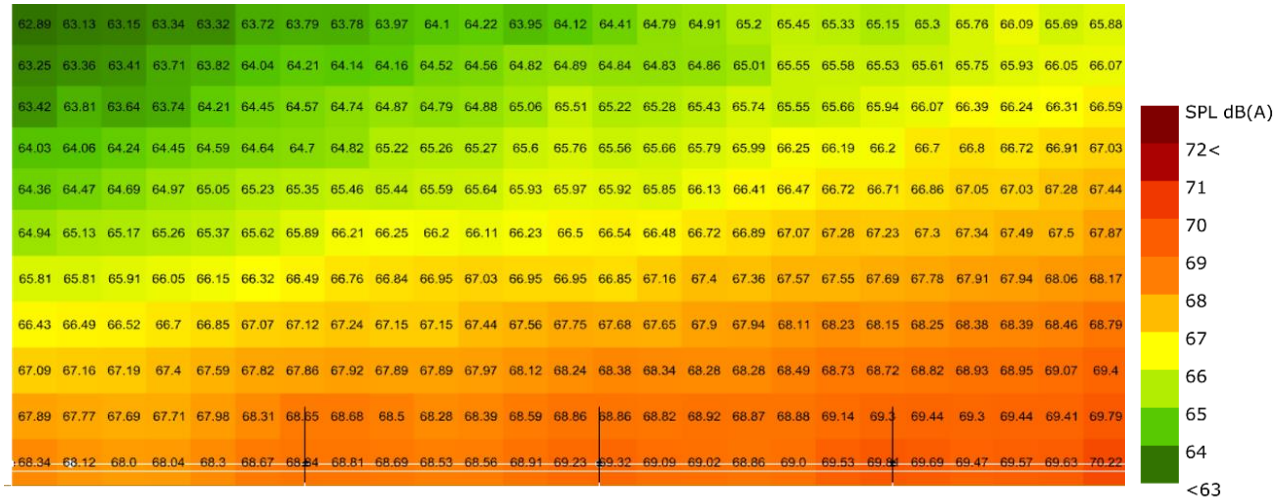

Figure 77 A-weighted SPL on the facade (X=5m and Y=10m)

5.1.5 Geomilieu

Geomilieu (Geo-environment) is a software package developed by DGMR for calculating and mapping environmental noise levels and air quality resulting from traffic and industry. The calculations are based on various national as well as international standards (see table 10). Depending upon the calculation method, it is also possible to compare calculated/ measured values with the tested values. The models can be stored in the

project, so multiple calculation methods can be implemented in a single project. The items in a model consist of sources, objects, calculation points, soil and material definition. Each item includes geographic information, which is related to 3D base data. In practice, the Dutch national coordinate system is used to store this geographic information, however, the coordinate system can be changed using any GIS software. More information regarding models and calculations can be found in [26].

Method	Description
Industrielawaai IL	Dutch calculation method for industrial noise
Industrielawaai windturbines	Dutch calculation method for industrial turbine noise
ISO9613-1/2	International calculation method for industrial and road traffic noise
Wegverkeersalwaai RMW-2012	Dutch road traffic noise method
Railverkeerslawaai RMR	Dutch rail traffic noise method
Harmonoise	European calculation method
SKM Wegverkeersalwaai	Standard mapping method for traffic noise
SKM railverkeerslawaai	Standard mapping method for rail traffic noise

Table 10 Noise calculation methods available in Geomilieu

5.1.5.1 Model set-up:

To keep the impartial comparison, Geomilieu is also tested with the ISO9613 outdoor noise calculation method and for the same facade. The 3D model is made using the same OSM file that was used to make the Rhino model and QGIS is used to define the "Netherlands RD New (EPSG:28992)". Figure 78 shows the 3D model in the Geomilieu environment. Point to note that the inclined geometries and extrusions cannot be modelled in Geomilieu, thus the roof profiles are missing in 3D geometry. Other calculation parameters like length of the line source, its position etc. are also modelled similar to the Grasshopper setup. Table 11 represents the simulation parameters used for the calculation.

Figure 78 Kervegan street in Geomilieu, Left: Plan view, Right: 3D perspective

Parameter	Value
Sound power level	80 dB (flat over all octave frequency)
Ground effect	0 (represent hard soil)
Distance between source to receiver surface	3.7m
Environmental factors	
1. Air temperature	20°C
2. Relative Humidity	50%
3. Static Air Pressure	10^5 Pa

Table 11 Simulation Parameter's used in Geomilieu calculations

Environmental factors like temperature, RH and static pressure are important for the calculation of 'sound attenuation due to air'. For the given values, Geomilieu calculates the air attenuation coefficient for the octave frequency band which can be seen in table 12.

Frequency (Hz)	63	125	250	500	1000	2000	4000	8000
Air absorption (dB/km)	0.12	0.45	1.32	2.73	4.66	9.86	29.42	103.91

Table 12 Frequency-based air absorption applied in Geomilieu

5.1.5.2 Mapping results: Geomilieu

Figure 79 represents the results from the Geomilieu simulation. Similar to the Grasshopper results, the SPL levels are decreasing with height as well as towards the open end of the street. Unlike the Grasshopper simulation, Geomilieu is capable of simulating line sources i.e. cylindrical spreading, thus the effect of point sources is not

present. However, it represents the values in contour points thus, colour contours are clearly visible.

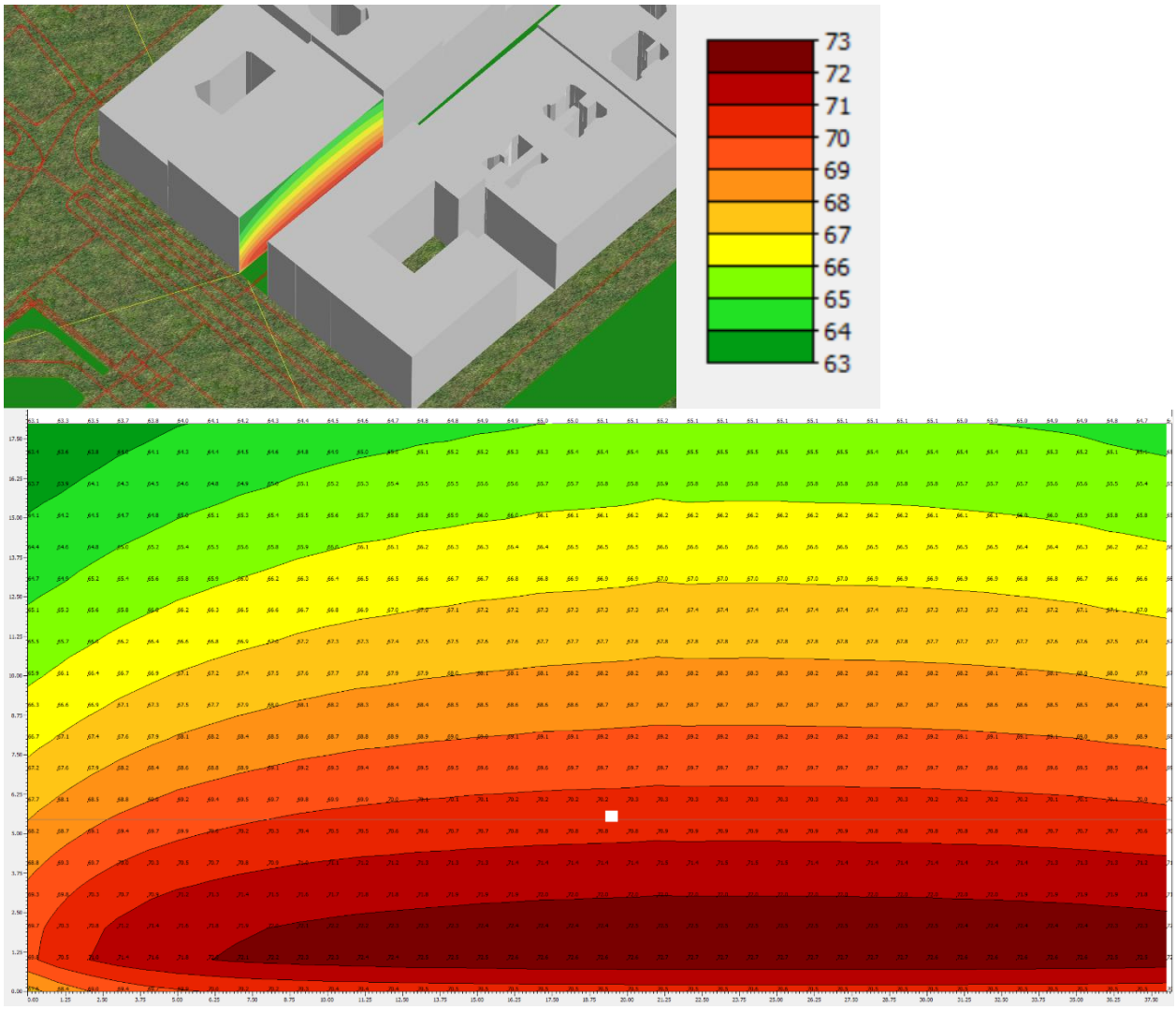

Figure 79 A-weighted SPL on façade for Geomilieu simulation

When these values are compared with the Grasshopper simulation (see Figure 80), a difference of 1 to 4 dB(A) is noted. Since the line source is represented as a point source in Grasshopper, the difference is greater with a variation of 4dB(A) near the source (dark red). However, this difference gradually decreases with increasing the distance between the source to the receiver. For example, towards the top left corner, the Geomilieu mapped 63.3 dB(A) while Grasshopper results also have SPL that ranges between 62-63 dB(A).

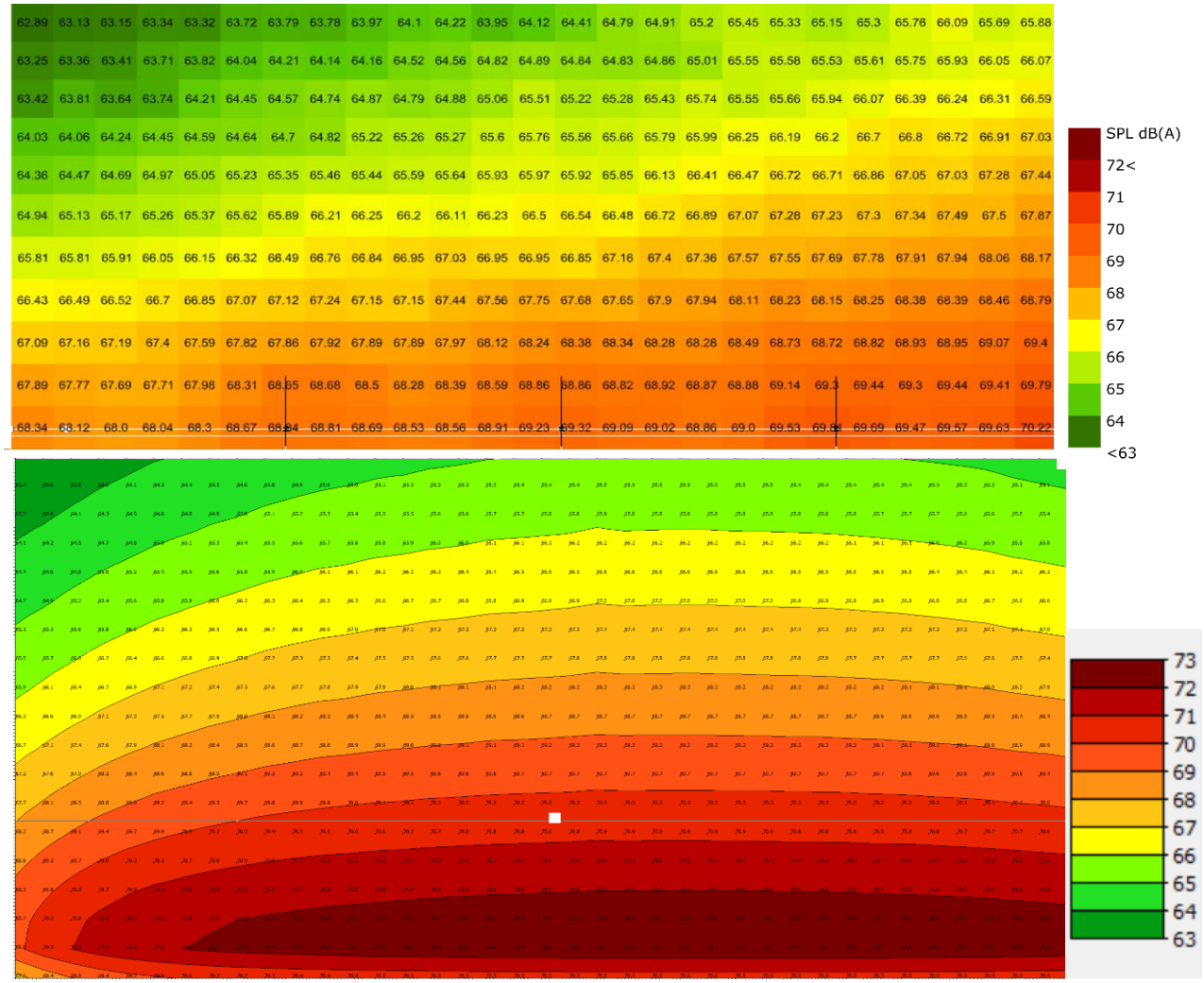

Figure 80 Top: Grasshopper SPL mapping results vs Bottom: Geomilieu mapping results

5.2 Summary

The most important findings from the validation study are listed below. These points serve as a design guide for designers who plan to use the workflow.

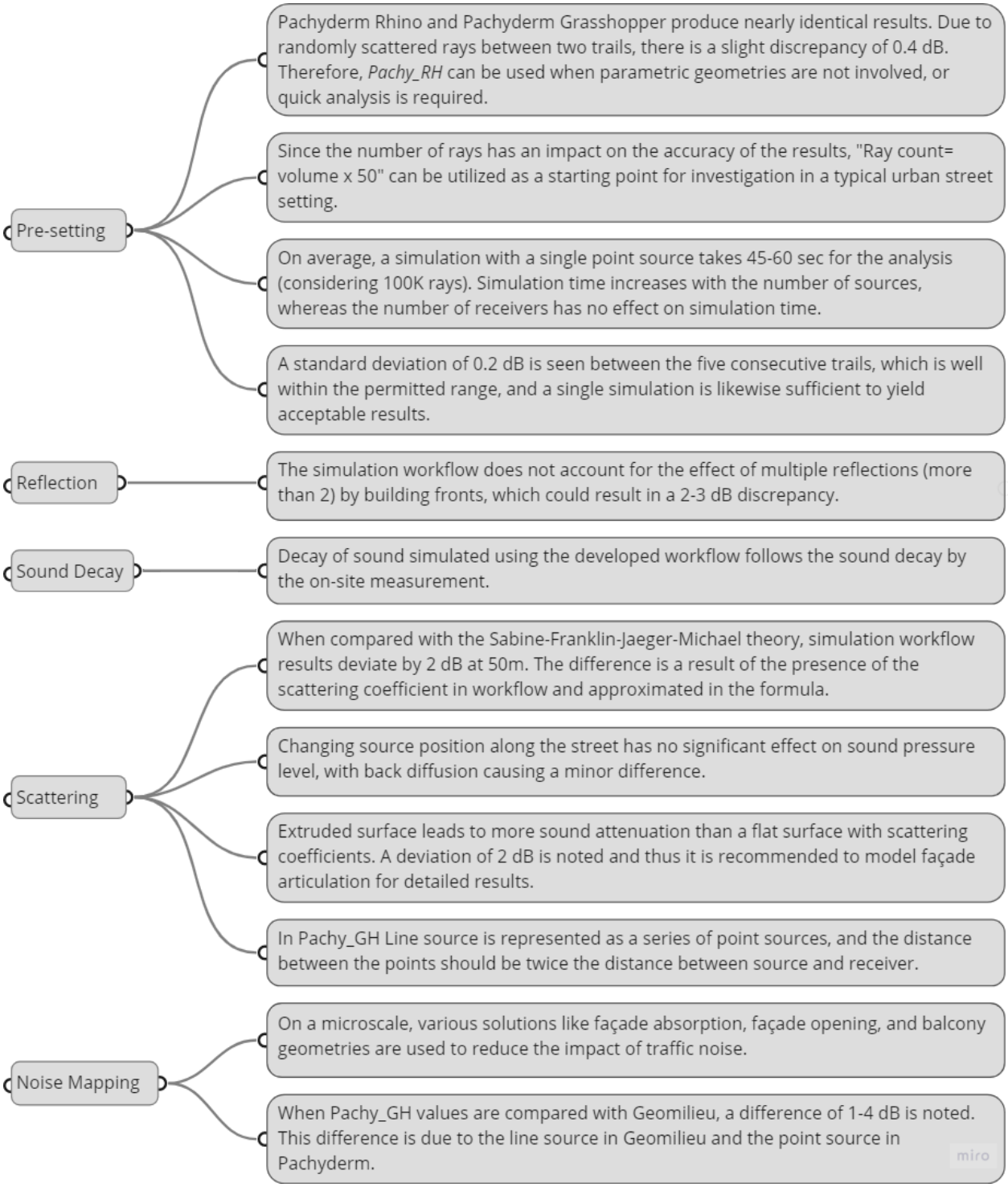

6

Design

Part 6 Design

6.1 Case Study

To test the developed parametric workflow a case study project called Entrée Zoetermeer is selected. Entrée is an innovative urban development that is going to be constructed in the new city district of Zoetermeer. It is critical for this project that the proposed geometrical and material variations lead to a quieter atmosphere. The mixed-use neighbourhood will be built on both sides of Afrikaweg and will include 4500 new houses, workplaces, and commercial spaces. The buildings are subjected to significant noise levels due to their proximity to the A12 national highway and Afrikaweg, making it an ideal context to test the proposed. Figure 81 illustrates the context.

6.1.1 Case Study Design Context

Because the area under the project Entrée is so large, just a small section of the design environment is chosen., as shown in figure 76. The length of the street was modelled in around 130m; the total width of the street (from building face to face) is 66 meters and consists of three roads with three lanes each. The buildings along the street consist of office/commercial spaces on lower stories and residential towers on top. The height of lower building blocks (offices) is 27m on both sides. Residential tower 1 (RT-1) is 45m high and residential tower 2 (RT-2) is 80 meters in height, see Figure 82. The design context also consists of a courtyard with a cross street opening width of 12.5m.

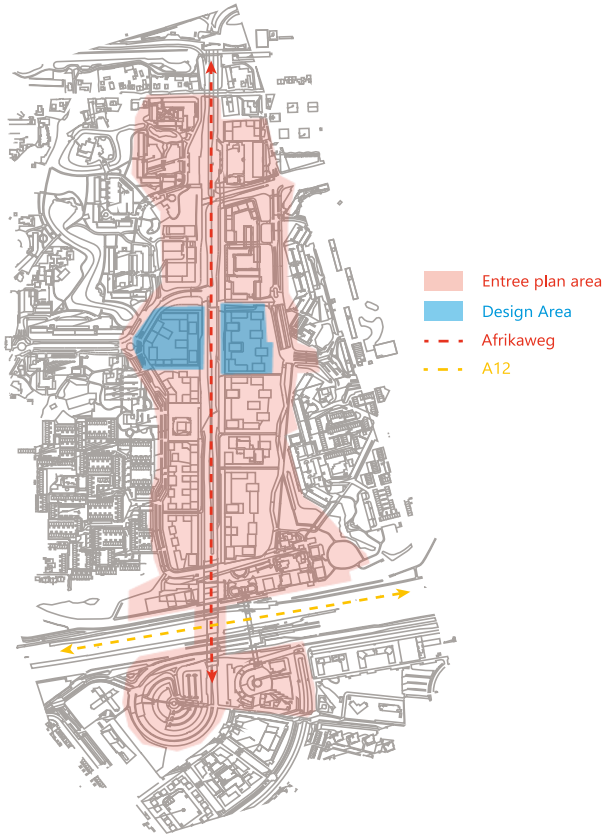

Figure 81 Entree Zoetermeer development plan

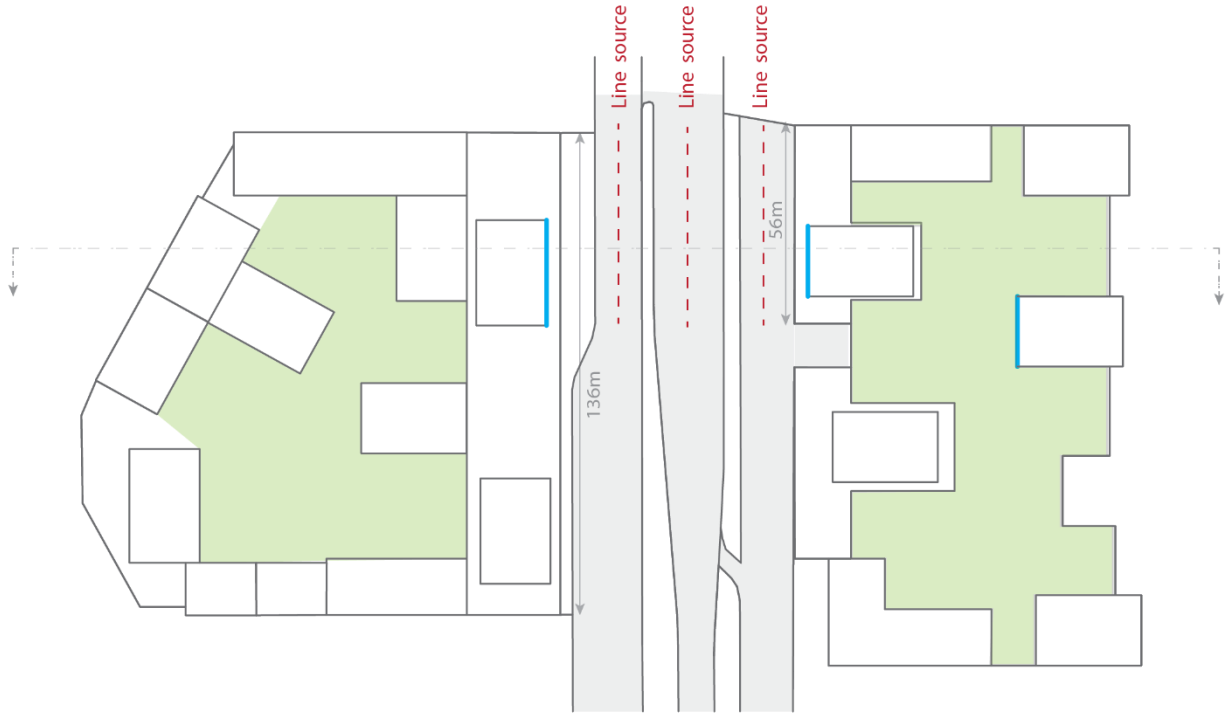

Figure 82 Design Context Plan

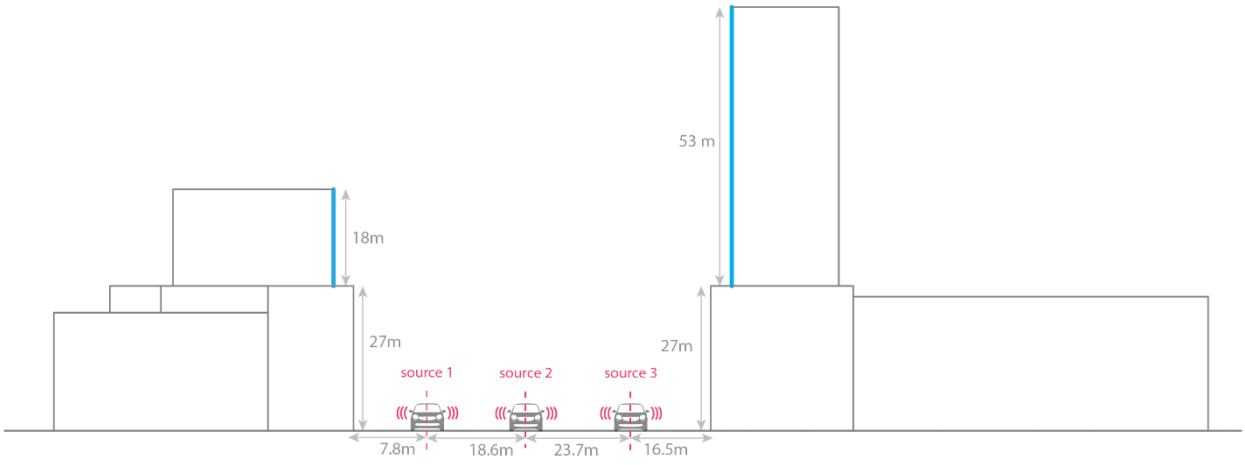

Figure 83 Design context section

6.2 Design variations

To evaluate the effects of urban context on noise reduction, several design variants are tested. These variants are chosen from the available literature about the effect of façade features on the acoustics of street canyons. In particular, the research by Echevarria Sanchez[81] explores the consequences of different façade features in reducing traffic noise. Given the context, the design variants are divided into two groups:

1. Acoustical consequences of geometrical variation
2. Acoustical consequences of material variation

6.2.1 Geometrical variation

First, the acoustical effects of geometrical sequences are tested without taking material variation into account. The geometrical sequences are separated into urban micro-scales, which are also criteria that designers consider early in the design process. For example, the inclination of the façade, openings in the façade, location of the courtyard and effect of semi-outdoor spaces and façade extrusion.

6.2.1.1 Façade inclination (F1)

Because the angle of the façade has a significant impact on sound reflection, three scenarios were tested: absolutely vertical, 80° downward inclination, and 100° upward inclination. These inclinations are applied to the facades on the lower stories (offices) and their impact is tested on the residential towers. These variations are illustrated in Figure 84. Point to note that, in the case of a perfectly vertical façade and 80° downward inclination case, the upper residential towers make an offset with lower building blocks. These offset distances are shown in Figure 84 and greatly affect the results.

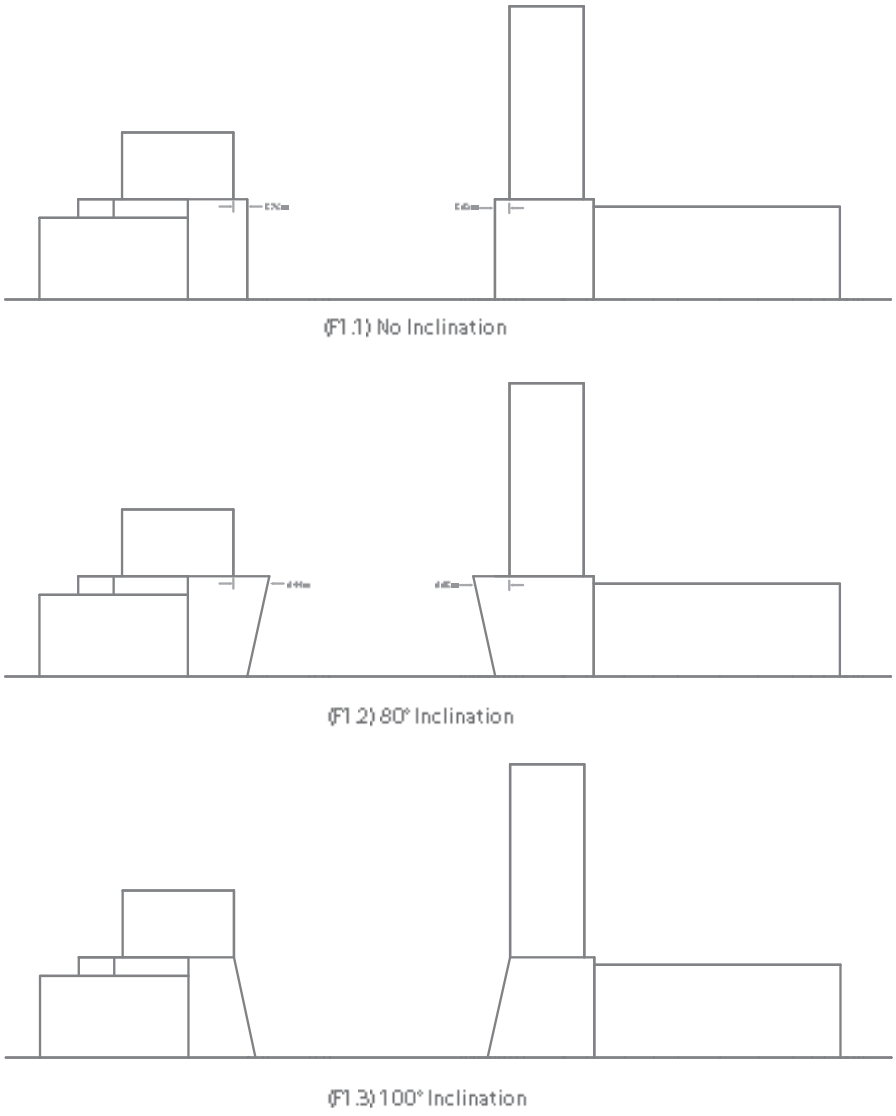

Figure 84 Facade inclination sequences

6.2.1.2 Façade Extrusion (F2)

Façade extrusions scatter the sound rays in different directions and thus play an important role in reducing the sound pressure level along the street. To test the effectiveness of the façade extrusion, two geometrical cases are made with triangular prominences. Figure 85 illustrates the variations and dimensions of the extrusion. In the first case, the lower and upper angle are arranged in such a way that they shift the apex of the triangle towards the top and the second case is just a mirror of the first with the apex toward the bottom. These extrusions are applied on a lower story façade and the consequences are tested for residential towers. Moreover, frequency depended scattering coefficients are also applied to these extrusions. and table 13 shows the scattering coefficients.

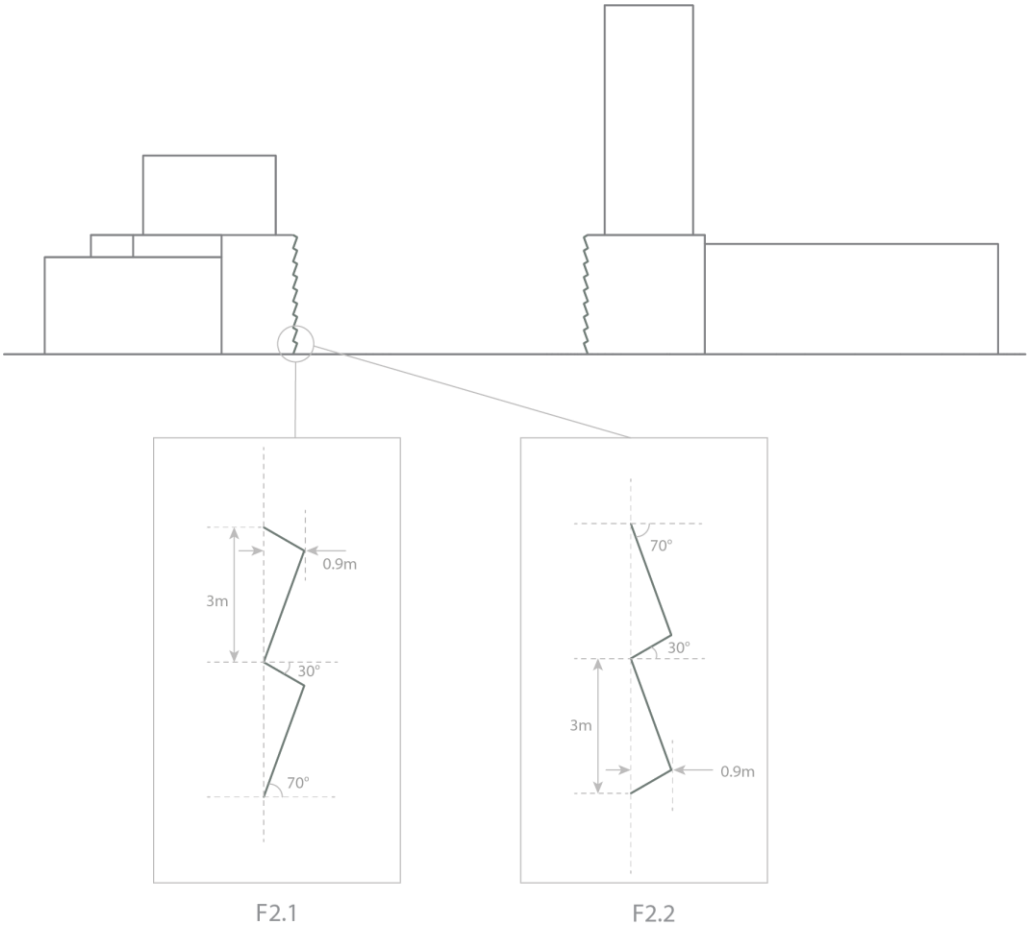

Figure 85 Facade extrusion sequences. F2.1: Apex toward the top, F2.2: Apex towards the bottom

Frequency	62.5	125	250	500	1000	2000	4000	8000
Scattering Coefficient	0.38	0.33	0.27	0.22	0.25	0.27	0.27	0.14

Table 13 Scattering coefficient applied to triangular extrusions[64]

6.2.1.3 Façade material (F3)

A green façade provides effective absorption as well as the scattering of sound, and in addition, creates a pleasing urban space. The effect of a green façade on sound absorption is studied in [143], [144]. Therefore, as a material variation, a green façade is tested by creating a uniform (checks) pattern on the façade in such a way that the effective area covered by the green façade is 50%. Similar to façade extrusions, this pattern is applied on the lower block of the building façade (Figure 86) and the upper residential façade is tested.

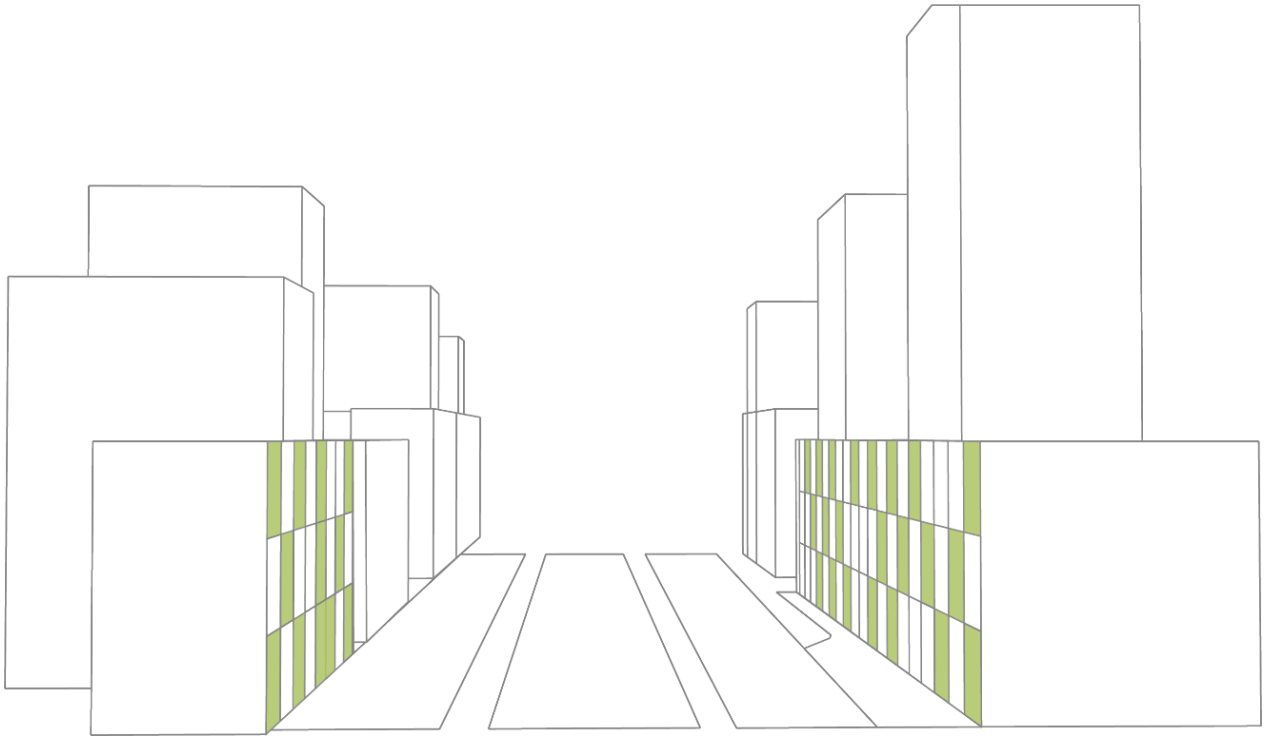

Figure 86 Material sequence: Green façade with (50%) pattern on façade

6.2.1.4 Courtyard

According to END, urban quiet side and quiet façades play an important role in urban environments. In a report[31] END proposed plans to protect these quiet areas against an increase in noise. Moreover, many large-scale residential projects include urban parks or courtyards in their urban planning. Therefore, it becomes necessary to check the noise levels of these protected areas which mostly depend on building heights, roof shapes and cross street opening. The impact of building height and roof shapes is greatly influenced by the diffraction phenomenon and better prediction can be done using wave-based simulation. The recent Pachyderm version does not support edge diffraction and therefore only the effect of the cross-street opening is tested as a courtyard variation.

In the early phases of the design, openings in the façade or entrance to the urban park still hold relevance because sound can penetrate through these openings and can affect the quiet side. In total, four variations are tested by considering two locations of street opening (C1.1 & C1.2) and two material variations (C2.1 & C2.2) please see Figure 87. In a material variation, a green façade is applied on the sidewalls of the entrance (C2.1 and C2.1 in Figure 87) by keeping the position of the street opening the same.

Figure 87 Courtyard sequences. C1.1: Entrance at 56m (Base case), C1.2: Entrance at 66m (10m offset case), C2.1: Base case with green wall at entrance, C2.2: 10m offset case with green wall at entrance

6.2.1.5 Balcony variation (B1)

Semi-outdoor spaces like balconies and loggia are important architectural features of the building which act as a buffer between outdoor noise and indoor space. Moreover, they also act as a diffusing element in a street, and their presence and shape have been greatly studied by many scholars. Thus, four variations are tested, two with normal acoustical ceiling extension and another two with the sound-absorbent ceiling (see Figure 88). To check the influence of height, two locations 20m and 30m from the ground are explored, thus making four cases.

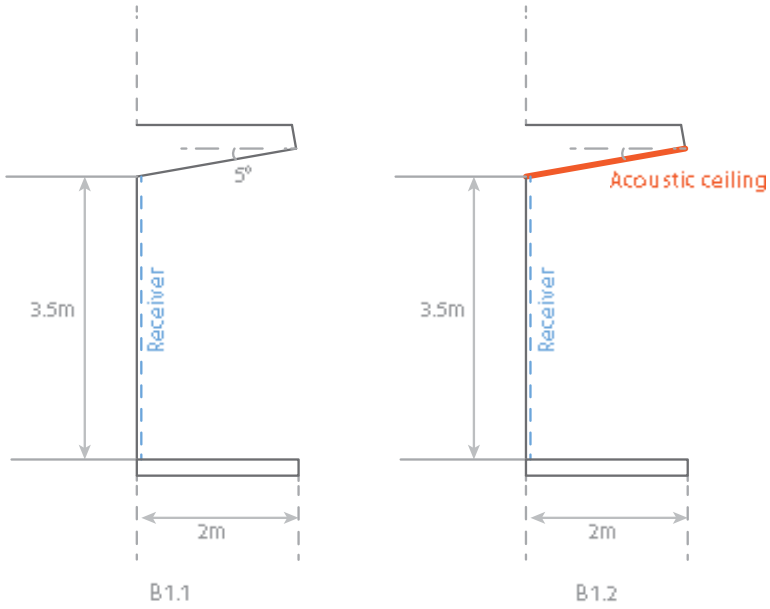

Figure 88 Balcony Sequences. B1.1: Balcony with the normal reflective ceiling. B1.2: Balcony with sound-absorbing ceiling

6.3 Simulation Parameters

6.3.1 Source

Three-line sources are modelled representing the centre of three lanes (Figure 83). The line sources are divided into points with a 16m distance between them (based on equation 28) and 0.5 m height from the ground (see Figure 89). Each point source is given 80dB power which is constant over the frequency band. Moreover, a hundred thousand (100,000) rays are casted from each point source so that the total number of rays are approximately equal to volume times 50

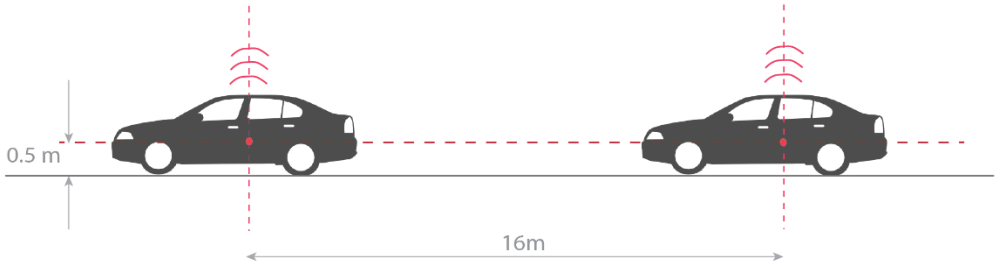

Figure 89 Line source concept used in the simulation

6.3.2 Receiver

Because of limited RAM, machine (computer) used for simulation can only handle data points (number of receivers) less than six hundred. Thus, testing surfaces are divided into data points with varying grid sizes so that fine mesh can be produced while compromising for computational power. The relationship between tested surface, grid spacing, and data points is given in table 14.

Tested Surface	Grid Size	No. of Points
Residential tower 1	1m x 1m	360
Residential tower 2	1.7m x 1.7m	510
Courtyard	1.2m x 1.2m	400
Balcony	0.2m x 0.2m	70

Table 14 Number of receivers corresponding to tested surface

6.3.3 Material Properties

All geometries are assigned with absorption coefficients given in Table 15.

Frequency	Road	Building facade	Grass cover	Green facade	Acoustic tiles
62.5	0.01	0.04	0.40	0.85	0.09
125	0.02	0.04	0.40	0.85	0.09
250	0.02	0.05	0.45	0.83	0.28
500	0.04	0.06	0.50	0.70	0.78
1000	0.10	0.08	0.20	0.68	0.84
2000	0.08	0.04	0.30	0.68	0.73
4000	0.05	0.06	0.35	0.66	0.64
8000	0.05	0.06	0.35	0.66	0.70

Table 15 Absorption coefficient used in the simulation [64][141][145]

6.4 Results and Discussion

Results are presented according to the tested sequences, where changes are made with respective base reference geometry (Figure 83). Sound pressure levels are represented along the façade surface in a colour grid format while the comparison is made using the box plot representing range of data points. Five cases evaluate the effect of façade shape and material properties (F), four cases assess the impact inside the courtyard (C) and two cases measure the impact of the balcony (B) and its materiality.

6.4.1 Sequence 1: Inclination of façade (F1)

Three variations of façade inclination are tested in this sequence (Figure 84). Only lower stories are geometrically adjusted and their consequences on upper-level façades are evaluated. Results demonstrate how overall façade inclination has a significant impact on noise levels.

In the case of a perfectly vertical façade (F1.1- standard case), the SPL values are increasing with height for RT-1 and decreasing with height for RT-2 (Figure 91). This variation is a result of the position of line sources. For RT-1, line source 1 (near the building) is blocked due to the 3.75m offset between two levels (see Figure 90) for most of the façade. However, that same line source then contributes to the additional 1 dB(A) at the top of the façade. The conclusion also holds for the results at the bottom of the façade, where only direct sound from source 3 and reflected rays from other two sources can reach. This effect is also visible for RT-2 where the offset is 3.92m. At the bottom of the façade, 3-4 dB(A) reduction is obtained because it is the shadow zone for line-source 3. At the extreme bottom (green stripe), no direct sound can reach, and the values are purely due to reflection from the opposite façade. The effect of the shadow zone is illustrated in Figure 90.

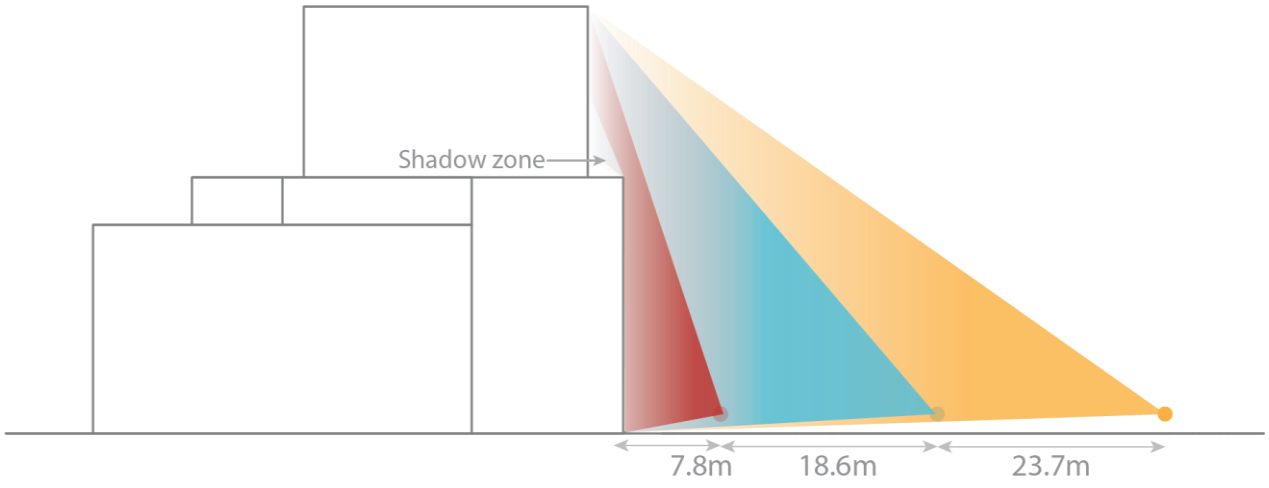

Figure 90 Effect of shadow zone

Upward inclined façade (F1.3-100°), should ideally reduce the sound pressure, as upward inclination reflects sound towards the sky. However, the effect is negative in the tested scenario. The sound pressure level of each tested point is increased as the inclination directs the reflected sound towards the tested façade. From Figure 92 and Figure , one can see that the number of data points are concentrated higher in the box plot, indicating an increased sound pressure level.

On the other hand, the downwardly inclined façade (F1.2-80°) restricts the sound within lower stories and the impact of sound on the higher residential tower is decreased. The mean as well as range of data points is reduced as compared to F1.1 and F1.3 cases (Figure 92 and Figure). The values below 51 dB(A) in Figure 92 is a result of the shadow region and thus can be ignored.

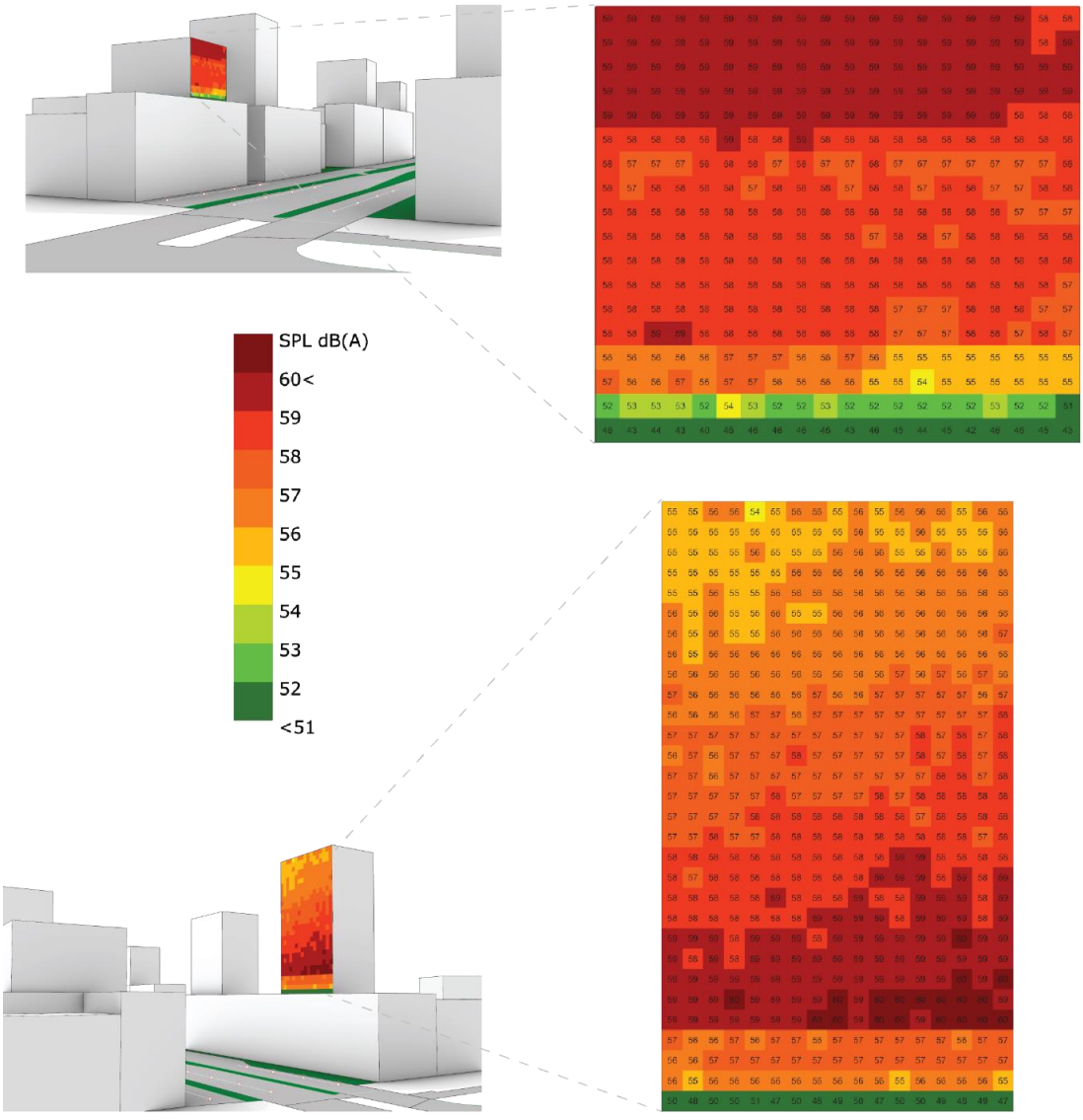

Figure 91 Sound pressure levels on façade for the Base case F1.1

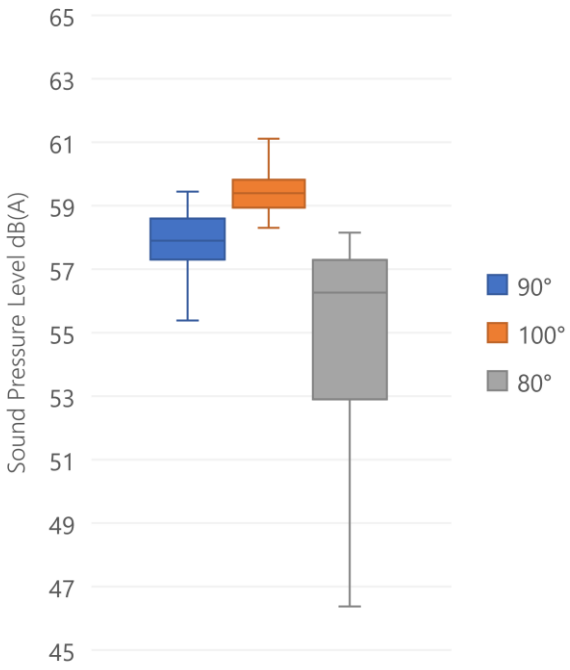

Figure 92 Box plot: SPL data distribution between different facade inclinations for RT-1

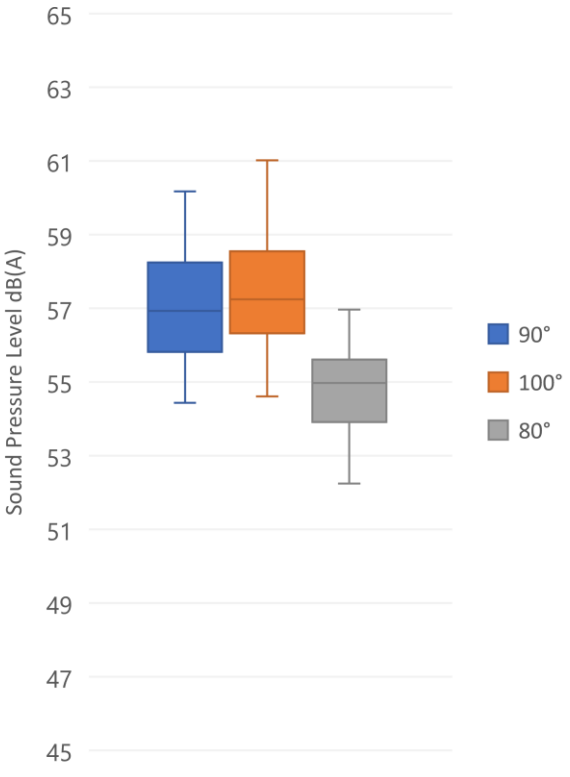

Figure Box plot: SPL data distribution between different facade inclinations for RT-2

6.4.2 Sequence 2: Façade Extrusion

Two variations are tested with triangular façade extrusion (F2) (Figure 85). Although the addition of triangular irregularities on the lower story façade scatters the sound, the intensity of the sound pressure level is not significantly reduced. When the results are compared with the base case, a slight decrease of 1-2 dB for each data point is observed (see Figure 93). Figure 94 shows the comparison between all three scenarios for residential tower-1. The figure illustrates that the decrease is more significant in the case of the extrusion with the apex at the bottom (F2.2) as compared to the case with the apex at the top (F2.2). A similar trend can be observed for residential tower 2, however, the effect is very less (Figure 95).

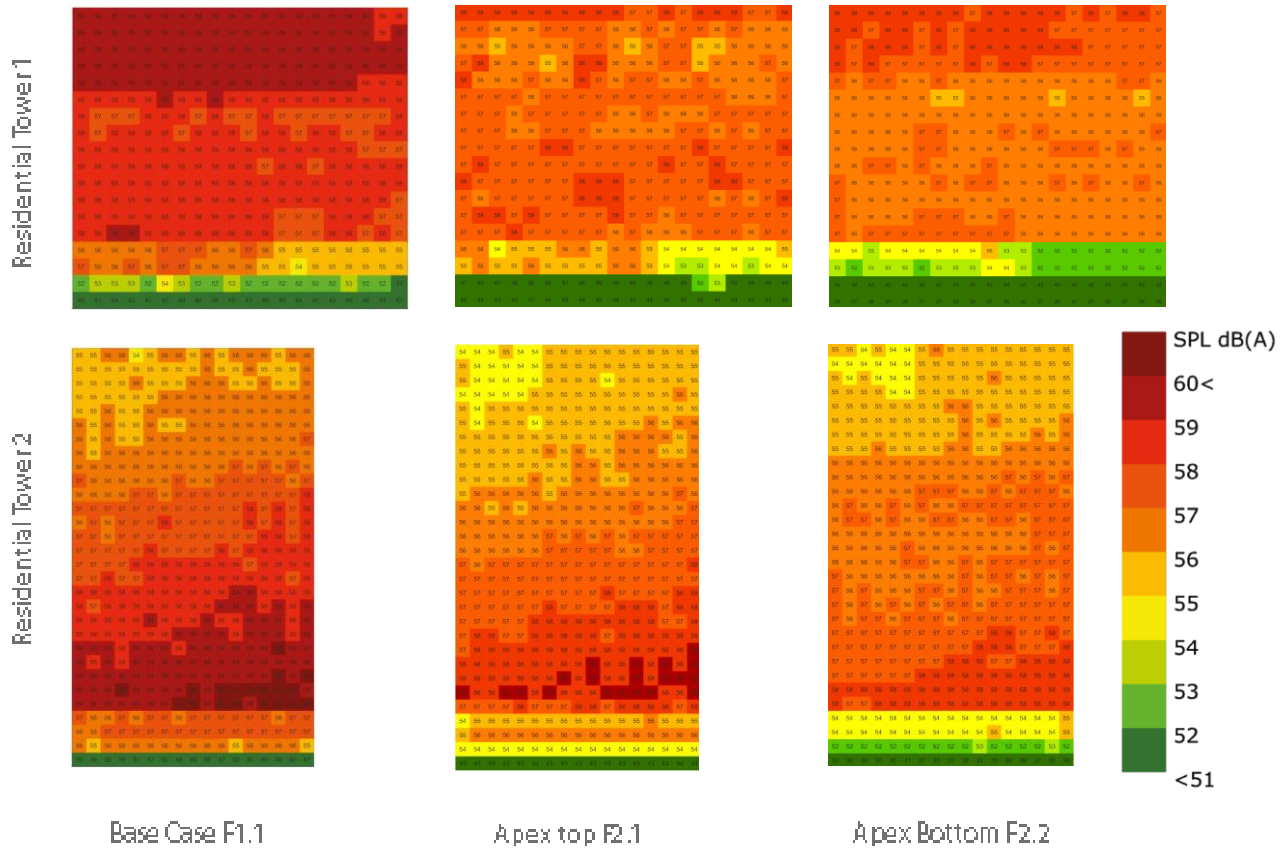

Figure 93 Sound pressure levels on façade for extrusion sequence F2.1 and F2.2 compared with base case F1.1

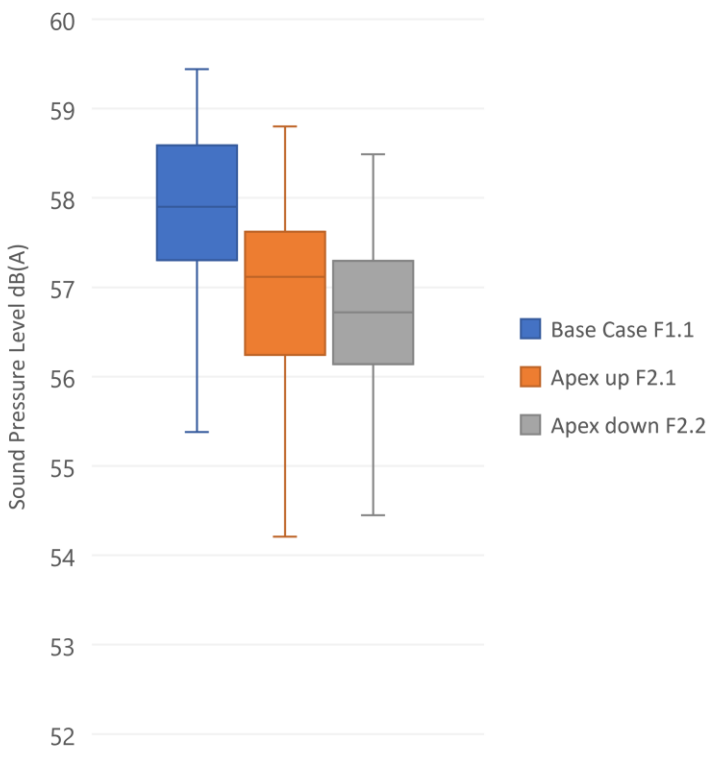

Figure 94 Box plot: SPL data distribution between different facade extrusion sequences for RT-1

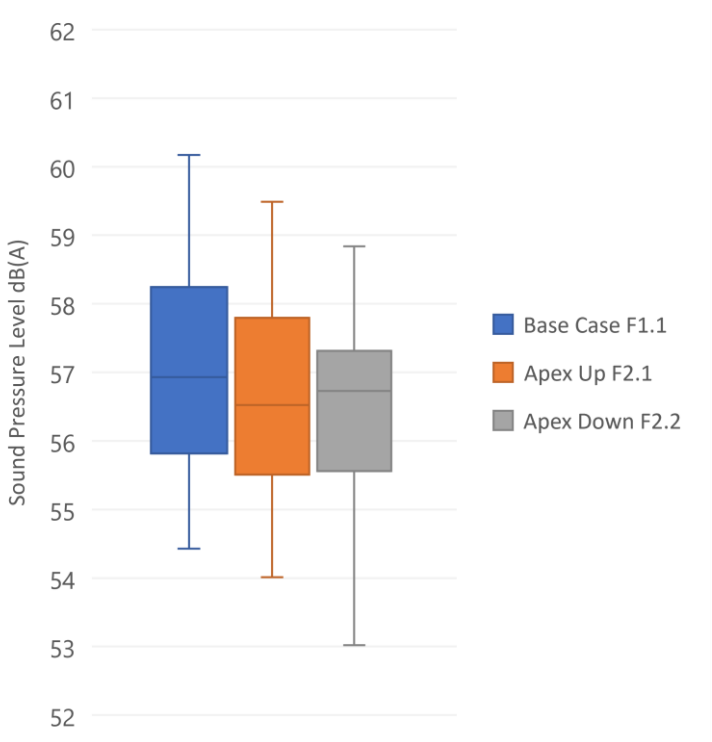

Figure 95 Box plot: SPL data distribution between different facade extrusion sequences for RT-2

6.4.3 Sequence 3: Façade material variation

All the previous cases were tested with the surface having a standard absorption coefficient according to table 2. Thus, in this sequence, the standard case is tested with 50% of the green façade applied in the lower façade in the pattern shown in Figure 86.

On average, the sound pressure level of each data point is reduced by 1-2 dB(A) as compared to the standard case without material variation (Figure 97). This reduction can be clearly seen in Figure 96, where a comparison is made with the standard case for residential tower-1. Even though the difference is not significant for residential tower-2 (Figure 98), the overall results demonstrate that the green façade could have an impact on reducing traffic noise. The location of the material plays a crucial role in sound absorption, and therefore more variation and patterns could be explored by using parametric optimization. Point to note that the lower values for RT-1 (light green grid) in figure 98 occurred due to a convergence issue during simulation.

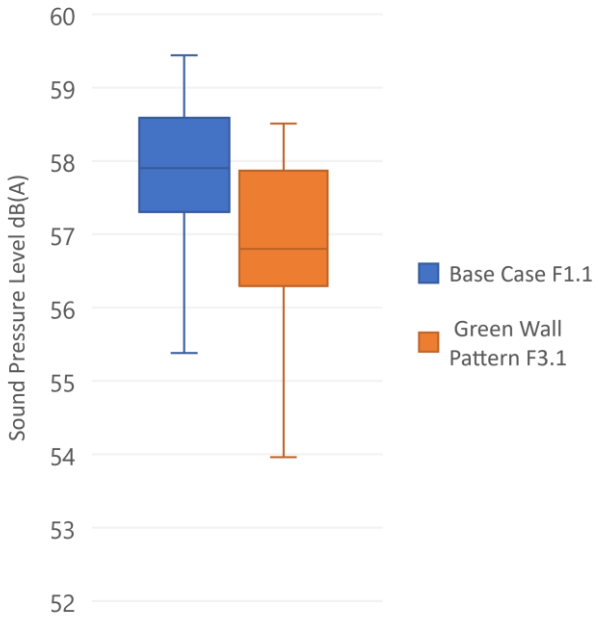

Figure 96 Box plot: SPL data distribution between base case (F1.1) and Green Wall (F3.1) tested for RT-1

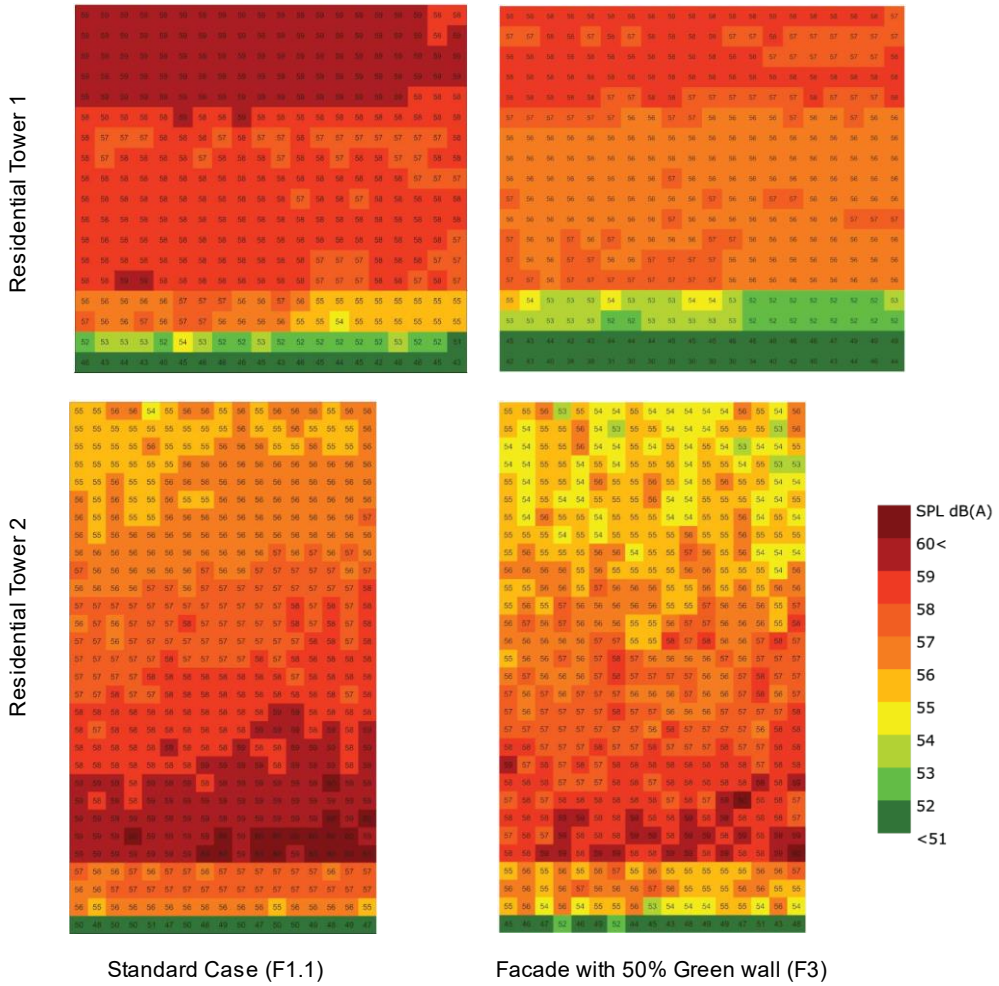

Figure 97 Sound pressure levels on façade for material sequence F3 compared with base case F1.1

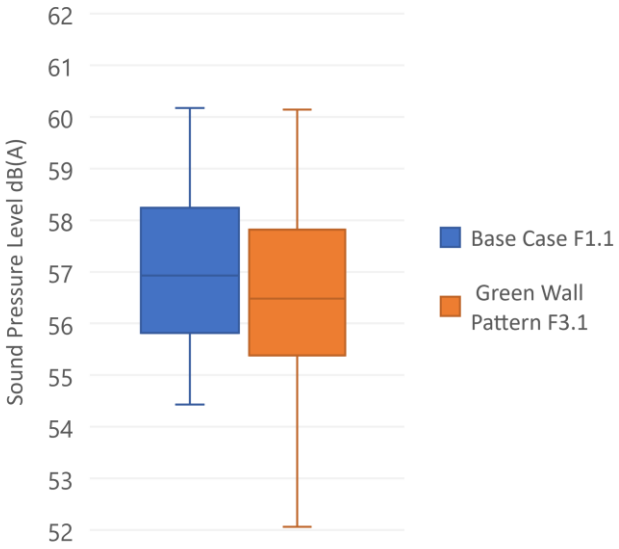

Figure 98 Box plot: SPL data distribution between base case (F1.1) and Green Wall (F3.1) tested for RT-2

6.4.4 Sequence 4: Courtyard variations

As stated earlier, the courtyards/urban parks are widely becoming popular among urban planners because of their added value to community development. In the early phases, it is also important to know the location of the entrances to these urban parks. Therefore, four courtyard sequences (Figure 87) are tested in which two represent the position of the courtyard entry and two present the material variation.

Figure 99 shows the results for the base case (C1.1) where the courtyard entrance is at the default location (56m from the first corner of the building). Towards the right higher sound pressure levels ranging 52-54 dB(A) can be seen as they are influenced by direct noise. These values lower down to 49-51 dB(A) toward the left as some protection is offered against direct sound sources by the buildings at the front.

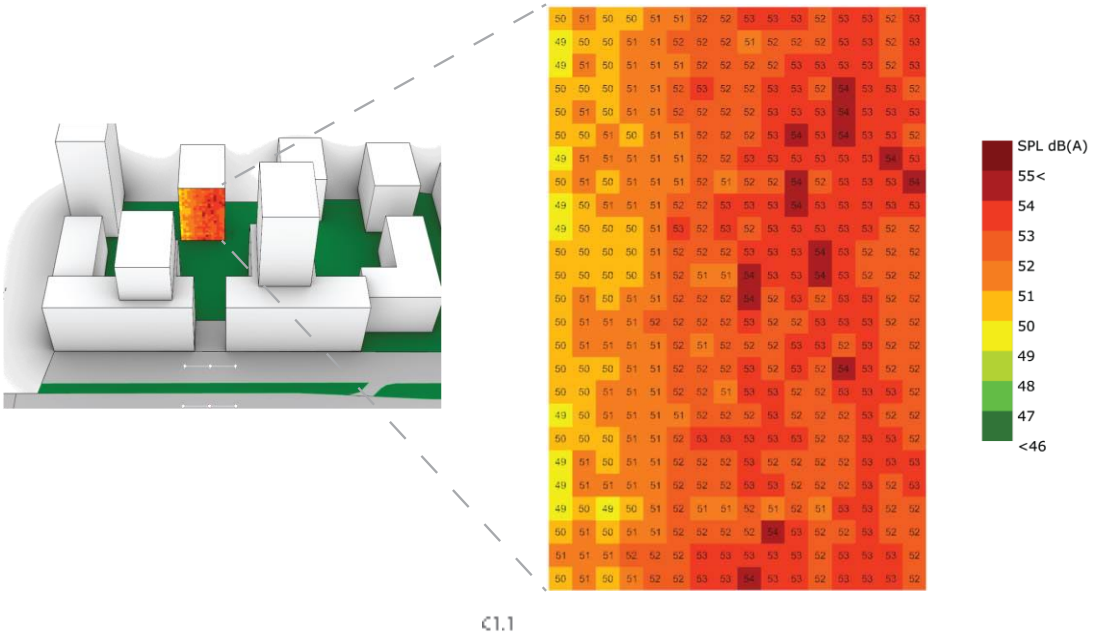

Figure 99 Sound pressure levels on façade for courtyard sequence C1.1

When the courtyard entrance is moved toward the right by 10m (case C1.2), more protection is offered by the buildings at the front. Therefore, the sound pressure level is reduced by 2-3 dB(A) compared to the base case (Figure 100). In this case, a higher decrease in SPL can be seen towards the left where only reflected sound can reach. The results are supported by Figure 101 where the mean value, as well as the distribution of data points, is lowered.

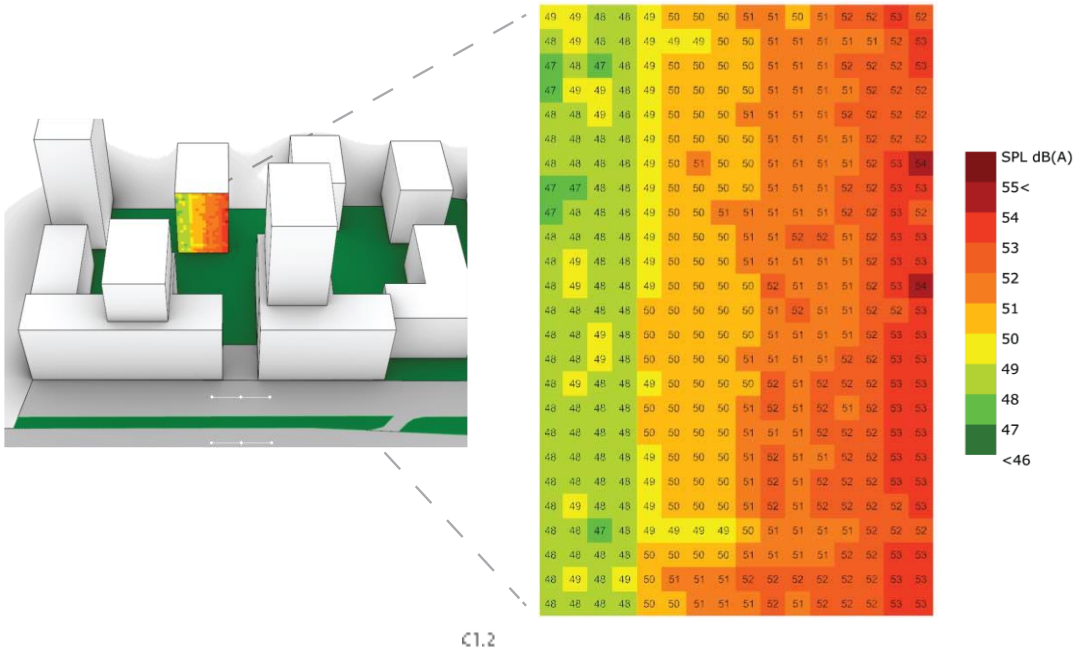

Figure 100 Sound pressure levels on façade for courtyard sequence C1.2

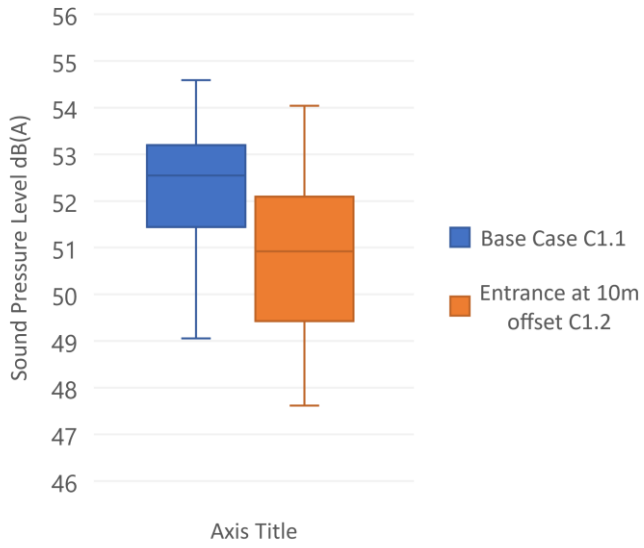

Figure 101 Box plot: SPL data distribution between base case (C1.1) and entrance at 10m offset (C1.2)

Results prove that the green façade also has a great impact on reducing the sound pressure levels inside the courtyard. When applied on the sidewall of the entrance, it significantly reduces the impact of reflected sound. On average 3 dB(A) decline is observed in both cases. This effect can be seen in Figure 103, where SPL values are distributed between 50-50 dB (A) for the case with a green wall as compared to concentrated values (52-54 dB) without the green wall. And as expected, C2.2 i.e.

combination of the green wall with 10m offset is the best among all. Figure 102, represents the comparison between all courtyard cases.

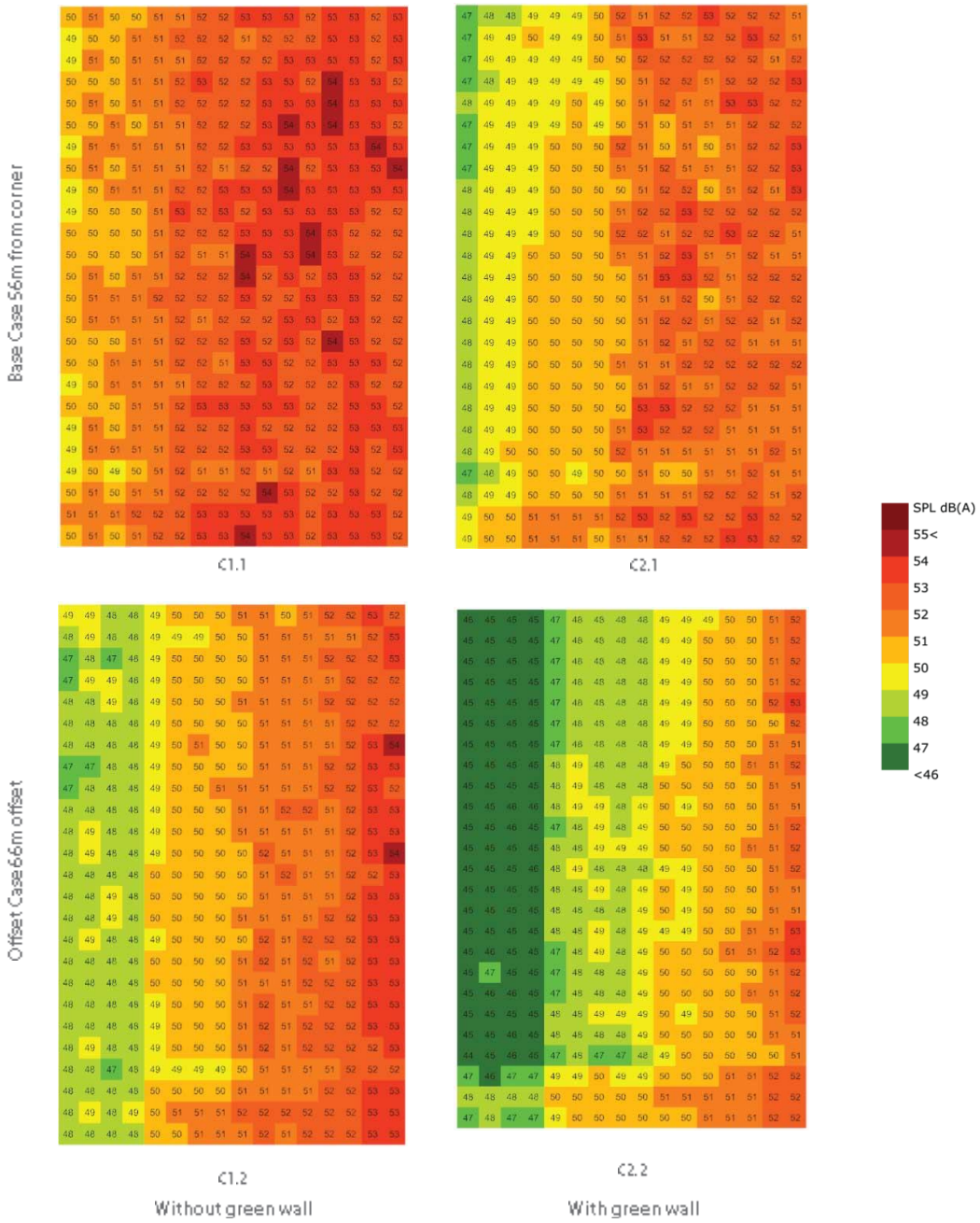

Figure 102 Sound pressure levels on façade for all four courtyard sequences

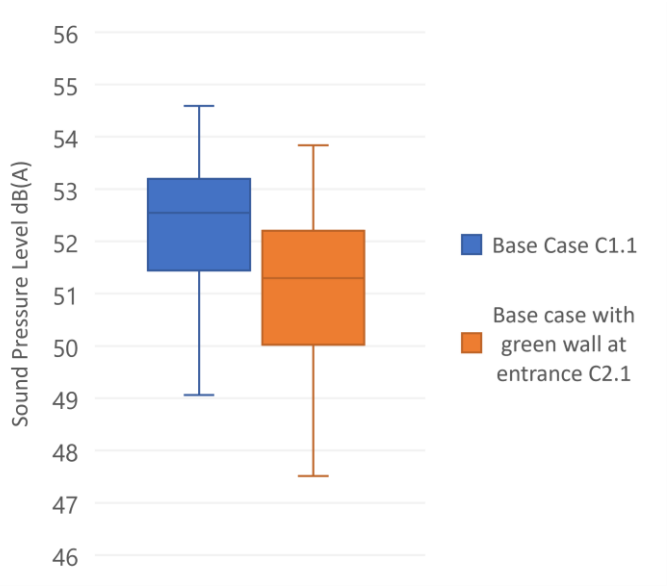

Figure 103 Box plot: SPL data distribution between base case (C1.1) and base case with green wall (C2.1)

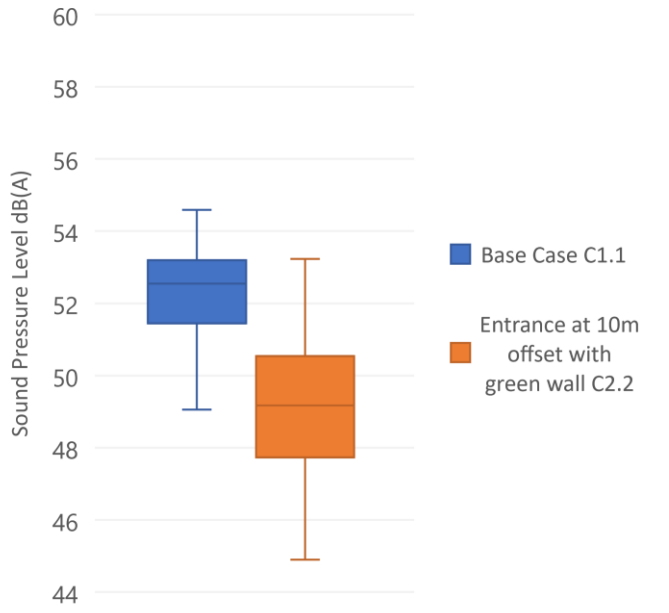

Figure 104 Box plot: SPL data distribution between base case (C1.1) and entrance at 10m offset with green wall (C2.2)

6.4.5 Sequence 5: Balcony variation

Two balcony variations are tested to check the effect of semi-outdoor spaces on sound attenuation (Figure 88). The horizontal extension of the balcony creates a shadow zone for direct sound and around 5 dB(A) reduction can be seen at lower levels (Figure 105).

The inclined ceiling also contributes to SPL by reflecting the sound toward the tested window.

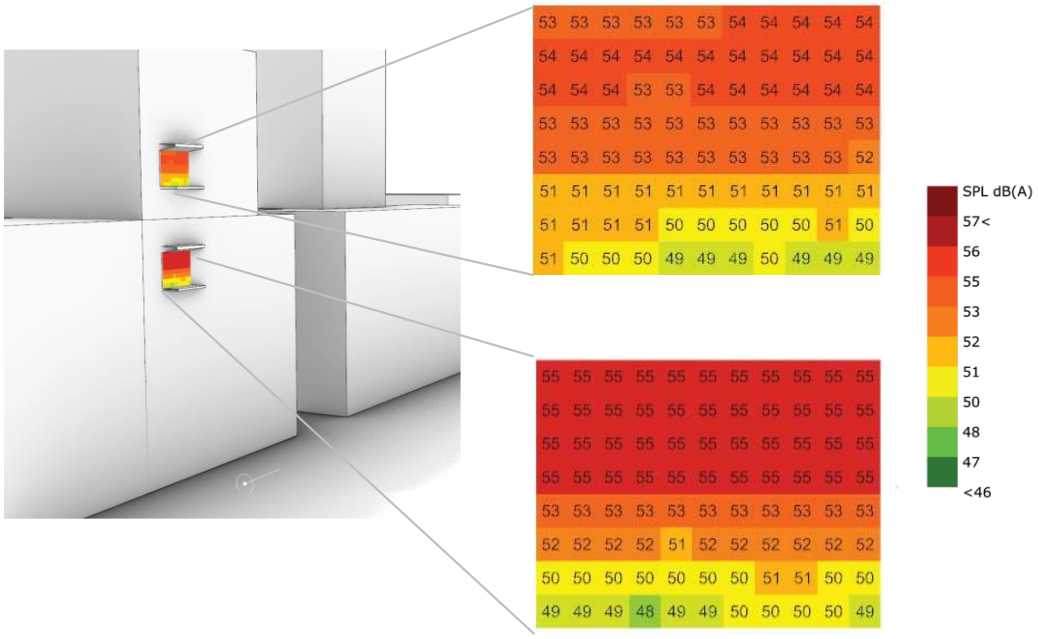

Figure 105 Sound pressure levels on façade for Balcony sequence B1.1 (without sound-absorbing ceiling)

The sound-absorbent ceilings are often used to reduce this impact of reflected sound. This impact can be seen in Figure 106, where the results of the balcony with and without absorbent ceiling are compared for the balcony at 20m height. 1-2 dB(A) reduction is noticed as the entire box plot shifts downward. On the other hand, 3-4 dB(A) reduction is achieved for the balcony at 30m (figure 108). This suggests that for different levels, different ceiling angles might be useful and therefore, optimizing the angle of the ceiling could be an interesting option.

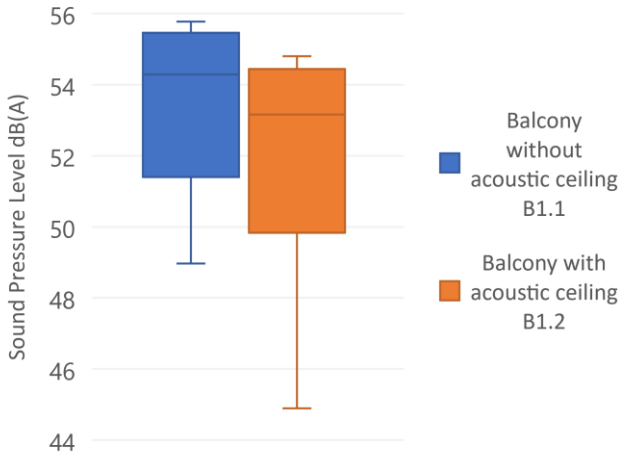

Figure 106 Box plot: SPL data distribution between balcony without acoustic ceiling (B1.1) and balcony with acoustic ceiling B1.2 at 20m.

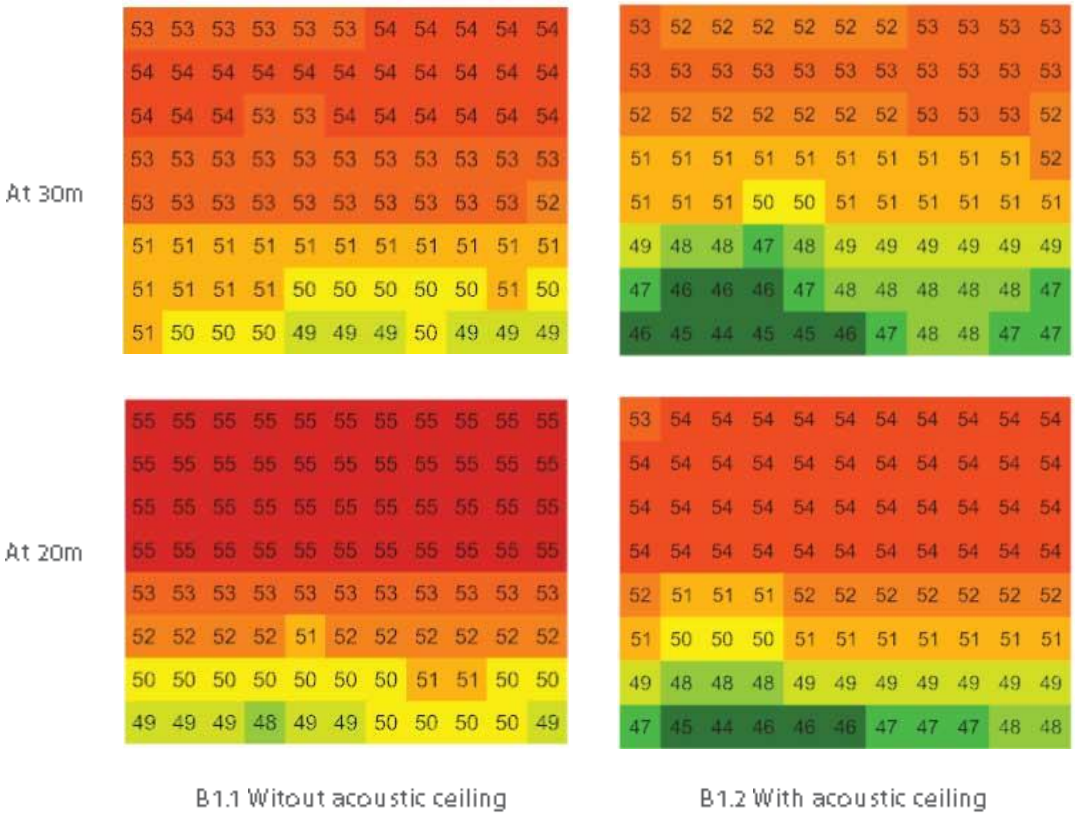

Figure 107 Sound pressure levels on façade for all four balcony sequences

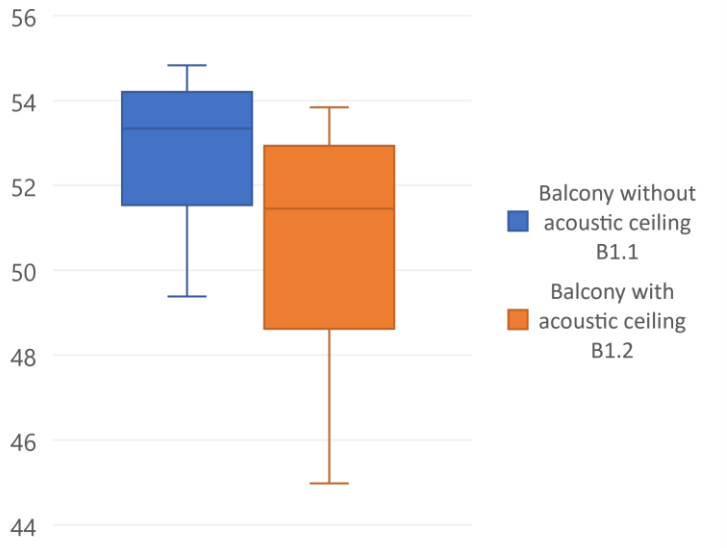

Figure 108 Box plot: SPL data distribution between balcony without acoustic ceiling (B1.1) and balcony with acoustic ceiling B1.2 at 30m.

6.5 Summary

Key takeaways from the design stage are listed below. These points can be considered during early-stage urban acoustic design.

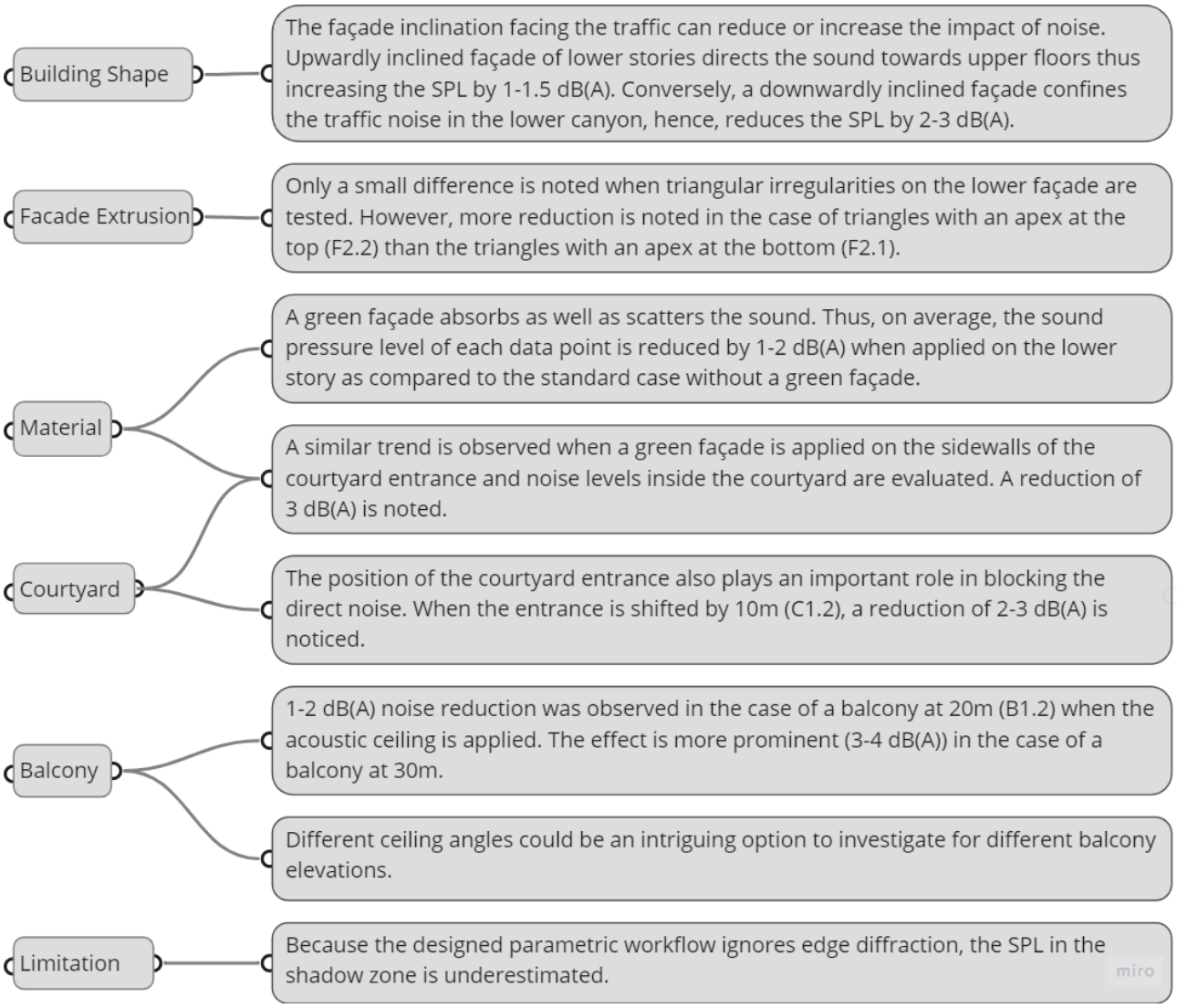

7

Optimization

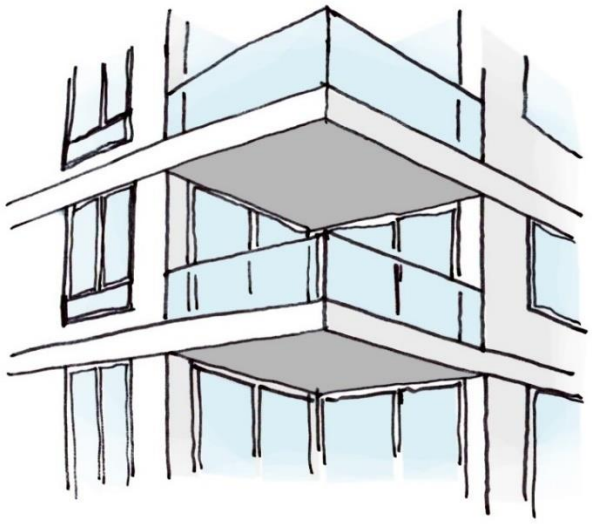

Part 7 Optimization

The process of finding the optimum solution to make a design as effective and functional as possible in regard to some specific performance indicators is referred to as optimization. The optimization can be set to minimize or maximize these indicators which might be related to various aspects of the design.

Since the research is focused on the development of the simulation workflow to predict traffic noise in an urban environment, optimization is carried out to test the capability of the developed workflow to incorporate the optimization process and further improved the design solutions. Therefore, this section answers questions like why and how to undertake optimization in an urban area to reduce noise impact and further represents the results from the tested workflow. Moreover, simplifications used for the optimization are also presented, which are critical for the successful execution of the optimization workflow. Readers should note that the purpose of optimization in this thesis is to illustrate the strategy of the optimization, set up the workflow and further test that optimization workflow, rather than to produce the best/optimal solution.

7.1 Relevance of optimization in urban acoustic

As mentioned in section 2.6.2, the first step of optimization is to identify whether the optimization is applicable in the first place. Often the design scenarios are simple enough to find the best solution by executing a few trials which might prove less time consuming than constructing and performing an optimization workflow. This is also true in this study; the design variations investigated are simple enough that an optimal solution can be found through a series of trials. However, noise exposure is not the only issue that influences building and urban design decisions. When a sustainable urban environment is considered, other performance criteria like, daylight, solar radiation, wind comfort, energy (heating and cooling demand), view factor, pedestrian comfort etc. also determine the design. These performance criteria are often related to each other which increases the complexity and decision making in the early phase of the design. As a result, the multi-objective optimization is a useful approach that allows designers to explore many design solutions and adjust proposals based on multiple performance evaluations.

Multi-objective building performance optimization is well-known, and it has been used in numerous studies over the last decade [127], [146], [147] along with its application in the real world [148]. When it comes to acoustics, the use of optimization for performance spaces, such as theatres, auditoriums, concert halls etc. is also well established [19][21].

However, there is very limited application of acoustic optimization is applied for urban scenarios. Therefore, a multi-objective optimization framework which considers acoustics as a performance indicator in combination with other parameters is very important in the early phases of the design process.

7.2 Optimization framework

During the design phase of this thesis, various geometrical, as well as material variations, are tested which opens up multiple cases for the optimization. However, optimizing all these variations is an exhaustive process and beyond the scope of this research. Given the various performance aspects involved in balcony design, it is thought to be the best possible case to optimize. Multiple performance indicators, such as sound pressure level on the window opening, view factor, energy demand (heating and cooling), and daylight, can be tested and optimized in this scenario. However, the last two are directly related to the amount of solar radiation falling on the opening. Therefore, to simplify the case, only two performance criteria are considered: Acoustics and Solar radiation. The concept behind the optimization is explained in Figure 109.

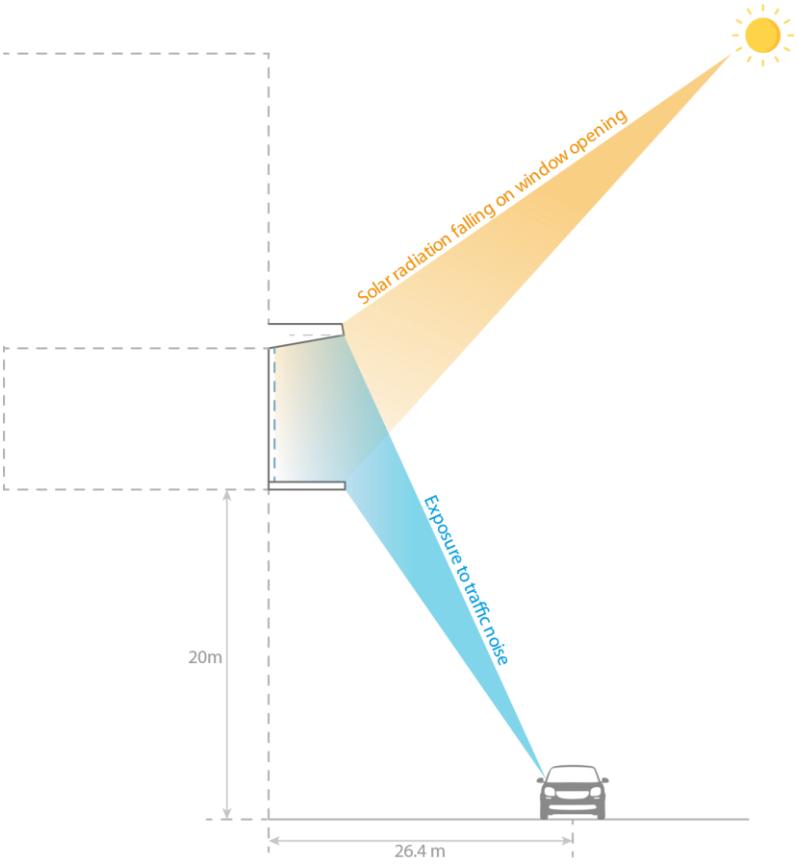

Figure 109 Logic behind the optimization considering solar radiation and traffic noise as performance criteria

Before starting the optimization and selection of optimization tool, the main framework of the optimization is made which is as follows.

7.2.1 Design variables

Design variables are the parameters which need to be optimized. These are usually related to the specific properties of the geometry (width, height etc). The results of the balcony case reveal that the angle of the ceiling and the sound pressure level are interconnected. Also, the depth of the balcony affects sound pressure level as suggested in the literature. Moreover, changing the angle of the ceiling would influence the size of the opening, thus will impact on the amount of solar gains/radiation.

Therefore, the *1) depth of the balcony* and *2) angle of the ceiling* are selected as the design variables for testing. Figure 110 (left), illustrates the concept behind design variables.

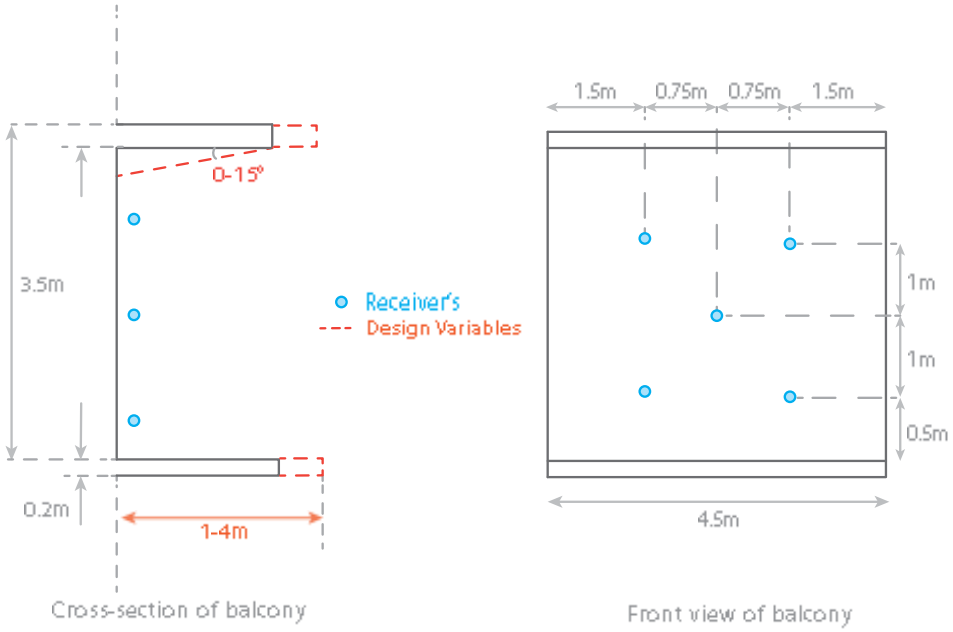

Figure 110 Left: Cross-section of the balcony with design variables, Right: front view of the balcony with receiver's position

7.2.2 Objectives

Objectives are the performance indicators to which one wants to optimize the design variables. In this case, two performance indicators are considered, one related to the acoustics and one based on solar radiation:

1. Minimization of average sound pressure level
2. Maximization of solar radiation (winter months) on the window opening

7.2.3 Constraints

The outputs of the optimization process usually fall within a certain range in order to simultaneously meet criteria relating to the practical limitations or the special solutions that are desired. Constraints are usually divided into two groups, one related to the parameters under optimization and the other associated with the objective of the optimization. In this case, only the constraints related to design variables are considered represented in 16.

Design Variable	Constraint	
	Lower limit	Upper limit
Depth of the balcony	1m	4m
Angle of the ceiling	0°	15°

Table 16 Design constraints considered in the optimization

7.3 Simulation

To perform multi-objective optimization, multiple plugins are available which can work in Grasshopper environments such as Galapagos, Opossum, Optimus, Wallacei and Octopus or in tandem with Grasshopper-like modeFRONTIER. In this research, Wallacei is used as an optimization plugin.

Wallacei[149] is a free evolutionary engine that allows users to run evolutionary simulations in Grasshopper. Wallacei offers a comprehensive set of analytic tools, as well as a choice of comprehensive selection methods, to enable users better understand their evolutionary simulations and make more informed decisions at every level. Additionally, after simulation, Wallacei allows users to select, reconstruct, and output any phenotype from the population.

Before setting up the workflow with Wallacei, parametric balcony definition is made using Grasshoppers' native components. Then the solar radiation definition is added to the previously developed acoustic workflow. Both the definitions are added in Appendix C: Grasshopper Definitions.

7.3.1 Simplifications

First, the trial was conducted on the original definition, which took a long time due to the large number of sources in the original script. Therefore, only a single point source is considered for optimisation. The ray count is lowered to 10K to further reduce the calculation time.

Moreover, Wallacei failed to analyse the sound mapping results. Therefore, the analysis surface (window opening) is divided into five receivers spaced in such a way that they represent the whole surface (see Figure 110). For the objective, the sound pressure level is calculated as an average of those five receivers.

Further, the post-processing step from the original definition is removed since the calculations are performed using a single source, however, frequency correction (A-weighting) is applied.

For solar radiation, the analysis period was set between the 1st of December to the 1st of March (winter months in Europe) given the fact that the objective was to maximize solar gains in winter.

The evolutionary algorithm in Wallacei tries to minimize every objective, therefore, the solar radiation value is multiplied by negative one.

7.3.2 Simulation setting

The settings within the Wallacei were mostly kept to their defaults, which apply the NSGA-2 algorithm[150], [151] as the primary evolutionary algorithm and the K-means method as the clustering algorithm. Population size has been set to 20 instances per generation, which results in 400 evaluated solutions. More detailed statistics are presented in Table 17.

Population	Generation Size	20
	Generation count	20
	Total	400
Algorithm Parameters	Crossover Probability	0.9
	Mutation Probability	1/n
	Crossover Distribution Index	20
	Mutation Distribution Index	20
	Random Seed	1
Simulation Parameters	No. of Genes (Sliders)	2
	No. of Values (Slider values)	20
	No. of fitness objectives	2
	Size of search space	6.4e1
Acoustics	Number of sources	1
	Number of receivers	5
	Sound power level	80 dB

Table 17 Simulation Parameters used in Optimization

7.4 Results

Both the objective functions i.e. minimization of average sound pressure level and maximization of solar radiation are inversely proportional. Increasing the depth of the balcony would decrease SPL along with solar radiation and vice versa. Similarly, increasing the angle of the ceiling would decrease the area of the opening, thus minimising solar gains and decreasing the sound pressure level. This is evident from the results. Figure 111, shows the parallel co-ordinate plot where the lines represent the relationship between both the objective. The negative sign in front of solar radiation value is due to simplification required to maximize the objective, and therefore can be ignored.

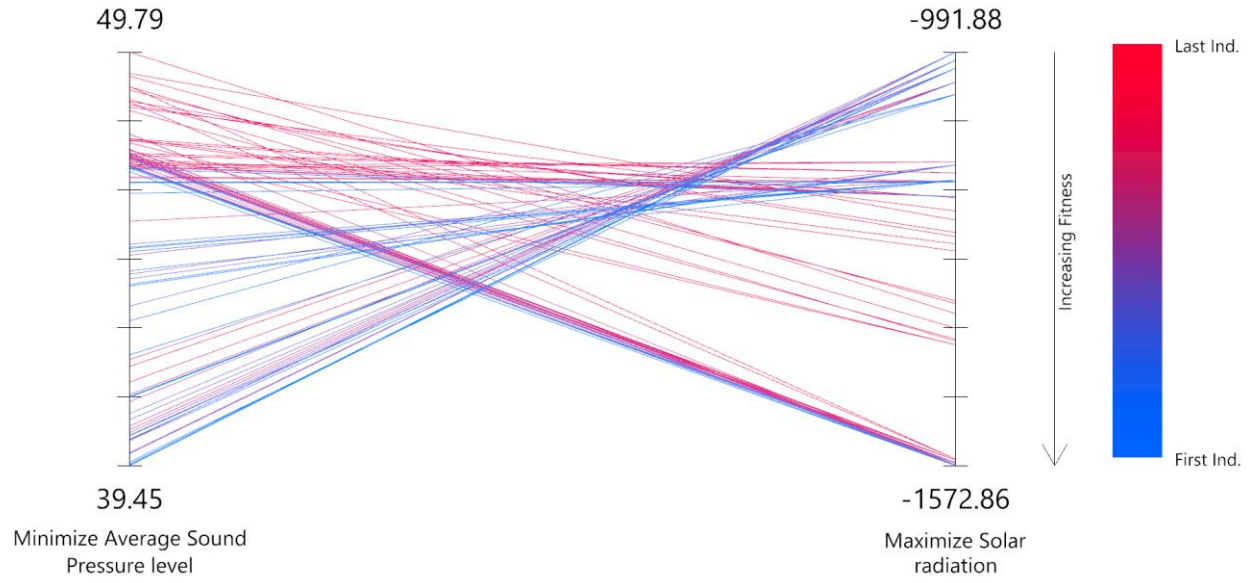

Figure 111 Parallel co-ordinate plot between objective functions. (Sound pressure levels are in dB(A) and solar radiation in kWh)

As it is apparent from the figure that when average sound pressure levels are minimized, solar radiation is also reduced. The fitness value for sound pressure levels varies from 39.45 to 49.79 dB(A), which shows that the tested design variables have the potential to enhance or also worsen the acoustic quality of space. Furthermore, because the evolutionary plugin seeks to meet the objective function, the cluster of lines may be seen near minimum SPL and maximum solar radiation.

In total, 20 generations are tested with 20 instances in each generation. Figure 112 shows how the evolutionary algorithm tries to evaluate all possible design variations for each generation, resulting in a line that fluctuates over the values. However, with every generation it tries to reach close to the fitness objective, thus the blue lines (latest generation) are closed to the objective than the red lines (first generation).

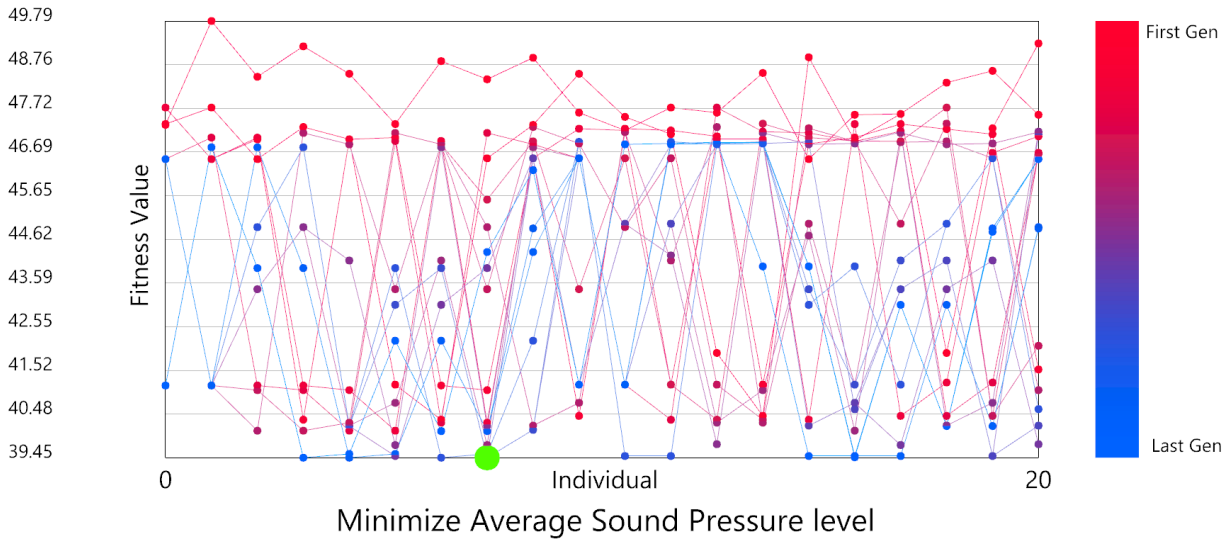

Figure 112 Fitness Value Graph for "minimize SPL" objective (vertical scale in dB(A))

7.4.1 Solutions

Wallacei allows users to select and represent the solution based on the defined objective. Therefore, based on the results of the optimization three solutions are selected, two representing the extremes (fittest for each objective), and one with average fitness ranking.

7.4.1.1 Minimize Average Sound Pressure Level:

This particular solution is obtained during the 14th generation and 11th instance. Figure 113 represents the parallel co-ordinate plot for the case along with extruded geometry. The solution results in the least average sound pressure level of 39.45 dB(A) with the lowest solar radiation of 991.88 kWh and obtained for a balcony with a depth of 4m and ceiling angle of 15°. Figure 114 presents the Pareto front[1] with a blue dot as the solution and a redline representing the 14th generation.

[1] The Pareto front is defined as the set of non-dominated solutions, where each objective is considered as equally good.

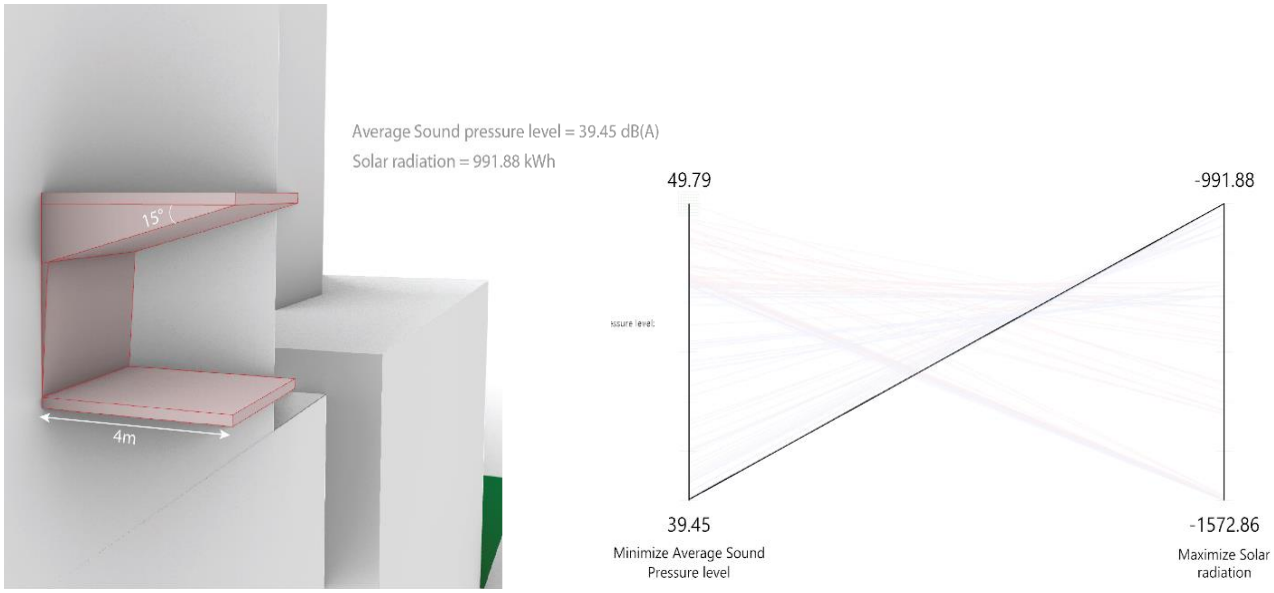

Figure 113 Balcony solution for the lowest average SPL. Left: Extruded Geometry, Right: Parallel co-ordinate plot

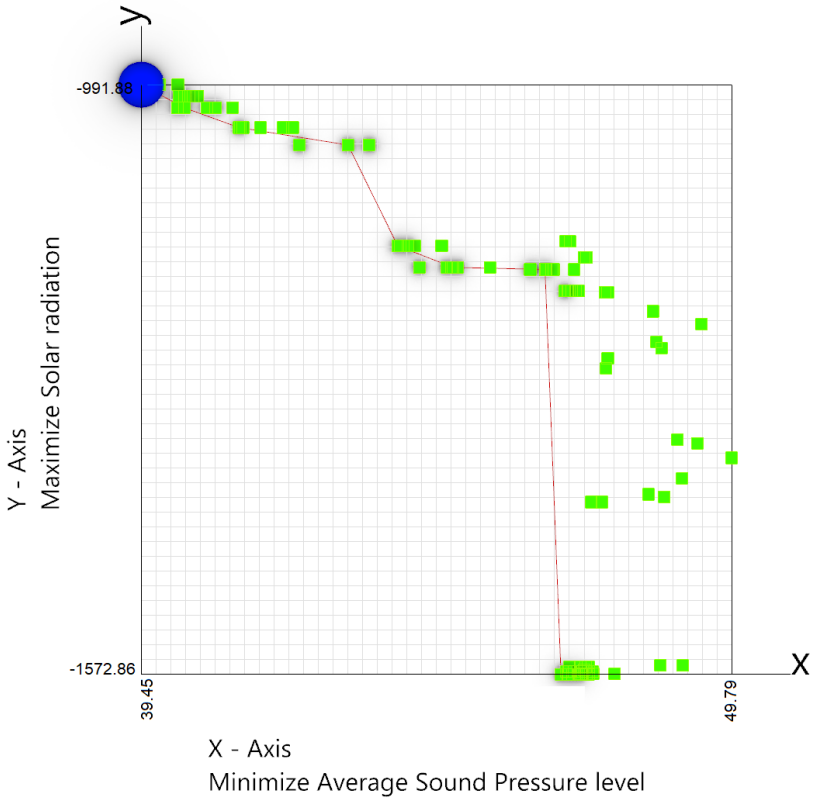

Figure 114 Pareto fronts for the solution with lowest average SPL (Blue circle representing solution and redline showing 11th generation)

7.4.1.2 Maximize Solar radiation:

The maximum solar radiation is obtained for the case with 1m depth and 5° ceiling angle during the 6th generation and 8th instance (Figure 115). The solution results in the highest solar radiation of 1572.86 kWh and with an average sound pressure level of 47.28 dB(A). Given the fact that maximum solar radiation should occur for the solution with a 0° inclined ceiling (which provides maximum area for the window opening), the results are slightly dubious. This ambiguity could be the result of the limited number of rays or a less number of generations used during the optimization. Therefore, it is advisable to use a large solution space with at least 100K rays. Also, Figure 116 represents the parallel co-ordinate plot for the case which shows that the maximum solar radiation doesn't necessarily result in the highest SPL.

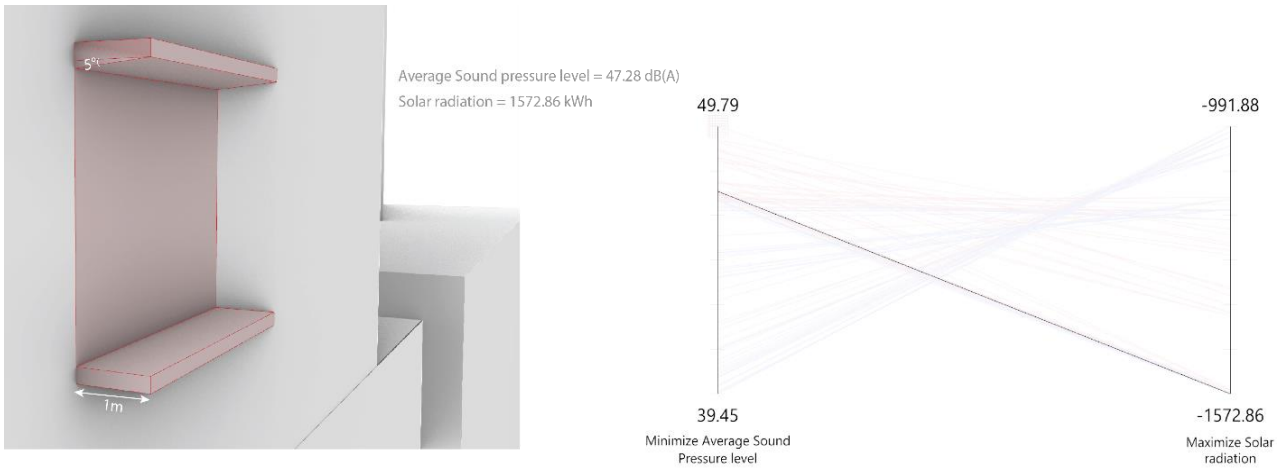

Figure 115 Balcony solution for the highest solar radiation. Left: Extruded Geometry, Right: Parallel co-ordinate plot

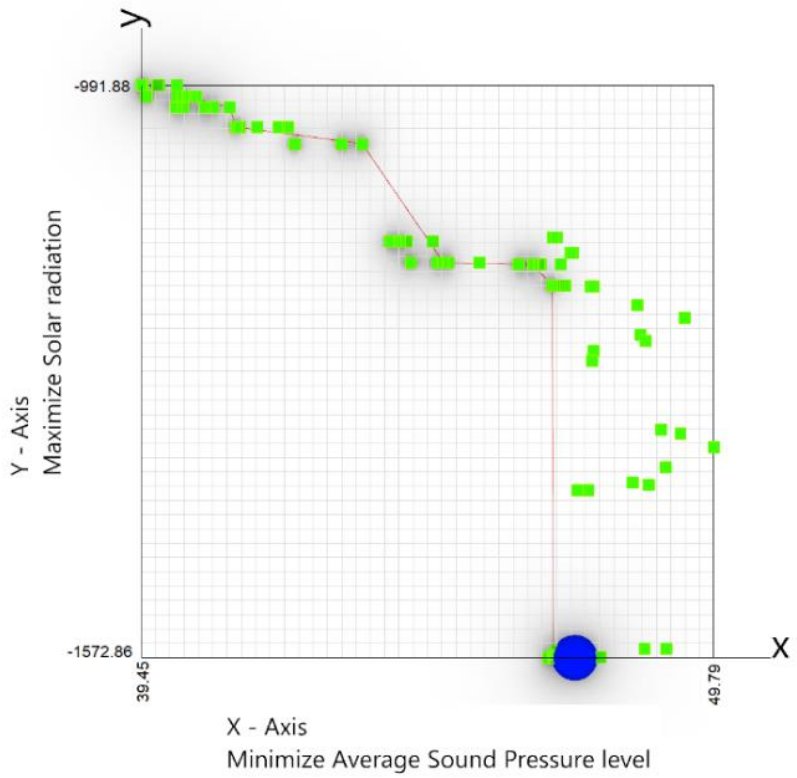

Figure 116 Pareto fronts for the solution with lowest average SPL (Blue circle representing solution and redline showing 6th generation)

7.4.1.3 Intermediate solution

The previous two solutions represent the case which satisfies extreme fitness functions. However, Wallacei allows users to find a solution with an average solution rank or with a specific intermediate objective using the relative difference method. For this case, a hypothetical objective is made that the average sound pressure level should be less than 45 dB(A) but gives maximum radiation. This specific solution is obtained during the 19th generation at the 7th instance which produces the balcony with a depth of 3m and ceiling angle of 14°. This solution has a sound pressure level of 44.32 dB(A), which is less than 45 dB(A), and solar radiation of 1171.82 kWh.

Figure 117 represents the parallel co-ordinate plot for the case along with extruded geometry and Figure 118 presents the Pareto front with a blue dot as the solution and the redline representing the 19th generation.

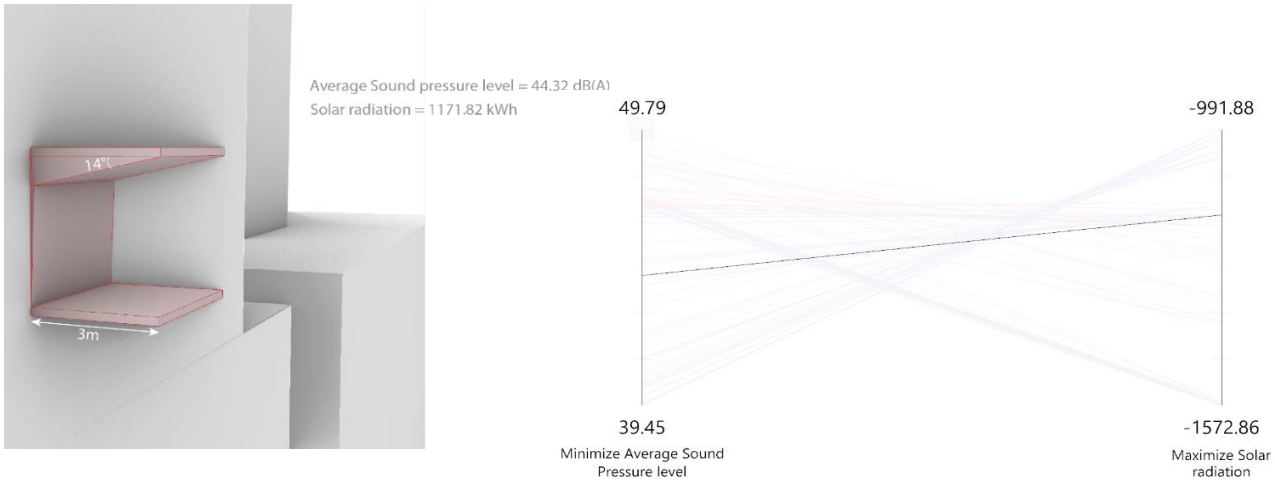

Figure 117 Balcony solution for the intermediate objectives. Left: Extruded Geometry, Right: Parallel co-ordinate plot

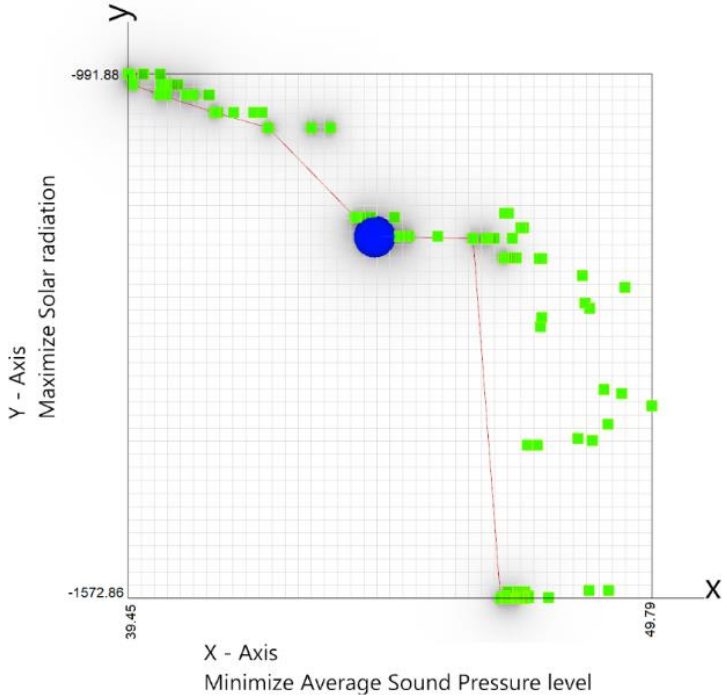

Figure 118 Pareto fronts for the solution with intermediate objective (Blue circle representing solution and redline showing 19th generation)

7.5 Summary

The important findings of optimization study are noted below.

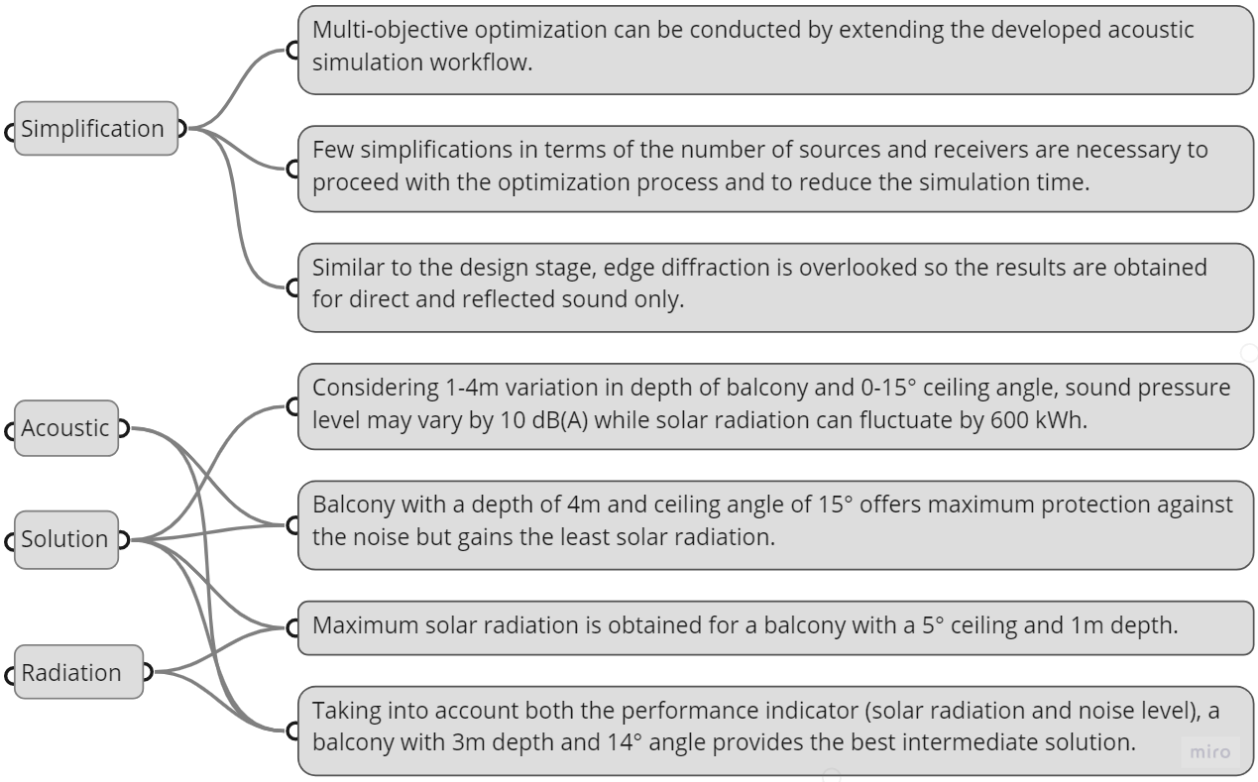

8

Discussion

Part 8 Discussion

This chapter discusses the potential limitations of the developed parametric workflow and its testing. These limitations are important in the light of accuracy and interpretation of the results. To overcome these limitations few simplifications are made in the workflow, these are also explained and will serve as a user guide for the people who intend to use the developed workflow. Moreover, recommendations are also proposed for every limitation, which might be interesting for future development.

8.1 Limitations, Simplifications and Recommendations

8.1.1 Calculation method

8.1.1.1 Limitation

The workflow is made using a combination of ray-tracing, image source and direct sound calculation methods which are based on Geometrical acoustics. The geometrical acoustic methods are suitable when boundary faces are larger than the wavelength of frequency, therefore making the workflow unsuited in lower frequencies (lower than 250 Hz octave).

8.1.1.2 Simplification

Considering this limitation of geometrical acoustics, all the surfaces are simplified as much as possible. For example, while validating the workflow, the façade articulation along the Kervagan street is not considered. Instead, all the surfaces are modelled flat. Moreover, street furniture like benches, traffic signs, post boxes, phone booths, streetlamps, fountains etc. are also excluded as these features are unlikely to make a significant difference in the results. In the case of balcony variation, frequencies smaller than 250 Hz are excluded from the analysis as their wavelength was greater than the balcony size.

8.1.1.3 Recommendation

Given that geometric methods are fast but inaccurate at lower frequencies and wave-based approaches are accurate but expensive at higher frequencies combining the two models makes sense. This means, that by using the wave-based approach in lower frequencies and geometric methods in higher frequencies, the simulation may become accurate over all frequency bands without consuming a lot of computing power. For example, Open PSTD[116], uses a wave-based approach and Blender as a 3D modelling

interface. Thus, its 3D modelling environment can be changed to Rhino 3D and then further can be combined with a Pachyderm for ray-tracing and image source method.

8.1.2 Meteorological Effects

8.1.2.1 Limitation

The meteorological effects such as atmospheric absorption, atmospheric refraction and atmospheric turbulence play important role in sound propagation in an urban environment. For longer distances i.e. more than 1 km, the effects are much more noticeable. Among three, the workflow only accounts for atmospheric absorption of sound. Therefore, in situations where atmospheric turbulence and refraction greatly affect the results (for larger distances) the application of the developed workflow is inadvisable.

8.1.2.2 Simplification

In this research, the design context under consideration was small enough that the effects do not contribute much to the results. Therefore, it is advisable that the current workflow should be used for an area within 500m x 500m.

8.1.2.3 Recommendation

The refraction and turbulence are highly dependent on the wind and temperature profile, therefore computer simulations require high computational power. Usually, the relationship between sound propagation and environmental factors like wind and temperature are established using empirical formulas. This can be done by scripting the custom components in Grasshopper. Further to include these effects, the temperature and wind data of the location are required. Few Grasshopper plugins like ladybug and honeybee have components which can read weather data from ewp weather files. This weather data will serve as input parameters for empirical formulas and accordingly the attenuation or amplification can be applied to the ray. However, a great amount of simplification is required because the environmental factors are constantly fluctuating for example direction of the wind or temperature during the day. Moreover, the amplification and reduction of sound also vary according to the direction of wind propagation. Hence, the process will require higher computational power to include all the variables and might prove costly and also time-consuming.

8.1.3 Interference effect

The amplification and reduction of the sound pressure level due to constructive and destructive interference have also excluded the workflow. The interference effects are particularly important when the sound source and receiver are close to the ground or when the sound travel along the surfaces which are parallel to each other. However, these

phenomena are characteristic of the wave, and therefore it is hard to simulate them using image sources or ray-tracing.

8.1.3.1 Simplification

No simplifications are carried out to overcome the effects of interference. However, the constructive and destructive interference are checked with hand calculation while validating the model.

8.1.3.2 Recommendation

As mentioned earlier, these phenomena are purely wave-based, their location of occurrence can only be predicted by simulating actual waves. Therefore, the recommendation given for the calculation method also holds in this situation. Although time-consuming, the other approach would be to check these interference effects using hand calculation for the given design context and accordingly add or subtract sound pressure levels in the post-processing step.

8.1.4 Source and receiver

8.1.4.1 limitation

One of the biggest limitations of the current workflow is the unavailability of the line source component. Thus, the traffic source is modelled as a number of point sources and therefore it fails to simulate the cylindrical spreading which occurs in the line source. Furthermore, the point sources are activated successively, and thus the simulation time is directly proportional to the number of sources. Considering 100k rays, each point source takes on an average of 40 seconds to simulate (machine with 32GB RAM Intel(R) Core(TM) i7-10850H CPU @ 2.70GHz). So for example, a 500m road with the point sources spaced at 10m will take around 30 minutes to calculate, losing its advantage of quick calculation.

Similarly, to map the SPL on the surface, the ladybug grid component is used which divides the surface into several point receivers. This process needs to be carried out before starting the actual calculation. Here, the generation of receiver points is dependent on the computational power of the machine. The machine used in this research can only process less than five hundred receivers at the same time. Therefore, limits the possibility to include more testing surfaces in a single simulation.

8.1.4.2 Simplification

As mentioned earlier, to represent the traffic source, a line is divided number of points. The distance between individual points depends on the distance between the source and receiver given by equation 28 ($x = 2y$) where x is the distance between point source along the line and y is the shortest distance between line source and receiver grid. However,

when the distance between the source and the receiver is large (more than 20m), the relationship does not apply. Therefore, it is recommended to perform a few trails to decide the exact distance between point sources along the line. For the receiver, the grid spacing is adjusted in such a way that the number of (receiver) points will be under five hundred (see Table 14)

8.1.4.3 Recommendation

The Pachyderm plugin for the Rhino environment is included with the line source component. Although it also simplifies the line as the number of points with a spacing of 10m, the rays are generated simultaneously from each point. This tremendously saves the calculation time. A similar concept can be implemented for the Grasshopper source component where rays are triggered all at once.

The receiver grid is directly proportional to the computational memory of the machine. Therefore, one has to use a machine with high Random-Access Memory (RAM) to include multiple testing surfaces in the same calculation.

8.1.5 Edge Diffraction

8.1.5.1 Limitation

This is the most important limitation of developed workflow and limits its practical use. Even though the current version of Pachyderm plugin includes the edge diffraction option, it does not work. Edge diffraction is particularly important while predicting the sound levels behind the object, for example, behind the barrier. As diffraction is not counted, the current workflow highly underestimates the sound pressure levels in the shadow zone. Therefore, the workflow is appropriate in situations where direct sound and reflected sound can reach. This means that the current workflow fails to calculate sound pressure levels behind the barrier considering no reflected sound is there.

8.1.5.2 Simplifications

Unavailability of the edge diffraction limits the testing possibilities in the design stage. Thus, all the design variations considered during the study are influenced by either direct noise or reflected noise. While data processing, it is advised that the values in the shadow region should be neglected. However, one can compare these values in the shadow region for different geometrical and material variations to make an estimated guess about the possible solutions.

8.1.5.3 Recommendation

There are several edge diffractions models available and also tested by the researcher (see section 2.4.4). It is possible to modify raytracing and image source solutions or to add diffraction components in simulation to take diffraction into account. For example,

the most popular commercial software based on geometrical acoustics such as CATT-Acoustics and Odeon includes the effect of edge diffraction. CATT-Acoustics considered the Biot-Tolstoy-Medwin (BTM) edge diffraction model which models diffraction around a finite edge in terms of virtual point sources located along the edge. This same principle can be implemented in Pachyderm component; however, it is computationally intensive.

Another way is to make surrogate models, that mimic the behaviour of the edge diffraction model as closely as possible. The data required to build a surrogate model can be constructed using CATT-Acoustic or Odeon simulations. This approach will prove to be time-consuming in front, but extremely useful and computationally cheaper once it is built. Finally, the most simplified approach would be to the model based on numerical equations, for example, Maekawa's principle.

9

Conclusion

Part 9 Conclusion

The main goal of this research was to develop and test the parametric simulation workflow that can be used to simulate traffic noise in the early design stage, allowing evaluation and optimization of building configurations in an urban microscale. The central question of this research was:

How can a parametric-driven workflow help to predict traffic noise levels in an urban environment and help analyse the building configurations in the early phases of the design?

The main question led to several sub-question and therefore this chapter summarises the main finding of this research by answering those sub-questions. In addition, the practical relevance of the developed workflow is presented along with recommendations for future improvements.

9.1 Conclusion

1. (a) what are the various meteorological effects which influence the propagation of noise in an urban context and to what extent do these aspects need to be considered in the early phases stage of acoustic design?

In an urban environment, sound travel through the atmosphere which is composed of varying temperature and wind speed which are constantly fluctuating. These atmospheric profiles and fluctuations lead to three dominant effects on sound propagation: atmospheric absorption, refraction by mean wind and temperature gradients and sound scattering from atmospheric turbulence.

Sound absorption in particular is a function of thermal conductivity of air (Temperature) and viscosity of the air (humidity). Since a correlation between these two can be established, the sound absorption due to the atmosphere is represented in terms of coefficient (dB/m). Atmospheric absorption plays a very important role when the distance between source and receiver is more and more often, and acoustic simulation software accounts for this effect.

The latter two, refraction and turbulence, are a function of temperature profile as well as the direction of the wind, which is itself a complex phenomenon. Moreover, these effects occur when the sound has to travel a significant amount of distance, for example in the case of aircraft noise. Therefore, most often, the refraction and turbulence effects are ignored for early design traffic noise simulation.

The proposed workflow is developed for the prediction of sound in a relatively smaller area (500m x 500m), therefore, only frequency depended sound absorption is considered while refraction and turbulence effects are ignored.

1. (b) To what extent are the results of a (simplified) parametric urban acoustic simulation workflow comparable to on-site reference measurements and acoustic software (Geomilieu)?

When the results from the developed parametric workflow are compared with onsite measurement for a cross-section of the street environment a difference of 1-4 dB is noted. Near the source, the difference is less as the results are influenced by a direct sound field, while the greater difference is observed far from the source. This is due to the fact that multiple reflections are not taken into account in ray-tracing solutions, but they do occur in reality.

Moreover, the evolution of sound pressure levels along the street for developed workflow are comparable to that of on-site measurement and a deviation of 2 dB is recorded at the end of the street (50m). This deviation is increased to 3 dB when the results are compared with the Sabine-Franklin-Jaeger-Michael theory.

Finally, a 1-4 dB(A) difference is observed when sound pressure levels on the façade are compared to Geomilieu (Geo-Environment: Urban noise modelling program). Near the source the difference is greater, nevertheless, the deviation gradually decreases with increasing the distance between the source to the receiver.

2. (a) How do sound waves emitted by the traffic interact with the geometrical features of the building?

The sound emitted by traffic propagates as a direct sound, reflected/scattered sound or diffracted sound. Results of the design stage show that a large share of energy is transferred through direct sound while reflected and diffracted sound are secondary. When this sound encounter with the building surfaces or geometry, the sound is absorbed, reflected, or transmitted through the material. The acoustical properties of the surface dictate the extent to which this phenomenon happens.

Building fronts (façades) and the ground surfaces like road pavement are typically made of hard materials which reflect the sound more often than they absorbed or scattered. Therefore, results illustrate that sound-absorbing materials like green façades have the potential to decrease the sound pressure level in an urban environment. In addition, scattering of sound due to façade irregularity also reduces the sound intensity, however, it increases the area influenced by the sound.

2. (b) How can different geometrical features and facade materials of the building contribute to enhancing the urban sound environment?

The simulation results presented in this thesis indicate that the building features, as well as the materiality of the façade, have an important influence on road traffic noise. The inclination of the façade (F1) is particularly important for the reflected noise. A flat upwardly inclined façade (F1.3) redirects the noise towards the tested façade and thus increases the noise level. On the other hand, a flat downwardly inclined façade entraps the noise within the lower canyon, and as a consequence shows 1-2 dB(A) less noise exposure on the upper storey. Having said that, this conclusion might differ for the façade in the lower canyon.

Although the addition of triangular irregularities (F2) on the lower storey façade scatters the traffic noise, the sound pressure levels are not significantly reduced. Nevertheless, the reduction is more significant (2 dB(A)) when the apex of the triangle is shifted at the top.

Along with scattering, the green façade is also effective in absorbing the sound. Hence, when 50% of the green façade (F3) is applied on the lower storey, it reduces almost 1.5 dB(A) noise exposure on upper stories. The green treatment was applied in a checkered pattern; therefore, a specific application (location and pattern) might be more effective.

For noise levels inside the courtyard, the location of the courtyard entrance highly influences the results. When the location of the entrance is shifted by 10m (C1.2) from the original position, sound pressure levels are declined by 1-3 dB(A). Of course, the results will differ with respect to locations and design context. Furthermore, the green façade treatment on the sidewalls of the entrance shows a remarkable effect. Reduction in the range of 1-4 dB(A) is predicted for the base variant (C2.1).To conclude, a combination of the green façade on the sidewalls of the entrance and shifting the location of the entrance (C2.2) proved to be the most effective solution in reducing the noise inside the courtyard.

Variations in smaller features of the building like semi-outdoor spaces (balcony) also protect from noise exposure. Balconies at two different elevations (20m and 30m) show variation in sound reduction when tested with a sound-absorbing ceiling. A reduction of 1-2 dB(A) is noticed for the balcony at 20m while a 3-4 dB(A) decrease is found with an absorption ceiling inclined at 5°.

2. (c) How can parametric optimization be implemented in urban acoustical design?

The multi-objective optimization performed in this research demonstrates the capability of the developed parametric workflow to handle the optimization process. However, simplifications in terms of source, shape, receiver, and data processing are crucial to incorporating the optimization in the original workflow.

Results reveal that the balcony with 4m depth and 15°ceiling angle is best suited to reduce the impact of noise on the window opening while the balcony with 1m depth and 5°ceiling angle is the best to maximize solar radiation in winter months. Finally, getting a fair amount of solar radiation while keeping the exposure to noise under 45 dB(A) is possible with the balcony having 3m depth and a 14° inclined ceiling.

These chosen solutions demonstrate the ability of workflow to analyse extreme solutions based on the objective, as well as the ability to identify a middle ground between the objectives. However, the findings are based on direct noise and reflected noise, thus the presence of edge diffraction might affect the results.

9.2 Practical Relevance

Overall, the developed workflow is able to predict the traffic noise levels on the façade with some simplification. The results of the validation study are comparable to the onsite measurements, and therefore the developed workflow can be used as an early design prediction tool to calculate noise in the street environment.

Moreover, the developed workflow is able to consider different geometrical and material configurations which shows that noise reduction on urban microscale can be achieved by geometrical design and application of absorbing material like green façades. However, underestimation of the results in the shadow zone due to the absence of edge diffraction limits its application to the cases where only reflection and direct noise can reach. This means the workflow is inadequate for predicting sound pressure levels in adjacent canyons and protected courtyards.

Nonetheless, the findings and simulation workflow are significant because modifying geometries and materials can be utilized as a tool in urban design (microscale) to reduce exposure to road traffic noise in the early stages of future projects. This is extremely important because traffic noise is a persistent and major environmental issue in urban areas.

In addition, the findings presented in this thesis suggest a possible link between urban acoustics and architecture, which are currently working in separation. The developed workflow uses Rhino and Grasshopper environment which gives opportunity to the architects and urban planners to test their solutions under one platform. This saves a significant amount of time given that the transition between 3D modelling software and acoustic simulation software is avoided.

Finally, the inclusion of a performance-based optimization workflow allows designers to combine acoustic performance objectives with other urban design aspects. This allows

designers to experiment with a variety of design options and alter proposals based on multiple performance assessments.

9.3 Recommendation for Future Research

The outcome of this study raised new questions for future research. First of all, in practice, the results might deviate from the simulated results due to multiple simplifications adopted while developing the workflow. Overcoming these limitations most importantly diffraction must be the first development. This will increase the practical scope of the developed workflow. The discussion section already contains recommendations for workflow development; hence, this section summarizes a few of the most important improvements for validation, design, and optimization.

9.3.1 Validation

Although validation is performed against reference on-site measurements and Geomilieu, validation of the results with respect to wave-based simulation or scale model measurements will increase the credibility of the Grasshopper workflow.

9.3.2 Design

Based on the results of the design stage, it is recommended to scrutinize the effect of façade inclination on the lower storey and more variations of façade extrusions.

Furthermore, a study of the specific location and pattern of the green façade would be useful. Testing more materials like glass façades, brick façades, or other absorbing and scattering materials will be more informative.

9.3.3 Optimization

In optimization, a simple case with only two performance criteria was considered since the purpose of the optimization in this research was to develop and test the optimization workflow rather than to find the best/optimal solution. Therefore, optimizing different design scenarios with the inclusion of other performance parameters like daylight, solar studies, wind comfort, energy etc. will further make the tool multifaceted. Moreover, it is recommended to perform optimization with more generations, more rays and multiple point sources representing lines to obtain the optimised and accurate solution. A few examples of multi-objective optimization which can be interesting for future work are as follow:

1. The apex angle in the case of the façade extrusion case (F2) also determines the amount of solar radiation gained by the building, which will further affect daylight, cooling demand and energy potential of PV façade panels.

2. Specific green wall patterns may improve the acoustical quality of the space as well as improve the indoor air quality in the case of natural ventilation. Further, reducing the urban heat island effect by a green wall can also be explored.

References

[1] L. Fritschi, A. L. Brown, R. Kim, D. Schwela, and S. Kephalopoulos, "Burden of disease from environmental noise: Quantification of healthy life years lost in Europe," 2011. doi: 10.1080/13504630.2011.629519.

[2] "NOISE GUIDELINES for the European Region," 2018, Accessed: Nov. 25, 2021. [Online]. Available: http://www.euro.who.int/pubrequest

[3] "WHO/Europe | Noise - Data and statistics." https://www.euro.who.int/en/health-topics/environment-and-health/noise/data-and-statistics (accessed Nov. 25, 2021).

[4] "Noise in Europe 2014," 2014.

[5] World Health Organization, "Guideline for Community Noise," *Ecotoxicol Environ Saf*, 1999.

[6] L.C. (Eelco) den Boer and A. (Arno) Schroten, "CE Delft Solutions for environment technology Traffic noise reduction in Europe," Delft, Mar. 2007.

[7] D. Łowicki and S. Piotrowska, "Monetary valuation of road noise. Residential property prices as an indicator of the acoustic climate quality," *Ecological Indicators*, vol. 52, 2015, doi: 10.1016/j.ecolind.2015.01.002.

[8] "Future noise policy: European commission green paper," *European Commission*, 1996, doi: 10.3397/1.3703028.

[9] "REPORT FROM THE COMMISSION TO THE EUROPEAN PARLIAMENT AND THE COUNCIL", Accessed: Nov. 27, 2021. [Online]. Available: http://whqlibdoc.who.int/hq/1999/a68672.pdf

[10] European Commission, "Report on the impact of demographic change," Jun. 2020.

[11] P. D. (2019). United Nations Department of Economic and Social Affairs, "World Urbanization Prospects 2018," New York.

[12] C. Lavalle *et al.*, "European territorial trends - Facts and Prospects for Cities and Region," Luxembourg, 2017. Accessed: Nov. 27, 2021. [Online]. Available: https://ec.europa.eu/jrc/en/territorial-policies

[13] European Environmental Agency, "Urban sprawl in Europe — Scattered urban areas continue to expand — Joint EEA-FOEN report," 2016, Accessed: Nov. 28, 2021. [Online]. Available: https://www.eea.europa.eu/publications/urban-sprawl-in-europe

[14] WHO & United Nations Human Settlements Programme, "Hidden cities: Unmasking and overcoming health inequities in urban settings," Kobe, Japan, 2010.

[15] S. Alves, L. Estévez-Mauriz, F. Aletta, G. M. Echevarria-Sanchez, and V. P. Romero, "Towards the integration of urban sound planning in urban development processes: The study of four test sites within the SONORUS project," *Noise Mapping*, vol. 2, no. 1, pp. 57–85, Jan. 2015, doi: 10.1515/noise-2015-0005.

[16] M. Hornikx, "Ten questions concerning computational urban acoustics," *Building and Environment*, vol. 106, pp. 409–421, Sep. 2016, doi: 10.1016/j.buildenv.2016.06.028.

[17] "Final Report Summary - SONORUS (The Urban Sound Planner) | FP7 | CORDIS | European Commission." https://cordis.europa.eu/project/id/290110/reporting (accessed Nov. 29, 2021).

[18] J. Sanz Soriano, O. Wright, E. van den Braak, and C. Day, "Exploration of stage acoustic considerations with parametric tools during early design stages," 2019.

[19] A. Bassuet, D. Rife, and L. Dellatorre, "Computational and Optimization Design in Geometric Acoustics," 2014.

[20] E. Badino, L. Shtrepi, and A. Astolfi, "Acoustic Performance-Based Design: A Brief Overview of the Opportunities and Limits in Current Practice," *Acoustics*, vol. 2, no. 2, pp. 246–278, May 2020, doi: 10.3390/acoustics2020016.

[21] A. Bassuet, "The Acoustical Design of the New National Opera House of Greece," 2010.

[22] N. Vlaun, A. van Waart, M. Tenpierik, and M. Turrin, "A Sound Working Environment: Optimizing the Acoustic Properties of Open Plan Workspaces Using Parametric Models," 2016.

[23] C. Calleri *et al.*, "Building façades optimization at preliminary design stage for outdoor noise mitigation," 2018.

[24] "Research — ORASE." https://www.orase.org/fields (accessed Dec. 04, 2021).

[25] "ISO - ISO 9613-2:1996 - Acoustics — Attenuation of sound during propagation outdoors — Part 2: General method of calculation." https://www.iso.org/standard/20649.html (accessed Apr. 05, 2022).

[26] "Geomilieu." DGMR. Accessed: Mar. 14, 2022. [Online]. Available: http://software.dgmr.nl/manuals/Geomilieu.pdf

[27] "Entree, een nieuw stukje Zoetermeer - Entree." https://entreezoetermeer.nl/projecten/entree-een-nieuw-stukje-zoetermeer/ (accessed Apr. 18, 2022).

[28] J. Picaut and L. Simon, "A scale model experiment for the study of sound propagation in urban areas," *Applied Acoustics*, vol. 62, no. 3, pp. 327–340, Mar. 2001, doi: 10.1016/S0003-682X(00)00028-1.

[29] P. Wannasawang and ir Martin Tenpierik ir Arie Bergsma, "BUILDING ENVELOPE IN AIRPORT REGIONS Sustainable Design Graduation Studio: 'Make some noise Schiphol.'"

[30] J. Niesten, M. J. Tenpierik, and J. Krimm, "Sound predictions in an urban context," *Building Acoustics*, 2021, doi: 10.1177/1351010X211034665.

[31] European Environmental Agency, "Good practice guide on quiet areas," Luxembourg, 2014. doi: 10.2800/12611.

[32] D. C. Hothersall, K. v. Horoshenkov, and S. E. Mercy, "NUMERICAL MODELLING OF THE SOUND FIELD NEAR A TALL BUILDING WITH BALCONIES NEAR A ROAD," *Journal of Sound and Vibration*, vol. 198, no. 4, pp. 507–515, Dec. 1996, doi: 10.1006/JSVI.1996.0584.

[33] M. Long, "Fundamentals of Acoustics," *Architectural Acoustics*, pp. 39–79, Jan. 2014, doi: 10.1016/B978-0-12-398258-2.00002-7.

[34] A.C. van der Linden, I.M. Kuijpers-van Gaalen, and A. Zeegers, "Building Physics," 2018.

[35] M. Pinterić, "Building acoustics," *Building Physics: From physical principles to international standards*, pp. 191–213, 2017, doi: 10.1007/978-3-319-57484-4_7.

[36] Higini Arau-Puchades, "Sound Pressure Levels in Rooms: A Study of Steady State Intensity, Total Sound Level, Reverberation Distance, a New Discussion of Steady State Intensity and Other Experimental Formulae," *BUILDING ACOUSTIC*, vol. 19, Nov. 2012, Accessed: Feb. 23, 2022. [Online]. Available: https://www.arauacustica.com/files/publicaciones/pdf_esp_36.pdf

[37] "How does the sound decrease with distance? ." http://www.sengpielaudio.com/calculator-SoundAndDistance.htm (accessed Dec. 31, 2021).

[38] "ISO - ISO 226:2003 - Acoustics — Normal equal-loudness-level contours." https://www.iso.org/standard/34222.html (accessed Mar. 30, 2022).

[39] "Roadway noise - Wikipedia." https://en.wikipedia.org/wiki/Roadway_noise (accessed Jan. 04, 2022).

[40] T. Beckenbauer, "Road Traffic Noise," *Handbook of Engineering Acoustics*, pp. 367–392, Jan. 2013, doi: 10.1007/978-3-540-69460-1_15.

[41] S. Grubesa and M. Suhanek, "Traffic Noise," *Noise and Environment*, Jun. 2020, doi: 10.5772/INTECHOPEN.92892.

[42] J. Krimm, "Acoustically effective façades," *A+BE | Architecture and the Built Environment*, vol. 8, no. 16, pp. 1–212, Jul. 2018, doi: 10.7480/abe.2018.16.2447.

[43] "Traffic Noise: Characteristics and Factors." https://www.environmentalpollution.in/noise-pollution/traffic-noise/traffic-noise-characteristics-and-factors/6092 (accessed Jan. 04, 2022).

[44] T. M. Barry and J. A. Reagan, "FHWA highway traffic noise: prediction model (USA).," 1978.

[45] United Kingdom Department of the Environment and Welsh Office Joint Publication/HMSO, "Calculation of Road Traffic Noise," London, 1975.

[46] C. Steele, "A critical review of some traffic noise prediction models," *Applied Acoustics*, vol. 62, no. 3, pp. 271–287, Mar. 2001, doi: 10.1016/S0003-682X(00)00030-X.

[47] Stylianos Kephalopoulos, Marco Paviotti, and Fabienne Anfosso-Lédée, "Common Noise Assessment Methods in Europe (CNOSSOS-EU) EUR 25379 EN", doi: 10.2788/31776.

[48] W. Yang, M. Cai, and P. Luo, "The calculation of road traffic noise spectrum based on the noise spectral characteristics of single vehicles," *Applied Acoustics*, vol. 160, 2020, doi: 10.1016/j.apacoust.2019.107128.

[49] Bert Peeters and Gijsjan v. Blokland, "IMAGINE: Improved Methods for the Assessment of the Generic Impact of Noise in the Environment The Noise Emission Model For European Road Traffic," Jan. 2007. [Online]. Available: www.imagine-project.org

[50] European Environmental Agency, "Environmental noise in Europe 2020."

[51] "Air Quality and Noise Legislation - Environment - European Commission." https://ec.europa.eu/environment/legal/law/5/e_learning/module_1_5.htm (accessed Jan. 06, 2022).

[52] E. van Kempen, M. Casas, G. Pershagen, and M. Foraster, "WHO environmental noise guidelines for the European region: A systematic review on environmental noise and cardiovascular and metabolic effects: A summary," *International Journal of Environmental Research and Public Health*, vol. 15, no. 2. 2018. doi: 10.3390/ijerph15020379.

[53] "Regulation - Noise Pollution Act - BWBR0003227." https://wetten.overheid.nl/BWBR0003227/2017-05-01#HoofdstukVI (accessed Jan. 06, 2022).

[54] "Health: Mapping health effects." https://kpvvdashboard-12.blogspot.com/2012/06/gezondheidseffecten-in-beeld-brengen.html (accessed Jan. 06, 2022).

[55] E. M. Salomons, "Unbounded homogeneous atmosphere," in *Computational Atmospheric Acoustics*, Dordrecht: Springer Netherlands, 2001, pp. 5–19. doi: 10.1007/978-94-010-0660-6_2.

[56] Martijn C Lugten, "Tranquillity by design: Architectural and landscape interventions to improve the soundscape quality in urban areas exposed to aircraft noise," University of Cambridge: Clare College, 2018.

[57] Simons. D.G, "Introduction to Aircraft Noise," 2019.

[58] E. M. Salomons, "Atmospheric refraction," in *Computational Atmospheric Acoustics*, Dordrecht: Springer Netherlands, 2001, pp. 37–65. doi: 10.1007/978-94-010-0660-6_4.

[59] André Filipe Garcia Peixoto de Oliveira, "The effect of wind and turbulence on sound propagation in the atmosphere," Maio, 2012.

[60] E. M. Salomons, "Atmospheric turbulence," *Computational Atmospheric Acoustics*, pp. 67–76, 2001, doi: 10.1007/978-94-010-0660-6_5.

[61] K. Attenborough, "Sound Propagation in the Atmosphere," *Springer Handbooks*, pp. 113–147, 2007, doi: 10.1007/978-0-387-30425-0_4.

[62] Michael Ermann, *ArchitecturAl Acoustics illustrAted*. 2015.

[63] P. S. Liu and G. F. Chen, "Porous Materials: Processing and Applications," *Porous Materials: Processing and Applications*, pp. 1–560, Aug. 2014, doi: 10.1016/C2012-0-03669-1.

[64] T. J. Cox and P. D'Antonio, *Acoustic absorbers and diffusers : theory, design and application*, 3rd ed. CRC Press Taylor & Francis Group, 2016.

[65] T. J. Cox *et al.*, "A tutorial on scattering and diffusion coefficients for room acoustic surfaces," *Acta Acustica United with Acustica*, vol. 92, no. 1, JAN-FEB, pp. 1–15, 2006.

[66] J. Piechowicz, "Sound Wave Diffraction at the Edge of a Sound Barrier," vol. 119, 2011.

[67] S. M. B. Fard, N. Kessissoglou, S. Samuels, and M. Burgess, "NUMERICAL STUDY OF NOISE BARRIER DESIGNS," *Proceedings of Acoustics 2013-Victor Harbor*, Nov. 2013.

[68] S. Kumar and G. S. Ranganath, "Geometrical theory of diffraction," *Pramana-J. Phys*, vol. 37, no. 6, pp. 457–488, 1991.

[69] Dirk Schr¨oder, Alexander Pohl, and Michael Vorl¨ander, "On the accuracy of edge diffraction simulation methods in Geometrical Acoustics," *Internoise*, Jan. 2012, Accessed: Apr. 12, 2022. [Online]. Available: https://www.researchgate.net/publication/258098587_On_the_accuracy_of_edge_diffraction_simulation_methods_in_Geometrical_Acoustics

[70] "Street Canyon - Wikipedia, the free encyclopedia." https://nl.wikipedia.org/wiki/Straatcanyon (accessed Apr. 12, 2022).

[71] R. G. Kouyoumjian and P. H. Pathak, "A Uniform Geometrical Theory of Diffraction for an Edge in a Perfectly Conducting Surface," *Proceedings of the IEEE*, vol. 62, no. 11, pp. 1448–1461, 1974, doi: 10.1109/PROC.1974.9651.

[72] L. Pisha, S. Atre, J. Burnett, S. Yadegari, and S. Marburg, "Approximate diffraction modeling for real-time sound propagation simulation Overview of geometrical room acoustic modeling techniques Approximate diffraction modeling for real-time sound propagation simulation," *Citation: The Journal of the Acoustical Society of America*, vol. 148, p. 1922, 2020, doi: 10.1121/10.0002115.

[73] M. A. Biot and I. Tolstoy, "Formulation of wave propagation in infinite media by normal coordinates with an application to diffraction Formulation of Wave Propagation in Infinite Media by Normal Coordinates with an Application to Diffraction*," *Journal of the Acoustical Society of America*, vol. 29, no. 3, 1957, doi: 10.1121/1.1908899ï.

[74] Z. Maekawa, "Noise reduction by screens," *Applied Acoustics*, vol. 1, no. 3, pp. 157–173, Jul. 1968, doi: 10.1016/0003-682X(68)90020-0.

[75] K. Takagi, "Some remarks on practical methods for calculating acoustical diffraction," *Applied Acoustics*, vol. 31, no. 1–3, pp. 119–132, Jan. 1990, doi: 10.1016/0003-682X(90)90056-Z.

[76] M. Hornikx and J. Forssén, "Noise abatement schemes for shielded canyons," *Applied Acoustics*, vol. 70, no. 2, pp. 267–283, Feb. 2009, doi: 10.1016/J.APACOUST.2008.04.002.

[77] R. H. Lyon, "Role of multiple reflections and reverberation in urban noise propagation," *Journal of the Acoustical Society of America*, vol. 55, no. 3, pp. 493–503, 1974, doi: 10.1121/1.1914527.

[78] H. Onaga and J. H. Rindel, "Acoustic characteristics of urban streets in relation to scattering caused by building facades," *Applied Acoustics*, vol. 68, no. 3, pp. 310–325, Mar. 2007, doi: 10.1016/J.APACOUST.2006.01.010.

[79] J. Kang, "Sound propagation in street canyons: Comparison between diffusely and geometrically reflecting boundaries," *J Acoust Soc Am*, vol. 107, no. 3, p. 1394, Feb. 2000, doi: 10.1121/1.428580.

[80] A. Can, N. Fortin, and J. Picaut, "Accounting for the effect of diffuse reflections and fittings within street canyons, on the sound propagation predicted by ray tracing codes," *Applied Acoustics*, vol. 96, pp. 83–93, Sep. 2015, doi: 10.1016/J.APACOUST.2015.03.013.

[81] G. M. Echevarria Sanchez, T. van Renterghem, P. Thomas, and D. Botteldooren, "The effect of street canyon design on traffic noise exposure along roads," *Building and Environment*, vol. 97, pp. 96–110, Feb. 2016, doi: 10.1016/J.BUILDENV.2015.11.033.

[82] K. Iu, K. L.-T. J. of the A. S. of America, and undefined 2002, "The propagation of sound in narrow street canyons," *asa.scitation.org*, vol. 112, no. 2, p. 537, Aug. 2002, doi: 10.1121/1.1492821.

[83] F. Aletta and J. Xiao, "Handbook of Research on Perception-Driven Approaches to Urban Assessment and Design," *Handbook of Research on Perception-Driven Approaches to Urban Assessment and Design*, pp. 1–641, Jan. 2018, doi: 10.4018/978-1-5225-3637-6.

[84] M. R. Ismail and D. J. Oldham, "A scale model investigation of sound reflection from building façades," *Applied Acoustics*, vol. 66, no. 2, pp. 123–147, Feb. 2005, doi: 10.1016/J.APACOUST.2004.07.007.

[85] J. Picaut and D. Scouarnec, "Using acoustic diffusors to reduce noise in urban areas," *Acta Acustica united with Acustica*, vol. 95, no. 4, pp. 653–668, Jul. 2009, doi: 10.3813/AAA.918194.

[86] N. H. Wong, A. Y. Kwang Tan, P. Y. Tan, K. Chiang, and N. C. Wong, "Acoustics evaluation of vertical greenery systems for building walls," *Building and Environment*, vol. 45, no. 2, pp. 411–420, Feb. 2010, doi: 10.1016/J.BUILDENV.2009.06.017.

[87] T. van Renterghem, M. Hornikx, J. Forssen, and D. Botteldooren, "The potential of building envelope greening to achieve quietness," *Building and Environment*, vol. 61, pp. 34–44, Mar. 2013, doi: 10.1016/J.BUILDENV.2012.12.001.

[88] E. Öhrström, A. Skånberg, H. Svensson, and A. Gidlöf-Gunnarsson, "Effects of road traffic noise and the benefit of access to quietness," *Journal of Sound and Vibration*, vol. 295, no. 1–2, pp. 40–59, Aug. 2006, doi: 10.1016/J.JSV.2005.11.034.

[89] Y. de Kluizenaar *et al.*, "Urban road traffic noise and annoyance: The effect of a quiet façade," *J Acoust Soc Am*, vol. 130, no. 4, p. 1936, Oct. 2011, doi: 10.1121/1.3621180.

[90] K. Heutschi, "A simple method to evaluate the increase of traffic noise emission level due to buildings, for a long straight street," *Applied Acoustics*, vol. 44, no. 3, pp. 259–274, Jan. 1995, doi: 10.1016/0003-682X(94)00027-S.

[91] S. K. Tang, "Noise screening effects of balconies on a building facade," *J Acoust Soc Am*, vol. 118, no. 1, p. 213, Jun. 2005, doi: 10.1121/1.1931887.

[92] H. H. el Dien and P. Woloszyn, "The acoustical influence of balcony depth and parapet form: experiments and simulations," *Applied Acoustics*, vol. 66, no. 5, pp. 533–551, May 2005, doi: 10.1016/J.APACOUST.2004.09.004.

[93] Y. G. Tong, S. K. Tang, and M. K. L. Yeung, "Full scale model investigation on the acoustical protection of a balcony-like façade device (L)," *J Acoust Soc Am*, vol. 130, no. 2, p. 673, Mar. 2012, doi: 10.1121/1.3598430.

[94] H. Hossam El Dien and P. Woloszyn, "Prediction of the sound field into high-rise building facades due to its balcony ceiling form," *Applied Acoustics*, vol. 65, no. 4, pp. 431–440, Apr. 2004, doi: 10.1016/J.APACOUST.2003.11.002.

[95] E. M. Salomons, H. Polinder, W. J. A. Lohman, H. Zhou, H. C. Borst, and H. M. E. Miedema, "Engineering modeling of traffic noise in shielded areas in cities," *J Acoust Soc Am*, vol. 126, no. 5, pp. 2340–2349, Nov. 2009, doi: 10.1121/1.3238238.

[96] W. Wei *et al.*, "Urban background noise mapping: The general model," *Acta Acustica united with Acustica*, vol. 100, no. 6, pp. 1098–1111, Nov. 2014, doi: 10.3813/AAA.918789.

[97] H. Kuttruff, "Room Acoustics, Fourth edition".

[98] "Simulation models," *Auralization*, pp. 147–173, 2008, doi: 10.1007/978-3-540-48830-9_11.

[99] L. Savioja and U. P. Svensson, "Overview of geometrical room acoustic modeling techniques," *Citation: The Journal of the Acoustical Society of America*, vol. 138, p. 708, 2015, doi: 10.1121/1.4926438.

[100] H. Carslaw, "Some multiform solutions of the partial differential equations of physical mathematics and their applications," *Proc. London Math*, vol. 30, no. 1, pp. 121–161, 1899.

[101] L. Cremer and H. Müller, *Die wissenschaftlichen grundlagen der raumakustik (The Scientific Basis of Room Acoustics: Geometrical Room Acoustics)*. 1978. Accessed: Apr. 15, 2022. [Online]. Available: https://www.ingentaconnect.com/content/dav/aaua/1985/00000058/00000003/art00003

[102] J. C. Allred and A. Newhouse, "Applications of the Monte Carlo Method to Architectural Acoustics," *J Acoust Soc Am*, vol. 30, no. 1, p. 1, Jun. 2005, doi: 10.1121/1.1909368.

[103] A. Krokstad, S. Strom, and S. Sørsdal, "Calculating the acoustical room response by the use of a ray tracing technique," *Journal of Sound and Vibration*, vol. 8, no. 1, pp. 118–125, Jul. 1968, doi: 10.1016/0022-460X(68)90198-3.

[104] M. Vorländer, "The accuracy of calculations using the room acoustical ray-tracing-model and its dependence on the calculation time," *Acustica*, vol. 66, no. 2, pp. 90–96, 1988.

[105] A. Kulowski, "Error investigation for the ray tracing technique," *Applied Acoustics*, vol. 15, no. 4, pp. 263–274, Jul. 1982, doi: 10.1016/0003-682X(82)90061-5.

[106] F. A. (Frederick A. Everest and K. C. Pohlmann, *Master handbook of acoustics*. McGraw-Hill, 2009.

[107] M. Reuben, "Wayverb: A Graphical Tool for Hybrid Room Acoustics Simulation," University of Hudderfield, 2017. Accessed: Apr. 17, 2022. [Online]. Available: http://eprints.hud.ac.uk/id/eprint/33919/

[108] "ODEON Room Acoustics Software." https://odeon.dk/ (accessed Apr. 20, 2022).

[109] "CATT Acoustics ." http://www.catt.se/ (accessed Apr. 20, 2022).

[110] "Olive Tree Lab - Suite." https://www.mediterraneanacoustics.com/olive-tree-lab-suite.html (accessed Apr. 20, 2022).

[111] "EASE." https://www.afmg.eu/en/ease-enhanced-acoustic-simulator-engineers#features (accessed Apr. 20, 2022).

[112] M. J. Beeson and D. T. Murphy, "ROOMWEAVER: A DIGITAL WAVEGUIDE MESH BASED ROOM ACOUSTICS RESEARCH TOOL," 2004, Accessed: Apr. 17, 2022. [Online]. Available: www.dat.dtu.dk/~odeon/

[113] "Ear." https://github.com/aothms/ear (accessed Apr. 20, 2022).

[114] "Pachyderm Acoustical Simulation | Food4Rhino." https://www.food4rhino.com/en/app/pachyderm-acoustical-simulation (accessed Mar. 14, 2022).

[115] "I-Simpa: I-Simpa." https://i-simpa.univ-gustave-eiffel.fr/ (accessed Apr. 20, 2022).

[116] "openPSTD." http://www.openpstd.org/ (accessed Apr. 20, 2022).

[117] "openPSTD." http://www.openpstd.org/index.html (accessed Apr. 17, 2022).

[118] S. Lu, X. Yan, W. Xu, Y. Chen, and J. Liu, "Improving auditorium designs with rapid feedback by integrating parametric models and acoustic simulation," *Building Simulation*, vol. 9, no. 3, pp. 235–250, Jun. 2016, doi: 10.1007/S12273-015-0268-X.

[119] W. Jabi, *Parametric design for architecture*. London : Laurence King Publishing, 2013.

[120] I. Caetano, L. Santos, and A. Leitão, "Computational design in architecture: Defining parametric, generative, and algorithmic design," *Frontiers of Architectural Research*, vol. 9, no. 2, pp. 287–300, Jun. 2020, doi: 10.1016/J.FOAR.2019.12.008.

[121] L.P.L. van der Linden, "Course Reader: Parametric Engineering," 2018.

[122] P. Schumacher, "Parametricism as Style-Parametricist Manifesto," 2008, Accessed: May 03, 2022. [Online]. Available: http://www.patrikschumacher.com/Parametricism%20as%20Style.htm

[123] X. Shi and W. Yang, "Performance-driven architectural design and optimization technique from a perspective of architects," *Automation in Construction*, vol. 32, pp. 125–135, Jul. 2013, doi: 10.1016/J.AUTCON.2013.01.015.

[124] "Karamba3D – parametric engineering." https://www.karamba3d.com/ (accessed May 03, 2022).

[125] "Ladybug Tools | Food4Rhino." https://www.food4rhino.com/en/app/ladybug-tools (accessed Apr. 30, 2022).

[126] Scott Marble, "Digital Workflows in Architecture," *Digital Workflows in Architecture*, Dec. 2012, doi: 10.1515/9783034612173/HTML.

[127] M. Turrin, P. von Buelow, and R. Stouffs, "Design explorations of performance driven geometry in architectural design using parametric modeling and genetic algorithms," *Advanced Engineering Informatics*, vol. 25, no. 4, pp. 656–675, Oct. 2011, doi: 10.1016/J.AEI.2011.07.009.

[128] Z. Liang and W. Wenshun, "PARAMETRIC ARCHITECTURAL DESIGN BASED ON OPTIMIZATION ALGORITHM," *Engineering Heritage Journal*, vol. 3, no. 1, pp. 13–17, Feb. 2019, doi: 10.26480/GWK.01.2019.13.17.

[129] "Genetic Algorithms - Fundamentals." https://www.tutorialspoint.com/genetic_algorithms/genetic_algorithms_fundamentals.htm (accessed May 11, 2022).

[130] Y. J. Grobman, A. Yezioro, and I. G. Capeluto, "Non-Linear Architectural Design Process," *International Journal of Architectural Computing*, vol. 8, no. 1, pp. 41–53, Jan. 2010, doi: 10.1260/1478-0771.8.1.41.

[131] "Evolutionary Engine for Grasshopper3D | Wallacei." https://www.wallacei.com/ (accessed May 03, 2022).

[132] "Rhino - Rhinoceros 3D." https://www.rhino3d.com/ (accessed Apr. 30, 2022).

[133] "Grasshopper - algorithmic modeling for Rhino." https://www.grasshopper3d.com/ (accessed Apr. 30, 2022).

[134] Arthur van der Harten, "Pachyderm Geometrical Acoustics - Geometrical Acoustics Simulation." https://app.gitbook.com/o/-MUFQGwbXTJbIrf7W5cD/s/-MDwhSkoNpBHNIRh8Fxr/ (accessed Feb. 17, 2022).

[135] "Ray Tracing: Rendering a Triangle (Barycentric Coordinates)." https://www.scratchapixel.com/lessons/3d-basic-rendering/ray-tracing-rendering-a-triangle/barycentric-coordinates (accessed Apr. 20, 2022).

[136] R. A. Tenenbaum, T. S. Camilo, J. C. B. Torres, and S. N. Y. Gerges, "Hybrid method for numerical simulation of room acoustics with auralization: part 1 - theoretical and numerical aspects," *Journal of the Brazilian Society of Mechanical Sciences and Engineering*, vol. 29, no. 2, pp. 211–221, 2007, doi: 10.1590/S1678-58782007000200012.

[137] "ISO - ISO 3382-1:2009 - Acoustics — Measurement of room acoustic parameters — Part 1: Performance spaces," 2009. Accessed: Apr. 20, 2022. [Online]. Available: https://www.iso.org/standard/40979.html

[138] S. Schlesinger *et al.*, "Terminology for model credibility," *SIMULATION*, vol. 32, no. 3, pp. 103–104, Mar. 1979, doi: 10.1177/003754977903200304.

[139] R. G. Sargent, "Verification and validation of simulation models," *Proceedings - Winter Simulation Conference*, pp. 166–183, 2010, doi: 10.1109/WSC.2010.5679166.

[140] J. Picaut, T. le Pollès, P. L'Hermite, and V. Gary, "Experimental study of sound propagation in a street," *Applied Acoustics*, vol. 66, no. 2, pp. 149–173, Feb. 2005, doi: 10.1016/J.APACOUST.2004.07.014.

[141] Christensen C. L and Koutsouris G., "User Manual: ODEON Room Acoustic Software." Odeon A/S, Lyngby, 2015.

[142] Y. Smyrnova, J. Kang, C. Cheal, E. Tijs, and H.-E. de Bree, "Laboratory Test of Sound Absorption of Vegetation," in *1st EAA - Euro Regio Congress on Sound and Vibration*, Sep. 2010, pp. 15–28.

[143] Z. Azkorra *et al.*, "Evaluation of green walls as a passive acoustic insulation system for buildings," *Applied Acoustics*, vol. 89, pp. 46–56, Mar. 2015, doi: 10.1016/J.APACOUST.2014.09.010.

[144] M. J. M. Davis, M. J. Tenpierik, F. R. Ramírez, and M. E. Pérez, "More than just a Green Facade: The sound absorption properties of a vertical garden with and without plants," *Building and Environment*, vol. 116, pp. 64–72, May 2017, doi: 10.1016/J.BUILDENV.2017.01.010.

[145] H. S. Yang, J. Kang, and C. Cheal, "Random-incidence absorption and scattering coefficients of vegetation," *Acta Acustica united with Acustica*, vol. 99, no. 3, pp. 379–388, May 2013, doi: 10.3813/AAA.918619.

[146] E. D. Giouri, M. Tenpierik, and M. Turrin, "Zero energy potential of a high-rise office building in a Mediterranean climate: Using multi-objective optimization to understand the impact of design decisions towards zero-energy high-rise buildings," *Energy and Buildings*, vol. 209, p. 109666, Feb. 2020, doi: 10.1016/J.ENBUILD.2019.109666.

[147] D. Yang, S. Ren, M. Turrin, S. Sariyildiz, and Y. Sun, "Multi-disciplinary and multi-objective optimization problem re-formulation in computational design exploration: A case of conceptual sports building design," *Automation in Construction*, vol. 92, pp. 242–269, Aug. 2018, doi: 10.1016/J.AUTCON.2018.03.023.

[148] A. Christodoulou, M. Vola, and G. Rikken, "Case study for the application of multidisciplinary computational design assessment and constructability optimisation tools," *Simulation Series*, vol. 50, no. 7, pp. 39–46, 2018, doi: 10.22360/SIMAUD.2018.SIMAUD.006.

[149] "Wallacei | About." https://www.wallacei.com/about (accessed May 08, 2022).

[150] "NSGA-II: Non-dominated Sorting Genetic Algorithm." https://pymoo.org/algorithms/moo/nsga2.html (accessed May 08, 2022).

[151] Y. Yusoff, M. S. Ngadiman, and A. M. Zain, "Overview of NSGA-II for Optimizing Machining Process Parameters," *Procedia Engineering*, vol. 15, pp. 3978–3983, Jan. 2011, doi: 10.1016/J.PROENG.2011.08.745.

[152] E. M. Salomons, "Appendix B : Free feild of a point source," in *Computational Atmospheric Acoustics*, Dordrecht: Springer Netherlands, 2001, pp. 37–65. doi: 10.1007/978-94-010-0660-6_4.

[153] "Vertical structure of the moist atmosphere," *Thermal Physics of the Atmosphere*, pp. 115–132, 2021, doi: 10.1016/B978-0-12-824498-2.00013-6.

[154] "Refraction of Sound Waves." https://www.acs.psu.edu/drussell/demos/refract/refract.html (accessed Jan. 24, 2022).

Table of figures

Appendix A: Atmospheric effects on sound propagation

A.1 Atmospheric Absorption

The amplitude of sound waves decreases with increasing distance *r* from the source (equations (5) and (6)). In the real atmosphere, however, the decrease in the amplitude of the wave is much larger. This is because sound waves lose their energy due to fluctuations in temperature and humidity [57]. The process of atmospheric absorption is originating from two physical effects:

i. Thermal conduction and viscosity of air
ii. Relaxation losses of gas molecules in the air

The temperature gradients present in the sound wave are partly reduced by the heat flow, which is a function of the thermal conductivity of air [152]. While velocity gradient in the sound wave is reduced by the momentum transfer, which is a function of the viscosity of air [152]. Also, the gas (oxygen, nitrogen and water vapour) molecules vibrate and rotate in the atmosphere, thus taking away the energy from the sound wave[57]. The atmospheric absorption not only depends on temperature and humidity but also on the frequency of the sound waves. Table 4 shows the absorption coefficient (dB/m) as a function of frequency, temperature and relative humidity. However, for most practical applications, the frequency-dependent effect is neglected [152]. The overall atmospheric absorption A_A and the effect of sound propagation are given by equation (10), in which, a is a attenuation coefficient [dB/m] and r is the distance between source and receiver [m].

$$A_A = -ar \tag{19}$$

The atmospheric attenuation coefficient can be derived by multiplying the sound absorption coefficient (m-1) with a factor equal to 8.686[57]. Then the sound pressure level at the source as a result of atmospheric absorption and spreading loss is given by equation (11).

$$L_p(r,\theta) = L_{p0} - 10{,}8 - A_r + DI(\theta) - A_A \tag{20}$$

In which, L_p is sound pressure level at source [dB], L_{p0} is the sound pressure level at 1m from the source [dB]. $A_r = 20\log(r)$ derived in chapter section 1.1.1 (equation (5)) and DI is the directionality index.

Temperature (°C)	Relative humidity (%)	63 Hz	125 Hz	250 Hz	500 Hz	1000 Hz	2000 Hz	4000 Hz	8000 Hz
30	20	0.212	0.717	1.86	3.40	6.00	14.6	47.6	167
	50	0.0904	0.346	1.24	3.56	7.03	11.7	24.7	74.2
	80	0.0573	0.223	0.852	2.90	7.41	13.3	23.3	56.4
20	20	0.259	0.706	1.39	2.59	6.55	21.6	74.9	218
	50	0.122	0.440	1.31	2.73	4.67	9.90	29.7	106
	80	0.0788	0.298	1.04	2.76	5.15	9.01	21.4	69.6
10	20	0.271	0.576	1.19	3.27	11.0	36.4	92.1	155
	50	0.160	0.481	1.05	1.89	4.27	13.3	47.2	157
	80	0.108	0.373	1.02	1.96	3.57	8.80	29.0	105
0	20	0.256	0.609	1.84	6.15	17.8	34.8	47.2	58.4
	50	0.180	0.408	0.818	2.08	6.84	23.9	71.6	148
	80	0.138	0.376	0.756	1.51	4.07	13.9	49.3	148

Table A1 Absorption coefficient (dB/m) as a function of frequency, temperature, and relative humidity[57]

A.2 Atmospheric Refraction

Atmospheric refraction is defined as a change in the propagation direction of a sound wave due to a sound speed gradient in the atmosphere [58]. The change in sound speed is occurred due to the density difference between atmospheric layers and wind speed [57]. In figure A1, the γ_1 (degree) correspond to the incoming angle made by sound ray, whereas γ_2 (degrees) is the refracted angle which is different from the incoming angle [58].

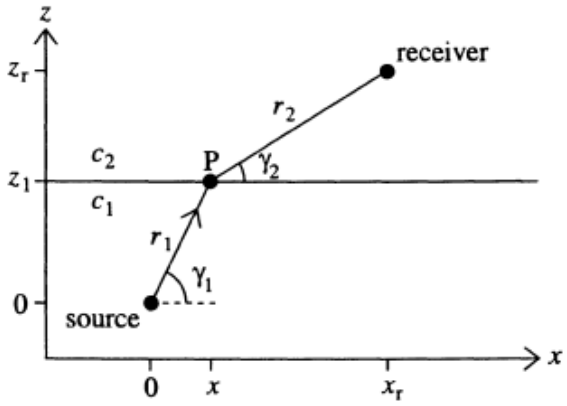

Figure A1 Refracted sound ray from source to receiver at the interface between two media[58]

The relation between two angles is given by Snell's law (equation-12) where c_1 and c_2 are the sound speed (m/s) in the corresponding media[57], [58].

$$\frac{\cos\gamma_1}{c_1} = \frac{\cos\gamma_2}{c_2} \tag{21}$$

The density of the atmospheric layer changes due to the temperature gradient, therefore in a non-moving atmosphere (without wind), sound speed c is the function of the temperature T of the atmosphere[58] and is defined by equation (13) [59],

$$c = c_0\sqrt{\frac{T}{T_0}} \tag{22}$$

In which, T is the temperature in Kelvin, $c_0 = 343\ m/s$ and $T_0 = 293\ K$

Higher temperature yields faster sound propagation due to less density [59]. During the day, the temperature near the ground surface is larger due to the heating of the earth's surface by solar radiation. The temperature decreases with elevation which is called as lapse rate (figure A2)

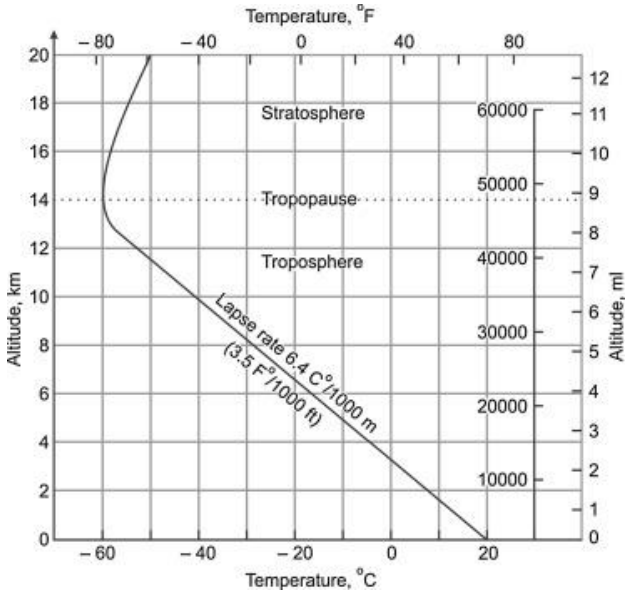

Figure A2 Variation of temperature with altitude (lapse rate), retrieved from [153]

Therefore, during the day, the sound wave travelling close to the ground is faster than the wave travelling far from the ground resulting in upward refraction [59]. This results in the formation of shadow zones where sound pressure levels are theoretically zero (see figure A3). During the night, the effect opposite where the ground surface cools faster than the atmosphere resulting in downward refraction[59].

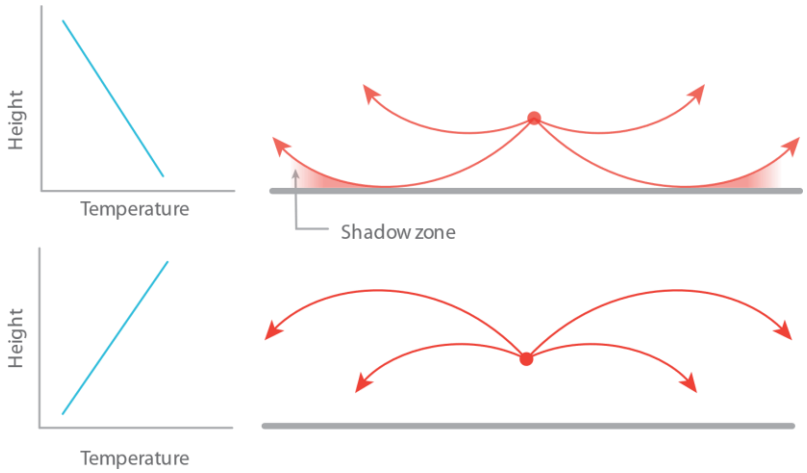

Figure A3 Top: upward refraction of sound, Bottom: downward refraction of the sound, based on[154]

In the above example, a non-moving atmosphere was considered, however, sound propagation in a moving atmosphere (with the wind) is more complex [58]. Refraction caused by the wind depends on the direction of the wind and often, simplification is carried out to include the effect of wind and the effective sound speed (c_{eff}) is given by equation (14), where c is the adiabatic sound speed (m/s) and u_r is the wind speed in the direction of sound propagation (m/s)

$$c_{eff} = c + u_r \tag{23}$$

The idea behind this simplification is that a sound wave travels slower when the wind is opposite to sound propagation ($u_r < 0$) and faster if sound moves in the direction of propagation ($u_r > 0$) [58] [59]. The latter case results in upward refraction while downward refraction occurs if the wind blows in the same direction [59].

Moreover, the roughness of the ground surface also determines the shape of the wind profile [58]; for example, a rough surface results in a lower wind speed near the ground [59]. To account for this effect, a logarithmic function is frequently used to simulate a realistic atmosphere [58].

$$c_{eff}(z) = c_0 + b\ln\left(\frac{z}{z_0} + 1\right) \tag{24}$$

In which, b is 1m/s for downward refraction and -1 m/s for upward refraction, and z_0 is roughness length of the ground surface (0.01m to 0.1m for grassland).

Therefore, after applying the correction for ground roughness and temperature the final resulting equation for sound speed c_{eff} at given height z is given by equation 16,

$$c_{eff}(z) = c_o \sqrt{\frac{T(z)}{T_o}} \pm u(z) \tag{25}$$

In which, $u(z)$ is horizontal wind speed function which is subtracted for upward refraction and added for downward wind speed. In crosswind conditions, $u(z)$ is zero [59]. Since the effect of atmospheric refraction is based on the wind and temperature, which is in itself a complex phenomenon, their effect is most often approximated in sound simulation programmes.

A.3 Atmospheric Turbulence:

Wind and temperature always fluctuate at short intervals in the real atmosphere, and these fluctuations are referred to as atmospheric turbulence. The atmospheric variability occurs due to shear instability (mechanical turbulence) and buoyancy (convective turbulence) [61]. Small temperature differences between air and ground combined with high wind velocities cause mechanical turbulence [61]. While convective turbulence is associated with a large temperature difference between ground and atmosphere [61]. These changes abrupt the general flow direction of fluid (wind in our case), forming swirls known as turbulent eddies[59] see figure A4. The formation of eddies is a continuous process, and their size increases with ground distance [59]. However, the larger eddies are transformed into smaller eddies and virtually all the kinetic energy is dissipated into heat [61][59].

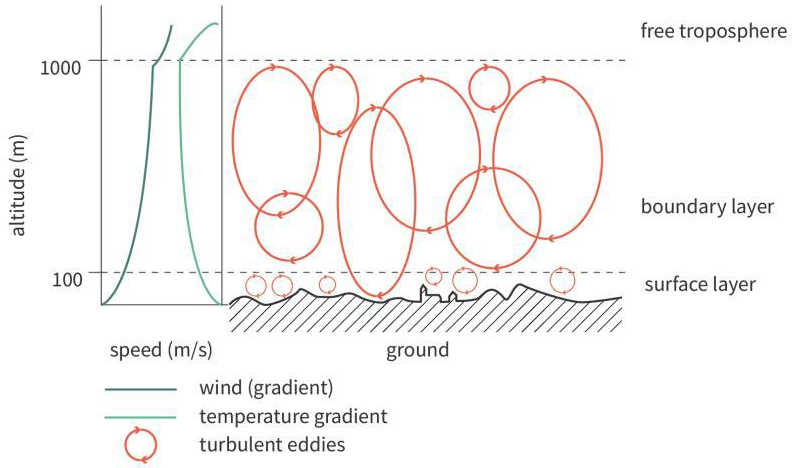

Figure A4 Schematic representation of the atmospheric boundary layer and turbulent eddy structure, adapted from [61]

To count these fluctuations in temperature and wind speed corresponding to turbulence, the acoustic refraction index n is used,

$$n = \frac{c_0}{c_{eff}} \tag{26}$$

In a turbulent atmosphere, the refractive index fluctuates around an average value[60] represented as n_d, and μ is fluctuating unit. Thus, equation (17) can be rewritten a [59] [60],

$$n(r,z) = n_d(z) + \mu(r,z) \tag{27}$$

In which, n_d only varies with the height z above the ground while μ varies with height as well as the distance between source and receiver $\left(r = \sqrt{x^2 + y^2}\right)$[60]. Since sound wave travels so fast that the medium can be considered 'frozen' and thus the amount of turbulence can be approximated [59] [60]. The fluctuation μ is depend on temperature fluctuation T_t and the turbulent wind velocity fluctuation u_t given by,

$$\mu = \frac{T_t}{2T_0} - \frac{u_t}{c_o} \tag{28}$$

Atmospheric turbulence results in a large increase in sound pressure level in the shadow region[60]. Oliveira[59] also concludes this phenomenon from his numerical application method in upward conditions. The increase in sound pressure level is a result of scattering by the turbulent eddies illustrated in figure A5 and results from [59]can be seen in figure A6.

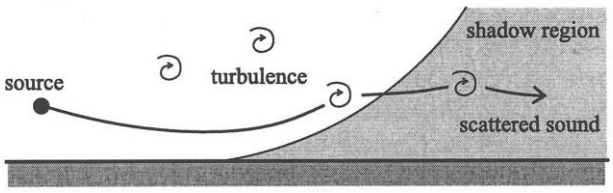

Figure A5 Scattering of sound into a refractive shadow region, adapted from[60]

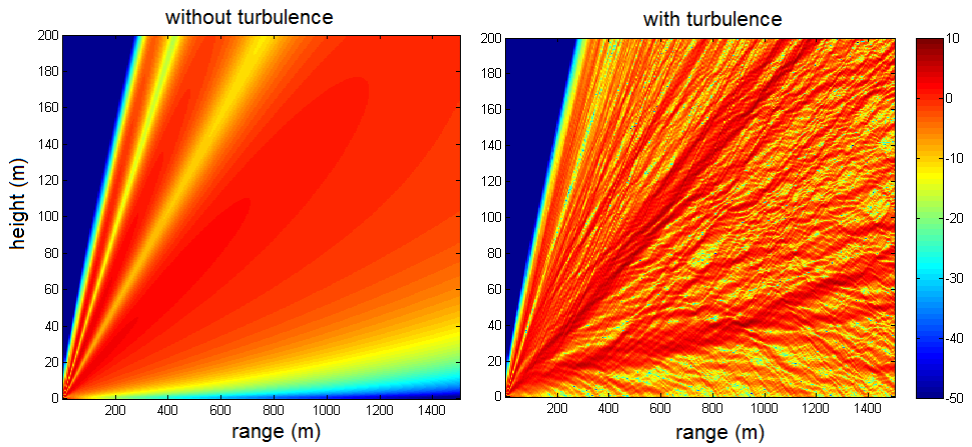

Figure A6 Relative sound pressure levels with and without turbulence, retrieved from[59]

Literature [60] suggests that the increase in sound pressure level in the shadow region is around 10 dB more than that of a non-turbulent environment. Although the effects due to atmospheric turbulence are large, it plays a less important role when the source and receiver are located near the surface [56]. Therefore, for traffic noise simulation, the effects are generally ignored [61].

Appendix B: Theoretical calculation for validation.

The ISO 9613-2 "Attenuation of sound during propagation outdoors- part 2 (A general method of calculation)" describes the calculation of damping of the noise during propagation outdoors. Thus, this appendix includes a sample calculation carried out for the validation process. Further B.2 shows sample calculation for interference effect.

B.1 Outdoor sound propagation

The resulting noise level is then given by,

$$L_{AT}(DW) = L_{WA} + D_C - A - C_{\text{met}}$$

Where, L_{WA} is source noise = 80dB

D_C is the directional correction for noise source given by,

$$D_C = D_\Omega - 0$$

D_Ω is calculated as,

$$D_\Omega = 10\lg\left\{1 + \left[d_p^2 + (h_s - h_r)^2\right]/\left[d_p^2 + (h_s + h_r)^2\right]\right\}$$

Where, h_s is the noise source height above terrain = 0.5m
h_r is the noise receptor height above terrain= 0.5m
d_p is the distance between a noise source and recipient projected on level terrain= 3.5m
Thus, D_Ω is calculated as 2,84 dB

A is the damping between the noise source and receiver given by

$$\mathrm{A} = \mathrm{A_{div}} + \mathrm{A_{atm}} + \mathrm{A_{gr}} + \mathrm{A_{bar}} + \mathrm{A_{misc}}$$

$\mathrm{A_{div}}$ is the damping due to geometry calculated by,

$$\mathrm{A_{div}} = 20\lg\,(\mathrm{d}/1\mathrm{m}) + 11\mathrm{dB}$$

Where d is the distance between source and receiver, therefore $\mathrm{A_{div}} = 21.88\ dB$

$\mathrm{A_{atm}}$ is the damping due to absorption of air given,

$$\mathrm{A_{atm}} = \alpha_{500}\mathrm{d}/1000$$

Where, α_{500} is air absorption coefficient at 500 Hz frequency (10°C and 70% humidity) = 1.9 dB/km. Therefore, $\mathrm{A_{atm}} = 6.65\ x\ 10\text{^} - 3$

$\mathrm{A_{gr}}$ is the terrain damping given by,

$$A_{gr} = 4{,}8 - (2h_m/d)[17 + (300/d)]$$

However, terrain damping is not applicable in this case since the surface is hard pavement.

$\mathrm{A_{bar}}$ is introduced to include the effect of the noise barrier, which is not applicable in this case. And $\mathrm{A_{misc}}$ is the damping due to other effects like vegetation, buildings and industry which are also excluded from the calculations.

Finally, C_{met} is the meteorological correction which is determined by means of the equation:

$$C_{\text{met}} = 0 \text{ for } dp < 10(h_s + h_r)$$
$$C_{\text{met}} = C0[1 - 10(h_s + h_r)/dp] \text{ for } dp > 10$$

Since $dp < 10(h_s + h_r)$, C_{met} becomes zero.

After substituting all the calculated values, $L_{AT}(DW) = 61\ dB$

B.2 Interference effect

According to [61], the first destructive interface occurs at $k(R2 - R1) = \pi$. Therefore, considering a sine wave, the constructive interface should occur at $k(R2 - R1) = 2\pi, 4\pi, 6\pi \ldots etc$, where $k = w/c$ and $k = 2\pi f$ (c being the speed of sound and f being the frequency)[61].

Table B.1 shows the calculations for the 10m distance where the first peak is observed. As one can infer, the values do not coincide with all the frequencies. Similar results are also obtained for the peaks at 24m, 32m and 46m and therefore it is concluded that the occurrence of these peaks is a result of certain building irregularities present along the street rather than the constructive or destructive interface.

Frequency	$k(R2-R1)$	Nearest π value
62.5	3.40	2π = 6.28
125	6.80	2π = 6.28
500	27.20	$\mathbf{8}\pi$ = 25.13
1000	54.40	$\mathbf{18}\pi$ = 56.55
2000	108.81	34π = 106.81
4000	217.61	$\mathbf{70}\pi$ = 219.91
8000	435.23	138π = 433.53

Table B.1 Calculations for the constructive interface at 10m

Appendix C: Grasshopper Definitions

C.1 Point Source to Point Receiver

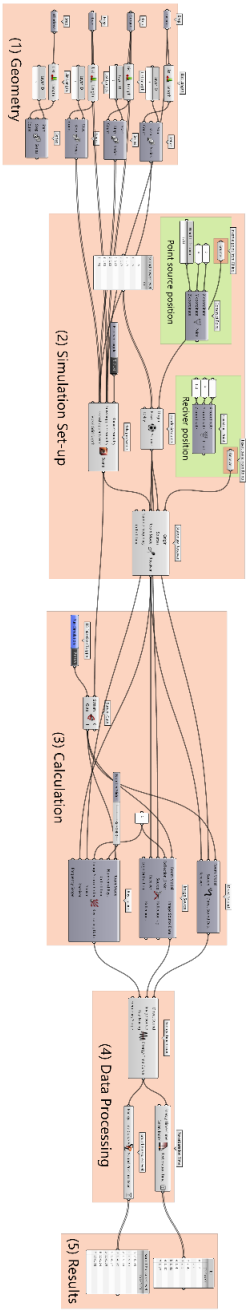

C.2 Line Source to SPL Mapping

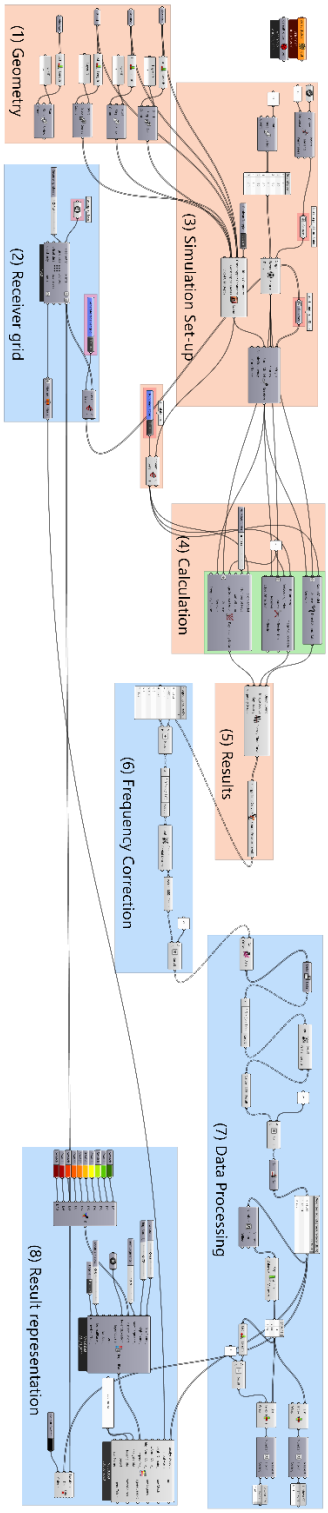

C.3 Parametric Balcony

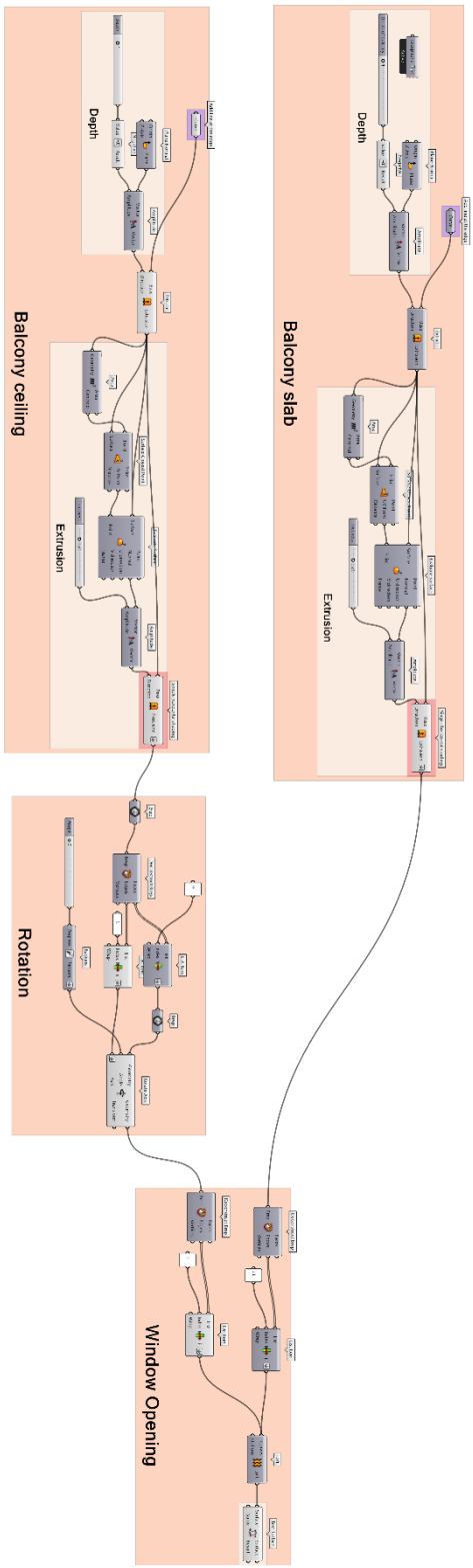

The parametric balcony definition is made using Grasshoppers' native components and can be seen as a four-step process. First, extrusions for balcony slab and balcony ceilings are created. Both the workflow takes a line from the Rhino as an input and creates a flat surface. The depth of these surfaces is controlled by the number slider. This number slider will be the design variable in the optimization workflow (see next section C5). Then these surfaces are extruded to make solid rectangles.

The extruded ceiling is then deconstructed into surfaces to take out the bottom surface (ceiling) and rotated by assigning the number slider. Again, this number slider will act as a design variable in the optimization workflow. Finally, by taking the edge of the ceiling and slab as input window opening is created.

C.4 Optimization

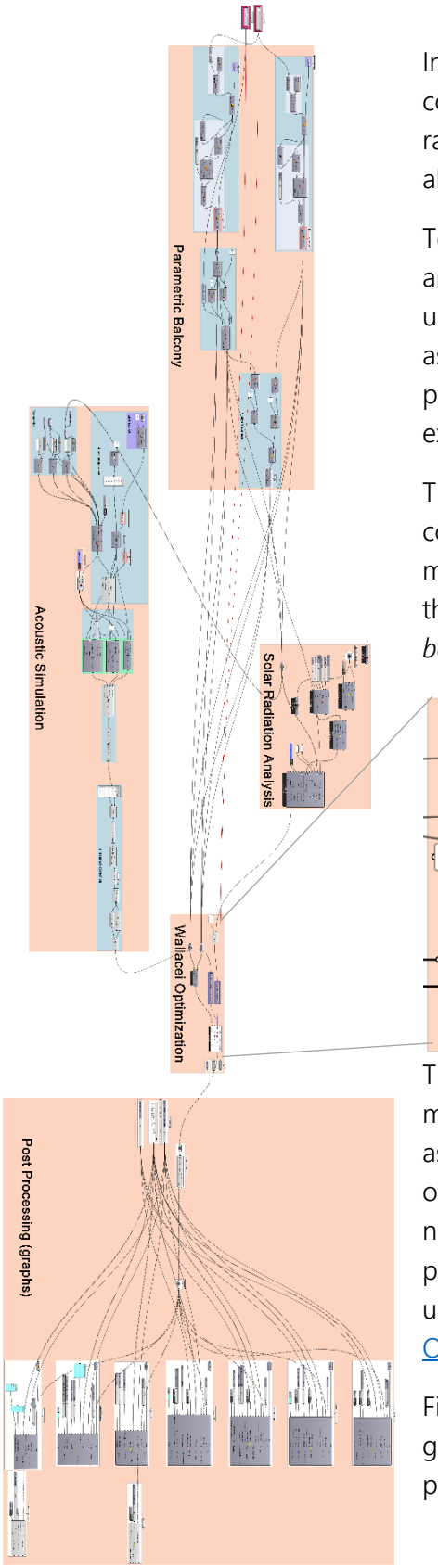

In this workflow, all the bits and pieces are combined i.e it is a combination of the parametric balcony, acoustic workflow, solar radiation analysis and Wallacei optimization. The first two are already explained.

To construct solar radiation definition, ladybug legacy components are used. The analysis period was set from 1st of Dec to 1st of March using a number slider and weather data from Amsterdam is used as an input. The previously created window opening in the parametric balcony script is set as the analysis surface and balcony extrusions as a context.

Then the optimization was carried out using the Wallacei X component which requires Genes, objectives and Phenotype as the main input. Genes mean the design variables to be optimized, therefore, the sliders used in the parametric balcony (*Depth of the balcony* and the *angle of the ceiling*) are inserted as an input.

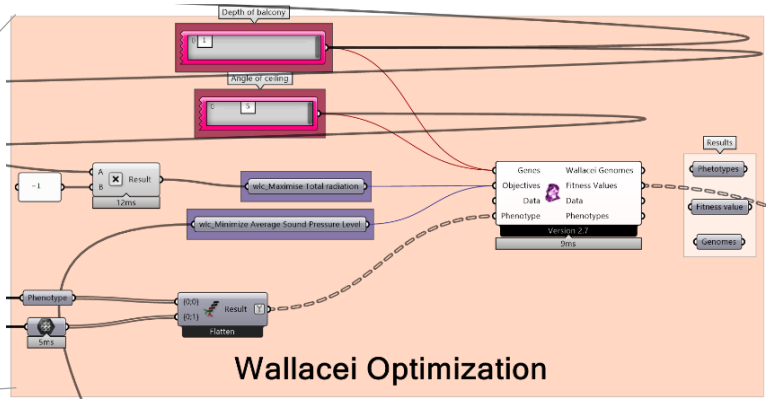

Then for the objective, first the solar radiation is multiplied by -1 to maximize the number and the average SPL from five receivers is set as a second objective. Phenotypes are the design solutions obtained after optimization, to get those solutions in 3D form one needs to insert geometry first, which is done by inserting the parametric balcony as a mesh. The detailed description for setting up the analysis using Wallacei is explained in [Multi-Objective Optimization with Wallacei - TOI-Pedia (tudelft.nl)]

Finally, the output from the optimization is processed by using the graphs like Standard deviation, mean trend line, Pareto front, and parallel co-ordinate plot.

Appendix D: Design stage results

D.1 Façade inclination (F1)

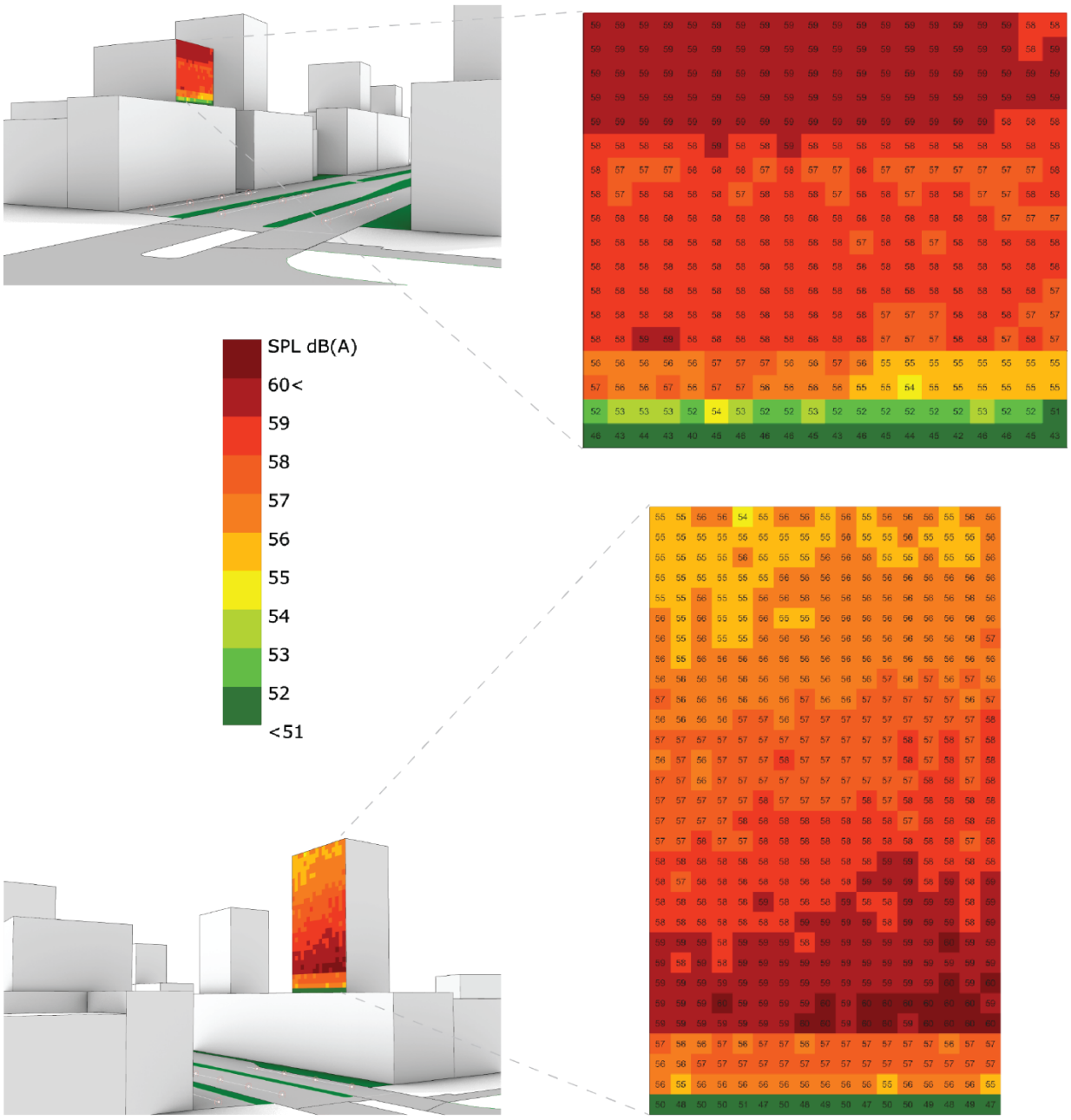

Figure D1 Sound pressure level for 90° facade (F1.1)

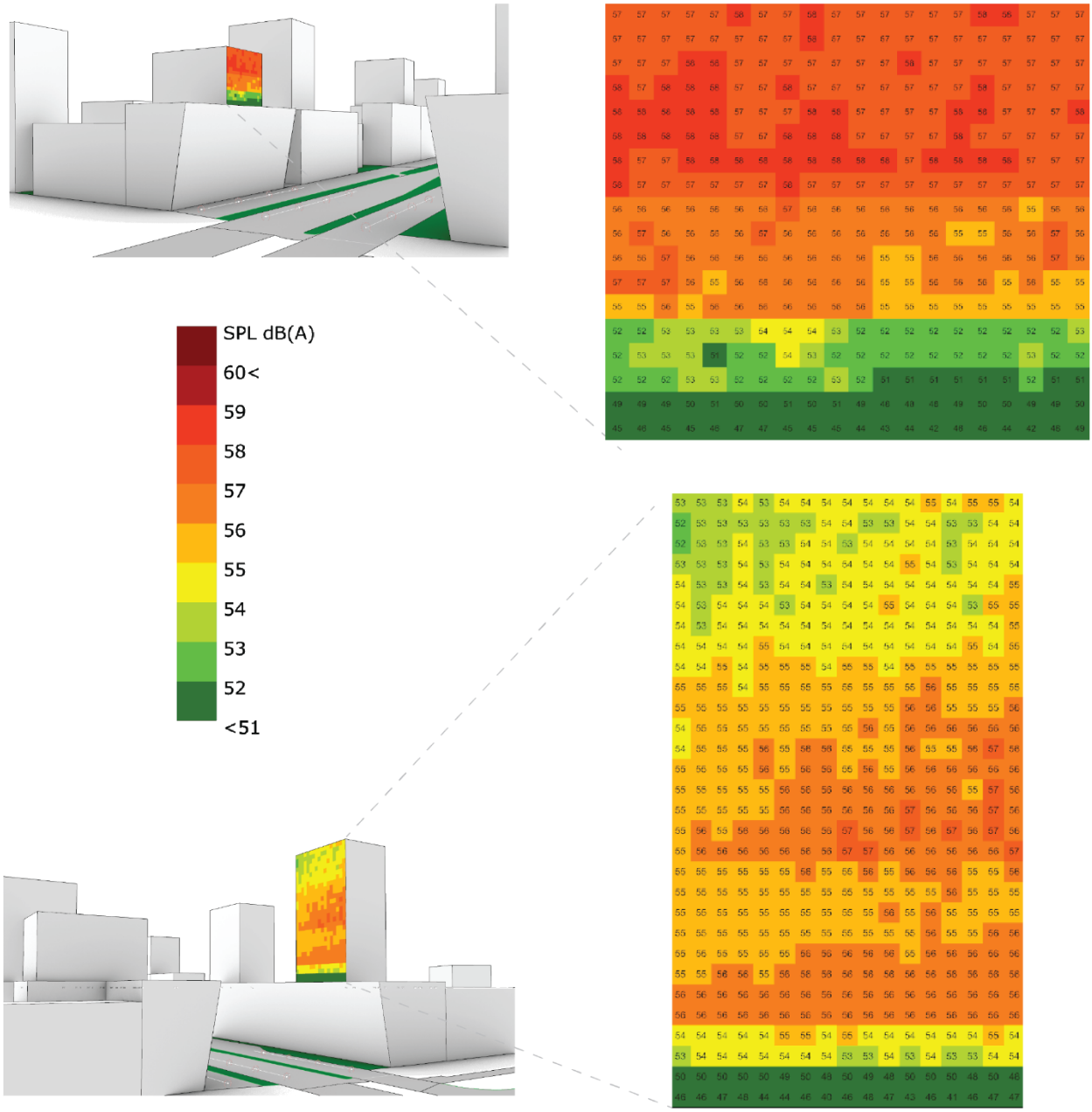

Figure D2 Sound pressure level for 80° facade (F1.2)

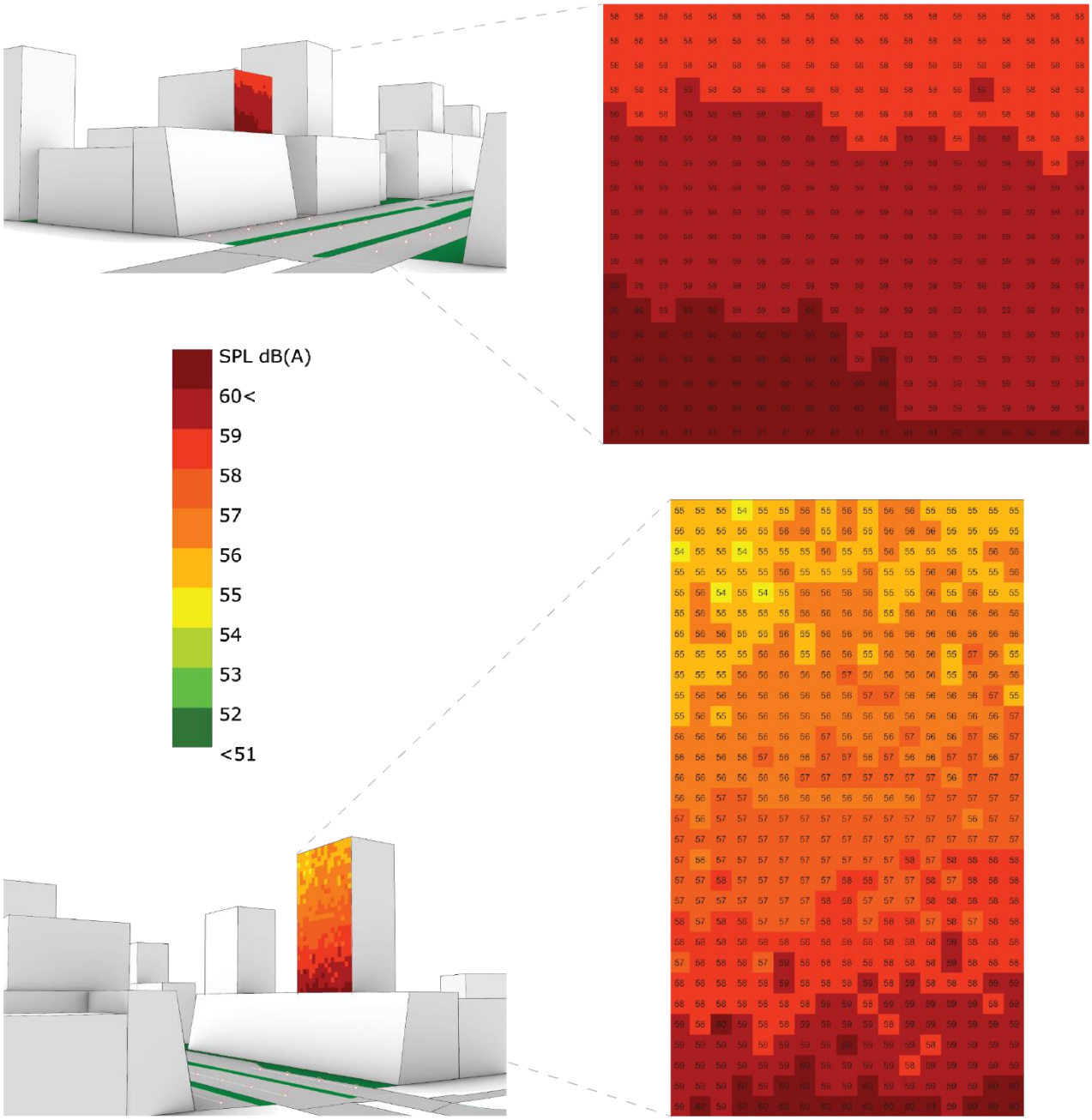

Figure D3 Sound pressure level for 110° facade (F1.3)

D.2 Façade Extrusion(F2)

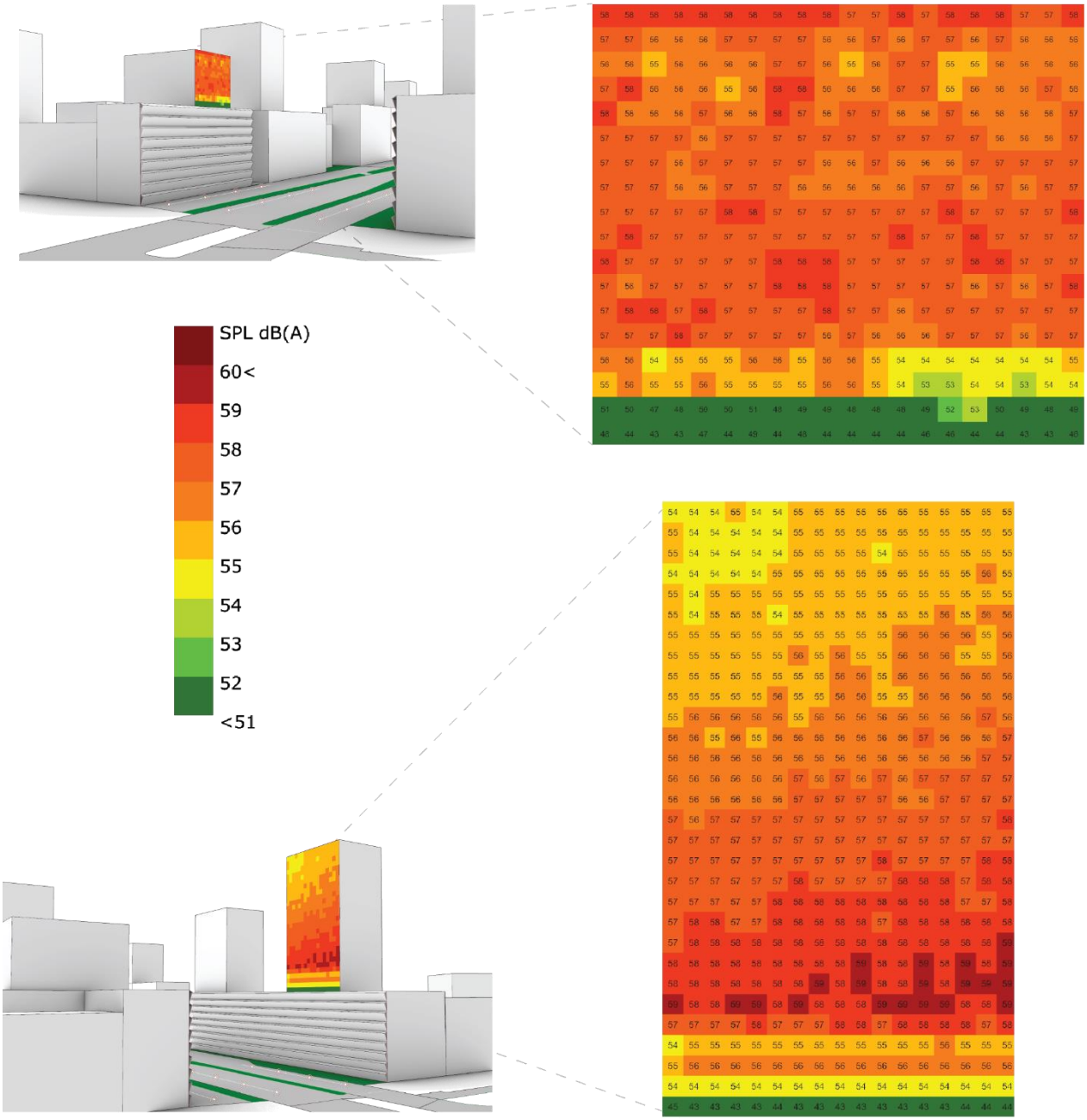

Figure D4 Sound pressure levels on façade with extrusion (apex up F2.1)

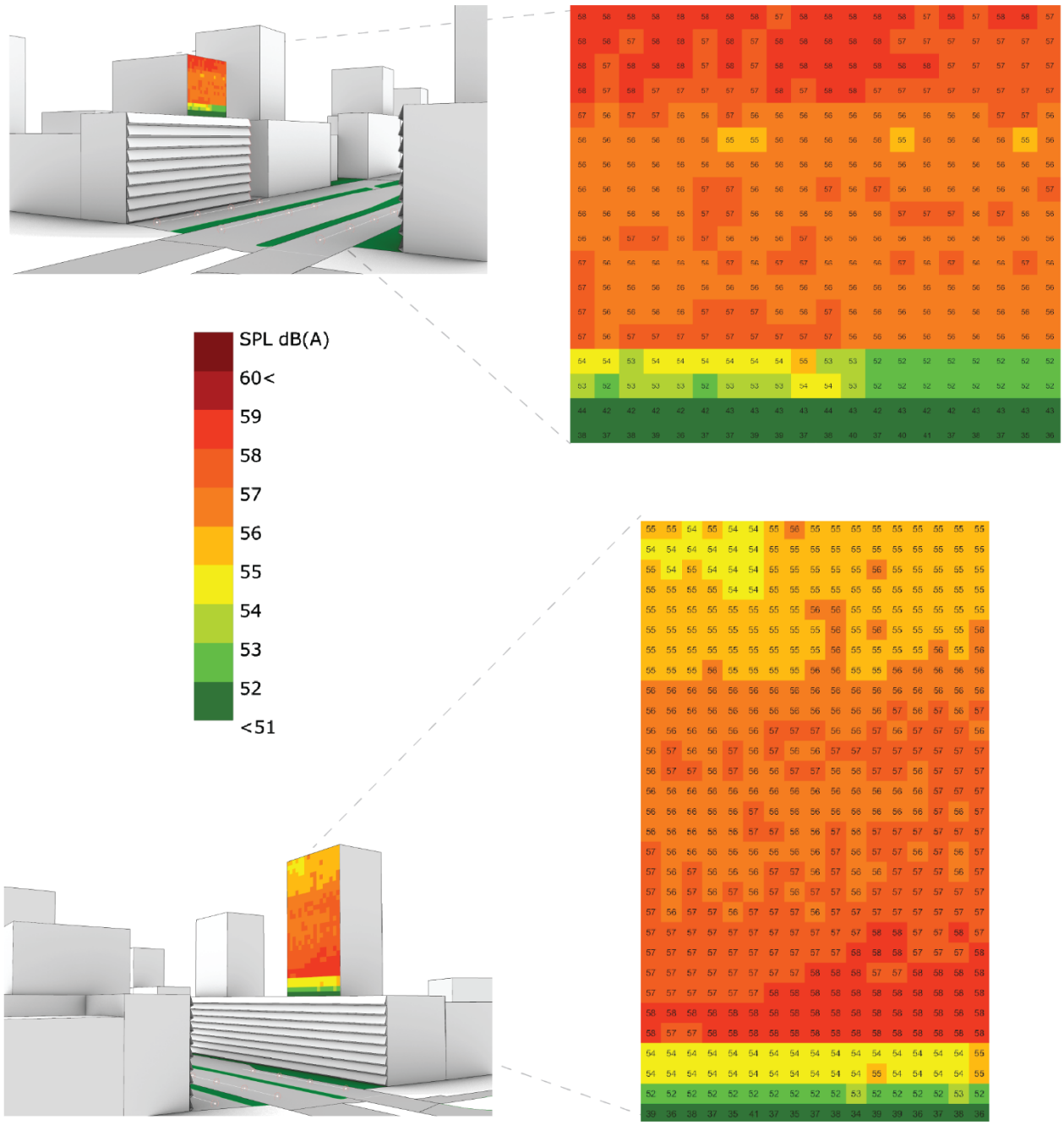

Figure D5 Sound pressure levels on façade with extrusion (apex up F2.1)

D.3 Façade Material (F3)

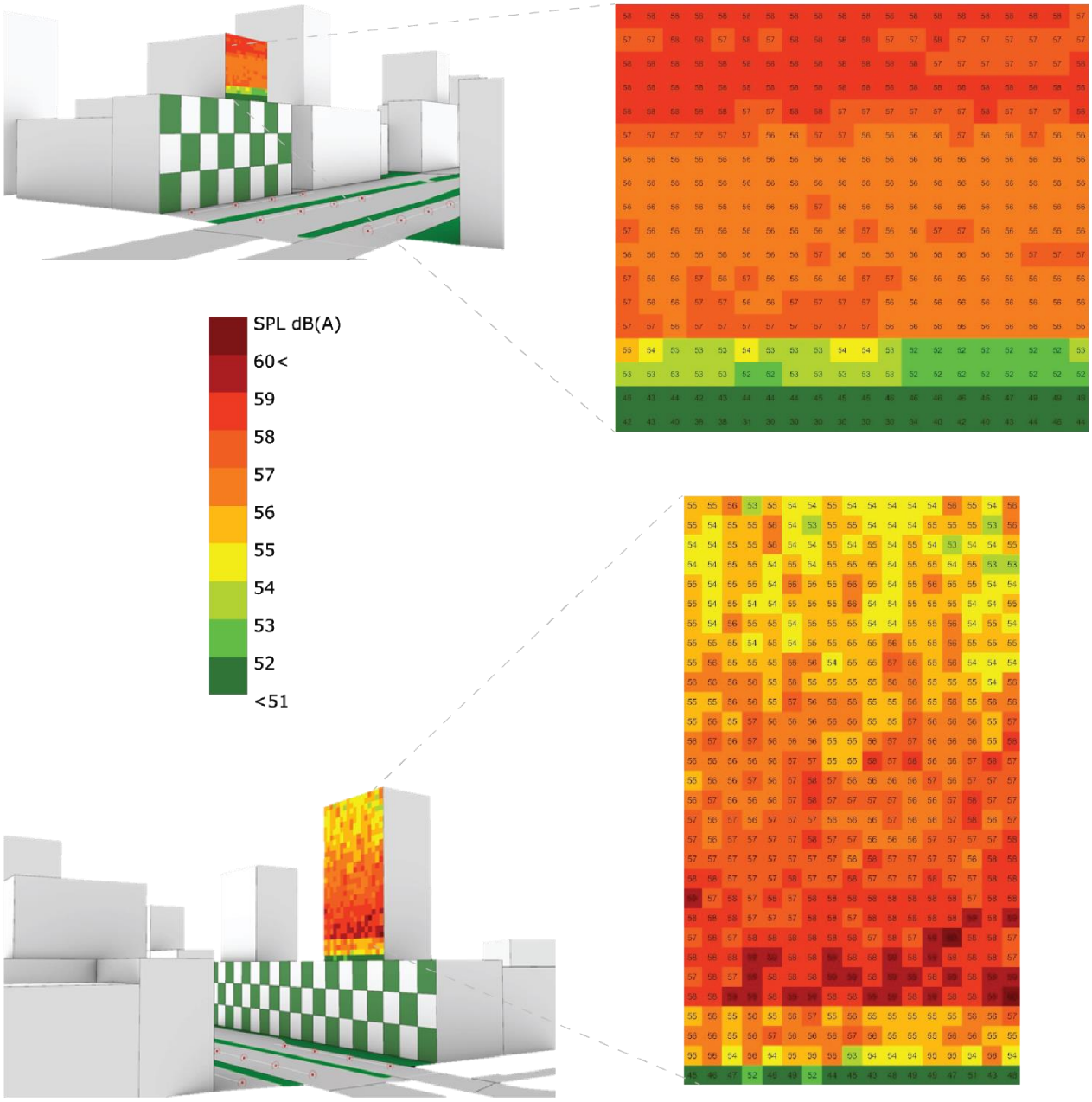

Figure D6 Sound pressure levels on façade with green pattern (F3)

D.4 Courtyard variation (C)

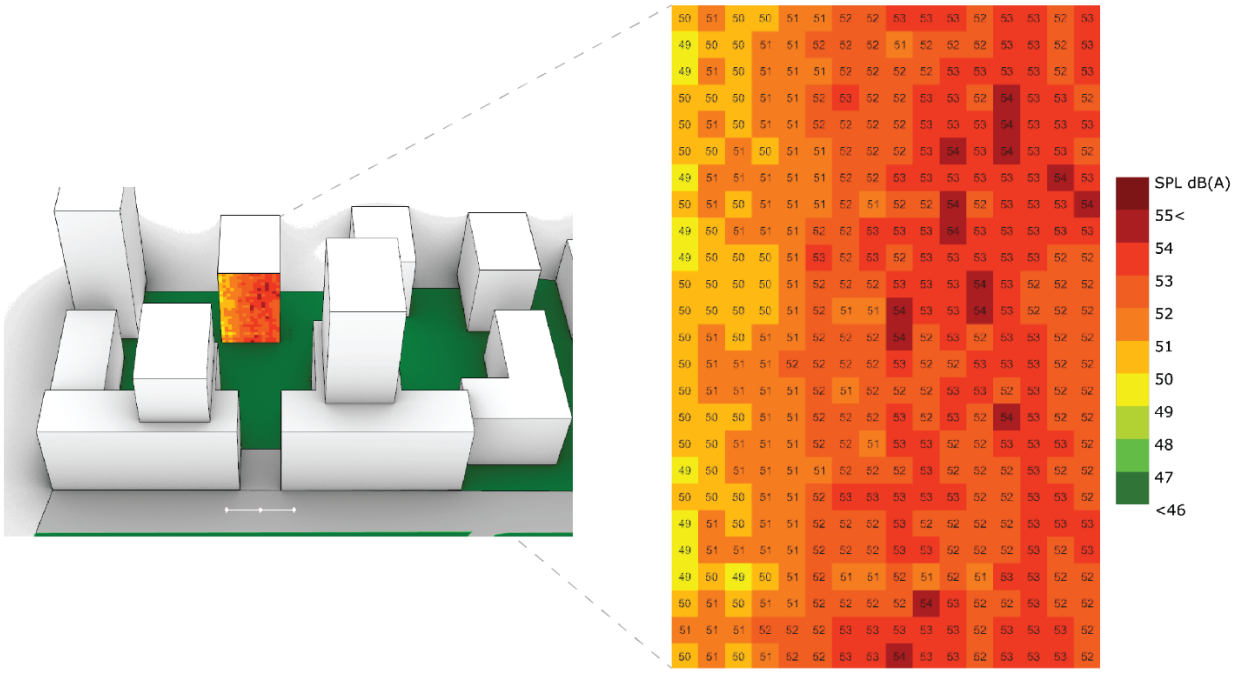

Figure D7 Sound pressure levels on façade for courtyard base sequence C1.1

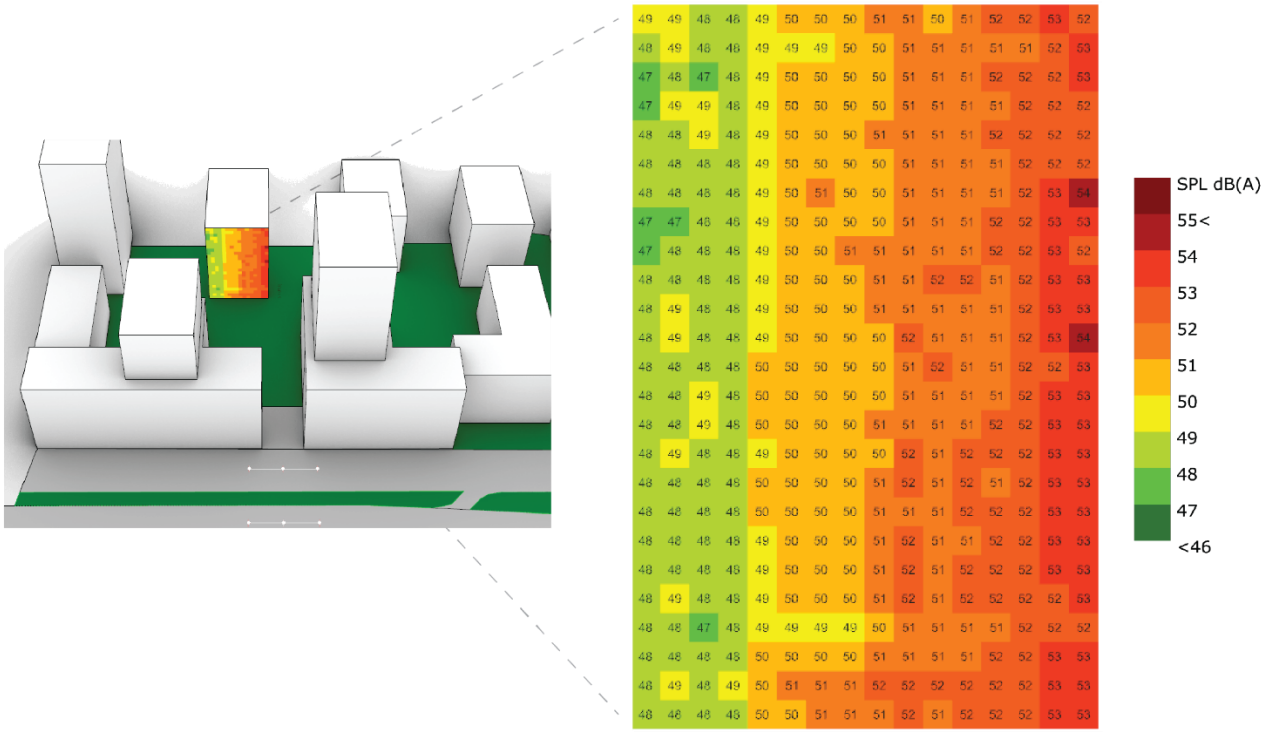

Figure D8 Sound pressure levels on façade for courtyard 10m offset sequence C1.2

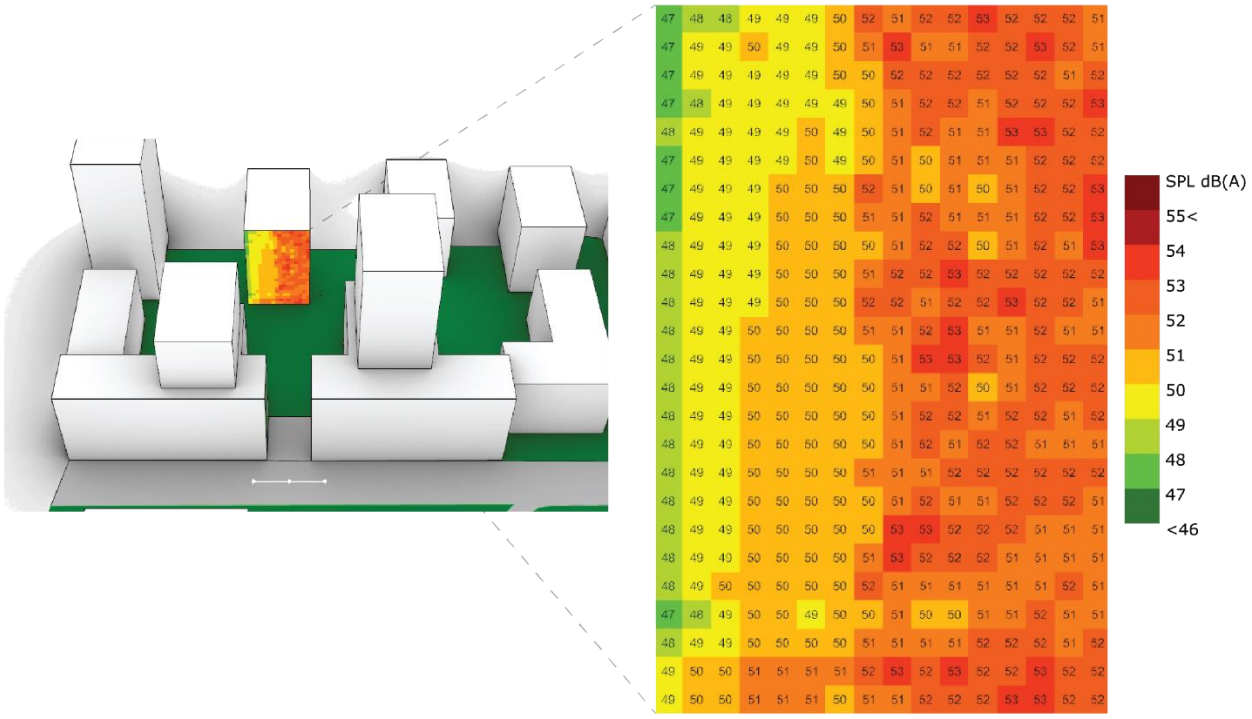

Figure D9 Sound pressure levels on façade for courtyard base sequence with green wall (C1.3)

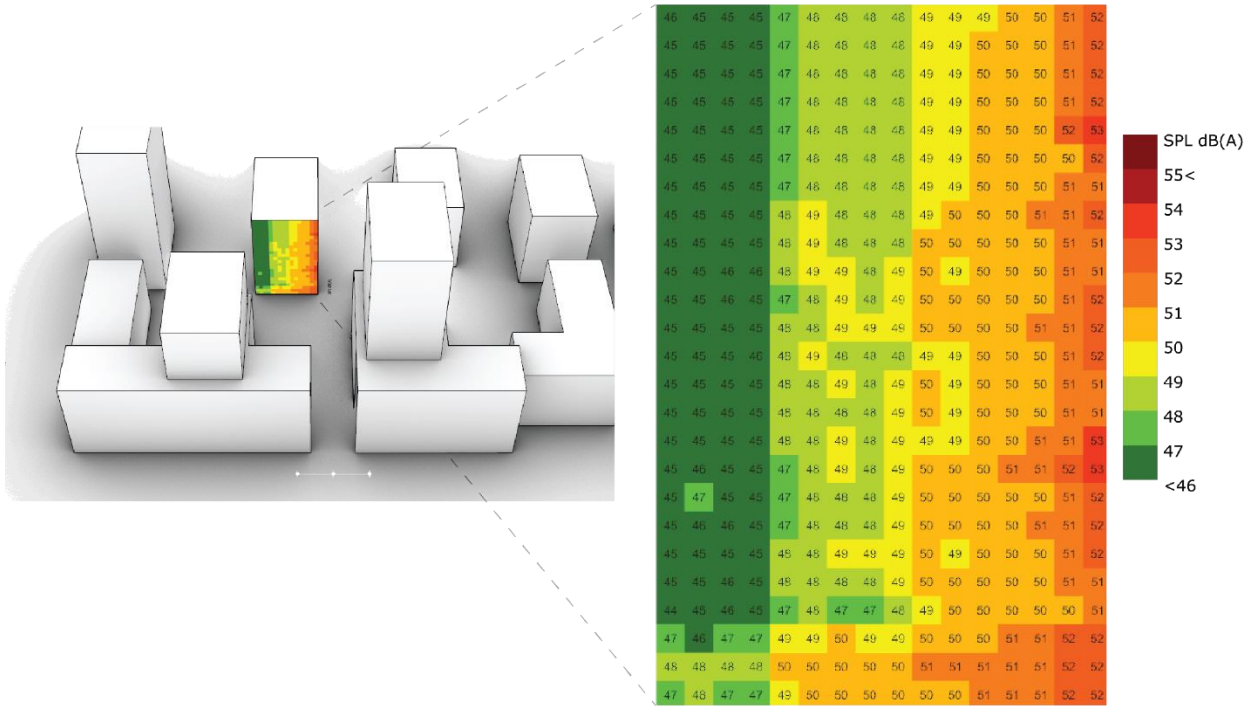

Figure D10 Sound pressure levels on façade for courtyard with 10m offset and green wall (C1.4)

D.5 Balcony variation (B)

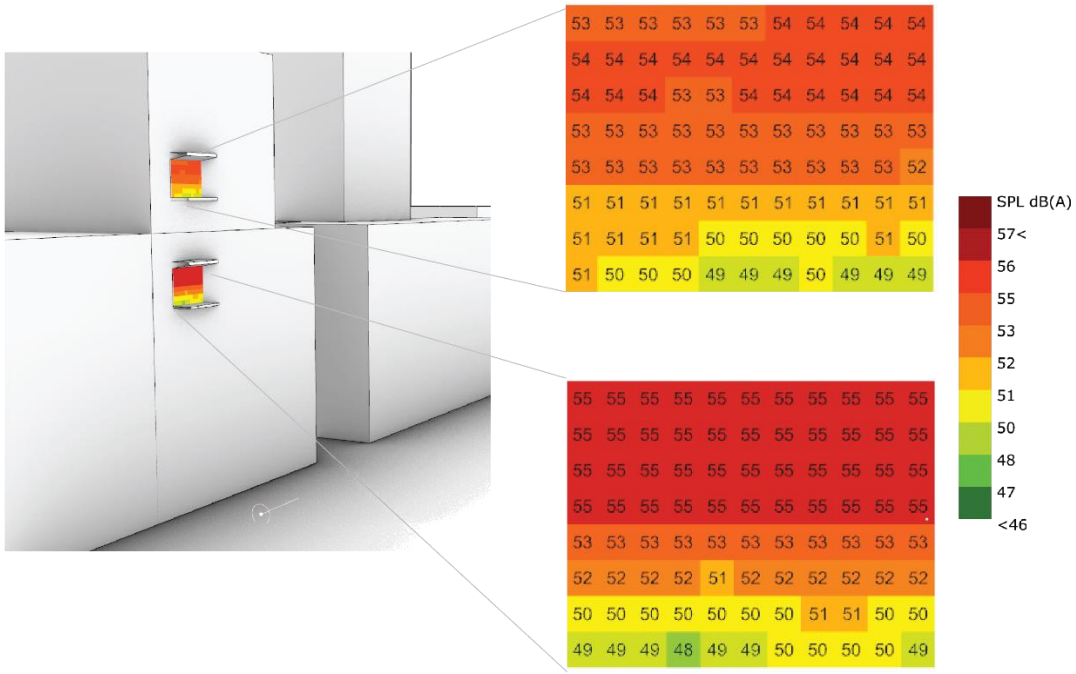

Figure D11 Sound pressure levels on façade for Balcony without sound-absorbing ceiling (B1.1)

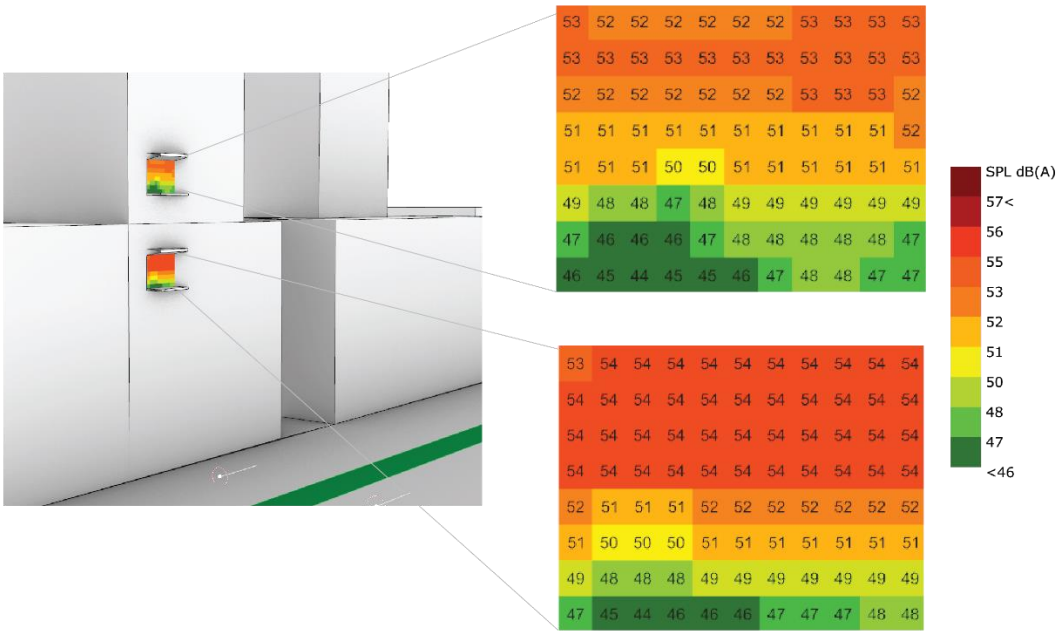

Figure D12 Sound pressure levels on façade for Balcony with sound-absorbing ceiling (B1.2)